Preparation, characterisation and selective hydrocarbon transformation applications of flat-model and zeolite-supported platinum catalysts

A thesis submitted in fulfilment of the requirements for the degree

Philosophiae Doctor

in the

DEPARTMENT OF CHEMISTRY
FACULTY OF SCIENCE

at the

UNIVERSITY OF THE FREE STATE

by

Nceba Magqi

Supervisor: Dr. E. Erasmus
Co-supervisor: Prof. J.C. Swarts

October 2014

Table of Contents

List of abbreviations and symbols

^{1}H NMR	proton nuclear magnetic resonance
AFM	atomic force microscopy
BE	binding energy
BTX	benzene, toluene and xylene
c/s	Counts per second
CA	cinnamyl alcohol
ca.	about (approximation symbol)
CAL	cinnamaldehyde
cm^{-1}	wave number
CNT	carbon nanotubes
CO	carbon monoxide
COD	1,5-cyclooctadiene
EELS	electron energy loss spectroscopy
EPMA	electron probe microanalysis
EXANES	Extended X-ray Absorption Fine Structure analysis
FT	Fischer-Tropsch
FTIR	Fourier transform infrared
FTS	Fischer-Tropsch syncrude
FWHM	Full width at half maximum
HCAL	hydrocinnamaldehyde
ICP-MS	inductively coupled plasma mass spectroscopy
IR	infrared
IRAS	infrared absorption spectroscopy
IWI	Incipient wetness impregnation
LAB	Linear alkyl benzene
MCP	Methyl cyclopentane

mp.	melting point
PED	photoelectron diffraction
PGM	Platinum group metals
PPA	3-phenyl-1-propanol
ppm	parts per million
RBS	Rutherford Backscattering Spectroscopy
RE	Rear earth
RON	research octane numbers
SFG	sum frequency generation
SMSI	strong metal-support interactions
STM	scanning tunnelling spectroscopy
TDS	thermal desorption spectroscopy
TEM	transmission electron microscopy
TGA	Thermogravimetric Analysis
TOF	Turnover frequency
TPD	temperature programmed desorption
TPO	temperature programmed oxidation
UHV	ultrahigh vacuum
UOP	Universal Oil Products
UPS	ultraviolet photoelectron spectroscopy
VPI	Vapour phase impregnation
WHSV	Weight hourly space velocity
XANES	X-ray Absorption Near Edge Structure
XPS	x-ray photoelectron spectroscopy
δ	chemical shift

List of selected structures and chemical reactions

List of selected Si wafer surfaces and flat model Pt/SiO_2/Si-wafer catalysts used in catalysis:

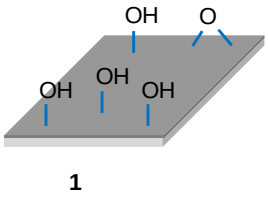

1

Si wafer with surface Si-OH groups

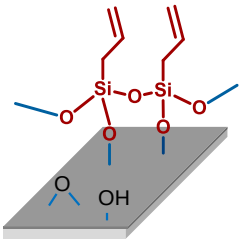

2

Si wafer with surface allyl groups

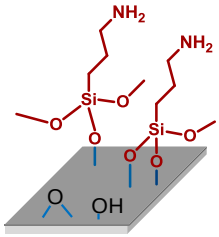

3

Si wafer with surface amino groups

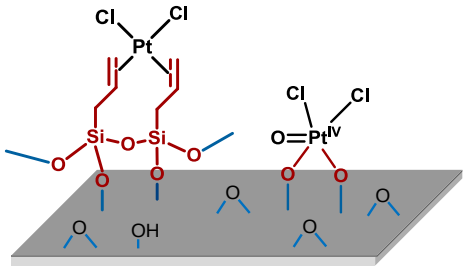

4

Si wafer with Pt spieces impregnated from H_2PtCl_6

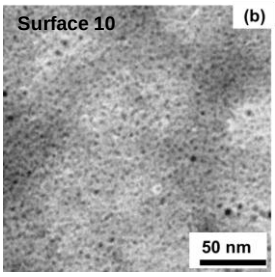

Si wafer with Pt particles obtained by grafting H_2PtCl_6 followed by calcination

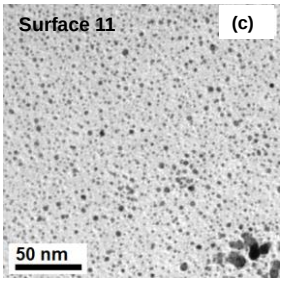

Si wafer with Pt particles obtained by spin coating of H_2PtCl_6 followed by calcination

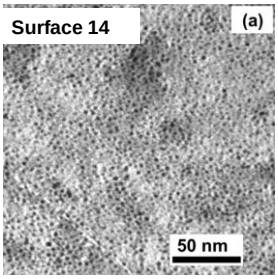

Si wafer with Pt particles obtained by grafting K_2PtCl_4

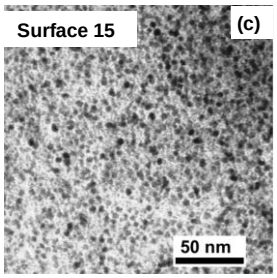

Si wafer with Pt particles obtained by grafting K_2PtCl_4 followed calcination

List of selected structures and chemical reactions

List of selected chemical reactions used to test the prepared catalysts:

1. Oxidation of 1-octadecanol

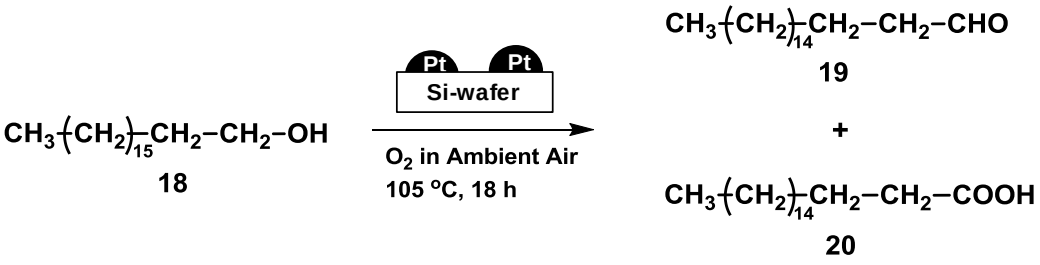

2. Oxidation of benzyl alcohol

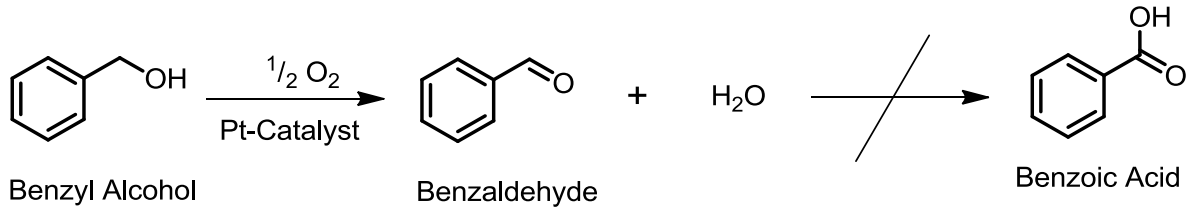

3. Oxidation of 1-octanol

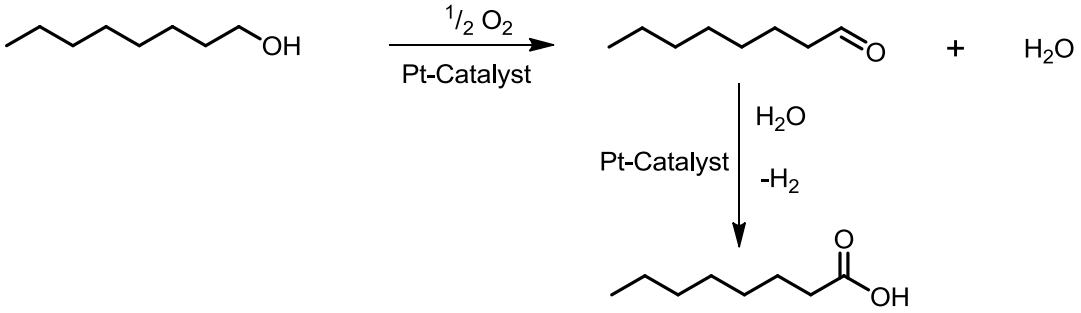

4. Hydrogenation of cyclohexene

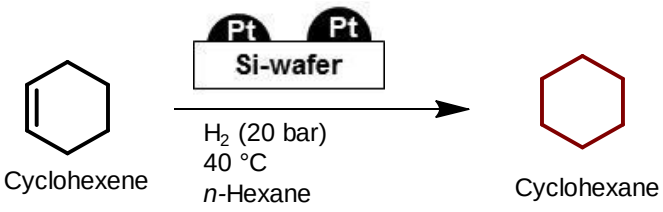

List of selected structures and chemical reactions

5. Hydrogenation of benzaldehyde

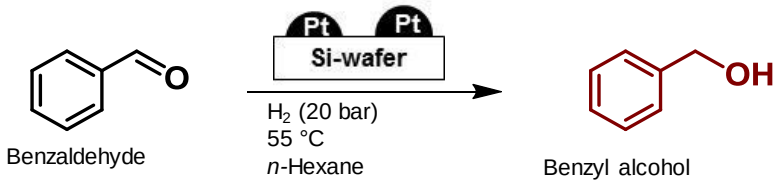

6. Hydrogenation of cinnamaldehyde

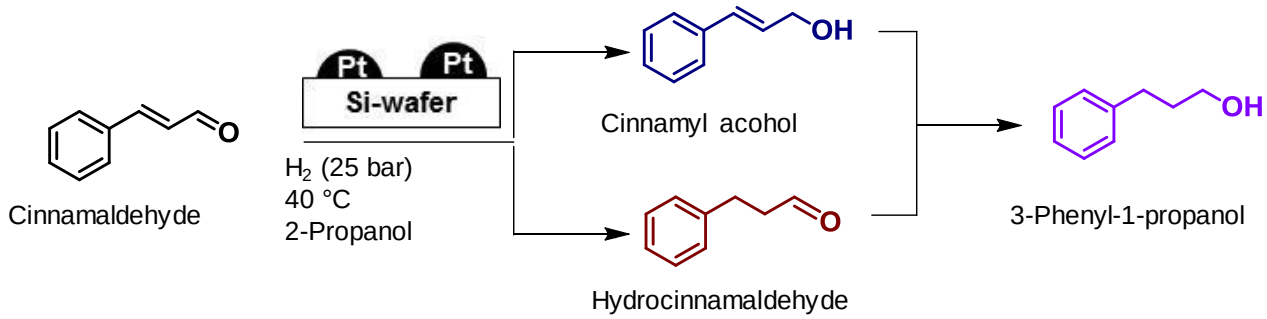

7. Aromatisation of various alkanes

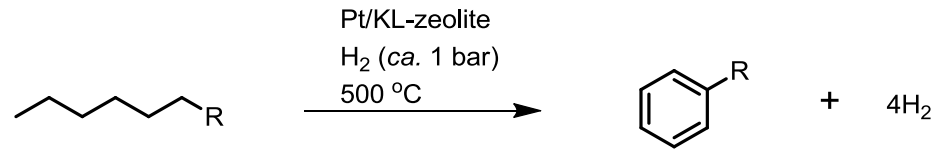

n-Hexane, R = H
n-Heptane, R = CH_3
n-Octane, R = CH_2CH_3

Acknowledgements

As the old saying goes, no man is an island. This study was made possible through the assistance and encouragement from a number of people whom I would like to thank.

I would like to extend my many thanks to my supervisor Dr Elizabeth Erasmus for her constant interest in my work and for giving me freedom to explore my own ideas. I would like to acknowledge her guidance in x-ray photoelectron spectroscopy and her supervision in many aspects of flat model catalysts. Her proficient and prompt review of my thesis allowed me to meet the set deadlines and milestones. I am sincerely grateful for her many hours spent reading my manuscript.

I would like to express my sincere gratitude to my co-supervisor Professor Jannie C. Swarts for allowing me to be a member of his research group, Physical Chemistry and supervising this study. I am grateful to him for an interesting topic in surface sciences and catalysis. His interest in my work and critical review of my thesis challenged me to go an extra mile to get a clear understanding of my work and to be more professional in my writing. The freedom and atmosphere in his research group made it possible to explore as many aspects of my study as possible.

I am deeply indebted to Sasol for the financial assistance to settle the costs associated with this study. I will always be grateful to Sasol for giving me the study leave and allowing me to further my studies in chemistry. This was made possible by my former manager Dr Pieter S. van Heerden who had an immense belief in me that I have what it takes to complete a doctoral study. I would like to say thank you to Pieter for his encouragement and his motivation to pursue this study. His discussion during the university visits highlighted many critical aspects of this study. Furthermore, I would like to acknowledge Pieter for his assistance in aromatisation work which was done at the Sasol research laboratory.

To the entire Physical Chemistry Group, I would like to express my great appreciation for making my stay in Bloemfontein an awesome experience and I would like to thank you for the ever important Friday afternoon discussions. Each and everyone of you made the Physical Chemistry

Acknowledgements

Group feel like home away from home. A special thank you goes to Professor Robbie Dennis for helping me with the Scientist software curve fittings. I would like to thank Dr Eleanor Müller for her assistance and for the refresher training in the Parr reactor. I would like to express my gratitude to Dr Ernie Langner, Stewart Tsai and Rikus Peens for their assistance and training in the ASAP Porosity Analyser. A special thank you to my office "neighbour", Chris Joubert who helped me learn a number of gas lines going in and out of our research lab and his help to learn unfamiliar equipment in the lab. To my European colleagues Uwe, Ron and Jasiu; thank you for the very informative discussions especially on Friday afternoons.

I would like to express my gratitude to Dr Linette Twigge for her assistance in running the ^{195}Pt NMR experiments at low temperature and the interpretation of the collected data. I wish to say thank you to Mrs Tessa Swarts for her assistance in all the administrative work relating to our research group. I would like to acknowledge Mr Itumeleng Daniel Fish for keeping our research laboratory in good condition to perform our experiments. I wish to thank the Microscopy Unit, UFS, for TEM analyses and iThemba Labs, Somerset West, for the RBS analyses.

To my friends outside of the chemistry circles, I would like to say thank you for all your support and your belief in my work ethics. A special thank you goes to Molly Matlotlo who has a special understanding of English and Japanese languages, for reading and for her instructive critic of my literature review to make it reader friendly even for the non-chemists like her. I would like to thank Pearl Gola, Mike Sibiya and Zinhle Marrengane for their confidence in me and for sharing their experiences with regard to doctoral studies.

My heartfelt gratitude goes to my parents and siblings who supported me even during the planning stages of my doctoral studies. Your emotional support, guidance and teachings about work ethics are highly appreciated.

Abstract

Allyl, amino and silanol (Si-OH) functionalised silicon wafers with epitaxial layer of SiO_2 (SiO_2/Si-wafers) were used as two-dimentional supports to prepare flat model Pt/SiO_2/Si-wafer catalysts by spin coating and grafting of suitable platinum precursors followed by calcination and reduction. X-ray photoelectron spectroscopy (XPS) revealed that H_2PtCl_6 reacted with surface allyl groups to form π-olefin Pt^{2+} supported complexes. Residual Si-OH groups also reacted with H_2PtCl_6 to form Pt^{4+} species. Together, the different surface Pt species formed a heterogeneous coating on the surface of Si-wafer. The platinisation of aminated silicon surfaces with K_2PtCl_4 dissolved in aqueous ethanol resulted in the reduction of the Pt(II) precursor and immobilisation of the resultant metallic Pt particles on the model Si-wafer. Calcination and reduction of the surface Pt species resulted in the formation of relatively small Pt particles, 1-5 nm average particle diameter, which interacted with the silicon surface *via* boundary Pt^{2+}-O-Si bonds or Pt^{2+}-N-Si bonds. The prepared flat model Pt/SiO_2/Si-wafer catalysts had catalytic activity in solvent-free aerobic oxidation of 1-octadecanol to carbonyl compounds. A selection of the prepared flat model Pt/SiO_2/Si-wafer catalysts were also shown to have activity in hydrogenation of alkene and carbonyl functional groups.

The preparation and characterisation of Pt catalysts supported on alkaline KL-zeolite and acidic HY-zeolites are also described. Two types of Pt/KL-zeolite catalysts were investigated. Those Pt/KL-zeolite catalysts prepared by vapour phase impregnation had a high particle dispersion (91.5 % *vs.* 75.8 %) and smaller particles sizes (average diameter = 1.2 nm *vs.*1.5 nm) compared to the equivalent Pt/KL-zeolite catalysts that were obtained by incipient wetness impregnation. In aromatisation of *n*-alkanes, the Pt/KL-zeolite catalysts obtained by vapour phase impregnation were more active and more tolerant to oxygenates present in the feed than the Pt/KL-zeolite catalysts obtained by incipient wetness impregnation. A correlation between the concentrations of acetic acid in the feed, the amount of coke deposit on spent catalysts and catalyst deactivation was established. Pt/KL-zeolite and Pt/HY-zeolite catalysts were also applied in liquid phase oxidation of primary alcohols under mild conditions (*ca.*100 °C and ambient pressure). Moderate substrate conversion (10-40 %) was achieved.

Keywords: Silicon wafer, Pt/SiO_2/Si-wafer, Pt/KL-zeolite, aromatisation, oxidation, hydrogenation, XPS.

Opsomming

Alliel, amino en silanol (Si-OH)-gefunksionaliseerde silikon wafers met epitaksiale SiO_2 (SiO_2/Si-wafers) lagies is gebruik as twee-dimensionele (2-D) ondersteunende platvorms om plat model Pt/SiO_2/Si-wafer katalisatore voorteberei met behulp van roterende verdampingsbedekking (die ekwivalent van nat chemiese impregnasie) van geskikte platinum uitgangstowwe gevolg deur kalsineering en reduksie. X-straal fotoelektron spektroskopie (XPS) het getoon dat H_2PtCl_6 met wafers wat oor oppervlak allielgroepe beskik reageer om π-olefien Pt^{2+} komplekse te vorm. Oorblywende (residuele) Si-OH groepe ondergaan ook interaksie met Pt^{2+} om Pt^{4+} spesies te vorm. Tesame vorm al die Pt spesiesoorte ‘n heterogene mengsel wat die oppervlakte van die Si-wafer bedek. Die platineering van geamineerde silikonoppervlaktes met K_2PtCl_4 opgelos in waterige etanol lei tot die reduksie van Pt(II) voorgangers en die immobilisasie van platinum metaaldeeltjies. Die kalsineering en reduksie van die oppervlak metaal Pt spesies lei tot die vorming van relatiewe klein Pt deeltjies met ‘n gemiddelde deeltjiedeursnit van 1-5 nm, wat ‘n interaksie met die ondersteunende silikon wafer ondergaan deur middel van grensvlak Pt^{2+}-O-Si of Pt^{2+}-N-Si bindingsmodes. Die voorbereide Pt/SiO_2/Si-wafer katalisatore toon katalitiese aktiwiteit in die oplosmiddelvrye lug oksidasie van 1-oktadekanol na karbonielverbindings. Sekere geselekteerde model Pt/SiO_2/Si-wafer katalisatore toon ook katalitiese aktiwiteit in die hidrogeneering van alkeen en karboniel funksionele groepe.

Die voorbereiding en karateriseering van Pt katalisatore ondersteun op KL-zeoliete en HY-zeoliete is ook beskryf. Twee soorte Pt/KL-zeoliet katalisatore is ondersoek. Pt/KL-zeoliet katalisatore wat voorberei is deur gasfase impregnasie het ‘n hoë deeltjiedispersie (91.5 % *vs.* 75.8 %) en kleiner deeltjiegroottes in vergelyking met die Pt/KL-zeoliet wat voorberei is deur aanvangsbenattingsimpregnasie (gemiddelde deursnit = 1.2 nm *vs.*1.5 nm). In die aromatisering van n-alkane, was die Pt/KL-zeoliet katalisatore wat voorberei is deur gasfase impregnasie meer aktief en meer verdraagsaam teen suurstof-bevattende verbindings as die Pt/KL-zeoliet wat voorberei is deur aanvangsbenattings impregnasie. ‘n Korrelasie tussen die konsentrasie van asynsuur in die voerstroom, die hoeveelheid neergeslane kooks op die uitgeputte katalisatore en katalis deaktiveering is vasgestel. Die Pt/KL-zeoliet katalisatore is ook aangewend in vloeistoffaseoksidasie van primêre alkohole onder matige kondisies (100 °C en omgewings druk) met matige sukses (10 - 40%) in substraat omskakeling.

Sleutelwoorde: Silicon wafer, Pt/SiO_2/Si-wafer, Pt/KL-zeolite, aromatisation, oxidation, hydrogenation, XPS.

Declaration

I, Nceba Magqi, declare that the thesis hereby submitted by me for the Philosophiae Doctor degree at the University of the Free State is my own independent work and has not previously been submitted by me at another university/faculty. I further more cede the copyright of the dissertation in favour of the University of the Free State.

Signed:_____ Date:_____

1. Introduction and Objectives

1.1 Introduction

The use of platinum in catalytic transformations of organic substrates dates back as early as the 1820s.[1] A useful feature of Pt in catalysis is the effortless addition or removal of electrons to form an element with one of the three different dominant oxidation states (*i.e.* Pt^0, Pt^{2+} and Pt^{4+}).[2] This feature makes it possible for Pt to adopt different oxidation states during any catalytic cycle. Notable reactions that are catalysed by Pt catalysts are hydrogenation reactions[3,4] and dehydrogenation reactions (including oxidation of alcohols and dehydrocyclisation reactions).[5,6,7] Supported Pt catalysts on durable and porous materials such as silica, alumina or zeolites have made it possible to extend the application of Pt catalysis to industrial processes which often have harsh conditions.[8]

The major challenges associated with the use of supported Pt catalysts in organic transformations are:

1. Poor selectivity to a specific product due to the diverse chemical reactions that can be catalysed by Pt catalysts. [9]
2. Catalyst deactivation by poisoning[i], thermal deactivation and leaching of the catalyst from the support. [8,9,10]

Poor product selectivity and catalyst deactivation contribute to the inevitable costs of separating the resulting catalytic products and the replacement of the deactivated catalysts. Understanding of the intrinsic properties of the catalyst at molecular level assists in refinement and design of industrial catalysts with better catalytic activity.[11] Given the complexity of the supported catalysts, it is not always feasible to study the intrinsic chemistry of the catalyst active site. The cost effective modelling techniques are sometimes used to simplify the industrial catalysts and make it

[i] Catalyst poisons such as sulphur compounds and oxygenates can competitively bind to the catalyst active site and prevent the interaction of the catalyst with the substrate.

more feasible to apply the modern spectroscopic tools to study the catalyst active sites.[11,12,13] Simulation of the industrial catalyst by impregnation of metal particles on the flat two-dimensional (2-D) model support provides simpler catalytic systems to study the intrinsic chemistry of the active site without the interference of the three-dimensional (3-D) porous support.[14]

The flat 2-D model catalyst systems used to simulate the industrial catalysts need to meet the following criteria: [15]

1. The electronic properties (*e.g.* conductance) and morphology of the model support must be conducive to the application of different surface science analysis tools without the disadvantages associated with the industrial 3-D porous support.
2. The 2-D model catalyst must be thermally stable against deactivation processes at high temperature.
3. The density of the metal particles per unit surface area must be sufficiently high to allow reactivity in the catalytic reactions and spectroscopic analysis.

It is also advantageous to use a versatile oxide support such as epitaxial SiO_2 that can be functionalised easily to form Si-OH groups which can interact with the metal-containing precursor.[11,14,16] Functionalised silicon wafers (Si-wafers) with a thin layer of surface SiO_2 have received a lot of attention in preparation of realistic flat 2-D model catalysts. The underlying Si substrate has a weak conductance which allows the use of spectroscopic techniques such as x-ray photoelectron spectroscopy (XPS).[14,15] The flat model Pt/Si-wafer catalysts have been successfully utilised in gas phase hydrogenation of α,β-unsaturated aldehydes to corresponding unsaturated alcohols.[17] Our research group has also utilised 2-D mono-metallic[18] and bi-metallic[19] catalysts supported on functionalised Si-wafers in solvent free aerobic oxidation of 1-octadecanol at 105 °C and ambient air.

Notably, a flat 2-D model $Pt/SiO_2/Mo(112)$ catalyst was used to study the aromatisation of *n*-heptane to toluene (see Scheme 1.1).[20] In this example, it was demonstrated using a batch reactor

system that aromatisation of *n*-heptane is dependent on particle size of Pt supported on flat 2-D model SiO_2 support where the optimum selectivity to toluene is obtained with Pt particle sizes of *ca.* 1.5 nm.[20] The example provided confirmed that dehydrocyclization reactions leading to aromatics are structure-sensitive.[21]

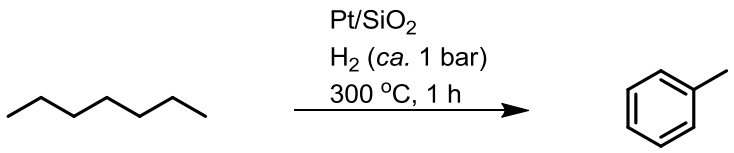

Scheme 1.1. Aromatisation of *n*-heptane over a flat 2-D model $Pt/SiO_2/Mo(112)$ catalyst.[20]

Pt catalysed aromatisation of *n*-alkanes to corresponding aromatics forms an integral part of catalytic reforming of low-value chemicals in the petroleum industry.[8] A notable commercial process which uses a bi-functional Pt catalyst on chlorinated Al_2O_3 (acidic support) is the Universal Oil Products (UOP) Platforming^{TM} process.[22,23] The disadvantage of this bi-functional Pt catalyst in the reforming of *n*-alkanes is the competing reactions on the acid sites.[24] Moreover, the chlorinated Pt/Al_2O_3 catalysts are also susceptible to leaching away of chloride ions to form corrosive waste in the presence of water.[25,26]

In mono-functional Pt catalysts, the metal is supported on non-acidic support to suppress the acid catalysed reactions and improve selectivity to aromatic products. Pt catalysts supported on non-acidic KL-zeolite have resulted in commercial processes such as the AROMAX^{TM} by Chevron Phillips Chemical Company[27] and the RZ-Platforming by UOP.[28] Pt/KL-zeolite catalysts have high activity in aromatisation of *n*-alkanes, especially *n*-hexane due to small Pt particles (*ca.* 2.5 nm) with high electron density[29] and the geometric properties of the L-zeolite channels which prevent the formation of secondary products from bimolecular reactions.[30,31]

Pt/KL-zeolite catalysts deactivate over a long period on stream due to irreversible adsorption of hydrocarbon on the surface of the active sites, followed by the dehydrogenation of the adsorbed specie to form carbonaceous deposits or coke.[32,33] In Pt/KL-zeolite catalysts obtained by vapour phase impregnation, the majority of Pt particles are located inside the L-zeolite channels which limit the bimolecular reactions that result in coke deposits. Thus the Pt/KL-zeolite catalysts obtained by vapour phase impregnation are more resistant to deactivation by carbonaceous deposits compared to catalysts obtained by incipient wetness impregnation or ion exchange impregnation.[34,35]

Beside the carbonaceous deposits, Pt/KL-zeolite catalysts are more susceptible to sulphur poisoning than bi-functional Pt catalysts.[36] The Pt/KL-zeolite catalysts are therefore more compatible with the Fischer-Tropsch syncrude (FTS) derived naphtha which is free from sulphur species.[37] The main challenge with the FTS naphtha is the oxygenates including water, alcohols, carbonyls and carboxylic acids which are inherent in FT products that over time deactivates the catalyst.[25,37] The only detailed study found in the literature about the impact of oxygenates in aromatisation of *n*-alkanes, is the conference communication by Dry and co-workers.[38] In this study the effect of alcohols and carbonyls in aromatisation of *n*-hexane over Pt/KL-zeolite catalyst obtained by incipient wetness impregnation was investigated. The authors concluded that the oxygenates decompose to form the same molecular amounts of carbon monoxide (CO) which chemisorb on the Pt active site and suppress its aromatisation activity. Although a reference to the possible formation of carbonaceous deposits was made, no quantification was provided. There is no literature found on the detailed effect of carboxylic acids in aromatisation of *n*-alkanes.

1.2 Objectives

The background given in the previous section outlines the versatility of Pt catalysts in industrially relevant chemical transformations and the opportunities provided by the flat model

catalyst systems in studying the intrinsic properties of the industrial catalysts. Against this background, this study set out to pursue the following goals:

1. Preparation and characterisation of flat 2-D model Pt catalysts supported on functionalised Si-wafers. Under this goal, the Si-wafers would be functionalised to make them suitable to immobilise the Pt precursors by wet chemical impregnation techniques.
2. Application of the prepared flat model Pt catalysts in transformation of organic compounds with different functional groups. The identified chemical reactions to pursue are solvent free aerobic oxidation of primary alcohols and hydrogenation of α,β-unsaturated aldehydes.
3. Preparation and characterisation of Pt catalysts supported on zeolites (KL-zeolite or HY-zeolite). The aim is to use incipient wetness impregnation and vapour phase impregnation methods to prepare Pt/zeolite catalysts with well dispersed Pt particles.
4. Application of Pt/KL-zeolite catalysts in aromatisation of *n*-alkanes in the presence of oxygenates, especially acetic acid.
5. Analysis of spent Pt/KL-zeolite to quantify the amount of adsorbed coke deposits and correlate it to the presence of oxygenates in the *n*-alkane feed and the catalyst deactivation.
6. To determine the effect of decoking (burning regeneration) on the physisorption and chemisorption properties of the Pt/KL-zeolite catalysts.
7. Application of Pt/zeolite catalysts in oxidation of primary alcohols.

1.3 References

[1] P. M. D. Collins, *Platinum Metals Rev.* **1986**, *30*, 141-146.
[2] V. I. Okafor, N. J. Coville, *S. Afr. J. Sci.* **1999**, *95*, 503-508.
[3] W. Yu, M. D. Porosoff, J. G. Chen, *Chem. Rev.* **2012**, *112*, 5780-5817.
[4] C. Lian, H. Liu, C. Xiao, W. Yang, K. Zhang, Y. Liu, Y. Wang, *Chem. Commun.* **2012**, *48*, 3124-3126.
[5] S. M. Kumar, D. Chen, J. C. Walmsley, A. Holmen, *Catal. Commun.* **2008**, *9*, 747-750.
[6] T. Mallat, Z. Bodnar, P. Hug, A. Baiker, *J. Catal.* **1995**, *153*, 131-143.

[7] M. Ilyas, M. Sadiq, *Chem. Eng. Technol.* **2007**, *30*, 1391-1397.
[8] B. C. Gates, J. R. Katzer, G. C. A. Schuit, in *Chemistry of Catalytic Processes.* McGraw-Hill, New York, **1979**, pp. 184-289.
[9] G. A. Somorjai, K. McCrea, *Appl. Catal. A.* **2001**, 222, 3-18.
[10] P. Meriaudeau, C. Naccache, *Catal. Rev. Sci. Eng.* **1997**, *39*, 5-48.
[11] F. Gao, D.W. Goodman, *Annu. Rev. Phys. Chem.* **2012**, *63*, 265-286.
[12] G. A. Somorjai, *Science*, **1985**, *227*, 902-908.
[13] J. W. Niemantsverdriet, in *Spectroscopy in Catalysis*. Weinheim:Wiley-VCH. **2007, pp.** 19-346.
[14] P.L.J., Gunter, J.W., Niemantsverdriet, F.H., Ribeiro, G.A., Somorjai, *Catal. Rev. Sci. Eng.* **1997**, *39*, 77-168.
[15] J. W. Niemantsverdriet, A.F.P. Engelen, A.M. de Jong, W. Wieldraaijer, G.J. Kramer, *Appl. Surf. Sci.* **1999**, *144-145*, 366-374.
[16] C.T. Campbell, *Surf. Sci. Rep.* **1997**, *27*, 1-111.
[17] A. Borgna, B. G. Anderson, A. M. Saib, H. Bluhm, M. Havecker, A. Knop-Gericke, A. E. T. Kuiper, Y. Tamminga, J. W. Niemantsverdriet, *J. Phys. Chem. B.* **2004**, *108*, 17905-17914.
[18] E. Erasmus, P. C. Thune, M.W.G.M. Verhoeven, J.W. Niemantsverdriet, J. C. Swarts, *Catal. Commun*. **2012**, *27*, 193-199.
[19] E. Erasmus, J. W. Niemantsverdriet, J. C. Swarts, *Langmuir*. **2012**, *28*, 16477-16484.
[20] M. J. Lundwall, S. M. McClure, X. Wang, Z. Wang, M. Chen, D.W. Goodman, *J. Phys. Chem. C*. **2012**, *116*, 18155−18159.
[21] R. M. Rioux, B. B. Hsu, M. E. Grass, H. Song, G. A. Somorjai, *Catal. Lett.* **2008**, *126*, 10−19.
[22] M. J. Sterba, V. Haensel, *Ind. Eng. Chem. Prod. Res. Dev.* **1976**, *15*, 2-17.
[23] V. Haensel, US Patent, 2479110A, **1949**.
[24] P. Meriaudeau, C. Naccache, *Catal. Rev. Sci. Eng.* **1997**, *39*, 5-48.
[25] A. de Klerk, E. Furimsky, in *Catalysis in the Refining of Fischer-Tropsch Syncrude*. RSC Publishing, Cambridge, **2010**, p. 193-207.
[26] D. J. O'rear, C. –Y., Chen, S. J. Miller, WO Patent, 2010/080360A2, **2010**.
[27] T. R. Hughes, W. C. Buss, P. W. Tamm, R. L. Jacobson, *Stud. Surf. Sci. Catal.* **1986**, *28*, 725-732.
[28] J. D. Swift, M. D. Moser, M. B. Russ and R. S. Haizmann, *Hydrocarbon Technol. Int.* **1995**, 86.
[29] C. Besoukhanova, J. Guidot, D. Barthomeuf, M. Breysse, J. R. Bernard, *J. Chem. Soc., Faraday Trans. 1*. **1981**, *77*, 1595-1604.
[30] S. J. Tauster, J. J. Steger, *J. Catal.* **1990**, *125*, 387-389.
[31] K. G. Azzam, G. Jacobs, W. D. Shafer, B. H. Davis, *J. Catal.* **2010**, *270*, 242–248.
[32] G. A. Somorjai, F. Zaera, *J. Phys. Chem.* **1982**, *86*, 3070-3078.
[33] S. M. Davis, F. Zaera, G.A. Somorjai, *J. Am. Chem. Soc.* **1982**, *104*, 7453-7461.
[34] S. Jongpatiwut, P. Sackamduang, T. Rirksomboon, S. Osuwan, W. E. Alvarez, D. Resasco, *Appl. Catal. A*. **2002**, *230*, 177-193.
[35] D. J. Ostgard, L. Kustov, K. R. Poeppelmeier, W. M. H. Sachtler, *J. Catal.* **1992**, *133*, 342-357.
[36] J. T. Miller, D.C. Koningsberger, *J. Catal*. **1996**, *162*, 209-219.
[37] A. de Klerk, *Green Chem.* **2007**, *9*, 560-565.
[38] M. E. Dry, R. J. Nash, C. T. O'Connor, in *Proc. 12th Inter. Zeolite Conf.* Baltimore, **1998**, 2557-2564.

2. Literature Review

This thesis deals with aspects regarding the preparation and applications of heterogeneous platinum-based catalysts supported on flat model supports and conventional powder supports. Before embarking on the crux of the thesis in the results and discussions in chapter 3, this chapter presents selected topics on the reported literature about realistic model catalysts on a flat support and the topics about Pt-based catalysts on conventional powder supports. The topics that are discussed in Section 2.1 to Section 2.6 in this chapter, clarify the rationale behind the study of model catalysts. This is achieved by reviewing the reported research breakthroughs that were achieved through model catalysts. The carefully selected literature review covers factors such as typical model supports, different types of metal deposition methods, characterisation techniques used in model catalysts and the validation of the model catalysts in catalytic reactions. All these factors are vital and influence the identity of a realistic model catalyst which mimics industrial processes.

Sections 2.7 to Section 2.9 present the reported literature about heterogeneous Pt-based catalysts for use in selective dehydrogenation reactions particularly, reforming of *n*-alkanes to aromatics and oxidative dehydrogenation of alcohols to corresponding carbonyls. The reforming of *n*-alkanes is one of the processes used in refining of vehicle fuel to make it suitable for the car engine. The factors that influence the unusually high aromatisation activity of Pt catalysts supported on alkaline support are discussed under this topic. Also discussed is the tolerance of Pt catalysts towards catalysts poisons that are found in petroleum naphtha and Fischer-Tropsch derived liquids.

Section 2.9 is the last section of this chapter and it gives a brief overview of the catalytic hydrogenation of α,β-unsaturated aldehydes. The topics discussed in this chapter are aligned with the objectives of this doctoral thesis as outlined in chapter 1.

2.1 General Introduction to Model Catalysts

The following discussion presents the literature review for goal 1 of this study as outlined in chapter 1.

Typical heterogeneous catalysts consist of a porous support with a large surface area as the major component with finely dispersed nano-size metal particles which are the catalytically active component on the walls of the support. The catalyst support serves a crucial role in maintaining the good separation and dispersion of the individual active sites, thus preventing agglomeration and loss of surface area during the catalytic reaction. However, the three dimensional (3-D) arrangement of the porous support housing the active metallic particles is not always ideal in studying the intrinsic chemistry of the technical (industrial) catalyst at a molecular level.[1] In the 3-D support, the metal particles hide inside the pores of the support. As a result, surface science techniques such as electron energy loss spectroscopy (EELS), scanning tunnelling spectroscopy (STM) and atomic force microscopy (AFM) cannot be applied to study the catalyst. Moreover, the durable supports used in industrial catalysts are insulating materials with large band-gaps which cause charge problems when spectroscopic techniques such as x-ray photoelectron spectroscopy (XPS) are used.

Due to the limitations outlined above, useful information that could be used to improve the design and fundamental study of industrial catalysts is not always accessible or runs the risk of being misinterpreted. [2,3,4] Model catalysts in the form of unsupported single crystal model and supported flat model catalysts provide an opportunity to study the intrinsic properties of the catalyst active sites which are not easily accessible in conventional heterogeneous catalysts.[5,6,7] Figure 2.1 depicts the XPS spectra of the supported ZrO_2 catalyst on silicon dioxide (SiO_2) powder and model ZrO_2 catalyst supported on epitaxial film of SiO_2 grown of Si(100) substrate.[8] Noteworthy is the loss of peak resolution on the spectra obtained from the analysis of the ZrO_2/SiO_2 powder catalyst. The XPS

spectra of $ZrO_2/SO_2/Si$ model catalyst exhibit well defined and resolved Zr 3d spin-orbit-split doublets.

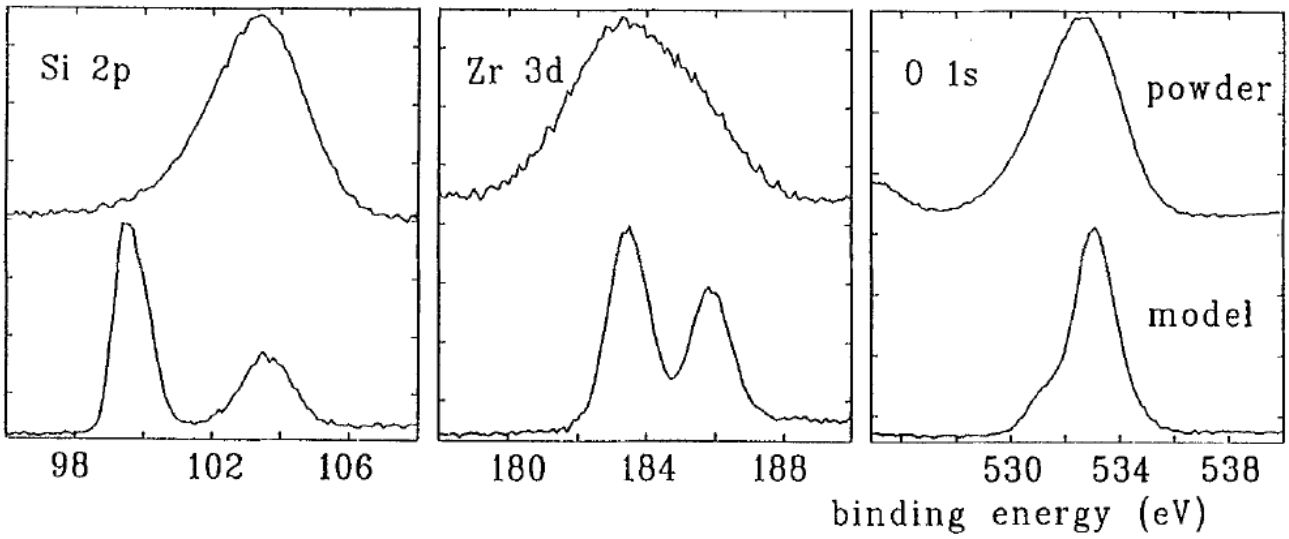

Figure 2.1. XPS spectra of the Si 2p (Si substrate and SiO_2 for model support), Zr 3d and O 1s peaks of the ZrO_2/SiO_2 powder catalyst (top) and $ZrO_2/SiO_2/Si$ flat model catalyst (bottom). The figure was adapted from Figure 1 of reference 8 with kind permission from Springer Science and Business Media. Copyright (1991) Springer Science and Business Media.

Extensive work has been done on single crystal model catalysts to help get an advanced understanding of the properties of conventional industrial catalysts.[9,10,11] In the single crystal model approach, the catalytic reaction may take place on modified metal single crystal surfaces. The data obtained in structure-insensitive reactions such as oxidation of CO on rhodium crystal surface, give a widely accepted intrinsic chemistry of the active site in terms of rate limiting kinetics.[7,12,13] As shown in Figure 2.2b, single crystal Rh and supported Rh give similar rates of CO_2 formation in CO oxidation by molecular oxygen.[12] In structure-sensitive reactions such as CO oxidation by NO, there are a number of factors involved in the rate-limiting steps. The rate of product formation is influenced by the structure and particle size of the metal species as shown in Figure 2.2a. [7,14]

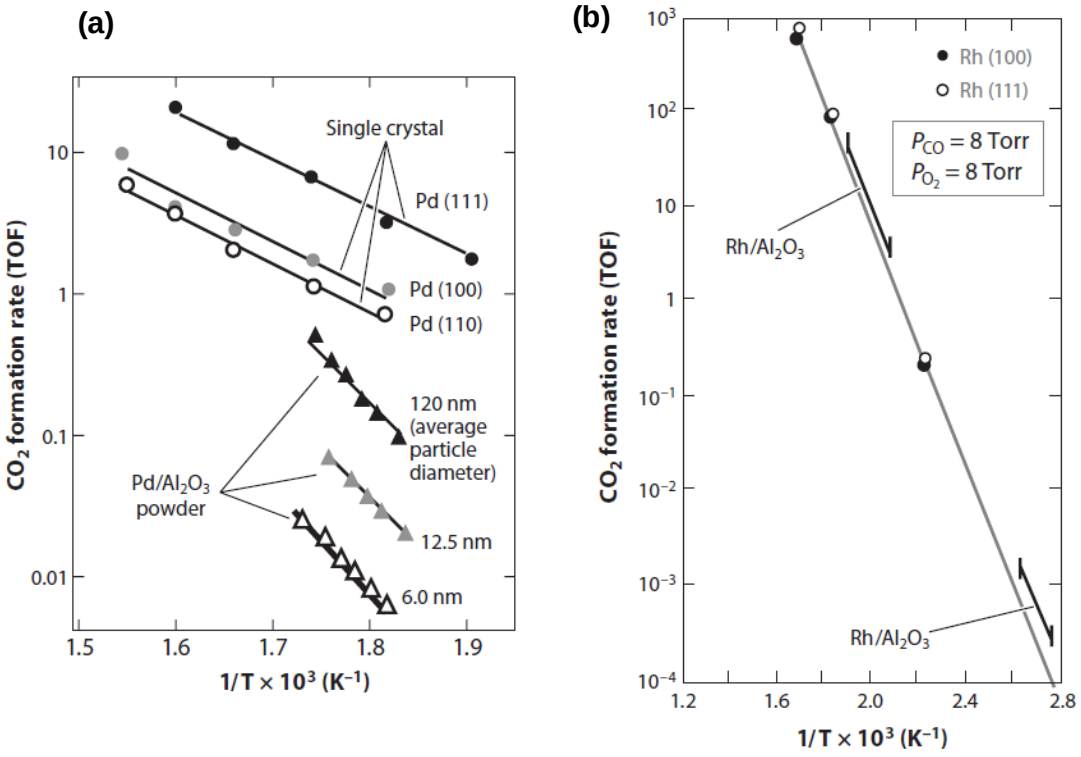

Figure 2.2. (a) A comparison of the rate of the CO_2 formation (TOF = Turnover Frequency) in oxidation of CO by NO on Pd surfaces; (b) a comparison of the rate of CO_2 formation (TOF) in oxidation of CO by O_2 over Rh(100), Rh(111) and supported Rh. Part (a) of the figure was adapted with permission from reference 14. Copyright (1997) by Elsevier and part (b) was adapted with permission from reference 12. Copyright (1986) by American Chemical Society.

The examples discussed in the previous paragraph outline the significance of single crystal model catalysts in simulating and simplification of heterogeneous catalyst systems. It must be noted that the single crystal systems have two major limitations which are the so-called "pressure-gap" and "material-gap". The pressure-gap arises from the fact that clean single-crystal surfaces are studied under ultrahigh vacuum (UHV) conditions. The catalytic data collected under these conditions may not match the data collected under realistic pressure conditions used in industrial applications. Furthermore, the single crystal approach does not consider the inevitable influence of the support on catalytic activity and the influence of the support on metal particle size variations. It also does not consider the morphological variations of the metal clusters and the metal-support interactions.[7,10] In

industrial catalysts, the active metal exists as nanoparticles on the support where metal-support interactions sometimes influence the characteristics of the catalyst.

To overcome the limitations of the single crystal catalyst systems, the UHV experimental techniques have been improved to allow studies at elevated pressure. The materials gap is eliminated by the use of flat (2-D) model oxidic supports similar to the material used in industrial catalysts.[7] Planar oxide-supported model catalysts provide intermediate catalyst systems to close the material-gap between single crystal model surfaces and industrial catalysts. The surface techniques used to unravel useful information in single crystal model catalysts can be applied in planar oxide-supported catalysts. At the same time, the size of the metal particle deposited on the support can be varied as desired. In the sections that follow, some of the research carried out to develop realistic catalysts on flat model supports is discussed.

2.2 Realistic Model Catalysts on Planer Oxide Supports

This section and the following subsections present literature on flat 2-D model oxide support which was the requirement for goal 1 (chapter 1).

The simulation of supported industrial catalysts by model supports varies with the method used to deposit the metal on the support and the characteristics of the support used. A realistic model catalyst needs to meet the following criteria: [15]

1. The model support must be conducting enough to allow the application of different surface science analysis tools without the loss of information due to charging problems. In addition to conducting characteristics, flat (2-D) model supports are more conducive for mechanistic studies of heterogeneous catalysts because the diffusion limitation caused by the 3-D pores in industrial catalyst is eliminated.
2. The model catalyst must be thermally stable against deactivation processes such as sintering, volatilization or encapsulation of metal species or reaction with the support *i.e.*

strong metal-support interactions (SMSI).

3. The number density of metal particles per unit surface area must be sufficiently high to allow reactivity in catalytic reactions and spectroscopic analysis.

It is also advantageous to use a versatile oxidic support that can be functionalised easily and stabilise the metal particles. A number of oxidic supports have been used successfully by different research groups to prepare flat model catalysts.[7,16,17] A few typical oxide supports which have been used to immobilise and prepare a variety of model catalysts include SiO_2, Al_2O_3, MgO and TiO_2.[17] The oxide support material can be used as a carefully prepared crystalline or bulk flat surface where metal particles can be deposited. The disadvantage of using bulk oxides as a flat support is the lack of conductivity which is useful in spectroscopic analysis tools.[18]

A thin layer of oxide prepared on a conducting material can be used as an alternative to bulk oxides. The epitaxial layer of oxide can be prepared by vacuum evaporation of the bulk oxide on conductive single crystal or evaporation of the metal in oxygen atmosphere on conducting material followed by annealing at high temperatures (about 300 to 1000 °C). Other popular methods to prepare epitaxial thin films are thermal oxidation of the metal single crystal substrate in air or near to ambient oxygen pressure (10^{-7}-10^{-6} Torr)[17] and anodic oxidation of the metal substrate.[19]

2.2.1 Silica (SiO_2) Supports for Model Catalysts

SiO_2 and *alumina* (Al_2O_3) are the most-used supports in heterogeneous catalysis. In flat model support, a thin layer of SiO_2 (-O-Si-O-) is prepared by reactive evaporation of silicon on conductive substrate in oxygen atmosphere[20,21] or thermal oxidation of silicon wafer in air or molecular oxygen. The amorphous thin -O-Si-O- layer derived from oxidation of crystalline silicon wafer has received a lot of attention in preparation of supported flat model catalysts due to the ease in which preparation procedures are carried out.[15] Deal and co-workers showed that the thickness of the -O-Si-O- layer can easily be varied by adjusting oxidation temperature and oxidation time.[22] It is important that

the -O-Si-O- layer is thin enough to allow the weak conductance of the underlying silicon when spectroscopic analysis tools are used.

2.2.2 Alumina (Al_2O_3) Supports for Model Catalysts

Al_2O_3, as mentioned above, is used extensively as a support in heterogeneous catalyst development. Preparation of a thin layer of alumina as a support for a model catalyst is complex and may result in surface defects that can heavily influence the metal-support interaction.[23] Surface defects can also effect variations in metal particle formation.[24] A good thin layer of Al_2O_3 is grown by thermal oxidation of aluminium alloys such as NiAl (110) or Ni_3Al (111), in the presence of molecular oxygen.[17] Alternatively, reactive evaporation of aluminium is used to prepare thin epitaxial alumina films on Ta(110),[25] Mo(110),[26,] Ru(0001)[27] or Re(0001).[28] Another method of preparing alumina is by passivation of aluminium by anodic oxidation. Anodic alumina films are mainly amorphous and porous but some order can be created by heating the amorphous layer to form γ-alumina.[19]

2.2.3 Titania (TiO_2) Supports for Model Catalysts

TiO_2 is used in model catalysts mostly in single crystalline forms of rutile and anatase especially in the study of the strong metal-support interactions (SMSI).[29,30] Titania thin layers are prepared by thermal oxidation of titanium foils, chemical vapour deposition on a conducting substrate and anodic oxidation of titanium. Model catalysts prepared by TiO_2 as a planar support material suffer from encapsulation of metal particles and loss of the CO chemisorption ability during reduction at high temperatures (about 500 ºC),[23,31] compared to support materials such as silica and alumina. [23,29]

2.2.4 Magnesium Oxide (MgO) Supports for Model Catalysts

MgO(100) cleaved from a bulk rock salt oxide is one of the well-known planar supports for model catalysts. The MgO(100) surfaces cleaved under UHV conditions are more preferable because their surface orientation have less defects compared to air-cleaved planes.[17] The epitaxial films of MgO can be prepared by evaporating MgO or Mg in oxygen atmosphere on conducting substrates. Unfortunately, the films of MgO on conducting substrates are not ideal model supports because MgO film forms mosaic type pattern on the underlying substrate.[32] Furthermore, the epitaxial MgO films often have wide bandgaps similar to bulk oxides.[18,32] These characteristics, especially the wide band-gap, limit the application of useful techniques such as STM, AES and XPS to their full potential in the analysis of model catalysts.

2.2.5 The Significance of Hydroxyl Groups on Model Supports

Inactivated hydrophobic oxide layer prepared by thermal oxidation is of minimal use in catalyst preparation by wet-chemical deposition methods because oxide supports such as silica are inert towards binding of the metal precursor in solution. Therefore, the surfaces of the oxide supports discussed above are activated by hydroxylation in water. Al_2O_3, SiO_2 and MgO are easily hydroxylated to corresponding surface hydroxyl groups.[33] TiO_2 is generally robust towards water hydroxylation.[34,35] A few reports on hydroxylation of TiO_2(110) are found in the literature and highlight the difficulty associated with TiO_2 hydroxylation.[36]

Alumina with surfaces which are terminated with oxygen layer is the easiest to hydroxylate to form up to 15 -OH groups per nm^2.[37,38] It is predicted that the hydroxylation of α-Al_2O_3(0001) proceed *via* the hydrolysis of Al-O-Al bonds to form surface $Al(OH)_3$.[39] Al_2O_3 is generally hydroxylated to form five different types of surface Al-OH groups as postulated by Peri[40] and later confirmed using several different techniques (Figure 2.3).[41,42,43]

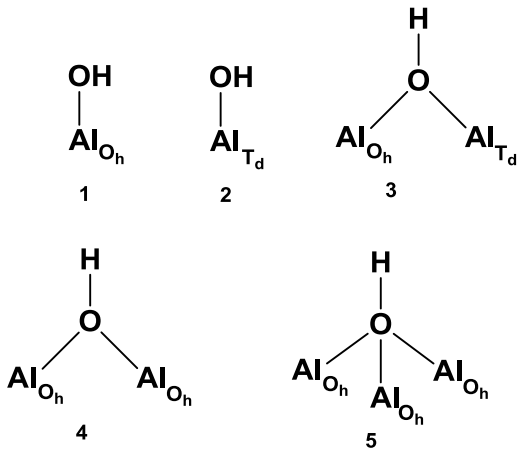

Figure 2.3. Different types of surface Al-OH groups as postulated by Peri.[40] O_h = octahedral, T_h = tetrahedral. The figure was adapted with permission from reference 41. Copyright (1986) by American Chemical Society

The density of surface hydrophilic silanol groups (Si-OH) on fully hydroxylated SiO_2 is about 4 - 5.5 OH per nm^2 which is *ca.* three times less than the surface Al-OH groups. The surface silanol groups are relatively stable at elevated temperatures which allow evaporation of excess water after hydroxylation. At temperatures above 500 °C, surface silanol groups dehydrate to form strained and stable siloxane bridges. The stable siloxane groups are very sluggish to re-hydroxylation.[44] Figure 2.4 depicts the temperature required to reverse silanol groups back to SiO_2.[17]

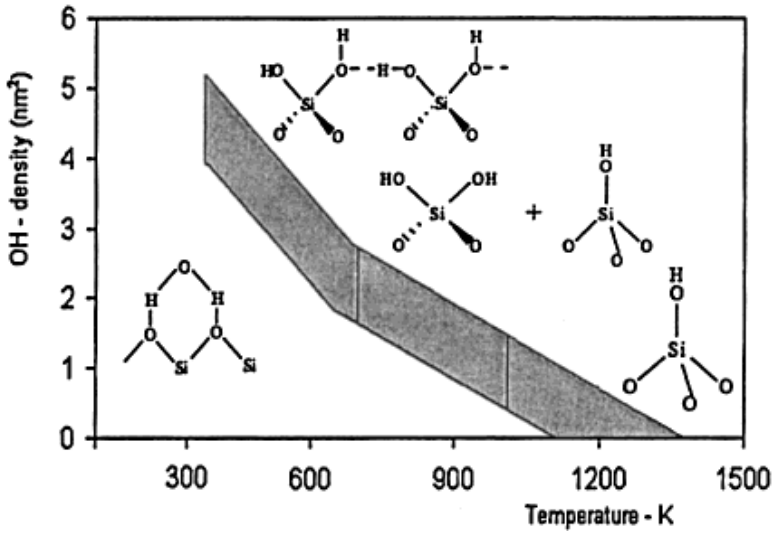

Figure 2.4. OH density on the surface of SiO_2 as a function of temperature. The figure was adapted with permission from reference 17. Copyright (1997) by Taylor and Francis.

In wet chemical impregnation of the metal species, the surface OH groups are used as anchors to immobilize metal clusters on the model support[45,46] or as wetting agents to enhance compatibility between the surface and the metal precursor loaded on the support.[17] In some cases, especially when spin coating, the 2-dimensional version of incipient wetness impregnation, is used to impregnate the model surface only weak interactions such as hydrogen bonding and electrostatic interactions develop between the metal centre and the OH group.[47,48] In chemical grafting, the metal centre interacts with OH to form a chemical bond with the O, as outline in Scheme 2.1.[45,47]

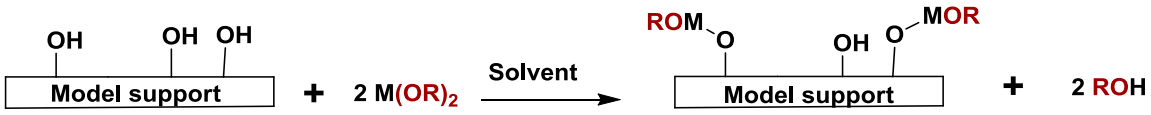

Scheme 2.1. Reaction of the OH groups on the surface of the model catalyst with the metal precursor.[45]

When a hydroxylated model support is used in vapour phase deposition of a metal precursor, the OH groups influence the adsorption and the distribution of metal particles on the surface. Baumer *et al.* showed using infrared absorption spectroscopy (IRAS) that the OH groups on the surface of planar alumina support are consumed during metal deposition and there is appreciable improvement of the density and particle distribution of Rh particles that are deposited by reactive evaporation of Rh metal (Figure 2.5).[49] Furthermore, the metal particles formed on hydroxylated model support are more stable to sintering deactivation.[33,49] The surface OH groups are consumed by the deposited metal leading to the formation of the oxidised metal and hydrogen ions.[33,43] It is still not clear whether the hydrogen ions from the OH group gets desorbed directly from the surface of the support or migrate to the metal cluster by reverse spill-over.[33]

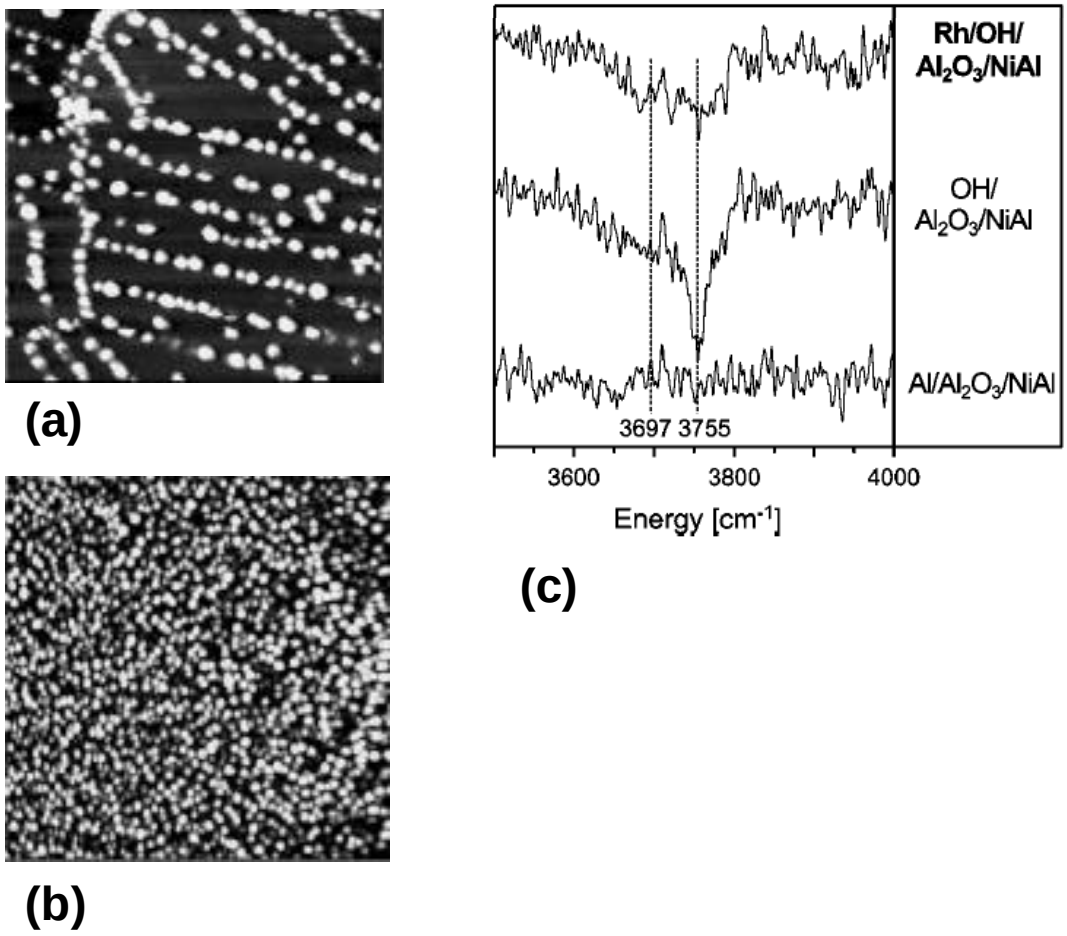

Figure 2.5. (a) and (b) Scanning tunnelling spectroscopy (STM) images of Rh particles on clean alumina and hydroxylated alumina respectively, and (c) infrared absorption spectroscopy (IRAS) data before and after Rh deposition on hydroxylated alumina. The figure was adapted with permission from reference 49. Copyright (2000) by Springer.

2.3 Metal Precursor Deposition Methods

The following discussion is about the literature on the wet chemical impregnation methods which were used to prepare catalysts in this study as prescribed in goal 1 and goal 3, chapter 1.

A number of methods used to deposit the metal precursor onto the surface of the support are known and discussed in the literature.[17] The most popular methods for metal deposition are *gas phase deposition methods* achieved by the evaporation of the metal source followed by deposition on the model support under ultrahigh vacuum conditions. The gas phase deposition methods include

metal vapour deposition, molecular vapour deposition and nanolithography.[7] Alternatively, there is *wet chemical deposition* of metal sources which is gaining considerable popularity in preparation of model catalysts due to their close similarity to preparatory methods of industrial catalysts.[15] Regardless of the method used to prepare the model catalysts, it is essential that the prototype developed is realistic *i.e.* it must be thermally stable under reaction conditions and that the amount of active sites per unit surface area is high enough for reactivity and characterization.[15,17] The following discussion focusses on wet chemical deposition methods which were used in this study.

2.3.1 Wet Chemical Impregnation of Metal Solutions on Model Support

The procedures that are often used to prepare catalysts on porous powder supports are ion exchange, grafting and incipient wetness impregnation. In the grafting approach, the metal species in solution react with -OH groups of the oxidic support to form chemical bonds.[46] The grafting of metal species in solution on the surface of -OH rich model oxide support mimics the process as outlined in Scheme 2.1.

Alkoxylation of -OH groups with a ligand has been shown to be the method of choice to immobilize ligands on the surface of silica support.[50] The complexes formed on the surface after reaction with the metal precursor can be used as immobilised homogeneous catalysts.[4,51] In Scheme 2.2, the preparation of immobilized homogeneous catalysts that can be used in hydrosilylation of olefins is outlined.[51,52] The ligands in the immobilised complexes can be decomposed by calcination followed by reduction to form catalytically active fine metal particles supported on the oxide layer.[53]

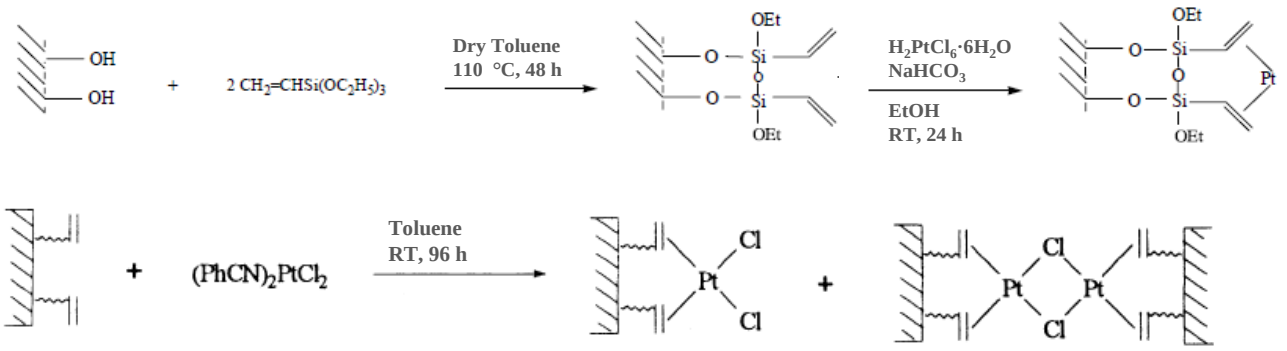

Scheme 2.2. The reaction of -OH groups on the surface of silica with silane followed by complexation with different Pt precursors. The figure was adapted with permission from reference 51. Copyright (2014) by Elsevier.

An equivalent of incipient wetness impregnation in flat model catalyst preparation is spin coating of the planar model support with metal solution. This method has received a lot of interest in the last decade in preparation of model catalysts on silicon wafers as shown by the reviews published by Niemantsverdriet and co-workers.[17,54] Spin coating utilises centrifugal and shear forces to form a very thin layer of metal solution on the surface of a flat model support spun in the spin coater. Eventually, the solvent evaporates from the surface of the support leaving behind metal species coating the substrate. Similarly to incipient wetness impregnation, drying of the spin coated surface followed by calcination result in metal particles distributed on the surface of the support.[55] The amount of the metal species deposited (m) can be quantified using formula 1 which has been used extensively in quantification of metal particles supported on SiO_2/Si-wafer.[54]

$$m = 1.35 \text{ x } C_o \sqrt{\frac{\eta}{\rho \omega^2 t_{evp}}} \quad (1)$$

Here, m is the number of moles of catalyst deposited onto the functionalised SiO_2/Si-wafer,
C_0 is the bulk concentration of the catalyst precursor in solution,
η is the viscosity of the solvent used to dissolve the metal precursor,
ρ is the density of the solvent used,
ω is the rotation speed (rotation per second – rps) and
t_{evp} is the evaporation time (in seconds).

2.4 Characterization and Analysis of Supported Model Catalyst

It is important to quantify the amount of active species in model catalyst. The amount of active species is used to determine the turnover numbers of the catalyst and ultimately the activity of the catalyst. It is also important to get a visual perspective of the supported metal particles since the morphology and particles size may play a role in catalytic activity, more so in structure-sensitive reactions. Other important properties of the supported model catalysts include electronic properties and metal-support interaction properties. This section looks at known characterisation techniques that can be used in studying the prepared catalysts (see goal 1, chapter 1).

2.4.1 Quantification of Supported Metal Particles

Determination of the amount of metal species deposited on the surface of model support is not straightforward and needs sensitive techniques since only a small amount of particles are deposited - in the order of nano moles per cm^2.

Rutherford Backscattering Spectroscopy (RBS) is one of the tools used to quantify the amount of metal species deposited on the surface of model support.[56] The major advantage of RBS is that it does not need a standard sample to quantify the analyte and it is non-destructive.[57] The basic principle of RBS is based on energy transfer during elastic collision of particles with at least one particle in motion.[58] During the RBS analysis a light monoenergetic ion beam (usually $^4He^+$) is shone on the analyte. This process facilitates the collision of the incident ion beam with the surface atoms and backscattering of the ion beam into the nuclear particle detector which gives an energy signal. The energy (E) of backscattered ions is proportional to the physical characteristics of the surface atoms and the number of backscattered ions (N) corresponds to the absolute amounts of surface elements in (atoms/cm^2). For instance, the energy signal detected after collision with a heavy atom will appear towards the high end of the energy scale in RBS spectrum as shown by E_B in Figure 2.6.[58,59] It is important to note that some of the incident ion beams penetrate the surface of the

analyte and collide with particles at depth (*t*) under the surface. The energy difference in ions backscattered from the surface and underneath the surface gives the depth profile of the element being analysed. For accurate data, it is important that the atomic mass of the deposited metal is higher than the support.

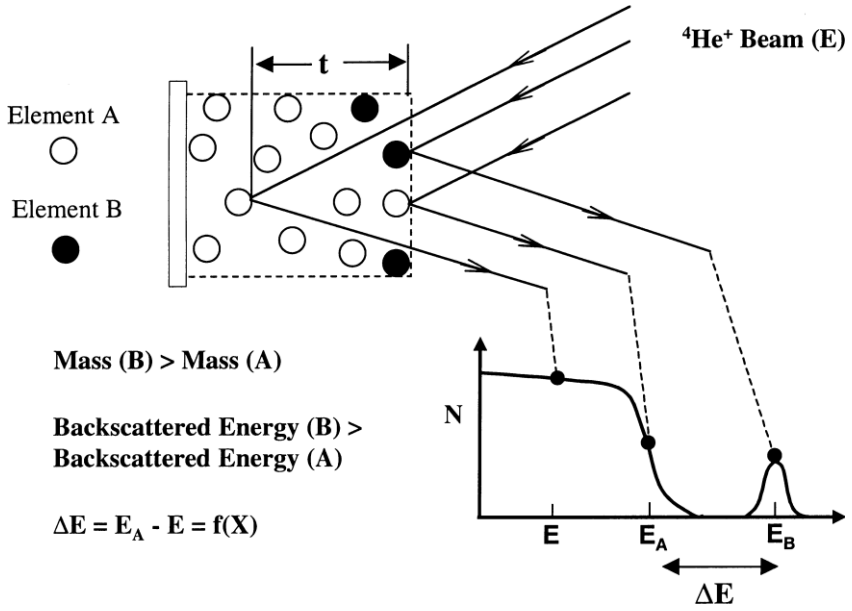

Figure 2.6. A simplified representation of the RBS analysis with typical resultant spectrum of two surface elements A and B. The figure was reprinted from reference 59 with permission from Elsevier (2000). The mass of element B is higher than the mass of element and energy E_B appears at the higher end of the energy spectrum. Element A is more abundant on the surface hence the number of backscattered ions (N) is higher for N_A than N_B as shown by the peak areas.

An XPS analysis can also be used to quantify the amount of metal species on the surface if suitable calibration is applied. Gothelid *et al.* used inductively coupled plasma mass spectroscopy (ICP-MS) data to calibrate the XPS Co peak intensity measurement which is directly proportional to the amount of cobalt on the same samples of model catalysts.[4]

When a model catalyst is prepared by metal vapour deposition, the evaporation rate and deposition time are used to predict the metal dose expressed as monolayer equivalent (MLE) on the surface of the support. The predicted MLEs are proportional to the XPS intensity[60] or the area under temperature programmed desorption (TPD) peaks.[61] This means that either XPS or TDP can be used

to determine the MLE when necessary calibration has been done. As discussed in section 2.3.1, the metal species in model catalysts prepared by spin coating can be predicted within 5-10% uncertainty using the formula in equation 1 and the associated parameters.[54]

2.4.2 Particle Size, Size Distribution and Morphology of Supported Metal

The microscopic techniques normally used to study the morphological properties of metal particles on a model support include atomic force microscopy (AFM), scanning tunnelling microscopy (STM), scanning electron microscopy (SEM) and transmission electron microscopy (TEM). AFM gives a very good indication of robust particle density per unit area and can be used effectively in comparative studies of the model catalyst preparation. One of the advantages of AFM is that it can be used to analyse metal particles in non-conducting model supports. It is essential to interpret the AFM data with caution especially where particle size is concerned. The metal particle size represented by the AFM image is usually bigger than the actual particle size.[62] This is due to the fact that the tip of the AFM probe is sometimes in few orders of magnitude bigger than the particle analysed.

The use of transmission electron microscopy (TEM) analysis in imaging metal particles on model support dates back as early as 1967.[63] Useful information such as the size and the distribution of metal particles can be accessed in TEM analysis. Limitations of TEM, including poor resolution of small particles (± 0.2 nm) and substrate dependent electron transmission, resulted in the development of more sophisticated variants of TEM *e.g.* aberration-corrected scanning TEM (STEM) and high resolution TEM (HRTEM).[64] To avoid the substrate dependency of TEM analysis, model supports with grids of transparent windows where metal particles can be deposited and analysed are used. These TEM grids are particularly useful in cases where Si wafers are used as model support.[17,65]

The scanning tunnelling microscopy (STM) "atomic imaging" is currently receiving increasing attention especially in the analysis of model catalysts prepared by metal vapour deposition on conducting substrates.[33,66] The STM images give more accurate data at atomic scale which can be used to determine the particle size and to study the influence of the support on particle sizes[67,30] The use of STM is limited to conducting substrates with a relatively low band-gap (< 3 eV).[18] Charging problems are alleviated with the use of thin layers of oxidic supports on conducting substrates.[68,69] One of the advancement of STM imaging is the use of *in situ* STM methodology to collect data in real time.[18] This approach is important in studying changes in size of metal particles during catalytic reaction[5], to probe encapsulation of metal particles due to strong metal support interaction (SMSI)[70] and to study the adsorption behaviour of volatile species on the surface of model catalysts.[71]

2.4.3 Electronic Structure and Metal-Support Interaction of Supported Metal Particles

XPS is by far the most used surface technique to study the electronic properties of supported metal particles especially the oxidation state of immobilized metal species on the surface of model support. The characteristic shift of the binding energy is useful in identifying the metal interaction with the support and is an indication of the changes in the oxidation state of the metal.[17,56,72] Extra caution needs to be taken when identifying the oxidation state of a particular metal using the observed binding energy from XPS analysis. Different compound types of the same metal and sharing the same oxidation state may exhibit a range of different binding energies depending on the electronic characteristics of the ligands attached to the metal centre. To exemplify this phenomenon, the normal binding energy of Pt^{2+} compounds such as $Pt(OH)_2$ ranges between 72.2 eV to 73.0 eV as summarised in Table 2.1.[73,74] At the same time, the binding energy of $PtCl_2$ and Pt(II) oxides exhibit an abnormally high binding energy of up to 74.0 eV.[74,75]

Table 2.1. A compilation of Pt $4f_{7/2}$ binding energies of different Pt compounds. The grey scales show the range of binding energies that has been reported in the literature for each Pt compound. The table was adapted with permission from reference 74.[i]

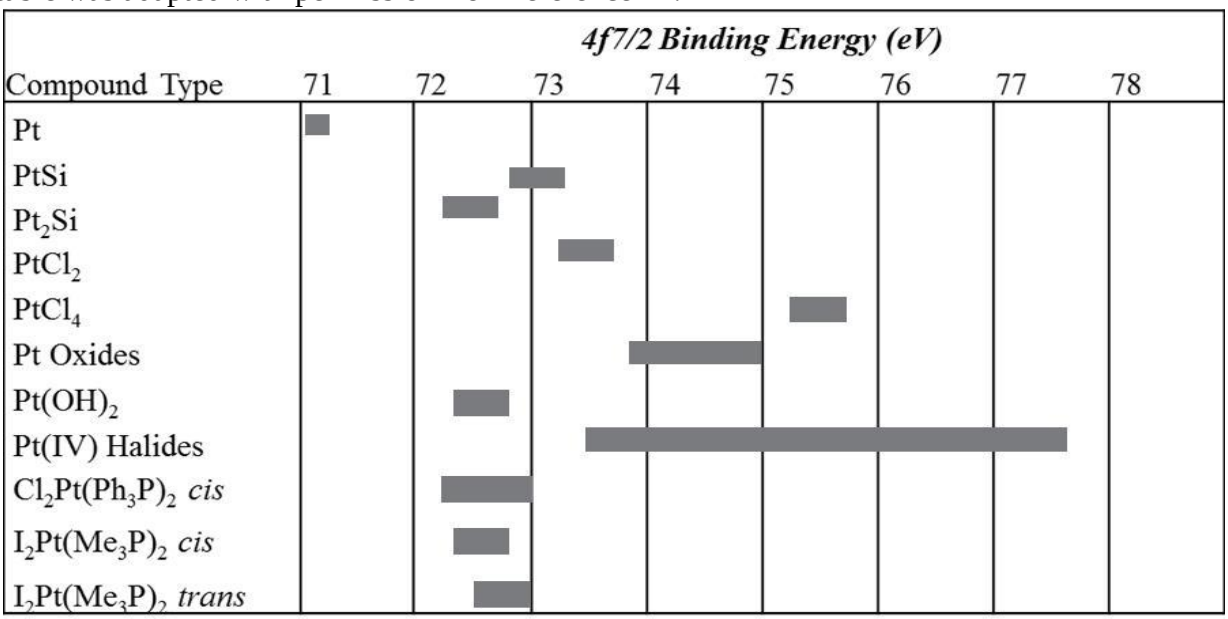

Besides the ligands outlined in Table 2.1, the interaction of the metal with the solid support also influence the shift in metal binding energy. A remarkable example where XPS was used to study the interaction of the metal with the support was the immobilisation of aqueous chromate on functionalised Si wafer.[56] In this study, the shift in binding energy of Cr $2p_{3/2}$ was used to explain the binding mode of immobilised Cr after the esterification of the silanol groups on the surface of the epitaxial silica with aqueous chromate. The results showed the Cr^{6+} oxidation state and the unusually high binding energy at 581.4 eV for Cr $2p_{3/2}$ (see Figure 2.7). The high binding energy revealed a unique Cr-silica interaction which is formed when chromate is anchored on the surface of model support.[56,76] The volatile Cr_2O_3 clusters are represented by the peak at 577.7 eV and they disappear as the calcination time continues as shown by the XPS peaks in Figure 2.7.

[i] The permission to use Table 2.1 was given by Perkin-Elmer Corp., the *X-Ray Photoelectroscopy* manufacturer, *via*. email communication.

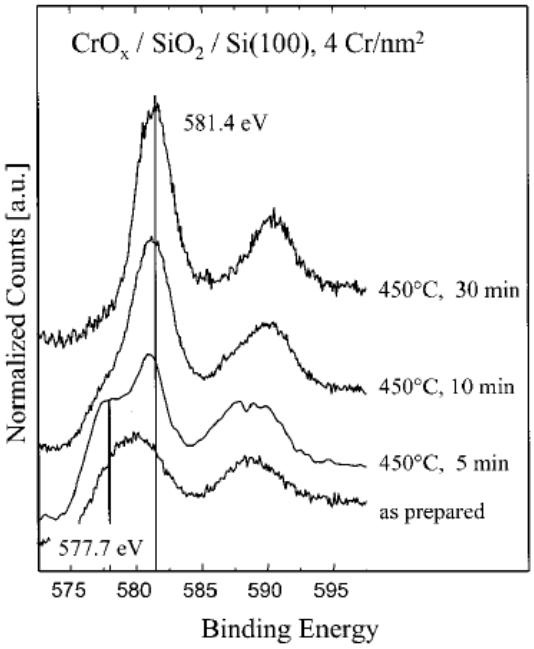

Figure 2.7. The XPS traces obtained after spin coating chromate solution on SiO_2/Si Wafer followed by calcination at 450 °C. The figure was adapted with permission from reference 56. Copyright (2001) by American Chemical Society.

The shift of binding energy does not only show the variations of oxidation states of the supported metal specie, but the binding energy may increase when the amount of metal deposited decreases.[77] Therefore, caution should be taken not to confuse the size-dependent binding energy shift with the shift due to the change of oxidation state.[78] Other techniques used to study electronic properties of metal particles on model support are Auger electron spectroscopy (AES) and to a certain extent, ultraviolet photoelectron spectroscopy (UPS)[78,79,80] and infrared (IR) spectroscopy in particular infrared absorption spectroscopy.[49]

2.4.4 Gas Chemisorption

Chemisorption of light gases on metal surfaces is sometimes used to study the reactivity of the supported metal particles or to determine the proportion of available metal particles on the support and the metal particle distribution. The common adsorbates used in chemisorption are CO, H_2, NO, O_2 and to a lesser extent formic acid and CO_2. The adsorption and desorption of these gases are

normally studied using thermal desorption spectroscopy. Through thermal desorption spectroscopy, the amount of adsorbed gas can be correlated to the concentration of metal particles and in conjunction with other surface analysis tools like ion scattering spectroscopy (ISS), the crystal orientation of the metal particles on the model support can be determined.[81]

The surface planes on supported metal particles can also be predicted using infrared absorption spectroscopy (IRAS) as illustrated by Goodman and co-workers using a mixture of CO and NO gases adsorbed on Pd particles on flat model support.[82] In this example, it was shown that CO and NO are sensitive to the facets of the Pd particles and the IR bands from these adsorbates are used to predict the distribution of the (100) and (111) facets. A detailed review on the use of IRAS to study gas chemisorption on flat model Pd catalysts was recently reported by Wilson and Brown.[83] Other techniques that can be used to study chemisorption of gas on model support include electron probe microanalysis (EPMA)[84], electron energy loss spectroscopy (EELS),[85,86] sum frequency generation (SFG)[87] and photoelectron diffraction (PED).[88] The major advantage of IRAS over these techniques is the high spectral resolution which gives an opportunity to identify closely related adsorbates [83] and can explain the type of interaction taking place between the metal and the support.[69]

2.5 Applications of Flat Model Catalysts in Catalysis

The literature covered in this section presents reported studies on the catalytic application of flat 2-D model catalysts to give a background to goal 2 of this study as described in chapter 1.

The catalytic applications of supported flat model catalysts in chemical transformations are done mostly in high pressure cells using gas phase reactions as probe experiments.[89] Simplified reactor designs have also been used for gas phase reactions under atmospheric pressure as shown in hydrogenation[90] and hydrodesulphurization reactions in continuous flow and batch mode.[91] Other gas phase reactions include aligned polymeric growth of carbon nanotubes (CNT) on the surface of the flat model catalyst.[92,93]

The application of model catalysts has gradually been extended to more complex industrial type reactions like Philips polymerization reactions,[56,94] Fischer-Tropsch synthesis[21] and reforming of *n*-alkanes to aromatics.[95] Lundwall *et al.*[95] demonstrated using a batch reactor system that reforming of n-heptane is dependent on particle size of Pt supported on model SiO_2 support where the optimum selectivity to toluene is obtained with a Pt particle size of *ca.* 1.5 nm (see Figure 2.8). Thermal desorption spectroscopy shows that the majority of the Pt particles with average particle size of 1.5 nm have C_6 surface sites.[96] This confirms that dehydrocyclization reactions are structure-sensitive.[97]

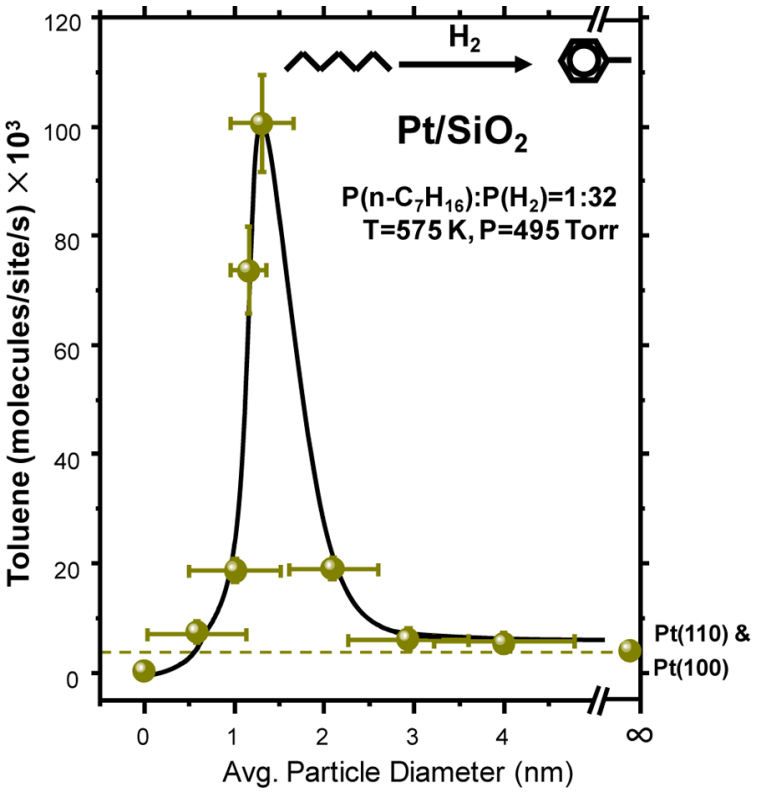

Figure 2.8. Dehydrocyclilization of n-heptane to toluene as a function of the particles size of Pt on SiO_2. Included is also data obtained from unsupported Pt(110) and Pt(100). The figure was adapted with permission from reference 95. Copyright (2012) by American Chemical Society.

In recent reports, supported flat model catalysts have been used in liquid phase catalytic oxidation of hydroquinone at ambient conditions.[4] Most recently, our research group reported the use of flat model catalysts in the solvent-free oxidation of molten 1-octadecanol in ambient air and low to moderate temperatures.[72]

The catalytic reactions described above outline the versatility of flat model catalysts in catalysis. However, the application of flat model catalysts has intrinsic limitations. The total surface area of the metal cluster (active species) of supported flat model catalyst is very small compared to the total surface area of metal clusters supported on conventional porous (large surface) support.[17] Since the available metal surface area is small in model catalysts, catalytic reactions are done at a very small scale and it can be difficult to detect and obtain a descent amount of products to be analysed. It is also relatively easy to poison the already small surface area of active species in flat model catalysts compared to conventionally supported catalysts.[21] It is important to handle the flat model catalysts with care to prevent contamination.

2.6 Hydrogenation of α,β-Unsaturated Aldehydes

This section is intended to give a brief overview on catalytic hydrogenation of cinnamaldehyde which is used as a model substrate to test the activity of flat 2-D model Pt catalysts prepared in this study (see goal 2, chapter 1). Catalytic hydrogenation plays an important role to add value in diverse industrial processes.[154] One important hydrogenation reaction is the chemoselective transformation of α,β-unsaturated aldehydes to corresponding unsaturated alcohols.[90,98] This reaction poses a fundamental challenge because the reduction of alkene group is thermodynamically favoured over carbonyl group.[99] When an aromatic analogue of benzaldehyde, cinnamaldehyde, is used as a model substrate, hydrogenation leads to a mixture of hydrocinnamaldehyde, cinnamyl alcohol and 3-phenyl-1-propanol (see Scheme 2.3).[100] Selective hydrogenation of cinnamaldehyde to either hydrocinnamaldehyde or cinnamyl alcohol is more challenging because the aldehyde function is as

reactive as it were in benzyldehyde. [101] Under unpromoted conditions, the catalytic hydrogenation of carbonyl group competes directly with alkene function to produce hydrocinnamaldehyde and cinnamyl alcohol.[101,102] It is desirable to selectively produce either hydrocinnamaldehyde or cinnamyl alcohol because these cinnamaldehyde derivatives are useful in fine chemicals and pharmaceuticals.

In heterogeneous catalysis, the commonly used unpromoted noble metals exhibit the following trend in selective hydrogenation of cinnamaldehyde to cinnamyl alcohol: Pd < Rh < Ru < Pt < Ir.[103] The selectivity of Pt catalysts can be improved by tuning the particles sizes to be > 3 nm.[104] Theoretical studies suggest that various adsorption states of α,β-unsaturated aldehydes on metal influence whether a saturated aldehyde or an unsaturated alcohol is formed.[105,106] Adsorption through C=O group is favoured in electron rich Pt particles and enhances the formation of unsaturated alcohol. However, on the acidic support such as β-zeolites, the Pt particles are electron deficient and only hydrocinnamaldehyde and acetals are formed in hydrogenation of cinnamaldehyde.[104] Bhogeswararao and Srinivas[107] revealed that addition of a base in the reaction medium increases the selectivity of cinnamyl alcohol from *ca.* 10% to 70% when Pt catalyst on acidic support is used.

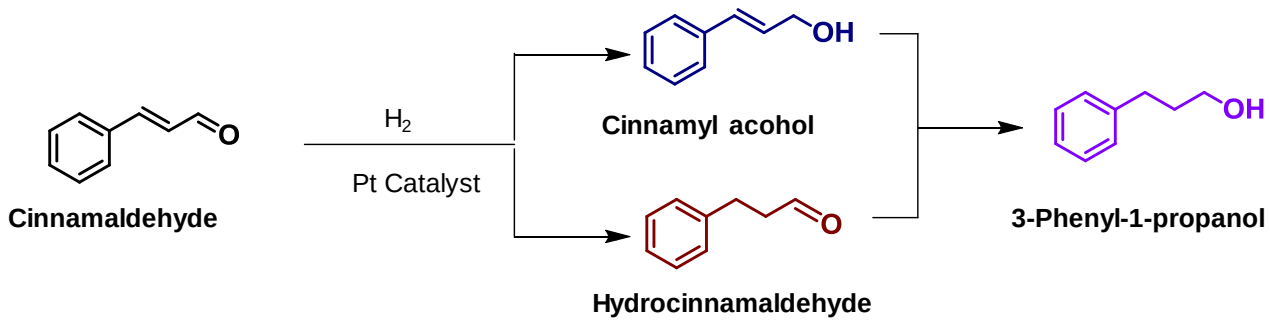

Scheme 2.3. An outline of the hydrogenation of cinnamaldehyde to various hydrogenation products

2.7 Supported Platinum in Catalysis

In this section and the following subsections, the focus shifts to the supported platinum catalysts on 3-D porous supports and their applications in hydrocarbon transformations, particular reforming of *n*-paraffins to aromatics (goals 3 and 4, chapter 1). Also discussed in this section is the literature on oxidative dehydrogenation of alcohols to corresponding carbonyls (goal 7, chapter 1).

The use of Pt in catalysed chemical reactions dates back to as early as the 1820s even before the term "catalysis" was coined in 1835.[108] Initially, attention was given to oxidation reactions which were inspired by the discovery of the famous pneumatic gas lighter by Dobereiner in 1822.[108,109] Over the past six to eight decades since the boom in petroleum and automobile industries, Pt based catalysts have been applied in a wide range of chemical reactions.[109,110]

A useful feature of Pt in catalysis is the effortless addition or removal of electrons to form an element with one of the three different dominant oxidation states *i.e.* Pt^0, Pt^{2+} and Pt^{4+}.[(109)] This feature makes it possible for Pt to adopt different oxidation states during catalytic life cycle. Similar to other noble metals, the bulk Pt has no or little catalytic activity. The catalytic activity of Pt catalysts is realised when the Pt metal is finely divided into nano-size particles.[108,111] Some reactions such as dehydrocyclisation have shown a clear dependence on the variation of Pt particle size and to a certain extent, even the shape of the metal particle.[112] To prevent agglomeration of metal particles in reaction, the metal particles are supported on high surface porous support such as silica, alumina or zeolites. The support also allows the introduction of a second metal or a promoter to improve the properties of the Pt catalyst.[113]

Large scale catalytic applications in chemical or petroleum industry mainly employ supported catalysts because they can be easily separated from the product mixture and are robust in harsh reaction conditions. Notable reactions that are catalysed by supported Pt catalysts are hydrogenation reactions,[114,115] dehydrogenation reactions (including oxidation of alcohols and dehydrocyclisation

reactions),[111,116,117] isomerisation of hydrocarbons [113,118] and hydrocracking reactions.[113,119] These reactions have resulted in well-known industrial processes such as the Universal Oil Products (UOP) Platforming™ and the Butamer™ Processes in oil refining industries and redox reaction by auto-catalyst in automobile industries.[120,121]

The catalytic reactions outlined in the previous paragraph emphasise the importance and versatility of Pt catalysts in different reactions. It is also important to note the challenges facing research in Pt catalysis. To name a few:

(1) The diverse chemical reactions that can be catalysed by Pt catalysts are a big disadvantage when it comes to product selectivity. Several transformations which take place per catalytic reaction result in a cocktail of products which are costly to remove from the product stream.[112]

(2) Supported Pt catalysts are susceptible to deactivation by poisoning, thermal deactivation and leaching.[112,113,122]

The availability of spectroscopic techniques and cost effective modelling techniques makes it possible for scientists and engineers to gain a better understanding of supported catalysts and thus improves the application of these catalysts.[123] The applicability of supported Pt catalysts in industrial chemical reactions has also improved in many aspects.[124] Given the numerous examples of Pt catalysed reactions found in the literature, it is impossible to review all the industrial chemical reactions which are catalysed by supported Pt catalysts. This study's main focus is concerned with dehydrogenation reactions catalysed by supported Pt catalysts. In dehydrogenation reactions, attention is given to the reforming of paraffinic hydrocarbons leading to aromatics and the oxidative dehydrogenation of alcohols to form respective carbonyls.

2.8 Reforming of Paraffins over Supported Pt Catalysts

Refining of vehicle fuel to make it suitable for the car engine requires a variety of catalytic processes. One of the catalytic processes used to upgrade the liquid feedstock to the fuel pool is

reforming which utilises platinum based catalysts. Dehydrogenation of saturated hydrocarbons to olefins and ultimately dehydrocyclisation to aromatics forms an integral part of catalytic reforming of low-value chemicals in petroleum industry. In reforming, the gasoline-range molecules or naphtha with low-octane numbers are re-arranged or reformed without changing the number of carbons to molecules with high-octane number. High-octane molecules regulate the burning of the fuel in the car engine chamber better than low-octane molecules. Low-octane molecules in fuel can cause an unregulated explosion or a knock that can damage the car engine.[113]

The low-octane naphtha contains C_{6+} straight chain paraffins that can be reformed through non-degradative dehydrogenation, cyclisation and isomerisation to form naphthenes, aromatics and branched-chain paraffins which have high octane numbers. It is important to note that degradative hydrogenolysis to C_1-C_4 gases and C_5 products also take places during the reforming process. The relative research octane numbers (RON) for paraffins, naphthenes and aromatics are listed in Table 2.2. The RONs of aromatics are clearly higher than the RONs of C_{6+} *n*-alkanes (*i.e. n*-alkanes with a minimum of six carbons).[113]

Aromatics, especially benzene, toluene and xylene (BTX), are formed mainly *via* dehydrocyclisation and dehydration reactions. Aromatics are still being used by refineries to boost fuel octane. At the same time, tight regulations to limit the use of aromatics, especially benzene, in fuel are imposed due to health and environmental concerns. Fortunately, the use of aromatics from catalytic reforming is not only limited to boosting gasoline octane, but can also be alkylated to useful petrochemicals such as linear alkylbenzene (LAB)[125,126] and cumene.[126,127,128]

Table 2.2. The relative research octane numbers (RON) for paraffins, naphthenes and aromatics.[113]

Hydrocarbon	Blending research octane number (RON)
Paraffins	
n-Butane	113
n-Pentane	62
n-Hexane	19
n-Heptane	0
n-Octane	-19
2-Methylhexane	41
2,2-Dimethylpentane	89
2,2,3-Trimethylbutane	113
Naphthenes (cycloparaffins)	
Methylcyclopentane	107
1,1-Dimethylcyclopentane	96
Cyclohexane	110
Methylcyclohexane	104
Ethylcyclohexane	43
Aromatics:	
Benzene	99
Toluene	124
1,3-Dimethylbenzene	145
Isopropylbenzene	132
1,3,5-Trimethylbenzene	171

The classical reforming processes are based on bi-functional Pt catalysts on acidic supports such as chlorinated Al_2O_3, SiO_2-Al_2O_3 and H-form zeolites. The metal centre and the acidic support have a synergistic effect on catalytic reforming of straight chain alkanes.[113] A notable commercial process which uses Pt catalyst on chlorinated Al_2O_3 is the Universal Oil Products Platforming™ process.[120,129] The disadvantage of bi-functional Pt catalysts in reforming of alkanes is poor selectivity to aromatics[130,131] due to competing reactions such as skeletal isomerisation,[113] hydrocracking[131,132] and the formation of coke (carbonaceous residue). [113] These side reactions are predominant on the acid site of the support.[122] Moreover, the chlorinated Pt/Al_2O_3 catalysts are also susceptible to leaching away of chloride ions to form corrosive waste in the presence of water.[154,182] The interest of this study is mono-functional catalysts thus the discussion that follows focuses on

non-acidic Pt catalysts on mono-functional supports as alternative cleaner catalysts for aromatisation of *n*-alkanes.

2.8.1 Reforming on Mono-functional Pt Catalysts

In mono-functional Pt catalysts, the metal is supported on non-acidic support to suppress acid catalysed reactions and allow only metal catalysed reactions to dominate the reforming process. The pathways followed by the metal catalysed reactions are influenced, to a large extent, by the surface crystallite configuration and the number of Pt atoms ensemble in active sites.[133,134] Essential mechanistic pathways involved in a typical reforming reaction on mono-functional Pt catalyst can be illustrated by the aromatisation of *n*-hexane in Scheme 2.4**.**[135] The sequence of catalytic steps is initiated by the adsorption of *n*-hexane on Pt active sites followed by either consecutive dehydrogenation to form alkenes [113,136,137] or 1,5-ring closure to the methylcyclopentanyl specie.[138]

The aromatisation of adsorbed hexenyl species is the main reaction taking place on three-atom Pt site in hexagonal symetry.[134,139] This reaction is preceded by 1,6-ring closure of adsorbed *cis*-*cis*-hexadienes or *cis*-*cis*-hexatrienes to adsorbed form cyclohexadiene. As outlined in Scheme 2.4, the final aromatic product is formed by the dehydrogenation and desorption of the cyclohexadiene. Beside the aromatic products, the adsorbed *cis*-dienes can reversibly isomerise on the surface of the metal to *trans*-isomers which can polymerise further to coke or otherwise desorb from the surface as hexenes. Isomerisation of *cis*-dienes to *trans*-isomers is prevented by optimum surface hydrogen.[136]

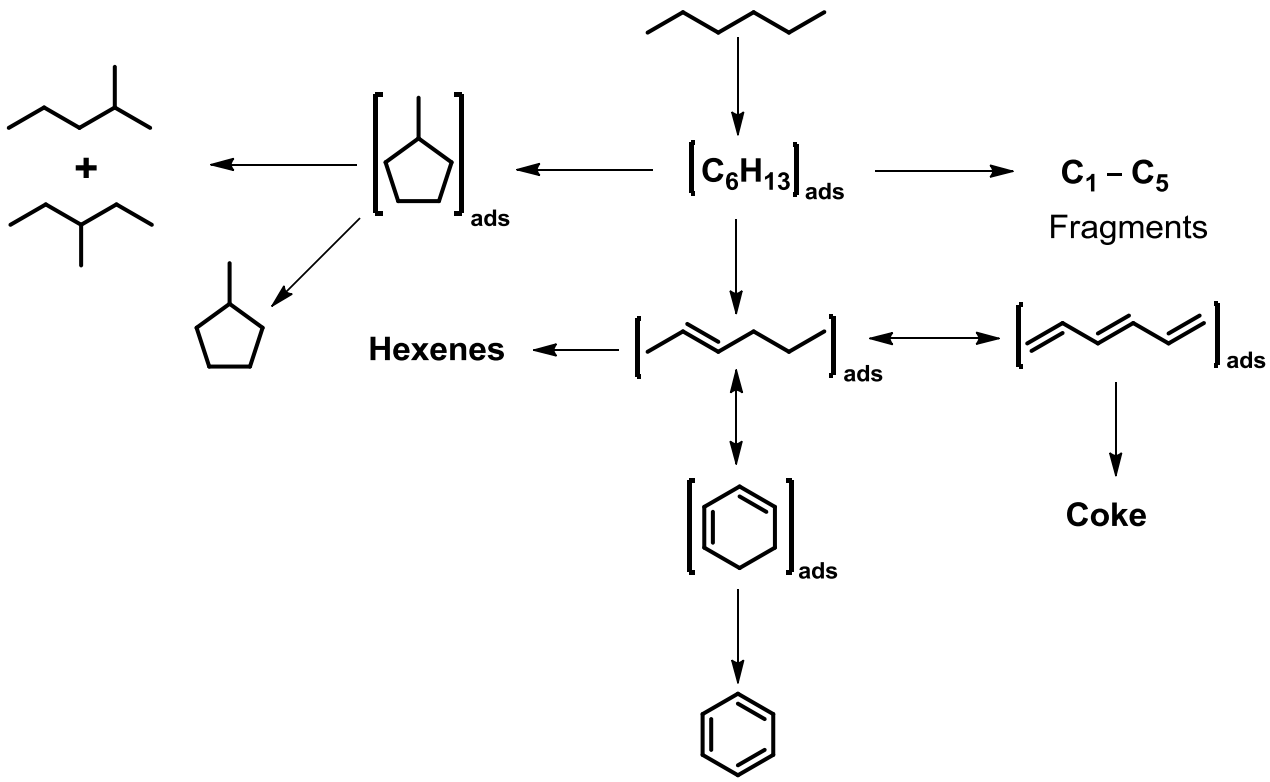

Scheme 2.4. The aromatisation of *n*-hexane on non-acidic Pt catalyst leading to benzene as the major product. Ads: adsorbed species. The scheme was adapted from reference 135 with permission of Elsevier (2006).

The minor products of reforming on mono-functional Pt catalysts are methylcyclopentane (MCP) and C_6 branch isomers which are formed by adsorbed methylcyclopentanyl specie on two-atom Pt site.[140,141] Even though C_6 branch isomers are formed in mono-functional Pt catalysts, they are minor products because they are mainly associated with acidic bi-functional Pt catalysts.[122] In addition to C_6-isomers, fragmentation to C_1-C_5 molecules takes place on the surface of the Pt active site. The fragmentation of the adsorbed species is favoured by the bigger Pt particles which are made of large ensemble of Pt atoms.[134,142]

2.8.2 Pt/KL-zeolite-Zeolite in Reforming of *n*-Alkanes

Zeolite-supported Pt catalysts, especially Pt on L-zeolite, are becoming popular catalysts for the study of reforming catalysis due to the unusually high yield and selectivity to benzene in the

catalytic aromatization of *n*-hexane.[122] The commercial reforming processes where Pt/KL-zeolite catalysts are used were published much later than the processes based on bi-functional catalysts. Notable commercial reforming processes that employ Pt/KL-zeolite catalysts include AROMAX™ by Chevron Phillips Chemical Company[143] and RZ-Platforming by Universal Oil Products.[144]

The acidity of the L-zeolite support is neutralised by ion-exchange with alkali Na^+ or K^+ cation. This approach works very well in minimising side reactions which are favoured by acidic catalyst such as isomerisation. Pt on K-exchanged L-zeolite has a remarkable selectivity towards *n*-hexane aromatisation compared to the other zeolite supported Pt catalysts. Bernard[145] demonstrated that under the same Pt loading (0.6 wt%) and same experimental conditions, Pt/KL-zeolite catalysts give better benzene selectivity than Pt catalysts on X-, Y- and Ω-zeolites (Table 2.3). It was further proposed that the basicity from exchanged alkali cations have a significant influence on the unusually high selectivity towards benzene.[145] Further theories to rationalise the high selectivity of Pt/KL-zeolite towards *n*-hexane aromatisation have been postulated. These theories are based on electronic properties of the Pt particles, geometric properties of the support and the effect of the particle size of the Pt crystallites, which will be discussed further in the following subsections.

Table 2.3. Product distribution (wt%) of the aromatization of *n*-hexane over various non-acidic zeolite-supported Pt catalysts and acidic $Pt/Cl/Al_2O_3$.

Catalyst	Conversion (wt%)	Yield (wt%)				Benzene selectivity
		C_1 - C_5	*i*-C_6 [a]	MCP [b]	Benzene	
Pt/KL-zeolite	59	2.9	3.5	5.3	47.2	80
Pt/NaX-zeolite	83	8.3	12.4	7.4	54.8	66
Pt/NaY-zeolite	41	2	5.3	9.8	23.7	58
Pt/NaΩ-zeolite	31	0.5	0.4	15	15.1	49
Pt/Na mordenite	17	0.8	4	11.2	0.9	5.5
$Pt/Cl/Al_2O_3$	48	4.8	9.1	10.5	23.5	49

a: iso-hexanes
b: Methylcyclopentane

2.8.2.1 Influence of Electronic Properties in High Aromatisation Activity

Electronic theories suggest that the metal-support interaction of Pt with alkaline exchanged L-zeolite support increases the electron density of the supported Pt particles.[146] The polarisation of metal particles is induced by the nearby cations in the support.[147] The electron-rich character of Pt particles can then be identified by the CO adsorption which will shift the IR stretch to lower wave-numbers (*ca.* 2060 to 2070 cm^{-1}).[146] This character is exemplified by the IR spectra in Figure 2.9 shows the IR stretch at 2075 cm^{-1} for CO adsorption on large Pt particles outside the L-zeolite channels. In comparison, the IR stretch at about 2060 to 2070 cm^{-1} identifies the CO adsorption on small Pt particles (1 to 2.5 nm average diameter) trapped inside the L-zeolite channels. The small Pt particles inside the channels are electron rich and are affected by the character of the cations on the support, hence the IR stretch for the adsorbed CO shifts to lower wave numbers.[146,148] The last CO stretch in Figure 2.9 appears at 2000 cm^{-1} and identifies very small Pt particles embedded inside the zeolite framework. These Pt particles are not accessible to participate in aromatisation reaction.[146]

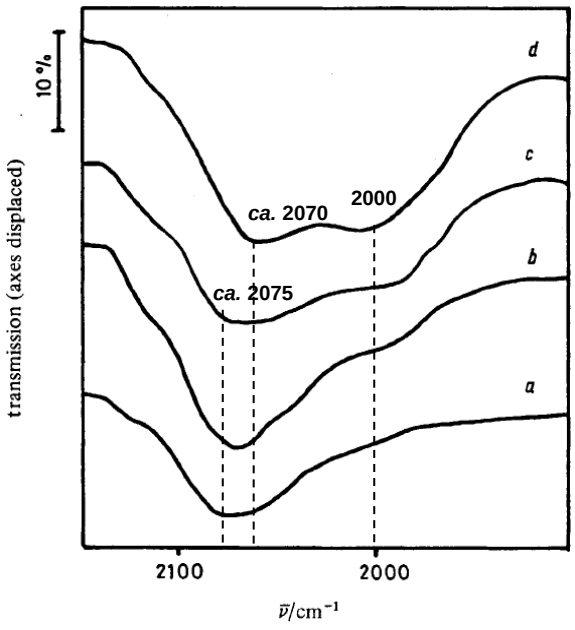

Figure 2.9. The IR data of CO adsorption on Pt/KL-zeolite sample. IR traces *a*, *b* and *c* were obtained after adsorption of CO at 0.013 bar for the duration of 5 min, 20 min and 48 h respectively. IR trace *d* was obtained after adsorption of CO at 0.08 bar for after 5 min. The figure was adapted from reference 146 with permission of The Royal Society of Chemistry (1969).

The electron rich Pt particles inside the L-zeolite channels and the alkaline support favour aromatisation of *n*-alkanes over side reactions such as hydrocracking. In fact, the influence of alkalinity on aromatisation reactions is evident even when Pt is supported on alkaline Mg(Al)O or SiO_2 which has less defined porous structures.[149,150] The aromatisation selectivity of Pt/SiO_2 doubles from 10 wt% to 19.8 wt% when alkalinity is introduced by co-impregnation of K^+ cation on the support (Table 2.4). What can also be noted is the suppression of hydrogenolysis reaction leading to C_1-C_5 products (from 16.2 to 4.1 wt%) in $Pt\text{-}K/SiO_2$ catalyst.[150]

Table 2.4. Aromatisation of *n*-hexane over Pt/SiO_2 and $Pt\text{-}K/SiO_2$ catalysts[150]

			Selectivity (wt%)			
Catalyst	Conv. (wt%)[a]	Bz yield (wt%)[b]	C_1-C_5[c]	*i*-C_5[d]	MCP[e]	Bz[b]
Pt/KL-zeolite	59.2	36.2	4.5	27	7.4	61.1
Pt/SiO_2	14	1.4	16.2	48.1	24.8	10.2
$Pt\text{-}K/SiO_2$	18.4	3.6	4.1	50	26.1	19.8

a: conversion, b: benzene, c: Hydrocabons with C_1 to C_5 carbon chain, d: isopentane, e: methylcyclopentane.

The preference of aromatisation reaction declines when acidity is introduced to the zeolite support.[151] In the presence of acid sites, hydrocracking to C_1-C_5 products and isomerisation reactions take over.[151,152] The catalytic activity of Pt/KL-zeolite is improved by the introduction of alkali earth Ba^{2+} ions which completely neutralise the residual acid sites to form Pt/BaKL catalysts.[132,153] Zheng and co-workers[132] demonstrated that the *n*-hexane conversion and aromatisation selectivity of Pt/KL-zeolite catalyst increases from 62 to 94 % and 82 to 96 % respectively when Ba^+ ion is co-impregnated in Pt/KL-zeolite.

2.8.2.2 Influence of Geometric Properties of L-zeolite in High Aromatisation Activity

Geometric theories state that the size and shape of the Pt/KL-zeolite channel network favour high aromatisation selectivity of C_{6+} *n*-alkanes by facilitating a head-on interaction with the Pt particles and by reducing the unintended reactions. The head-on attachment of *n*-alkane on the Pt

surface is the pre-requisite of 1,6-ring closure in aromatisation using mono-functional Pt catalyst (Figure 2.10).[154]

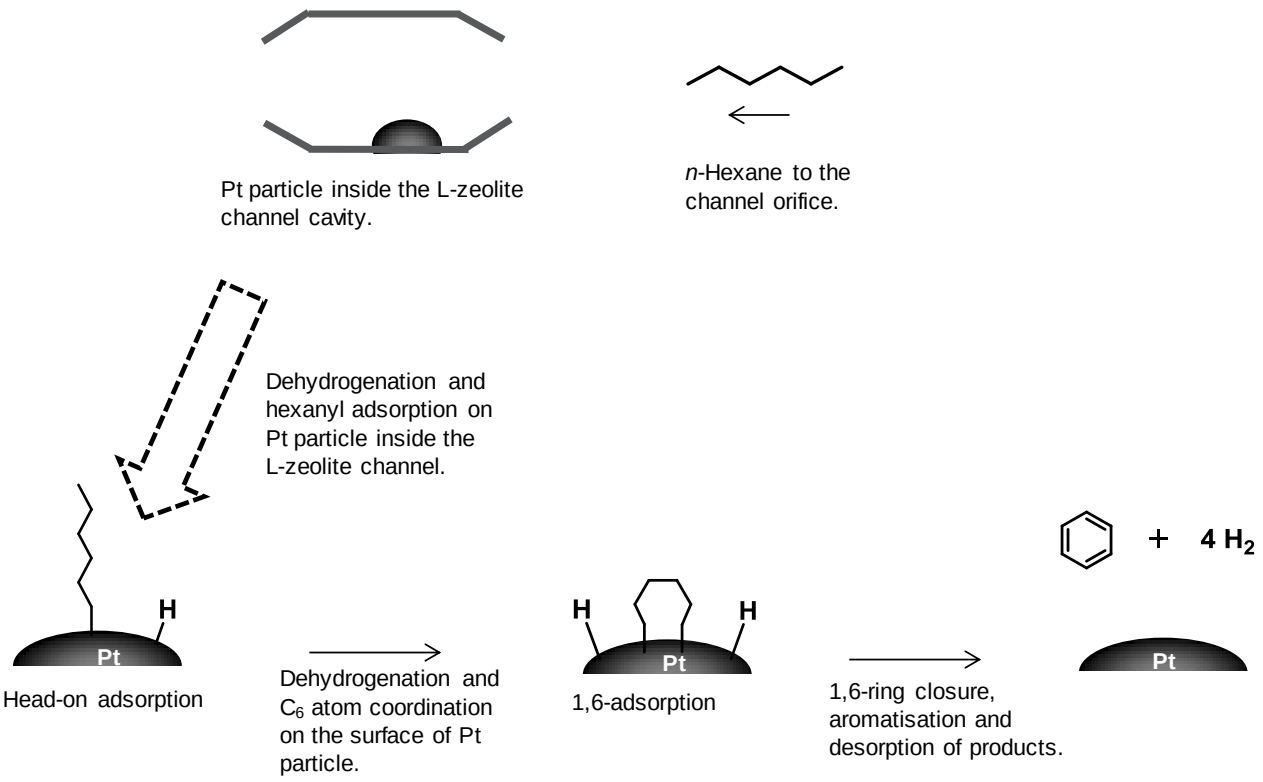

Figure 2.10. Schematic model of head-adsorption and 1,6-adsorption of *n*-hexane on Pt surface leading to 1,6-ring closure.[154]

The channel orifices (*ca.* 0.73 nm diameter) and interlinked channel cavities (*ca.* 1.3 nm diameter) determine the orientation of the *n*-alkane before adsorbing on the metal particle and stabilise the aromatisation intermediate products.[155] Metal particles are trapped inside the channel cavities, inside the L-zeolite channels, to form interlinked yet isolated catalytically active sites within the channels. The dimensions for channel orifices and channel cavities are illustrated by the L-zeolite model in Figure 2.11.[156]

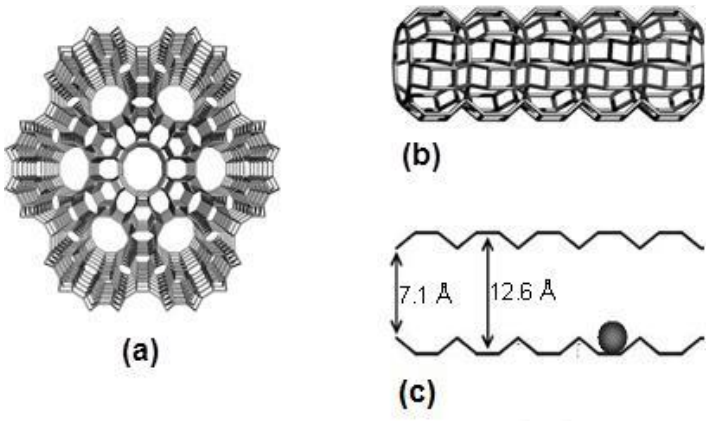

Figure 2.11. Model of L-zeolite showing (a) a cross section of unidimensional channels (b) a side-view of the main channel and (c) the dimensions of channel orifice and channel cavity. The figure was adapted from reference 156 with kind permission from Springer Science and Business Media (2004).

According to the "molecular die" theory, the high *n*-hexane aromatisation of Pt/KL-zeolite is ascribed to the orientation effect of the channel orifices.[155] The orifice to the L-zeolite channel network allows *n*-alkane molecules with longer chain length (*ca.* 0.7 nm long) to enter the channels lengthwise one molecule at a time.[157] This orientation of *n*-alkane especially *n*-hexane, as it enters the channel, will facilitate terminal adsorption on the surface of Pt clusters that are trapped in the channel passage (Figure 2.10).[155] The terminal (C_1) atom adsorption is sequentially followed by C_6 atom coordination on the surface of Pt cluster, the 1,6-ring closure and ultimately aromatisation. Azzam *et al.*[157] suggested that the controlled diffusion of *n*-hexane, one molecule at a time, into the channel cavity ensures that dehydrocyclisation takes place and eliminates secondary reactions that lead to side products and catalyst deactivation. The "molecular die" concept was also used to explain the high benzene selectivity observed in aromatisation of *n*-hexane catalysed by Pt on dealuminated faujasite.[151] The orifices (0.71 – 0.74 nm diameter) of Faujasite framework allow *n*-hexane to enter the active sites lengthwise in a similar manner as in KL-zeolite channel network (see Figure 2.10).[155] It is important to note that the molecular die approach does not explain the relationship between reduced acidity of the faujasite support and the aromatisation selectivity.

Derouane and Vanderveken[158] used molecular modelling techniques to explain the role played by the L-zeolite intracrystalline channels in pre-organisation of *n*-hexane molecule into a pseudo-cycle. In the proposed mechanism, *n*-hexane molecule diffuses through the orifices, meet head-on with Pt particles inside the channels and partially dehydrogenate to form a Pt-C_1 bond with terminal methyl group. The rest of the *n*-hexane chain curves inside the limited space of the channel and the free methyl group is forced closer to the Pt active site to form a pseudo-cyclic species which resembles 1,6-ring closure transition state. The free methyl group attaches to the Pt active site leading to 1,6-metallocycle with the platinum and in the end a liberated benzene. Figure 2.12 shows an adapted computer model depiction of liberated benzene molecule next to six-atom Pt cluster inside the L-zeolite channel.[159] Besides the theoretical data reported by the authors, the pre-organisation technique was not proven experimentally.

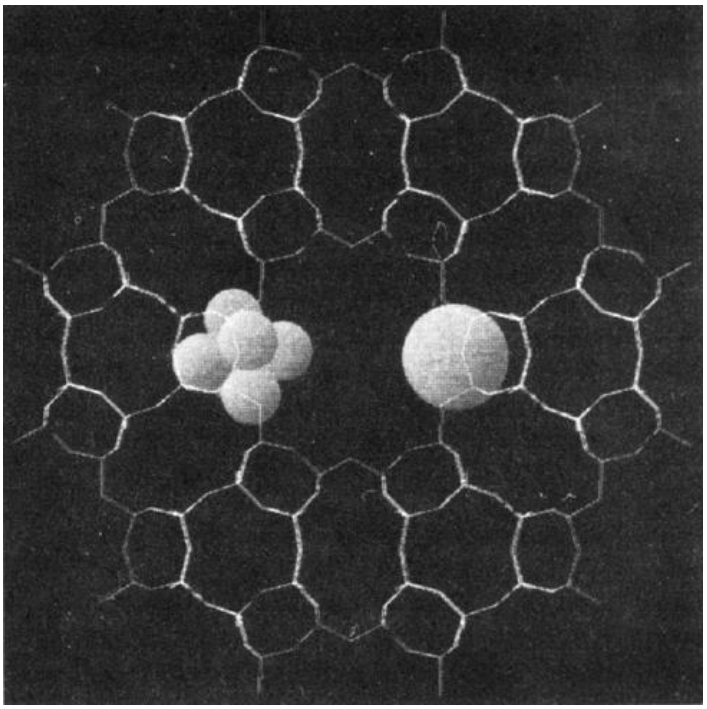

Figure 2.12. A computer model of L-zeolite channel with six-atom Pt cluster and a space filling circle approximately the size of benzene molecule. The figure was adapted with permission from reference 159. Copyright (1995) by American Chemical Society.

2.8.2.3 Role of Metal Particle Morphology and Size in Reforming by Pt/KL-zeolite

Besoukhanova *et al.* [146] identified four types of Pt particles in Pt/KL-zeolite catalyst:

1. Large Pt particles (10-60 nm) outside the zeolite channels
2. Pt crystals (1-2.5 nm) inside and outside the L-zeolite channels
3. Small metallic cylinders (1.5-7 nm) inside and outside the channels
4. Very small Pt particles (*ca*. 0.6-0.8 nm diameter) embedded in channel cavities.

The Pt crystals and metallic cylinders inside the channel cavities are largely responsible for the aromatisation activity of Pt/KL-zeolite catalyst. The very small Pt particles which are embedded in the walls of channel cavities are not accessible to hydrocarbons, hence these particles do not participate in catalysis.[146] Large particles outside the channels are active in dehydrocyclisation reaction despite that they are not influenced by the electronic properties of the support. Large particles deactivate rapidly during catalysis and result in non-selective dehydrocyclisation and hydrogenolysis which will lower the yield of aromatic products. [160]

Dehydrocyclisation of *n*-alkanes to aromatic products is sensitive to small Pt atom ensembles[134,139] and is inherently dependent on clean Pt surfaces.[160] Small Pt ensembles dispersed on the support favour aromatisation over hydrogenolysis irrespective of the support type. The effect of metal dispersion on aromatisation of *n*-hexane is summarised in Table 2.5 where H_2 uptake measurements produce high H/Pt values for Pt/KL-zeolite and Pt/Faujasite-zeolite catalysts (1.56 and 1.10 respectively). These H/Pt values correspond to high Pt dispersion which indicates that the Pt particles were smaller on KL-zeolite and Faujasite supports relative to the other supports listed in Table 2.5. At 13 to 15 % *n*-hexane conversion, Pt/KL-zeolite and Pt/FAU catalysts give higher aromatisation selectivity compared to catalysts with poor Pt particle dispersion (Pt/microporous silica SSZ-34 and Pt/SiO_2). Hydrogenolysis to C_1-C_5 products is remarkably high on Pt catalysts with low metal dispersion such as Pt on microporous silica SSZ-34 and on macroporous silica SiO_2.

Table 2.5. Aromatisation of *n*-hexane over various Pt catalysts with different metal dispersion[161]

			Selectivity (%)	
Catalyst	H/Pt	Conversion (%)	Benzene	C_1-C_5
Pt/KL-zeolite	1.56	15.4	57.1	4.7
Pt/Faujasite	1.1	13.2	35.4	9.8
Pt/microporous silica SSZ34	0.72	14.3	23.1	16.7
Pt/SiO_2	0.78	15.3	20.3	18.9

The data in Table 2.5 highlight the fact that Pt catalyst with small metal particles supported on different supports favour high aromatisation selectivity of *n*-alkanes. However, the results do not show the effect of different Pt particle sizes supported on the same support, KL-zeolite. Sachtler and co-workers[162] comparative study proved that Pt/KL-zeolite-IWI catalysts prepared by the incipient wetness impregnation (IWI) method have smaller metal particles relative to catalysts prepared by the ion exchange method (Pt/KL-zeolite-IE). As a result of small metal particles and high metal dispersion, Pt/KL-zeolite-IWI catalyst has a higher turnover frequency (TOF = 1.01 min^{-1}) towards aromatisation compared to Pt/KL-zeolite-IE catalyst (see Table 2.6). Furthermore, Pt/KL-zeolite-IE (which has a low metal dispersion, CO/Pt = 0.45 *vs* 0.69) has a high propensity for hydrogenolysis as shown by high TOF (2.1 min^{-1}) towards C_1 to C_5 products.

Table 2.6. Aromatisation of *n*-hexane over 0.5 % Pt/KL-zeolite catalysts.[162]

		Turnover Frequencies (TOF) (min^{-1})[a]			
Catalyst	CO/Pt ratio	Benzene	C_1-C_5	*i*-C_6	MCP
Pt/KL-zeolite-IE[b]	0.45	0.68	2.1	0.95	0.77
Pt/KL-zeolite-IWI[c]	0.69	1.01	0.61	0.68	0.72

a: Reaction conditions: 350 °C, ambient pressure, 20 h time on stream, b: Pt/KL-zeolite prepared by ion exchange, c: Pt/KL-zeolite prepared by incipient wetness impregnation.

A different study by Jongpatiwut *et al.*[163] further confirms that the aromatisation activity of Pt/KL-zeolite catalysts increases as the Pt particle size gets smaller. In this study, the aromatisation selectivity of *n*-hexane was compared between Pt/KL-zeolite catalysts prepared by the incipient

wetness impregnation (IWI) with $Pt(NH_3)_4(NO_3)_2$ and the vapour phase impregnation (VPI) with $Pt(acac)_2$. X-ray absorption analysis (X-ray Absorption Near Edge Structure and Extended X-ray Absorption Fine Structure analysis - XANES and EXAFS) and TEM analysis revealed that Pt/KL-zeolite-VPI catalysts have small Pt particles containing about 6-10 Pt atoms.[163,164] The Pt particle sizes in Pt/KL-zeolite-VPI catalysts were estimated to be below 0.7 nm.[122,165] H_2 chemisorption data further showed that Pt/KL-zeolite-VPI catalysts have better Pt particle dispersion compared to Pt/KL-zeolite-IWI catalysts as shown by H/Pt values of 0.91 and 0.56 respectively.[163]

Pt/KL-zeolite-VPI catalyst with high Pt dispersion gives higher *n*-hexane conversions than Pt/KL-zeolite-IWI catalyst.[163] The overall difference in *n*-hexane conversion between these catalysts is *ca*. 15 to 20 % over 30 h on stream as shown in Figure 2.13. The Pt/KL-zeolite-VPI catalyst also gives higher benzene selectivity (93.7 %) than Pt/KL-zeolite-IWI catalysts (84 % selectivity) after 9 h on stream. This study also showed that Pt/KL-zeolite-VPI is more tolerant to deactivation over time on stream as shown by reaction profile in Figure 2.13b.

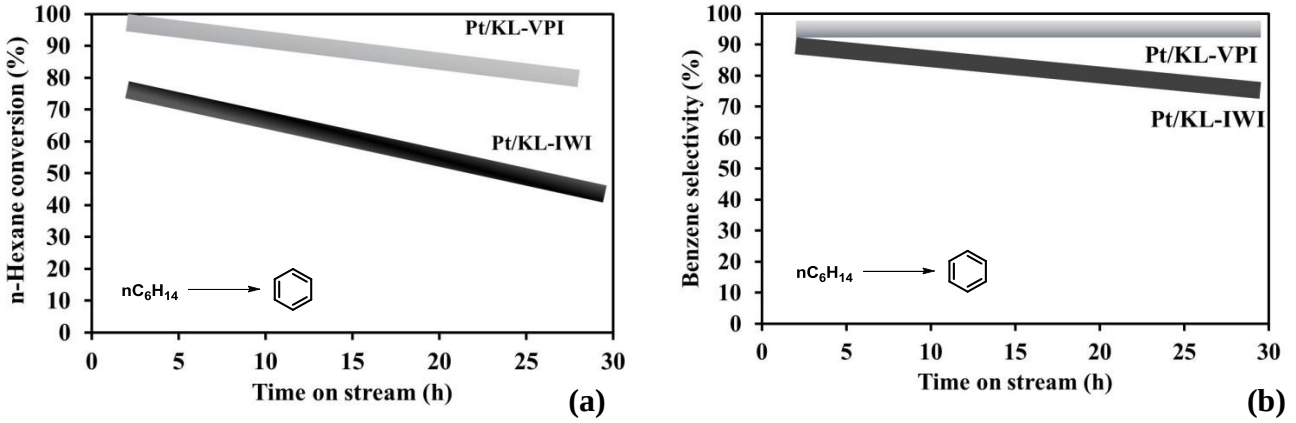

Figure 2.13. Reaction trendline for *n*-hexane conversion (a) and benzene selectivity (b) against time on stream over Pt/KL-zeolite catalyst prepared by vapour phase impregnation (Pt/KL-VPI) and Pt/KL-zeolite catalyst prepared by incipient wetness impregnation (Pt/KL-IWI). Reaction conditions: Weight Hourly Space Velocity (WHSV) = 5 h^{-1}, H_2/*n*-hexane = 6, 500 °C.[163]

Iglesia and Baumgartner[160] showed that small Pt crystallites (*ca*. 1.5 nm diameter) on non-porous silica give 5.5 s^{-1} initial turnover rates in aromatisation of *n*-heptane which is higher than 2.4 s^{-1} turnover rate observed in Pt/KL-zeolite catalyst. This is summarised in Table 2.7. Pt particles supported on non-porous silica have neither the high electronic density nor the channel confinement effect which were previously identified as contributing factors for high aromatisation activity of Pt/KL-zeolite catalysts by the other authors.[150,158] Iglesia and Baumgartner [160] concluded that the confinement and electronic effects are not necessary for the high aromatisation activity observed in Pt/KL-zeolite but intrinsic property of clean Pt surfaces and small Pt ensembles are necessary.

Table 2.7. Reforming of *n*-heptane over Pt/SiO_2 and Pt/KL-zeolite catalysts.

			Turnover Rate (s^{-1})[a]	
Catalyst	H/Pt	Particle size (nm)	Toluene	C1-C5
Pt/SiO2				
Initial	0.64	1.4	5.5	2.2
Steady state [b]	0.15	1.5	0.4	0.7
Pt/KL-zeolite				
Initial	0.85	< 0.7	2.4	1.3
Steady state [b]	0.76	< 0.7	2.2	1.3

a: Reaction conditions: 410 °C, 8 bar, H_2/nC_7 = 5.5, b = After *n*-hexane reaction at 500 °C for 2-5 h

It is important to note that aromatisation catalysed by Pt on SiO_2 support is not sustainable as the catalyst deactivates rapidly (*ca.* 2-5 h on stream, see Table 2.7) due to coke deposits on catalyst active sites.[160,164] Coke deposits on clean Pt surface inhibit dehydrocyclisation activity. Due to coke deposits, Pt/SiO_2 loses the *n*-alkane aromatisation activity two times faster than Pt/KL-zeolite catalyst.[166] In Pt/KL-zeolite catalysts, extremely small Pt clusters are stabilised within the L-zeolite channels[167] where bimolecular reactions leading to intracrystalline coke deposits are inhibited.[157,160]

There is remarkable evidence that small Pt particles, high dispersion of Pt particles and the L-zeolite unidimensional channels with internal cavities play a significant role in the unusually high aromatisation activity of Pt/KL-zeolite-catalysts. A review by Meriaudeau and Naccache[122]

summarises the unique characteristic factors that contribute to high aromatisation activity of Pt/KL-zeolite catalysts as follows:

1. The non-acidic character of Pt/KL-zeolite which eliminates side reactions
2. The extremely small size of Pt particles dispersed within L-zeolite channels
3. The size and morphology of the L-zeolite channels which inhibit the bimolecular reactions leading to coke formation
4. The stability of Pt crystallites derived from metal-support interaction with KL support and unique dimensions of L-zeolite channels.

The unique characteristics of KL support make Pt/KL-zeolite catalysts superior to other non-acidic Pt reforming catalysts. Despite the characteristics listed above, Pt/KL-zeolite catalysts are sensitive to a wide range of catalyst poisons which reduce the *n*-alkane aromatisation activity. In the following section, factors leading to the deactivation of Pt/KL-zeolite catalysts are outlined.

2.8.3 Deactivation and Poisoning of Pt/KL-zeolite Catalysts

Pt based catalysts used in the hydrocarbon conversions are sensitive to N, O and S compounds which react with Pt and reduce the catalytic activity. As a result of catalyst poisons, commercial naphtha reformers are preceded by hydroprocessing steps which rigorously reduce the catalyst poisons before the hydrocarbon stream enters the reforming reactor.[154] Among the hydrocarbon streams used in the Pt reformer, the Fischer-Tropsch syncrude (FTS) derived naphtha is free from N- and S-species.[168] The major concern in the FTS naphtha is the oxygenates including water, alcohols, carbonyls and carboxylic acids which are inherent in FT products.[154,168] Crude oil naphtha inevitably contains very stable and refractory S and N heterocyclic rings. Consequently, severe hydrodesulphurisation and hydrodenitrogenation play a crucial role to reduce S and N species in naphtha feed to acceptable levels. Even traces of S (*e.g.* ppb levels) in naphtha feed will reduce the aromatisation activity of Pt/KL-zeolite catalysts in reforming catalysis.[153]

In addition to catalyst poisons, Pt catalysts are also susceptible to metal particle sintering and build-up of carbonaceous deposits which alter the reactivity of the fresh Pt catalyst. Research

towards the understanding of the mechanisms leading to carbonaceous deposits during the reforming process are reported in the literature. [162,169,170] Interest on the refining of Fischer-Tropsch (FT) syncrude has also led to the study of Pt/KL-zeolite catalysts in the reforming of oxygenated syncrude and *n*-alkanes.[154]

2.8.3.1 Deactivation by Carbonaceous Deposits

Without hydrocarbon adsorption on Pt active site, there will be no reforming of *n*-alkane. The hydrocarbon must adsorb on the Pt active site and dehydrogenate to form an adsorbed aromatic precursor which subsequently desorb as an aromatic final product. Irreversible adsorption of hydrocarbon followed by the dehydrogenation over a long time on stream eventually results in carbonaceous deposits or coke. Somorjai and others[169,170] claimed that a clean Pt surface has catalytic activity towards aromatisation while Pt surface covered with 3-dimentional (3-D) carbonaceous deposits is totally inactive. The Pt sites covered by one or more single carbon atom still have the dehydrogenation activity and residual aromatisation activity.[171,172,173]

An accurately prepared Pt/KL-zeolite catalyst with most of the Pt particles inside the L-zeolite channels is resistant to 3-D carbonaceous deposits due to the protected environment provided by the channels where bimolecular reactions leading to coke are inhibited.[160] After a prolonged catalytic reaction, irreversible carbonaceous deposits are accumulated in Pt/KL-zeolite catalysts due to the irreversible adsorption of aromatic precursors and C_1 side products. The irreversibly adsorbed hydrocarbons on the surface of Pt dehydrogenate to form the deactivated Pt-C which accumulates to coke.[174] Ostegard *et al.* [162] illustrated by temperature programmed oxidation (TPO) that coke can deposits on Pt site or on the support of Pt/KL-zeolite catalysts. The TPO spectra showed a peak at 200 °C corresponding to coke on Pt particles and a peak at 280 °C assigned to coke on the support. Using the TPO data, the amount of coke determined in this study corresponded to the magnitude of catalyst deactivation in *n*-hexane aromatisation as shown in Table 2.8. Pt/KL-zeolite catalyst

prepared by ion exchange (Pt/KL-zeolite-IE) severely deactivated (61.2 % deactivation) after 20 h on stream in the aromatisation of *n*-hexane and had the highest amount of coke deposited on the Pt sites compared to Pt/KL-zeolite catalyst prepared by incipient wetness impregnation (Pt/KL-zeolite-IWI). The superiority of Pt/KL-zeolite-IWI catalyst over Pt/KL-zeolite-IE is due to better Pt particle dispersion as determined by CO/Pt values in Table 2.8 (0.69 *vs* 0.45).

Table 2.8. Catalyst deactivation data after *n*-hexane aromatisation and corresponding temperature programmed oxidation (TPO) data for coke deposition on Pt/KL-zeolite catalysts.[162]

Catalyst	% Deactivation	Coke/Pt	Coke/Zeolite	CO/Pt
Pt/KL-zeolite-IE[a]	61.2	9	1.7	0.45
Pt/KL-zeolite-IWI[b]	20.5	4.1	1.6	0.69

a: Pt/KL-zeolite catalyst prepared by ion exchange, b: Pt/KL-zeolite catalyst prepared by incipient wetness impregnation.

The *n*-alkane aromatisation activity of Pt/KL-zeolite catalysts deteriorates fast when longer chain-length hydrocarbons such as *n*-octane are used as the feed. Jongpatiwut *et al.*[175] reported that the aromatisation activity of Pt/KL-zeolite catalysts decreases fast and the amount of coke adsorbed on catalyst was about two folds higher when *n*-octane was used as aromatisation feed instead of *n*-hexane under the same conditions. The authors[175] concluded that the diffusion of bigger C_8-aromatics from *n*-octane aromatisation is limited in the confined L-zeolite channels compared to a smaller *n*-hexane aromatisation product, benzene. Therefore, the C_8-aromatics trapped inside the channels dehydrogenate to form coke and plug the channels.[175,176,177] The channel and pore plugging was proven by isobutane sorption of the spent catalysts and the results showed that there was two times more space available in spent Pt/KL-zeolite catalyst from *n*-hexane aromatisation than the spent catalyst from *n*-octane aromatisation.[175]

Regeneration of coked catalyst is possible by oxidation of the carbon deposits to CO_2 under air flow, followed by reduction under H_2. The results obtained after catalyst regeneration are comparable to results observed in fresh Pt/KL-zeolite catalyst as shown by the conversion of

n-octane to aromatics in Figure 2.14.[175] The selectivity of aromatic products is also similar to the product selectivity in fresh catalyst.

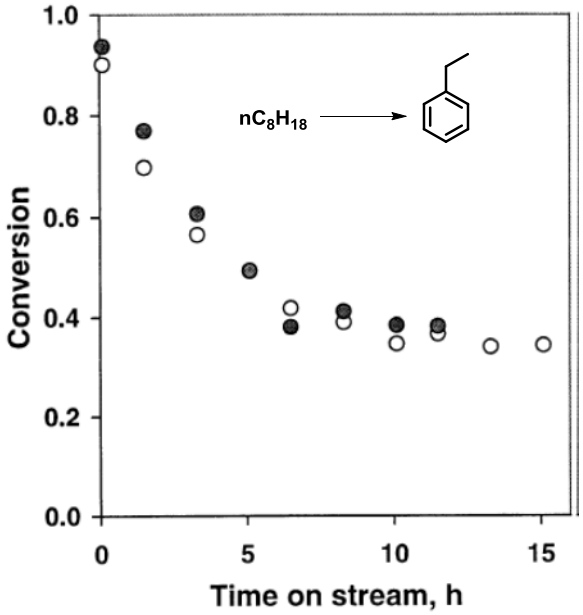

Figure 2.14. Total *n*-octane conversion before and after regeneration in air at 400 °C as function of time on stream. Open symbols: first reaction cycle, and full symbols reaction cycle after catalyst regeneration. The figure was adapted with permission from 175. Copyright (2003) by Elsevier.

2.8.3.2 Sulphur Poisoning of Pt/KL-zeolite Catalysts

The application of Pt/KL-zeolite catalyst in the reforming of crude oil-based naphtha is limited by the extreme sensitivity of this catalyst in sulphur poisoning. Pt/KL-zeolite catalysts are more sensitive to sulphur poisoning than the conventional bi-functional reforming catalysts such as $Pt/Cl/Al_2O_3$.[178] As a result of sulphur sensitivity, the hydrocarbon feed is passed through sulphur removal systems to deplete the sulphur content below 0.05 ppm prior to reforming over Pt/KL-zeolite catalyst.[153,179]

Attempts to understand the sensitivity of Pt/KL-zeolite catalyst to sulphur poisoning have been made by different research groups.[178,180,181] Vaarkamp *et al.*[180] concluded that S adsorbs on the Pt active sites and enhances the growth of Pt clusters by agglomeration and eventually plugging the L-zeolite channels. These claims were confirmed by McVicker *et al.*[181] where it was revealed that even

a low concentration of thiophene in the feed accelerates sintering and subsequent deactivation of Pt particles.

Besides the particle growth, other reports claim that the K^+ in the KL support is responsible for high sulphur sensitivity of Pt/KL-zeolite catalysts.[150] Under sulphur free conditions, the presence of alkali cations such as K^+ in the L-zeolite support increase the electronic density of Pt particles and promote the aromatisation of *n*-hexane.[146] Sulphur in *n*-hexane feedstock interacts strongly with K^+ and supresses the ability of K^+ to promote aromatisation.

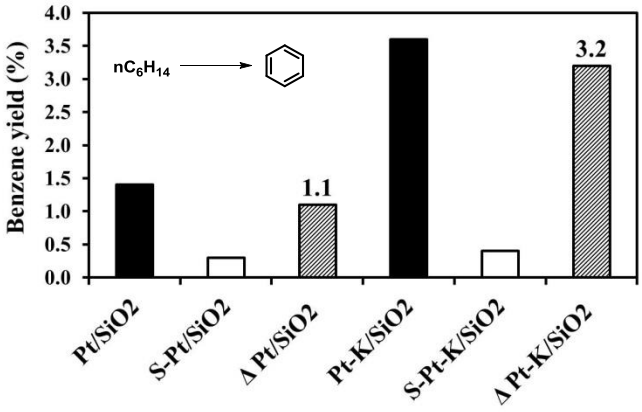

Figure 2.15. Benzene yield from aromatisation of neat *n*-hexane feed (*black columns*) and *n*-hexane feed spiked with 0.5 wt% sulphur (*white columns*). The difference between aromatisation of neat *n*-hexane and spiked hexane is shown by stripped columns.[150]

The role played by K^+ in sulphur poisoning is illustrated by comparative study between Pt/SiO_2 and $Pt\text{-}K/SiO_2$ in the aromatisation of *n*-hexane spiked with 0.5 wt% sulphur as shown by the relative benzene yields in Figure 2.15.[150] Severe negative impact on aromatisation due to sulphur poisoning was observed on the benzene yield which was reduced by 3.2 wt% when $Pt\text{-}K/SiO_2$ catalyst was used in aromatisation of *n*-hexane. Only 1.1 wt% reduction on benzene yield was observed in K^+ free Pt/SiO_2 catalyst which implies that K^+ plays a role in sulphur induced deactivation of Pt-K/catalyst.[150]

Jongpatiwut *et al.*[163] proved that Pt/KL-zeolite catalysts promoted with rare earth (RE) metal have a better tolerance to sulphur poisoning than un-promoted Pt/KL-zeolite catalysts. It was postulated that RE oxides, especially Ce, interact and trap sulphur so to keep Pt particles active for the aromatisation. When Ce oxides in the support are saturated with sulphur, the rate of Pt deactivation increases.

2.8.3.3 Oxygenate Poisoning of Pt/KL-zeolite Catalysts

The FT derived naphtha is rich in oxygenates compared to petroleum naphtha.[168] Hydroprocessing and drying of the charge stock to remove the oxygenates before the reformer are inevitable when using chlorinated bi-functional catalysts. Conventional reforming of hydrocarbons on bi-functional catalyst requires oxygenates depleted feed with less than 10 ppm oxygenate content.[182]

The disadvantage of excess oxygenates, especially water, is the leaching away of chloride ions in chlorinated bi-function catalysts such as $Pt/Cl/Al_2O_3$.[154,182] At the same time, a controlled addition of water in the charged feedstock is beneficial to regulate the halogen content in chlorinated Pt/KL-zeolite catalysts during the reforming of hydrocarbons.[183] Furthermore, Blessing *et al.*[184] claimed that the presence of water (*ca.* 5 ppm) in the feedstock to the reformer loaded with chlorinated Pt/KL-zeolite catalyst increases the concentration of benzene by 8% from 40% to 48%. However, when water (3%) is added to the feed stream to the reformer loaded with Cl^- free Pt/KL-zeolite catalyst, a reduction in aromatisation activity is observed.[163] A study by Jongpatiwut *et al.*[163] in Figure 2.16, showed that *n*-hexane conversion and benzene selectivity by Pt/KL-zeolite catalysts drop when water is added to the feed for 1 h. It was observed that the catalyst deactivation was more severe in un-promoted catalysts Pt/KL-zeolite-IWI and Pt/KL-zeolite-VPI which were prepared by incipient wetness impregnation (IWI) and vapour phase impregnation (VPI) methods respectively. The authors[163] pointed out that the exposure to water accelerates Pt particle growth by

sintering which is followed by the increase in coke formation and ultimately catalyst deactivation. To alleviate the particle growth in the presence of water, a promoter Ce is added to stabilise the Pt particles and improve resistance to sintering.

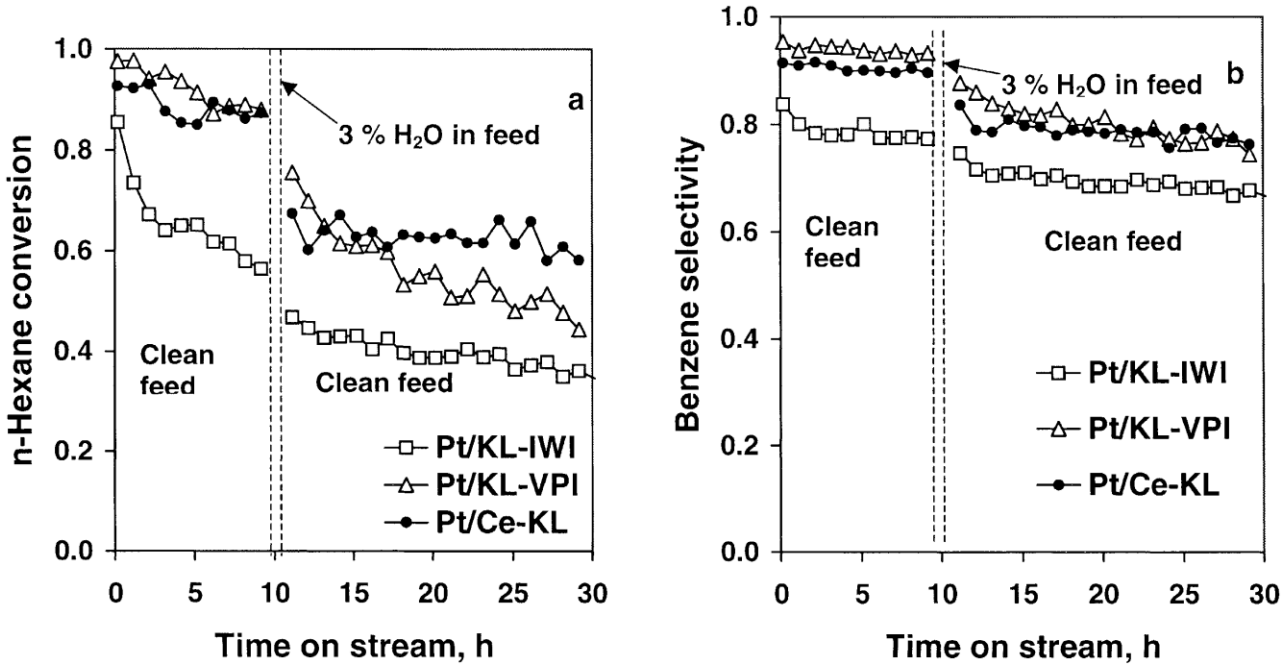

Figure 2.16. (a) *n*-Hexane conversion and (b) benzene selectivity over Pt/KL-zeolite catalysts *vs* time on stream. Water vapour (3 %) was introduced at 9 h for duration of 1 h and then the reaction was run again as normal. Pt/KL-IWI: Pt/KL-zeolite prepared by incipient impregnation, Pt/KL-VPI: Pt/KL-zeolite prepared by vapour phase impregnation. The figure was adapted with permission from reference 163. Copyright (2002) by Elsevier.

In addition to water, the oxygenate-tolerance of Pt/KL-zeolite catalyst in *n*-hexane aromatisation in the presence of alcohol, ketone and aldehyde was investigated by Dry and co-workers.[185] It was found that the oxygenates in the feedstock have a negative effect on *n*-hexane conversion and benzene selectivity at 450 °C and 1 bar H_2. Under the same relative molecular concentration of oxygenates, the magnitude of the negative effect induced by oxygenates on aromatisation ability was similar. At reforming conditions, the oxygenates decompose to similar amounts of CO which chemisorb on Pt active site and supress aromatisation activity in the same magnitude. The catalyst deactivation caused by oxygenates is alleviated when H_2 pressure is

increased to 4 bar. The authors concluded that the impact of oxygenates on Pt/KL-zeolite aromatisation activity is negligible when the oxygenate content is *ca.* 1 mole %.[185]

2.9 Oxidation of Alcohols over Supported Pt Catalysts

The literature on oxidation of alcohols was studied to understand the properties of catalysts used for oxidation of primary alcohols which is the requirement for goal 7 (chapter 1). Supported noble metals especially Platinum Group Metals (PGM) are seen as attractive alternatives in catalytic oxidation of hydrocarbons relative to stoichiometric inorganic reagents. When used as oxidants, the inorganic reagents generate large amounts of side products and contribute to chemical waste and environmental issues.[186] In a catalytic approach using a green oxidant such as oxygen or H_2O_2, the transformation of alcohol to carbonyl and finally carboxylic acid results in water as the only side product. When carboxylic acid is the target product, water is the solvent of choice. A number of organic solvents are also used as solvent for water insoluble alcohols.[187] In addition to atom efficiency, oxidation of alcohols catalysed by supported metals requires mild experimental conditions under atmospheric pressure. In fact, catalytic oxidation of alcohols to achieve up to 99% yield of corresponding carbonyls can be done using Au-Pt based bimetallic catalysts at temperatures as low as 25 °C.[188,189]

The advantages associated with the use of supported metal catalysts in oxidation of alcohols are clearly significant. At the same time there are still a number of challenges with regard to the product selectivity and sustainable catalyst activity to different substrates.[190,191,192] The common cause of catalyst deactivation is the over-oxidation of the catalyst active sites to form metal oxides which are less active towards oxidation. In addition to over-oxidation, destructive chemisorption of intermediate oxidation products and polymeric by-products deactivate the catalyst active sites.[191] Among the PGMs, Pt is less susceptible to over-oxidation due to higher redox potential compared to the other metals in the group.[193,194] However, the un-promoted Pt catalysts are still susceptible to

chemical poisoning by destructive chemisorption of by-products. The addition of a second metal such as bismuth (Bi) to the Pt catalyst can suppress the chemical poisoning[195] but poses further challenges because Bi can leach from the catalyst and contaminate the final product quality.[196] Pt catalysed oxidation reactions especially selective dehydrogenations of alcohols to corresponding carbonyls are discussed in the following sections.

2.9.1 Oxidative Dehydrogenation of Primary Alcohols

PGMs exhibit excellent activities in oxidation of alcohols to carboxylic acids. In some instances such as the oxidation of glyoxal to glyoxylic acid, Pt exhibits a higher rate of product formation than the rest of PGMs.[197,198] A more notable application of Pt-base catalysts is the selective oxidative dehydrogenation of primary alcohols to form respective carbonyls.[199] The typical oxidation of alcohols proceeds *via* oxidative dehydrogenation to aldehydes for primary alcohols or ketones for secondary alcohols.[200] A widely accepted pathway followed in oxidative dehydrogenation of alcohols is initiated by the adsorption of alcohol on the metal active site. On the surface of the metal, the alcohol dehydrogenates to give the adsorbed metal alkoxide which subsequently undergoes a β-hydride elimination to form a corresponding carbonyl and two adsorbed hydrogen atoms ($2H_{ads}$) on the surface of the metal (see Scheme 2.5).[201,202,203] In the presence of oxygen, the adsorbed hydrogen atoms are removed from the surface by reacting with the dissociatively adsorbed oxygen to form water.[202]

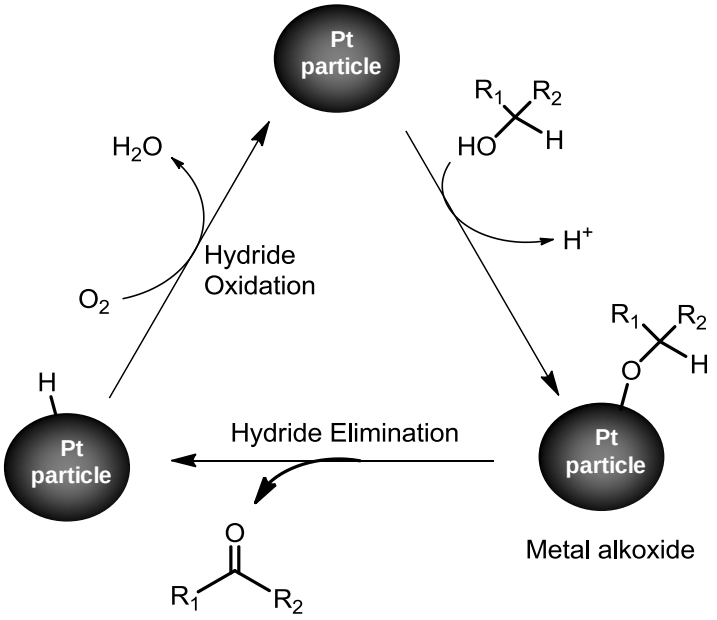

Scheme 2.5. Illustration of postulated mechanism of oxidative dehydrogenation of primary or secondary alcohols on supported Pt catalyst. The figure was adapted with permission from reference 203. Copyright (2009) by American Chemical Society.

Oxidative dehydrogenation of primary alcohols especially simple aliphatic alcohols to form aldehydes presents challenges due to poor reactivity in catalytic oxidation[204] and subsequent oxidation of aldehydes to form carboxylic acids. A conversion to form a carboxylic acid can either follow a slow process of oxygen insertion or a rapid hydration to geminal diol followed by dehydrogenation to carboxylic acid.[195,205]

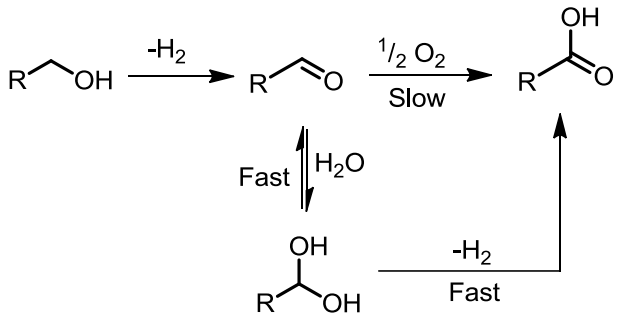

Scheme 2.6. The illustration of a postulated reaction mechanism in oxidation aldehydes to form corresponding carboxylic acids. The figure was adapted with permission from reference 205. Copyright (2004) by American Chemical Society.

The dehydration to carboxylic acids is sometimes prevented by gas phase oxidation of alcohols at high temperature (310-550 °C),[206] replacing the standard aqueous medium with organic medium[207,208] or maintaining very low alcohol conversions (*ca*. 20 %).[195] In transfer dehydrogenation, the unsaturated organic reagent is used to react with the adsorbed hydrogen atoms and thus eliminate the formation of water which can hydrate the aldehyde.[207]

2.9.2 Typical Pt Catalysts Used in Oxidative Dehydrogenation of Primary Alcohols

A number of advances have been made in oxidative dehydrogenation of alcohols since the reduced platinum oxides were used to dehydrogenate a series of primary and secondary alcohols in the presence of oxygen.[204,209] In these studies, oxidative dehydrogenation is catalysed by the unsupported Pt particles which are produced *in situ* by the reduction of Pt oxides using H_2 gas[204] or the alcohols.[209]

Much of the subsequent investigations in selective oxidation of primary alcohols have been done using 5% Pt supported on carbon support (Pt/C).[191,199] Activated carbon or graphite supports are stable in wide range of pH and suitable for applications in the presence of complexing molecules.[191] The activity of the Pt/C catalyst in selective oxidation of alcohols is improved by the addition of the second metal as a promoter especially bismuth (Bi) to make a bi-metallic catalyst. The promoter improves the catalyst activity and the selectivity of oxidation products.[210,211] A notable commercial oxidation Pt catalyst is 5%Pt-5%Bi/C (CF 196RA/W) supplied by Degussa. Other metals that are used as promoters in Pt/C catalysts include palladium (Pd) and gold (Au).

Beside the carbon supported catalysts, Al_2O_3 supported Pt catalysts (Pt/Al_2O_3) have also received a lot of attention in selective oxidation of aromatic[191] and allylic alcohols.[195,212] Selective deposition of Bi onto Al_2O_3 supported Pt particles suppresses the rapid deactivation of Pt active sites and improve catalysts activity compared to monometallic Pt/Al_2O_2. The Bi particles decrease the size

of the Pt active sites and suppress the chemisorption of polymeric secondary by-products. This process is known as geometric blocking effect.[195]

Other catalysts that have been used in oxidative dehydrogenation of primary alcohols include 5% Pt/BN (BN = Boron nitride), 2% Pt/SiO_2 and 3% Pt/TiO_2. These catalysts have all been used in oxidative dehydrogenation of 1,6-hexanediol to achieve more than 95 % selectivity to 6-hydroxyhexanal at 7 to 22 % alcohol conversion.[213]

2.9.3 Case Studies in Oxidative Dehydrogenation of Primary Alcohols Using Pt Catalysts

Sneeden and Turner[204] studied oxidative dehydrogenation of 1-octanol and benzyl alcohol using unsupported Pt particles which were formed by H_2 reduction of PtO_2. Under ambient conditions, the dehydrogenation of 1-octanol yielded 21 % octanal while 72 % benzaldehyde yield was achieved in dehydrogenation of benzyl alcohol. No carboxylic acids were detected in both transformations. The relative yields of aldehydes obtained from different substrates highlighted the poor activity of Pt catalysts in oxidative dehydrogenation of primary aliphatic alcohols compared to primary aromatic alcohols.

Similar oxidative dehydrogenation work was done by Griffin and co-workers[199] where a series of Pt catalysts on different solid supports were used to oxidatively dehydrogenate 1-octanol in toluene (see Table 2.9). In mono-metallic catalysts, a very high selectivity to octanal (more than 90 %) was observed at low conversion of the starting material. Addition of a promoter Bi to the Pt catalyst improved the activity to the oxidative dehydrogenation but a noticeable amount of octanoic acid (10-20 % selectivity) also formed. A similar trend was observed by Baiker and co-workers[195] in oxidative dehydrogenation of 1-dodecanol over 5% Pt-3%Bi/Al_2O_3 in aqueous medium. At 5 % alcohol conversion, the selectivity to dodecanal was as high as 80 %. A dramatic decrease to about 50 % aldehyde selectivity is observed when the conversion is increased to about 45 %.

Table 2.9. Oxidative dehydrogenation of 1-octanol over 5 % Pt catalysts. The initial alcohol: metal ratio was 80:1.

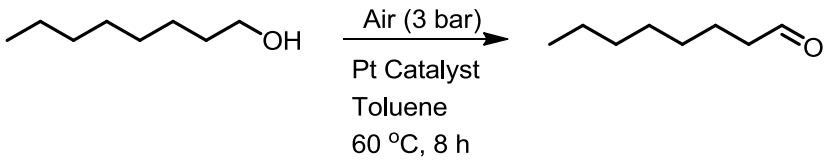

Catalyst	Conversion (%)	Aldehyde selectivity (%)
5% Pt/Al2O3	34	94
5% Pt-1% Bi/Al2O3	66	87
5% Pt/C	29	86
5% Pt-1% Bi/C	60	81

The oxidative dehydrogenation of aromatic and allylic primary alcohols using supported Pt catalysts is much easier than the aliphatic primary alcohols and the problem of over-oxidation to corresponding carboxylic acid is very minimal.[203,195] A classic example of the dehydrogenation of aromatic primary alcohol is the transformation of 2-hydroxybenzol alcohol to salicylaldehyde in 97 % yield over Pt-Bi/C catalyst at 45 °C.[214]

Baiker and co-workers have done extensive investigations in selective oxidation of allylic primary alcohol, cinnamyl alcohol.[195,212] A selective oxidation of cinnamyl alcohol over 5 % Pt-Bi/Al_2O_3 in aqueous medium achieves 98.5 % selectivity to cinnamaldehyde at 95 % alcohol conversion. The conjugate C=C bond in cinnamaldehyde and the aromatic ring in the aromatic aldehydes destabilised the geminal diol which is formed by the hydration of the aldehydes.[195] Thus the formation of the corresponding carboxylic acids is supressed (see Scheme 2. 7).

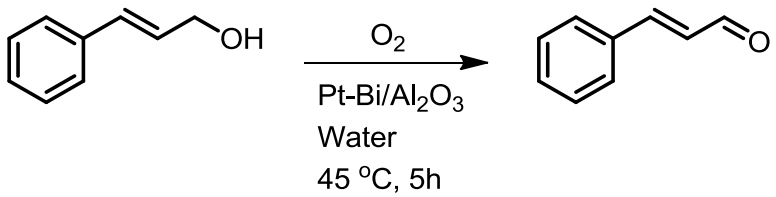

Scheme 2. 7. Oxidative dehydrogenation of cinnamyl alcohol to cinnamaldehyde in aqueous medium.

There is still a big opportunity to increase the scope of Pt catalysts applications in oxidative dehydrogenation of alcohols in particular, primary aliphatic alcohols and to improve the catalyst activity without the use of promoters. Ikeda and co-workers[203] showed that *n*Pt@*h*C catalyst which has Pt nanoparticles embedded in microporous carbon support is two times more active in oxidative dehydrogenation of alcohols than the commercial Pt/AC catalyst on activated carbon. *n*Pt@*h*C catalyst was more tolerant to deactivation and exhibited no obvious change in particle dispersion even after use in catalytic oxidation. Further analysis showed that secondary by-products that lead to chemical poisoning do not adsorbed on Pt particles that are embedded on porous support in *n*Pt@*h*C.

Beside *n*Pt@*h*C catalyst, there is limited literature on the application of the Pt catalysts on well-defined porous support like zeolites. Some literature exists on the use of zeolites to support catalysts derived from other noble metals such as cobalt,[215] iron[216] and gold[217] for selective oxidation of toluene[216] and benzyl alcohol.[215,217] It is worth exploring whether the Pt catalysts supported on well-defined support such as zeolites will have an impact on oxidative dehydrogenation of primary alcohols. Structured pores of the support are known to protect the metal particles and improve the catalyst activity in dehydrocyclisation reactions.[122] In this thesis, Pt particles that are supported on porous supports KL-zeolite and Y-zeolite are tested in oxidative dehydrogenation of alcohols.

2.10 References

[1] J. W. Niemantsverdriet, in *Spectroscopy in Catalysis*. Weinheim:Wiley-VCH. **2007, pp.** 19-346.
[2] X. Lai, D. W. Goodman, *J. Mol. Catal. A. Chem.* **2000**, *162*, 33-50.
[3] X. Lai, T. P. St Clair, D. W. Goodman, *Faraday Discuss.* **1999,** *114*, 279-284.
[4] K. L. E Eriksson, W. W. Y. Chow, C. Puglia, J. E. Backvall, E. Gothelid, S. Oscarsson, *Langmuir*. **2010**, *26*, 16349-16354.
[5] A. Kolmakov, D. W. Goodman, *Surf. Sci.* **2001**, *490*, L597-L601.
[6] T. Worren, K. H. Hensen, E. Laegsgaard, F. Besenbacher, I. Stensgaard, *Surf. Sci.* **2001**, *477*, 8-16.
[7] F. Gao, D.W. Goodman, *Annu. Rev. Phys. Chem.* **2012**, *63*, 265-286.
[8] L.M. Eshelman, A.M. de Jong, J.W. Niemantsverdriet, *Catal. Lett.* **1991**, *10*, 201-210.
[9] G. Ertl, *Surf. Sci.* **1994**, *299*, 742-754.
[10] F. Zaera, *Prog. Surf. Sci.* **2001**, *69*, 1-98.
[11] G. A. Somorjai, R. L. York, D. Butcher, J. Y. Park, *Phys. Chem. Chem. Phys.* **2007**, 9, 3500–3513.
[12] D.W., Goodman, C.H.F.M., Peden, *J. Phys. Chem.* **1986**, *90*, 4839-4843.
[13] M.J.P., Hopstaken, W.J.H., van Gennip, J.W., Niemantsverdriet, *Surf. Sci.* **1999**, *69*, 433-435.
[14] D. R. Rainer, S. M. Vesecky, M. Koranne,W. S. Oh, and D. W. Goodman, *J. Catal.* **1997**, *167*, 234-241.
[15] J. W. Niemantsverdriet, A.F.P. Engelen, A.M. de Jong, W. Wieldraaijer, G.J. Kramer, *Appl. Surf. Sci.* **1999**, *144-145*, 366-374.
[16] C.T. Campbell, *Surf. Sci. Rep.* **1997**, *27*, 1-111.
[17] P.L.J., Gunter, J.W., Niemantsverdriet, F.H., Ribeiro, G.A., Somorjai, *Catal. Rev. Sci. Eng.* **1997**, *39*, 77-168.
[18] A.K. Santra, D.W. Goodman, *J. Phys. Condens. Matter*. **2003**, *14*, R31-62.
[19] G. Patermarakis, N. Nicolopoulos, *J. Catal.* **1999**, *187*, 311-320.
[20] M. S. Chen, A. K. Santra, D. W. Goodman, *Phys. Rev. B.* **2004**, *69*, 155404
[21] Z. Wang, S. Skiles, F. Yang, Z. Yan, D. W. Goodman, *Catal. Today.* **2012**, *181*, 75-81.
[22] B.E. Deal, A.S. Grove, *J. Appl. Phys.* **1965**, *36*, 3770-3778.
[23] C. Linsmeier, E. Taglauer, *Appl. Catal. A.* **2011**, *391*, 175-186.
[24] M. Baumer, M. Frank, M. Heemeier, R. Kuhnemuth, S. Stempel, H.-J. Freund, *Surf. Sci.* **2000**, *454-456*, 957-962.
[25] P. J. Chen, D.W. Goodman, *Surf. Sci.* **1994**, *312*, L767-L773.
[26] M.-C. Wu, D. W. Goodman, *J. Phys. Chem.* **1994**, *98*, 9874-9881.
[27] Y. Wu, E. Garfunkel, T.E. Madey, *J. Vac. Sci. Technol. A*. **1996**, *14*, 2554-2558.
[28] Wu, Y., Garfunkel, E., Madey, T.E., *Surf. Sci.* **1996**, *365*, 337-352.
[29] S. J. Tauster, S. C. Fung, R.L. Garten, *J. Am. Chem. Soc.* **1978**, *100*, 170-175.
[30] S. Bonanni, K. Ait-Mansour, H. Brune, W. Harbich, *ACS Catal*. **2011**, *1*, 385-389.
[31] E. Labich, S. Taglauer, H. Knozinger, *Top. Catal.* **2001**, *14*, 153-161.
[32] S. Schintke, W. – D. Schneider, *J. Phys. Condens. Matter*. **2004**, *16*, R49–R81.
[33] M. Sterrer, H. –J. Freund, *Catal. Lett.* **2013**, *143*, 375-385.
[34] L. Liu, C. Zhang, G. Thornton, A. Michaelides, *Phys. Rev.* **2010**, *82*, 161415.
[35] G. Ketteler, S. Yamamoto, H. Bluhm, K. Andersson, D. E. Starr, D. F. Ogletree, H. Ogasawara, A. Nilsson, M. Salmeron, *J. Phys. Chem. C.* **2007**, *111*, 8278-8282.
[36] S. Wendt, R. Schaub, J. Matthiesen, E. K. Vestergaard, E. Wahlstrom, M. D. Rasmussen, P. Thostrup, L. M. Molina, E. Lægsgaard, I. Stensgaard, B. Hammer, F. Besenbacher, *Surf. Sci.* **2005**, *598*, 226–245.
[37] M. M. Ivey, K. A. Layman, A. Avoyan, H. C. Allen, J. C. Hemminger, *J. Phys. Chem. B.* **2003,** 107, 6391-6400.
[38] Z. Vit, L. Nondek, *React. Kinet. Catal. Lett.* **1984**, *24*, 137-139.
[39] K. C. Hass, W. F. Schneider, A. Curioni, W. Andreoni, *Science.* **1998**, *282*, 265-268.
[40] J. B. Peri, *J. Phys. Chem.* **1965**, *65*, 220-230.
[41] G. Piedra, J. J. Fitzgerald, N. Dando, S. F. Dec, G. E. Maciel, *Inorg. Chem.* **1996**, *35*, 3474-3478.
[42] H. Konzinger, P. Ratnasamy, *Catal. Rev. –Sci. Eng.* **1978**, *17*, 31-70.
[43] Q. Fu, T. Wagner, M. Ruhle, *Surf. Sci.* **2006**, *600*, 4870–4877.

[44] H. E. Berg, in *The Colloid Chemistry of Silica*, (H. E. Bergna, ed). American Chemical Society, Washington, DC, **1990**, p 25.
[45] L. T. Zhuravlev, *Langmuir*. **1987**, *3*, 316-318.
[46] J. F. Lambert, M. Che, *J. Mol. Catal. A-Chem.* **2000**, *162*, 5-18.
[47] E. Erasmus, J.W. (Hans) Niemantsverdriet, J. C. Swarts, *Langmuir.* **2012**, *28*, 16477-16484.
[48] A. Siani, K.R. Wigal, O.S. Alexeev, M.D. Amiridis, *J. Catal.* **2008**, *257*, 16-22.
[49] M. Heemeier, M. Frank, J. Libuda, K. Wolter, H. Kuhlenbeck, M. Baumer, H.-J. Freund, *Catal. Lett.* **2000**, *68*, 19-24.
[50] K. Ro´zga-Wijas, J. Chojnowski, W. Fortuniak, M. S ´ cibiorek, Z. Michalska, Ł. Rogalski, *J. Mater. Chem.* **2003**, *13*, 2301–2310.
[51] Q. J. Miao, Z. -P. Fang , G. P. Cai, *Catal. Commun.* **2003**, *4*, 637-639.
[52] Z. M. Michalska, Ł. Rogalski, K. Rózga-Wijas, J. Chojnowski, W. Fortuniak, M. Scibiorek, *J. Mol. Catal. A.* **2004**, *208*, 187–194.
[53] T. Chang, S. L. Bernasek, J. Schwartz, *J. Am. Chem. Soc.* **1989**, *111*, 758-760.
[54] J. W. Niemantsverdriet, A. F. P. Engelen, A. M. de Jong, W. Wieldraaijer, G.J. Kramer, *Appl. Surf. Sci.* **1999**, *144-145*, 366-374.
[55] E. W. Kuipers, C. Laszlo, W. Wieldraaijer, *Catal. Lett.* **1993**, *17*, 71-79.
[56] P. C. Thune, R. Linke, W. J. H. van Gennip, A. M. de Jong, J. W. Niemantsverdriet, *J. Phys. Chem. B.* **2001**, *105*, 3073-3078.
[57] L. J. van IJzendoorn, M. J. A. de Voigt, J.W. Niemantsverdriet, *React. Kinet. Catal. Lett.* **1993**, *50*, 131-137
[58] J. Perriere, *Vacuum***. 1987**, *37*, 429-432.
[59] D. R. Pesiri, R. C. Snow, N. Elliott, C. Maggiore, R. C. Dye, *J. Membrane Sci.* **2000**, *176*, 209-221.
[60] C. J. Weststrate, A. Resta, R. Westerstrom, E. Lundgren, A. Mikkelsen, J. N. Andersen, *J. Phys. Chem. C.* **2008**, *112*, 6900-6906.
[61] J. W. Niemantsverdriet, P. Dolle, K. Markert, K. Wandelt, *J. Vac. Sci. Technol.* **1987**, A5, 875-878.
[62] P. C. Thüne, J. W. Niemantsverdriet, *Surf. Sci.* **2009**, *603*, 1756–1762.
[63] H. Poppa, *J. Appl. Phys.* **1967**, *38*, 3883-3894.
[64] W. Zhou, I. E. Wachs, C. J. Kiely, *Curr. Op. Sol. Stat. Mat. Sci.* **2012**, *16*, 10–22.
[65] F. Enquist, A. Spetz, *Thin Solid Films*. **1987**, *145*, 99-104.
[66] H.-F., Wang, H. Ariga, R. Dowler, M. Sterrer, H.-J., Freund, *J. Catal*. **2012**, *286*, 1–5.
[67] M. Baumer, M. Frank, M. Heemeier, R. Kuhnemuth, S. Stempel, H.-J. Freund, *Surf. Sci*. **2000**, *454*, 957-962.
[68] A. K. Santra, B. K. Min, D. W. Goodman, *Surf. Sci.* **2002**, *515*, L475–L479.
[69] J. B. Giorgi, T. Schroeder, M. Baumer, H. J. Freund, *Surf. Sci.* **2002**, *498*, L71-
[70] R. A. Bennett, P. Stone, M Bowker, *Catal. Lett.* **1999**, *59*, 99-105.
[71] S. Takakusagi, K. Fukui, R. Tero , K. Asakura, Y. Iwasawa, *Langmuir*. **2010**, *26*, 16392-16396.
[72] E. Erasmus, J. W. (Hans) Niemantsverdriet, J. C. Swarts, *Langmuir.* **2012**, *28*, 16477-16484.
[73] W. M. Riggs, *Anal. Chem.* **1972**, *44*, 830-832.
[74] J. F. Moulder, W. F. Stickle, P. E. Sobol, K. D. Bomben, in *Handbook of X-Ray Photoelectroscopy*, (J. Chastain, ed.). Perkin-Elmer Corp., USA, **1992**, p. 181.
[75] J. D. Cooper, V. P. Vitullo, D. L. Whalen, *J. Am. Chem. Soc.* **1971**, *93*, 6297-6297.
[76] R. Merryfield, M. McDaniel, G. Parks, *J. Catal.* **1982**, *77*, 348-359.
[77] C. R. Henry, *Surf. Sci. Rep.* **1998**, *31*, 231-323.
[78] Y. Wu, E. Garfunkel, T. E. Madey, *J. Vac. Sci. Technol. A*. **1996**, *14*, 1662-1667.
[79] M. Frank, R. Kuhnemuth, M. Baumer, H. J. Freund, *Surf. Sci.* **1999**, *427-428*, 288-393.
[80] F. S. Ohuchi, R. H. French, R. V. Kasowski, *J. Appl. Phys.* **1987**, *62*, 2286-2289.
[81] J. Yoshihara, C.T. Campbell, *Surf. Sci*. **1998**, *407*, 256-267.
[82] X. Xu, P. Chen, D. W. Goodman, *J. Phys. Chem.* **1994**, *98*, 9242-9246.
[83] E. L. Wilson, W. A. Brown, *J. Phys. Chem. C.* **2010**, *114*, 6879-6893.
[84] Y. Sakamoto , K. Okumura, Y. Kizaki, S. Matsunaga, N. Takahashi, H. Shinjoh, *J. Catal.* **2006**, *238*, 361–368.
[85] M. Rocca, *Surf. Sci. Rep.* **1995**, *22*, 1-71.
[86] J.G. Chen, J.E. Crowell, J.T. Yates, *Surf. Sci.* **1987**, *187*, 243-264.

[87] T. Dellwig, J. Hartmann, J. Libuda, I. Meusel, G. Rupprechter, H. Unterhalt, H.-J. Freund, *J. Mol. Catal. A.* **2000**, *162*, 51–66.
[88] C. T. Campbell, A. W. Grant, D. E. Starr, S. C. Parker, V. A. Bondzie, *Top. Catal.* **2001**, *14*, 43-51.
[89] F. Rumpf, H. Poppa, M. Boudart, *Langmuir*. **1988**, *4*, 722-728.
[90] A. Borgna, B. G. Anderson, A. M. Saib, H. Bluhm, M. Havecker, A. Knop-Gericke, A.E.T. Kuiper, Y. Tamminga, J. W. Niemantsverdriet, *J. Phys. Chem. B.* **2004**, *108*, 17905-17914.
[91] A. Borgna, E. J. M. Hensen, L. Coulier, M. H. J. M. de Croon, J. C. Schouten, J. A. R. van Veen, J. W. Niemantsverdriet, *Catal. Lett.* **2003**, 90, 117-122.
[92] P. Moodley, J. Loos, J. W. Niemantsverdriet, P. C. Thune, *Carbon*. **2009**, *47*, 2002-2013.
[93] H. Liu, G. Cheng, R. Zheng, Y. Zhao, C. Liang, *J. Mol. Catal. A:* **2006**, *247*, 52-57.
[94] P. C. Thune, C. P. J. Verhagen, M. J. G. van den Boer, J. W. Niemantsverdriet, *J. Phys. Chem. B.* **1997**, *101*, 8559-8563.
[95] M. J. Lundwall, S. M. McClure, X. Wang, Z. Wang, M. Chen, D.W. Goodman, *J. Phys. Chem. C.* **2012**, *116*, 18155−18159.
[96] M. J. Lundwall, S. M. McClure, D. W. Goodman, *J. Phys. Chem. C.* **2010**, *114*, 7904−7912.
[97] R. M. Rioux, B. B. Hsu, M. E. Grass, H. Song, G. A. Somorjai, *Catal. Lett.* **2008**, *126*, 10−19.
[98] G. Szollosi, B. Torok, L. Baranyi, M. Bartok, *J. Catal*. **1998**, *179*, 619-623.
[99] M. A. Vannice, B. Sen, *J. Catal.* **1989**, *115*, 65-78.
[100] P. Gallezot, D. Richard, *Catal. Rev. Sci. Eng.*, **1998**, *40*, 81-126.
[101] P. Raylander, in *Catalytic hydrogenation in organic synthesis*, **1979**, page 78, Academic Press, New York.
[102] J. H. Billman, J. I. Stiles, J. Tounis, *Syn. Commun.* **1971**, *1***,** 127-131.
[103] A. Giroir-Fendler, D. Richard, P. Gallezot, *Stud. Surf. Sci. Catal*. **1988**, *41*, 171-178.
[104] M. Lashdaf, V.-V. Nieminem, M. Tiitta, T. Venalainen, H. Osterholm, O. Krause, *Micropor. Mesopor. Mater.*, **2004**, *75*, 149-158.
[105] F. Delbecq, P. Sautet, *J. Catal.* **1995**, *152*, 217-236.
[106] D. Loffreda, F. Delbecq, F. Vigne, P. Sautet, *J. Am. Chem. Soc.* **2006**, *128*, 1316-1323.
[107] S. Bhogeswararao, D. Srinivas, *J. Catal.* **2012**, *285*, 31-40.
[108] P. M. D. Collins, *Platinum Metals Rev.* **1986**, *30*, 141-146.
[109] V. I. Okafor, N. J. Coville, *S. Afr. J. Sci.* **1999**, *95*, 503-508.
[110] C. J. Campbell, J. H. Laherrere, *Scientific American*. **1998,** *March*, 78-84.
[111] S. M. Kumar, D. Chen, J. C. Walmsley, A. Holmen, *Catal. Commun.* **2008**, *9*, 747-750.
[112] G. A. Somorjai, K. McCrea, *Appl. Catal. A.* **2001**, 222, 3-18.
[113] B. C. Gates, J. R. Katzer, G. C. A. Schuit, in *Chemistry of Catalytic Processes.* McGraw-Hill, New York, **1979**, pp. 184-289.
[114] W. Yu, M. D. Porosoff, J. G. Chen, *Chem. Rev.* **2012**, *112*, 5780-5817.
[115] C. Lian, H. Liu, C. Xiao, W. Yang, K. Zhang, Y. Liu, Y. Wang, *Chem. Commun.* **2012**, *48*, 3124-3126.
[116] T. Mallat, Z. Bodnar, P. Hug, A. Baiker, *J. Catal.* **1995**, *153*, 131-143.
[117] M. Ilyas, M. Sadiq, *Chem. Eng. Technol.* **2007**, *30*, 1391-1397.
[118] F. Garin, G. Maire, *Acc. Chem. Res.* **1989**, *22*, 100-106.
[119] H. Du, C. Fairbridge, H. Yang, Z. Ring, *Appl. Catal. A.* **2005**, *294*, 1-21.
[120] M. J. Sterba, V. Haensel, *Ind. Eng. Chem. Prod. Res. Dev.* **1976**, *15*, 2-17.
[121] H. Connor, *Platinum Metals Rev.* **1961**, *5*, 9-12.
[122] P. Meriaudeau, C. Naccache, *Catal. Rev. Sci. Eng.* **1997**, *39*, 5-48.
[123] G. A. Somorjai, *Science*, **1985**, *227*, 902-908.
[124] A. K. Aboul-Gheit, S. A. –W. Ghoneim, *Recent Patents Chem. Eng*. **2008**, *1*, 113-125.
[125] C. T. O'connor, E. van Steen, M. E. Dry, in *Recent Advances and New Horizons in Zeolite Science and Technology*, (H. Chon, S. I. Woo, S. –E. Park, eds.), *Stud. Surf. Sci. Catal.* **1996**, *102*, 323-362.
[126] C. Perego, P. Ingallina, *Catal. Today*. **2002**, *73*, 3-22
[127] T. F. Degnan Jr, C. M. Smith, C. R. Venkat, *Appl. Catal. A.* **2001**, *221*, 283-294.
[128] A. de Klerk, R. J. J. Nel, *Energy Fuels*. **2008**, *22*, 1449-1455

[129] V. Haensel, US Patent, 2479110A, **1949**.
[130] S. Sivasanker, S. R. Padalker, *Appl. Catal.* **1988**, *39*, 123-126
[131] P. G. Smirniotis, E. Ruckenstein, *Appl. Catal.* **1995**, *123*, 59-88.
[132] J. Zheng, J. –L. Dong, Q. –H. Xu, Y. Liu, A. –Z. Yan, *Appl. Catal. A.* **1995**, *126*, 141-152.
[133] J. Biswas, G. M. Bickle, P. G. Gray, D. D. Do, in *Proc. 4th Int. Symposium*, (B. Delmon, G.F. Froment, eds.), *Stud. Surf. Sci. Catal.* **1987**, *34*, 553-565.
[134] P. Biloen, J. N. Helle, H. Verbeek, F. M. Dautzenberg, W. M. H. Sachtler, *J. Catal*. **1980**, 63, 112-118.
[135] A. Wootsch, Z. Paal, N. Gyorffy, S. Ello, I. Boghian, J. Leverd, L. Pirault-Roy, *J. Catal.* **2006**, *238*, 67-78.
[136] Z. Paal, P. Tetenyi, *J. Catal.* **1973**, *30*, 350-361.
[137] B. H. Davis, *Catal. Today*. **1999**, *53*, 443-515.
[138] Y. Barron, G. Maire, J. M. Muller, F. G. Gault, *J. Catal.* **1966**, *5*, 428-445.
[139] Z. Paal, R. Schlögl, *Surf. Sci.* **2009**, *603*, 1793–1801.
[140] A. Djeddi, I. Fechete, F. Garin, *Top. Catal.* **2012**, *55*, 700-709.
[141] Z. Paal, *Adv. Catal*. **1980**, *29*, 273-334.
[142] J. W. A. Sachtler, G. A. Somorjai, *J. Catal.* **1983**, *81*, 77-94
[143] T. R. Hughes, W. C. Buss, P. W. Tamm, R. L. Jacobson, *Stud. Surf. Sci. Catal.* **1986**, *28*, 725-732.
[144] J. D. Swift, M. D. Moser, M. B. Russ and R. S. Haizmann, *Hydrocarbon Technol. Int.* **1995**, 86.
[145] J. R. Bernard, in *Proc. 5th Int. Conf. Zeolite*, (L. V. Rees, ed.). Heyden London, **1980**, p. 686-695.
[146] C. Besoukhanova, J. Guidot, D. Barthomeuf, M. Breysse, J. R. Bernard, *J. Chem. Soc., Faraday Trans. 1*. **1981**, *77*, 1595-1604.
[147] A. P. J. Jansen , R. A. Van Santen, *J. Phys. Chem.* **1990**, *94*, 6764–6772.
[148] A. Y. Stakheev, E. S. Shpiro, N. I. Jaeger, G. Schulz-Eldoff, *Catal. Lett.* **1995,** *32*, 147-158.
[149] R. J. Davis, E. G. Derouane, *Nature*. **1991**, *349*, 313-315
[150] T. Fukunaga, V. Ponec, *J. Catal.* **1995**, *157*, 550-558.
[151] D. E. W. Vaughan, A. K. Ghosh, US Patent 4832824, **1989**.
[152] E. Mielczarski, S. B. Hong, R. J. Davis, M. E. Davis, *J. Catal.* **1992**, *134*, 359-369
[153] T. R. Hughes, W. C. Buss, P. W. Tamm, R. L. Jacobson, *Stud. Surf. Sci. Catal.* **1986**, *28*, 725-732.
[154] A. de Klerk, E. Furimsky, in *Catalysis in the Refining of Fischer-Tropsch Syncrude*. RSC Publishing, Cambridge, **2010**, p. 193-207.
[155] S. J. Tauster, J. J. Steger, *J. Catal.* **1990**, *125*, 387-389.
[156] A. Z. Ruiz, D. Bruhwiler, T. Ban, G. Calzaferri, *Monatshefte fur Chemie*. **2005**, *136*, 77–89.
[157] K. G. Azzam, G. Jacobs, W. D. Shafer, B. H. Davis, *J. Catal.* **2010**, *270*, 242–248.
[158] E. G. Derouane, D. J. Vanderveken, *Appl. Catal.* **1988**, *45*, L15-L22.
[159] B. C. Gates, *Chem. Rev.* **1995**, *95*, 511-522.
[160] E. Iglesia, J. F. Baumgartner, in *New Frontiers in Catal.* (L. Guczi, F. Solymosi, P. Teteny, eds.), *Proc. 10th Int. Congr. Catal.* Akad Kiado, Budapest, **1993**, *B*, 993-1006.
[161] E. Mielczarski, S. B. Hong, R. J. Davis, M. E. Davis, *J. Catal.* **1992**, *134*, 359-369.
[162] D. J. Ostgard, L. Kustov, K. R. Poeppelmeier, W. M. H. Sachtler, *J. Catal.* **1992**, *133*, 342-357.
[163] S. Jongpatiwut, P. Sackamduang, T. Rirksomboon, S. Osuwan, W. E. Alvarez, D. Resasco, *Appl. Catal. A*. **2002**, *230*, 177-193.
[164] G. Jacobs, F. Ghadiali, A. Pisanu, A. Borgna, W. E. Alvarez, D. Resasco, *Appl. Catal. A*. **1999**, *188*, 79-98.
[165] C. Dossi, R. Psaro, A. Bartsch, A. Fusi, L. Sordelli, R. Ugo, M. Bellatreccia, R. Zanoni, G. Vlaic, *J. Catal.* **1994**, *145*, 377- 383
[166] S. B. Sharma, P. Ouraipryvan, H. A. Nair, P. Balaraman, T. W. Root, J. A. Dumesic, *J. Catal.* **1994**, *150*, 234-242
[167] W. J. Han, A. B. Kooh, R. F. Hicks, *Catal. Lett.* **1993**, *18*, 193-208.
[168] A. de Klerk, *Green Chem.* **2007**, *9*, 560-565.
[169] G. A. Somorjai, F. Zaera, *J. Phys. Chem.* **1982**, *86*, 3070-3078.
[170] S. M. Davis, F. Zaera, G.A. Somorjai, *J. Am. Chem. Soc.* **1982**, *104*, 7453-7461.
[171] Z. Paál, H. Groeneweg, J. Paál-Lukács, *J. Chem. Soc., Faraday Trans.* **1990**, *86*, 3159-3166.
[172] A. Sárkány, *J. Chem. Soc., Faraday Trans. 1*. **1988**, *84*, 2267-2277.

[173] A. Sárkány, *Catal. Today*. **1989,** *5*, 173-184.
[174] K. Matusek, Z. Paal, *React. Kinet. Catal. Lett.* **1999**, *67*, 241-246.
[175] S. Jongpatiwut, P. Sackamduang, T. Rirksomboon, S. Osuwan, D. E. Resasco, *J. Catal.* **2003**, *218*, 1-11.
[176] S. Trakarnroek, S. Ittisanronnachai, S. Jongpatiwut, T. Rirksomboon, S. Osuwan, D. E. Resasco, *Chem. Eng. Comm.* **2007**, *194*, 946–961.
[177] M. M. J. Treacy, *Micropor. Mesopor. Mater.* **1999**, *28*, 271–292.
[178] J. T. Miller, D.C. Koningsberger, *J. Catal*. **1996**, *162*, 209-219
[179] W. C. Buss, L.A. Field, R.C. Robinson, US Patent, 4456527, **1984**.
[180] M. Vaarkamp, J. T. Miller, F. S. Modica, G. S. Lane, D. C. Koningsberger, *J. Catal.* **1992**, *138*, 675-685.
[181] G. B. McVicker, J. K. Lao, J. J. Ziemiak, W. E. Gates, J. L. Robbins, M. M. J. S. B. Rice, T. H. Vanderspurt, V. R. Cross, A. K. Ghosh, *J. Catal*. **1993**, *139*, 48-61.
[182] D. J. O'rear, C. –Y., Chen, S. J. Miller, WO Patent, 2010/080360A2, **2010**.
[183] L. A. Field, US Patent, 4627912, **1986**.
[184] C. D. Blessing, S. H. Brown, T. P. Cheung, D. J. Glova, D. M. Hasenberg, D. L. Holtermann, G. P. Khare, D. B. Korr Jr, US Patent, 20080027255A1, **2008**.
[185] M. E. Dry, R. J. Nash, C. T. O'Connor, in *Proc. 12th Inter. Zeolite Conf.* Baltimore, **1998**, 2557-2564.
[186] J. H. Clarke, *Green Chem.* **1999**, *1*, 1-8.
[187] N. Dimitratos, J. A. Lopez-Sanchez, G. J. Hutchings, *Chem. Sci.* **2012**, *3*, 20-45.
[188] J. Han, Y. Liu, R. Guo, *Adv. Funct. Mater.* **2009**, *19*, 1112-1117.
[189] H. Miyamura, R. Matsubara, S. Kobayashi, *Chem. Commun.* **2008**, 2031-2033.
[190] T. Mallat, A. Baiker, *Catal. Today*. **1994**, *19*, 247-284.
[191] M. Besson, P. Gallezot, *Catal. Today*. **2000**, *57*, 127-141.
[192] T. Mallat, A. Baiker, *Chem. Rev.* **2004**, *104*, 3037-3058.
[193] H. E. van Dam, L. J. Wisse, H. van Bekkum, *Appl. Catal.* **1990**, *61*, 187-197.
[194] M. S. Ide, D. D. Falcone, R. J. Davis, *J. Catal.* **2014**, *311*, 295-305.
[195] T. Mallat, Z. Bodnar, P. Hug, A. Baiker, *J. Catal.* **1995**, *153*, 131-143.
[196] Y. Liu, H. Abe, H. M. Edvenson, T. Ghosh, F. J. DiSalvo, H. D. Abruna, *Phys. Chem. Chem. Phys.* **2010**, *12*, 12978-12986.
[197] P. Gallazot, R. de Mesanstourne, Y. Christidist, G. Mattioda, A. Schouteeten, *J. Catal.* **1992**, *133*, 479-485.
[198] A. Deffernez, S. Hermans, M. Devillers, *Appl. Catal. A.* **2005**, *282*, 303-313.
[199] R. Anderson, K. Griffin, P. Johnston, P. L. Alters, *Adv. Synth. Catal.* **2003**, *345*, 517-523.
[200] H. G. J. de Wilt, H. S. van der Baan, *Ind. Eng. Chem. Prod. Res. Dev.* **1972**, 11, 374-378.
[201] L-W. H. Leung, M. J. Weaver, *Langmuir*. **1990**, *6*, 323-333.
[202] R. DiCosimo, G. M. Whitesides, *J. Phys. Chem.* **1989**, *93*, 768-775.
[203] Y. H. Ng, S. Ikeda, Y. Morita, T. Harada, K. Ikeue, M. Matsumura, *J. Phys. Chem. C.* **2009**, *113*, 12799-12805.
[204] R. P. A. Sneeden , R. B. Turner, *J. Am. Chem. Soc.* **1955**, *77*, 190-191.
[205] T. Mallat, A. Baiker, *Chem. Rev.* **2004**, *104*, 3037-3058.
[206] G. Kolb, V. Hessel, V. Cominos, C. Hofmann, H. Lowe, G. Nikolaidis, R. Zapf, A. Ziogas, E. R. Delsman, M. H. J. M. de Croon, J. C. Schouten, O. de la Iglesia, R. Mallada, J. Santamaria, *Catal. Today*. **2007**, *120*, 2-20.
[207] C. Keresszegi, T. Burgi, T. Mallat, A. Baiker, *New J. Chem.* **2001**, *25*, 1163-1167.
[208] G. J. teb Brink, I. W. C. E. Arends, R. A. Sheldon, *Adv. Synth. Catal.* **2002**, *344*, 355-369.
[209] J. W. E. Glattfeld, S. Gershon, *J. Am. Chem. Soc.* **1938**, *60*, 2013-2022.
[210] H. Kimura, K. Tsuto, *Appl. Catal. A.* **1993**, *96*, 217-228.
[211] H. H. C. M. Pinxt, B. F. M. Kuster, G. B. Marin, *Appl. Catal. A.* **2000**, *191*, 45-54.
[212] C. Keresszegi, T. Mallat, J-D Grunwaldt, A. Baiker, *J. Catal.* **2004**, *225*, 138-146.
[213] M. S. Ide, D. D. Falcone, R. J. Davis, *J. Catal.* **2014**, *311*, 295-305.
[214] H. Lefranc, *EP 0667331B1*. Rhodia Chimie, France, **1999**.
[215] D. Nakashima, Y. Ichihashi, S. Nishiyama, S. Tsuruya, *J. Mol. Catal. A.* **2006**, *259*, 108-115.
[216] X. Li, B. Lu, J. Sun, X. Wang, J. Zhao, Q. Cai, *Catal. Commun.* **2013**, *39*, 115-118.
[217] T. Sanada, C. Murakami, K. Gora-Marek, K. Iida, N. Katada, K. Okumura, *Catalysts*. **2013**, *3*, 599-613.

3. Results and Discussion

3.1 The Model Pt Catalysts on Flat Two-Dimensional Support

This chapter describes the experimental work performed by the author. Supported platinum catalysts were prepared on flat two-dimensional (2-D) model supports and on three-dimensional (3-D) porous zeolite supports for selective transformations of organic materials. Results generated in preparation of model Pt catalysts are grouped in Section 3.2. This is followed by the results describing the catalytic applications of these catalysts in organic transformations in Sections 3.3 to 3.4. The last section of this chapter, Section 3.5, is dedicated to the preparation of Pt catalysts supported on zeolites and their applications in dehydrogenation reactions, especially dehydrocyclisation of alkanes to aromatic compounds.

Characterisation of model Pt catalysts on a flat 2-D support was performed utilising surface science techniques such as X-ray photoelectron spectroscopy (XPS), transmission electron microscopy (TEM) and Rutherford Backscattering Spectroscopy (RBS). The zeolite supported catalysts were characterised by physisorption and chemisorption studies, thermal analysis and inductively coupled plasma – optical emission spectroscopy (ICP-OES). Other general techniques used included ^{1}H NMR and Fourier Transform Infrared (FTIR).

3.2 Preparation of Model Pt Catalysts on Flat 2-D Supports

The flat 2-D support used to prepare the model Pt catalysts in this study was a single sided polished silicon wafer (Si-wafer) with (100) surface orientation. Before platinisation of the Si-wafer with the Pt precursor, surface silanol groups (-Si-OH) were generated and reacted with allyltrimethoxysilane and 3-aminopropyltrimethoxysilane to generate an allyl or an amino surface. The surface silanol groups and immobilised surface allyl and amino derivatives were used as anchoring sites or reactive surface points to react with a suitable Pt precursor during platinisation.

3.2.1 Pre-treatment of Silicon Wafer (Si-wafer) as a Model Catalyst Support

The surface of a Si-wafer was activated in a 3-step process first by thermal oxidation to produce a thin surface layer of amorphous SiO_2 (a bridged -Si-O-Si- network). This layer was previously characterised to be 3-90 nm thick. [1,2,3] Hydroxylation of this Si-O-Si layer to liberate surface silanol groups (Si-OH) followed. Finally, subsequent silanation of the surface Si-OH groups with appropriate silanes liberated a surface with pseudo-bidentate ligands. The preparation sequence is outlined in Scheme 3.1.

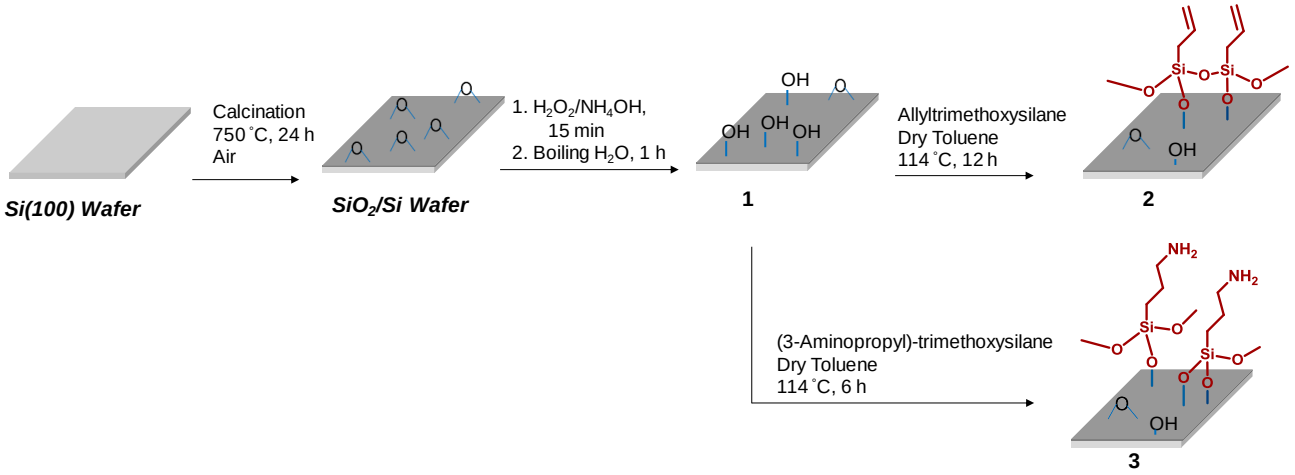

Scheme 3.1. The outline of the 3-step procedure used to activate the polished surface of Si-wafer.

The success of the first step, thermal oxidation to form a thin layer of surface silicon dioxide (SiO_2) was first noted by a slight colour change from grey to a slightly darker grey colour of the surfaces of the Si-wafer (Figure 3.1b). The colour changes which indicate the increasing thickness of the SiO_2 on the surface of Si-wafer are more pronounced when thermal oxidation is done at 1000 °C using wet molecular oxygen as an oxidant. When wet oxidation is used, the oxidised Si-wafer becomes green in colour which indicates a rather thick layer of surface SiO_2 (Figure 3.1c). Si-wafer samples that were oxidised by wet oxidation were not used in subsequent steps due to a concern that the resultant SiO_2 layer is too thick and might reduce the weak conductance of the elemental Si. This would be detrimental in XPS analysis.

XPS analysis further confirmed that the amount of native SiO_2 on the surface of Si-wafer increased after thermal oxidation at 750 °C. The XPS data in Figure 3.2a shows peaks at binding energies 103 eV and 99.5 eV due to Si 2p core level electrons of the native SiO_2 layer and bulk elemental Si of the untreated Si-wafer respectively. The intensity of the Si 2p peak at 103 eV (for SiO_2 contribution) increased from 400 c/s (c/s = counts per second) to about 800 c/s while the Si 2p peak at 99.5 eV (for elemental Si contribution) was not detectable after thermal oxidation (Figure 3.2b). As the top layer of SiO_2 increases *via* thermal oxidation, the electrons from elemental Si underneath the surface SiO_2 layer has insufficient energy for emission and detection during XPS analysis. The SiO_2 layer grown by thermal oxidation at 750 °C for 24 h, can be as thick as 90 nm which is enough to prevent the detection of the electrons from underneath the surface.[1]

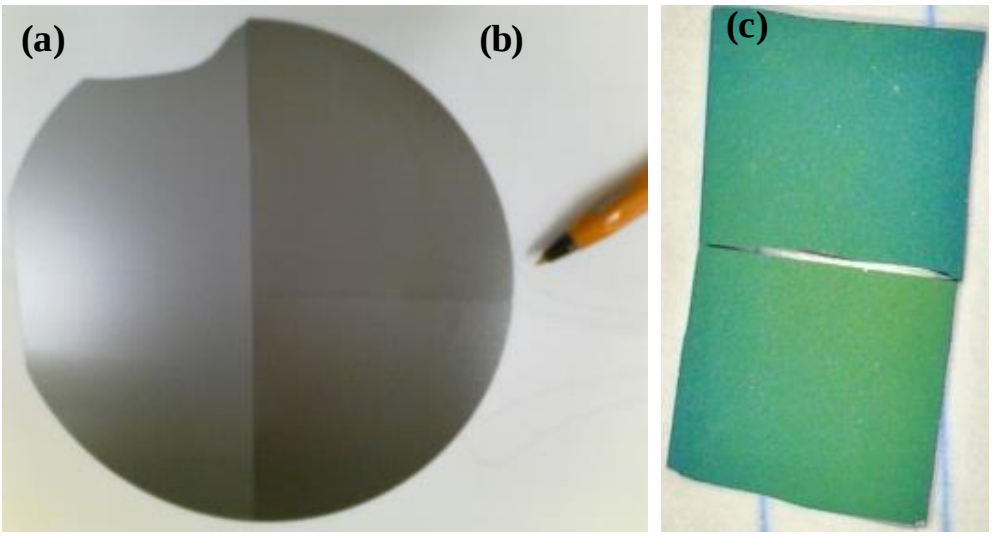

Figure 3.1. Photographs of Si-wafer samples (a) before thermal oxidation (*i.e.* a metallic 100 Si surface, (b) thermal oxidation in air at 750 °C to generate a thin Si-O-Si surface and (c) wet oxidation in wet molecular oxygen at 1000 °C (a much thicker Si-O-Si surface is generated).

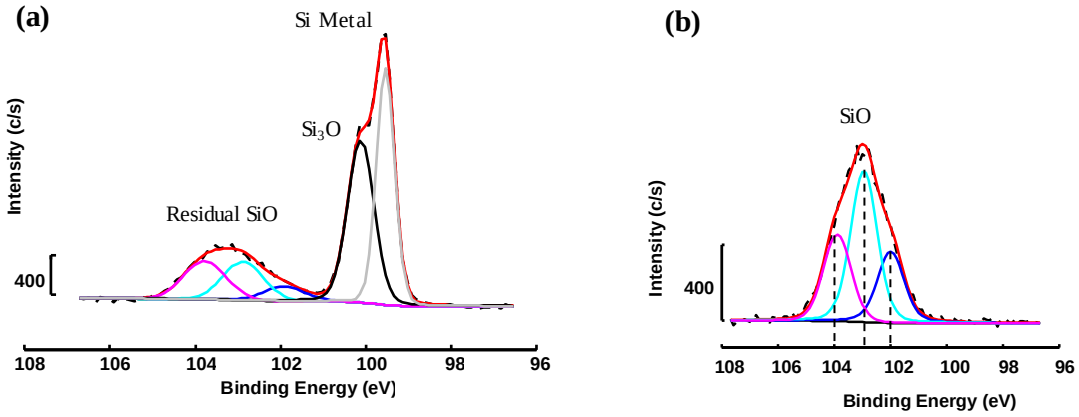

Figure 3.2. A comparison of XPS Si 2p spectra collected from (a) an untreated sample of Si-wafer (b) a sample of Si-wafer after thermal oxidation. (see Table 3.1 for explanation of the different peaks fitted having $1 \leq n \leq 4$. Dotted black line: experimental curve. Red line: Theoretically fitted curve. Other lines: Peaks theoretically introduced to replicate the experimentally determined curve.

The curve fitting of Si 2p signals obtained from XPS analysis of untreated Si-wafer showed three peaks at about 103 eV and two peaks at about 100 eV. These peaks correspond to Si^0 (elemental Si) and oxides of Si^+ (interphase layer), Si^{2+}, Si^{3+} and Si^{4+} as summarised in Table 3.1. After thermal oxidation, only Si oxides species nearer to the surface were detected by XPS. The interphase layer which is made of Si^+ oxide and the elemental Si were not detected due to the thickness of surface SiO_2.

Table 3.1. Relative binding energies of Si 2p core level electrons obtained from XPS analysis of untreated and oxidised Si-wafers.

	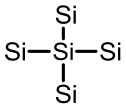 Si^0	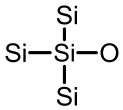 Si^+	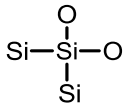 Si^{2+}	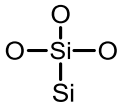 Si^{3+}	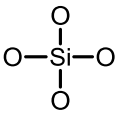 Si^{4+}
	Binding energy (eV)				
Clean Si-wafer	99.5	100.1	101.9	102.9	103.8
Oxidised Si-wafer	-	-	101.9	102.8	103.7
Comparative literature data[4]	99.5	100.5	101.1	102.4	103.9

The oxidised Si-wafer with a layer of surface SiO_2 is still not suitable to immobilise the Pt species in solution because the silica layer is inert towards metal complexation and has poor wetting capability.[5] Therefore, the surface of SiO_2 was hydroxylated to form silanol groups on surface **1** which were immediately silanated without further characterisation (see Scheme 3.1).

XPS samples including Si-wafer samples most often have adventitious carbon contamination which is detected by XPS analysis[6,7] and at times the C 1s spectral peak of the residual carbon contamination overlaps with the crucial surface anchored compound C peaks of interest during the XPS measurements.[8,9] The intensity of XPS carbon spectral peak at 284.8 eV due to residual carbon on the surface of hydroxylated Si-wafer **1** was used as background blank and subtracted in analysis of silanated wafer **2**. Successful silanation with allyltrimethoxysilane to form surface **2** was confirmed by XPS data which showed an increase in intensity of the C 1s residual peak (284.8 eV) from 620 c/s in surface **1** to 1315 c/s after silanation. This increase can be attributed to allyl C 1s contribution from immobilised allyltrimethoxysilane. Furthermore, the XPS spectrum of surface **2** showed a C 1s peak with a new asymmetrical shape which indicated overlapping peaks at 283 – 288 eV region (Table 3.2). The overlapping C 1s peaks were deconvoluted into two peaks which were centred at binding energies 286.7 eV and 284.8 eV, and are respectively consistent with the binding energies of C 1s in methoxy groups and C 1s in allyl groups ($=CH_2$, =CH and $-CH_2$) of allyltrimethoxysilane.[10] The intensity of C 1s at binding energy 284.8 eV is 1315 c/s. This value includes the contribution from allyl atoms as well as the 620 c/s from residual carbon on clean Si-wafer surfaces. Therefore the peak intensity due to allyl atoms only is 695 c/s. Based on these calculations, the ratio of the peak intensities at 286.7 and 284.8 eV due to the allyl-anchored derivative is 1:3. The same ratio was obtained when the peak areas at 286.7 eV and 284.8 eV were used instead of peak intensities. The observed peak ratio implies that on average only one methoxy group per reacting allylsilane is chemically bound to the Si surface, one remained unreacted and is

still bound to the silane Si centre and the third may form a bridge between the two silane Si centres (see Table 3.2).

Table 3.2. XPS spectra of C 1s region from the analysis of surfaces **1** and **2**. In both XPS peaks, the black line represents the experimentally measured curve. In the XPS peak of surface **1**, the blue line is the theoretical fitted curve. In the XPS peak of surface **2**, the red line is the theoretically fitted curve and the other lines are peaks theoretically introduced to replicate the experimentally determined curve.

Pre-treated Si-wafer	XPS C 1s peak	C 1s description and Binding energy (eV)
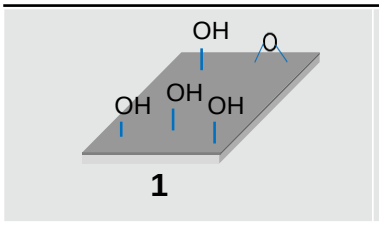	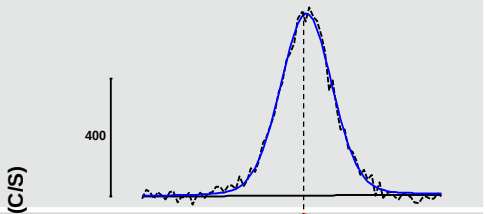	Residual C 1s at 284.8 eV
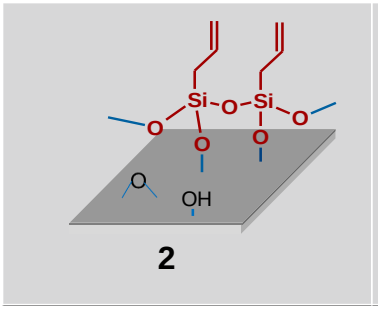	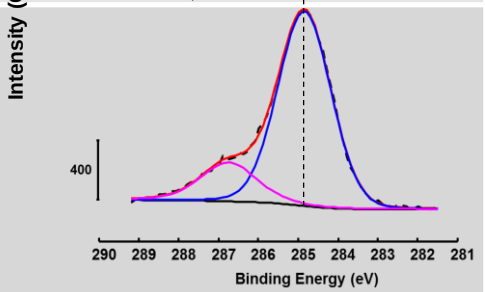	Allyl C 1s at 284.8 eV Methoxy C 1s at 286.7 eV Intensity Ratio = 1:3

Complete hydrolysis of the methoxy groups can be achieved by a prolonged silanation step to more than 48 h.[11] However, refluxing methoxysilanes for extended period to achieve complete silanation also runs a risk of cluster formation as shown by a TEM micrograph of silanated Si-wafer samples after silanation for 12 h and 48 h in Figure 3.3. It is important to use dilute silanation solutions under dry conditions to prevent polymerisation and cluster formation. Only surface **2** (see Scheme 3.1) with typical TEM micrograph in Figure 3.3a which was obtained by silanation for 12 h, was used in platinisation procedure. The surface used is free from clusters that might interfere in subsequent analysis and yet it has immobilised surface allyl groups to react in platinisation step.

The results discussed in this section showed that the flat model support, Si-wafer was successfully oxidised followed by silanation with allyltrimethoxysilane to form surface **2**. The results from silanation with 3-aminopropyltrimethoxysilane to form aminated surface **3** (Scheme 3.1) are discussed in section 3.2.5.

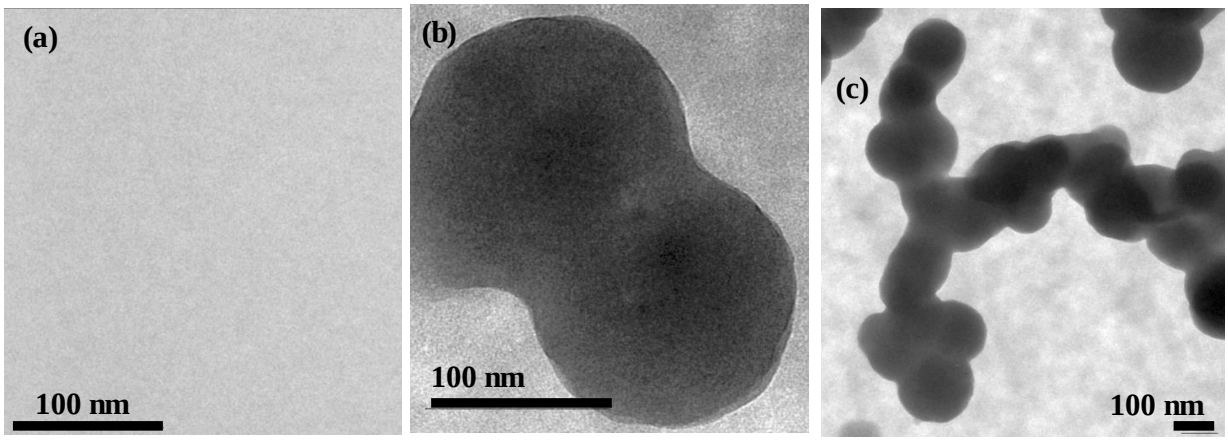

Figure 3.3. TEM micrographs of Si-wafer with allyl groups obtained (a) after silanation with allyl methoxysilane for 12 h under reflux and (b)-(c) after silanation for 48 h. Surface **2** represented by TEM micrograph (a) which is free from clusters was used in platinisation step.

3.2.2 Platinisation of Si-wafer: Pt(IV) Coordination to Immobilised Pseudo-Bidentate Ligands

Two procedures, chemical grafting and spin coating (schematically illustrated in Scheme 3.2), were followed to react the $H_2PtCl_6 \cdot 6H_2O$ with allyl groups on surface **2**. Chemical grafting was used to mimic the well-known reductive complexation of platinum salts with olefins *via* ligand exchange[12] and spin coating is the 2-D equivalent of wet incipient impregnation which is used to immobilise metal species on 3-D solid support. In the chemical grafting approach, a solution of 10 mM hexachloroplatinic acid ($H_2PtCl_6 \cdot 6H_2O$) in ethanol was reacted with the immobilised allylsilane at room temperature (*ca.* 25 °C) for 24 h. This method was also adapted by refluxing the reactants at 60-70 °C for 30 min.

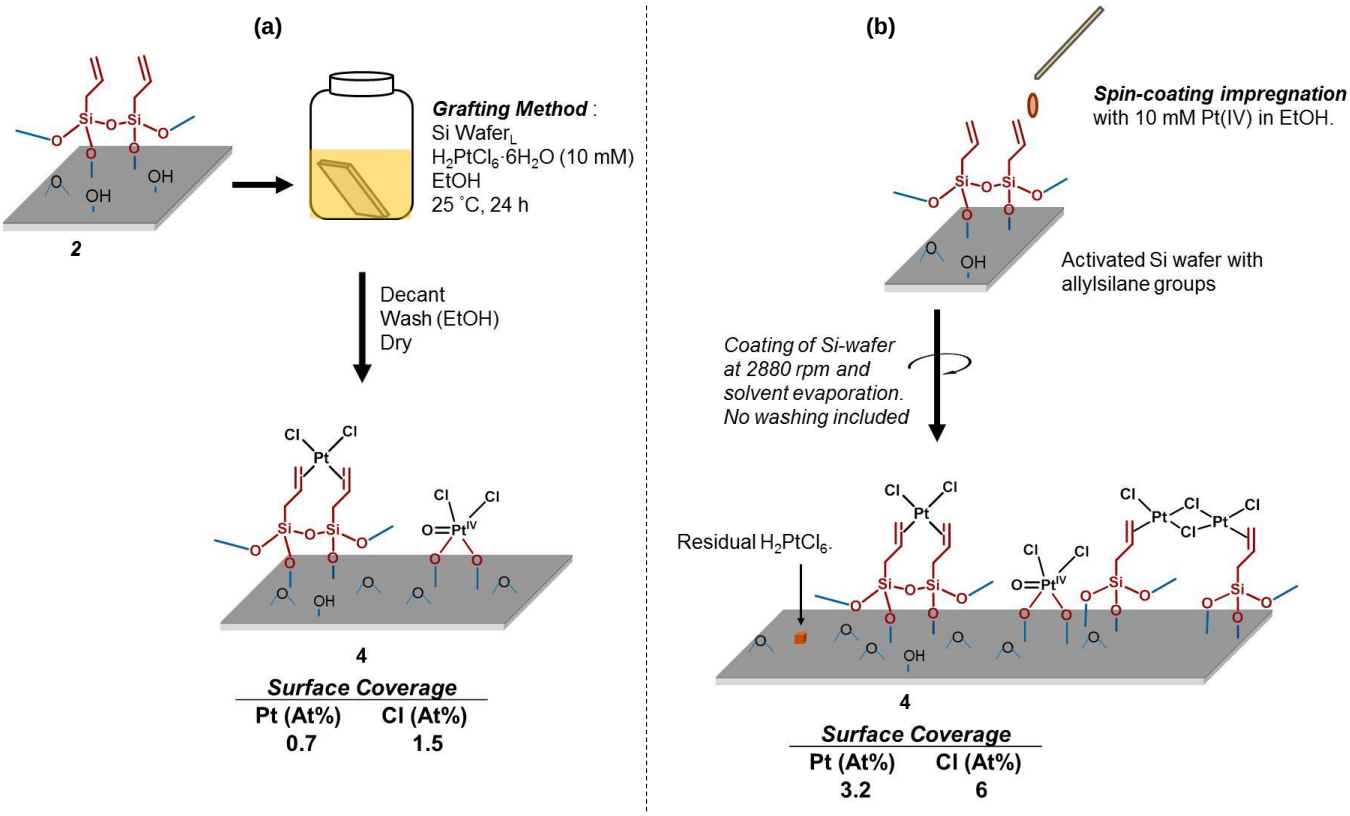

Scheme 3.2. (a) The outline of the procedure used to graft 10 mM Pt(IV) solution on activated Si-wafer and (b) the outline of the spin coating procedure. Also provided are the atomic ratios of Pt to Cl on surface **4**. The bonding motives of surface **4** are idealised but serve to explain qualitatively what happens on the surface. XPS data which are consistent with the shown bounding motives are in Figure 3.4.

XPS analysis of the platinum-grafted and spin coated Si-wafers (surface **4**, Scheme 3.2) gave a quantitative indication of the atomic composition and the oxidation states of Pt in the resultant species coating the surface of the Si-wafer. Among the species detected, the XPS spectra of the Pt on surface **4** showed distinct Pt 4f spin-orbit-split doublets[i] or spin doublets[13] (Pt $4f_{7/2}$ and Pt $4f_{5/2}$) and overlapping spin doublets of Cl 2p (Cl $2p_{3/2}$ and Cl $2p_{1/2}$) in all platinised samples as illustrated in Figure 3.4.

[i] The spin-orbit-split doublet are spin doublets caused by the split which takes place in p, d, and f levels due to x-ray ionisation. The resultant XPS peaks are spin doublets caused by the vacancies in $p_{1/2}$, $p_{3/2}$, $d_{3/2}$, $d_{5/2}$, $f_{5/2}$, and $f_{7/2}$.

(a) Grafting Method

Pt 4f7/2 (eV)		FWHM(eV)	Chi Sq
Pt^{2+}	72.4	2.2	2.0
Pt^{4+}	73.6	2.0	

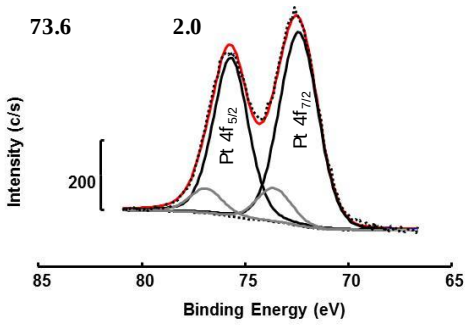

Cl 2p (eV)		FWHM(eV)	Chi Sq
Pt-Cl	198.5	1.6	1.0
Pt-Cl	200.1	1.5	

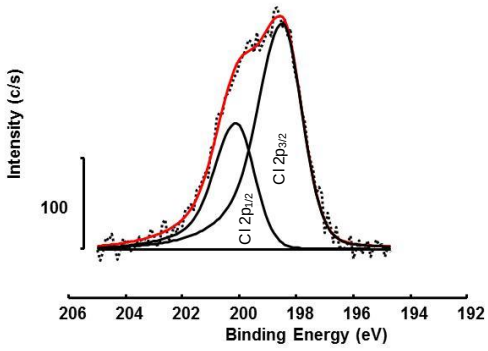

O 1s(eV)		FWHM(eV)	Chi Sq
Pt^{4+}=O	530.0	1.3	0.6
Pt^{4+}-O	531.1	1.3	
Si-O	532.6	1.9	

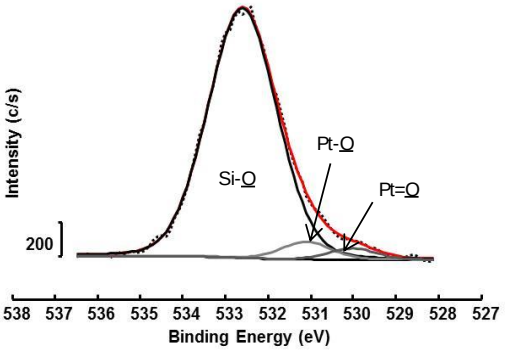

(b) Spin Coating Method

Pt $4f_{7/2}$ (eV)		FWHM	Chi Sq
Pt^{2+}	73.0	2.1	6.5
Pt^{4+}	75.2	1.8	

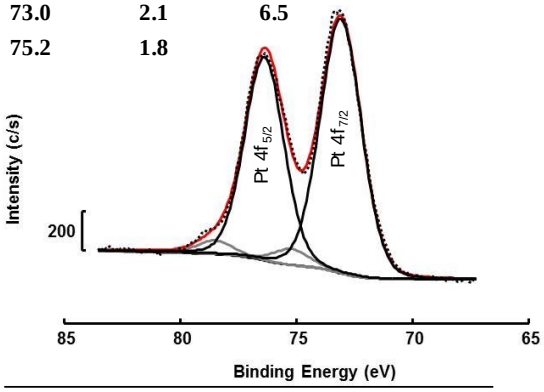

Cl 2p (eV)		FWHM(eV)	Chi Sq
Pt-Cl	198.7	1.5	1.2
Pt-Cl	200.3	1.5	
μ-Cl	199.9	1.4	
μ-Cl	201.5	1.5	

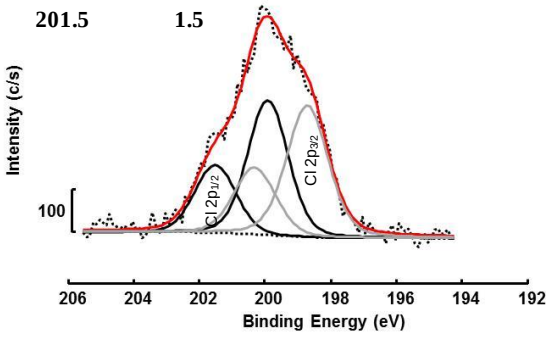

O 1s (eV)		FWHM (eV)	Chi Sq
Si-O	532.6	1.7	3.0

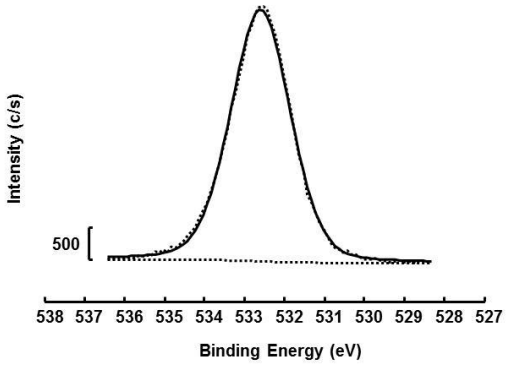

Figure 3.4. XPS data of Pt 4f, Cl 2p and O 1s from the analysis of platinised Si-wafers **4** prepared by (a) grafting and (b) spin coating. FWHM: Full Width at Half Maximum, Chi Sq: Chi Square, a goodness of fit. Red line: theoretical fitted. Dotted black line: experimentally measured curve. Other lines: peaks theoretically introduced to replicate the experimentally determined curve.

On the basis of peak area obtained for Pt 4f and Cl 2p peaks, the relative ratio of atomic Pt to Cl was calculated to be 1:2 in both samples prepared by spin coating and grafting at room temperature. The observed ratio of Pt to Cl implies that $H_2PtCl_6 \cdot 6H_2O$ retains only two Cl atoms during the reaction with the immobilised pseudo-bidentate ligand in surface **2** as shown by the proposed structures in Scheme 3.2 and Figure 3.5. The retained Cl atoms are attached to the Pt as can be confirmed by the Pt^{2+} oxidation state which is derived from the binding energies of the symmetrical Pt $4f_{7/2}$ peaks at 72.4 and 73.0 eV in grafted and spin coated samples respectively.

The shift in binding energies of the Pt $4f_{7/2}$ peaks are within the range of the Pt^{2+} oxidation state[14] and confirm that $H_2PtCl_6 \cdot 6H_2O$ was reduced from the Pt^{4+} oxidation state (found at 75.3 eV based on the Pt $4f_{7/2}$ peak)[15] to form an immobilised Pt^{2+} complex on surface **4**. Since the separation of the Pt 4f spin-orbit-split doublets is always constant at 3.3 eV, the binding energy of Pt $4f_{5/2}$ is not elaborated in determining the oxidation states of the Pt species. The retained Cl atoms in the Pt complex were detected at binding energies in the 198.5 - 199.9 eV due to Cl $2p_{3/2}$ contribution in grafted and spin coated samples. The observed Cl $2p_{3/2}$ corresponds to the literature value of 199.1 eV for the crystalline dichloro(1,5-cyclootadiene)platinum (II) which has adjacent Cl atoms as the Pt^{2+} complex proposed in surface **4** (Figure 3.5).[16]

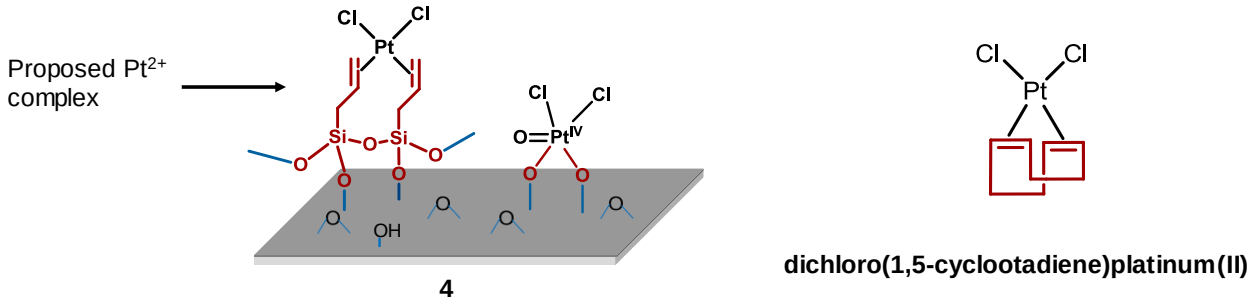

Figure 3.5. Proposed π-olefin Pt^{2+} complexation in surface **4** and a chemical structure of dichloro(1,5-cyclootadiene)platinum (II).

Based on the atomic ratio obtained for Pt and Cl (*i.e.* 1:2), and the Pt^{2+} oxidation state of the Pt specie on surface **4**, one can conclude that $H_2PtCl_6 \cdot 6H_2O$ reacted on the grafting approach with the allyl groups attached on surface **2** to form an immobilised π-olefin $Pt(allyl)_2Cl_2$ complex as depicted in Figure 3.5. At the same time, the C 1s signal at *ca*. 283.5 eV which correspond to the Pt-C contribution[17] could not be resolved from the large residual carbon peak at 284.8 eV and thus the binding mode of allyl groups to the Pt centre could not be confirmed. The C 1s signal contribution by Pt-C interaction was probably overshadowed by the large C 1s signal contributed by the immobilised allylsilane and residual carbon contamination. Since the XPS data could not prove unambiguously the coordination mode of the allyl groups to Pt in surface **4**, additional Pt-alkene coordination reactions in homogeneous solutions were performed as discussed in Section 3.2.3 below.

In both the grafting and spin coating procedures used to prepare platinised surface **4**, additional Pt $4f_{7/2}$ peaks were observed at binding energies of 73.6 eV and 75.2 eV due to the presence of Pt^{4+} species in surface **4**. In the grafted sample (see Figure 3.4a), the Pt^{4+} species was most likely due to the adsorbed $-(SiO)_2-Pt(O)Cl_2$ complex which is formed by the reaction of $H_2PtCl_6 \cdot 6H_2O$ with the residual surface Si-OH groups. The binding energy of the core level electrons of O 1s at 531.1 eV and 530.0 eV in the grafted sample confirmed the presence of surface Pt-O and Pt=O respectively (Figure 3.4a). According to the published literature, the Pt-O specie has a binding energy of about 530.5 eV [17] while Pt=O specie has a binding energy of 530.0 eV.[18]

The abnormally high binding energy of Pt^{4+} (*i.e.* 75.2 eV) in spin coated sample was due to the small amount of the unreacted $H_2PtCl_6 \cdot 6H_2O$ (*ca.* 6% of the surface Pt) which remained on surface **4** after the solvent evaporation. Pt^{4+} halides have higher binding energies compared to other Pt^{4+} analogues.[13] The literature value of $H_2PtCl_6 \cdot 6H_2O$ binding energy is 75.3 eV based on the Pt $4f_{7/2}$ peak and the Cl $2p_{3/2}$ binding energy is 199.1 eV.[15] In the case of surface Cl species in spin coated samples, the Cl 2p peak could be deconvoluted into two sets of spin doublets with Cl $2p_{3/2}$ binding energies of 198.7 eV and 199.9 eV presented in Figure 3.4b. The Cl $2p_{3/2}$ peak with binding energy

of 198.7 eV is due to Pt-Cl contribution. The Cl $2p_{3/2}$ peak at 199.9 eV is due to the Pt-μ-Cl)-Pt bridge and is mutually consistent with the Cl $2p_{3/2}$ at 200.5 eV for di-μ-chlorobis[(1,2-η-)-1-hexene]diplatinum(II).[ii] In summary, the overall XPS data suggest that grafting at ambient conditions and spin coating impregnation of 10 mM Pt^{4+} solution successfully platinised the pre-treated Si-wafer samples to form immobilised Pt^{2+} complexes on surface **4**, although more than one species exists on the surface.

Grafting by refluxing the Pt^{4+} solution at 60 °C was also attempted to optimise the platinisation protocol. After heating the Pt solutions under reflux for 30 min in the presence of silanated Si-wafer **2**, a considerable amount of Pt^{4+} was reduced to Pt^{2+} and coordinated to the immobilised allyl ligands. This was ascertained by XPS analysis of the platinised sample which exhibited a Pt $4f_{7/2}$ core level signal with binding energy at 72.7 eV due to the Pt^{2+} contribution (see Figure 3.6).

Unlike grafting at room temperature for 24 h which achieved a Pt^{2+} complex on surface **4**, grafting at elevated temperatures also exhaustively reduced the Pt^{4+} precursor to form a zero-valent Pt species as suggested by the Pt $4f_{7/2}$ peak at 71.7 eV (see Figure 3.6). Of the Pt species detected on the surface of platinised Si-wafer, about 54 % were due to Pt^{2+} species and 26 % due to Pt^{0} species on the basis of peak area measurements. The rest of the analysed Pt was due to the non-reduced Pt^{4+} which contributed to the Pt $4f_{7/2}$ with the binding energy of 74.0 eV.

The calculated atomic ratio of Pt:Cl on the surface of platinised Si-wafer was 1:3. This ratio gives an indication that the Pt complexes retain some Cl atoms after grafting at 60 °C. Since Cl atoms are distributed between the unreacted Pt^{4+} precursor and Pt^{2+} complex similar to that of surface **4**, it was deemed inaccurate to interpret the calculated ratio between Pt and Cl atoms at 60 °C experiment in terms of all possible bonding motives.

[ii] di-μ-chlorobis[(1,2-η-)-1-hexene]diplatinum(II) was prepared by reaction of 1-hexene with $H_2PtCl_6 \cdot 6H_2O$ at 60 °C for 1 h. For more details on preparation and characterisation of di-μ-chlorobis[(1,2-η-)-1-hexene]diplatinum(II), see section 3.2.3.

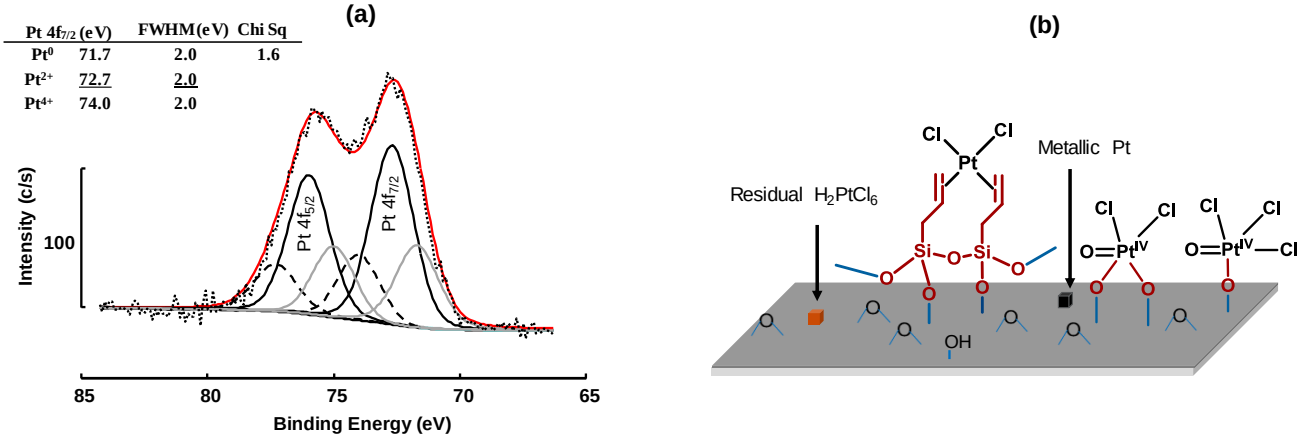

Figure 3.6. (a) XPS data of Pt 4f from the analysis of platinised Si-wafers prepared by grafting at 60 °C (Scheme 3.2 and Figure 3.4 show results for grafting at 25 °C). FWHM: Full Width at Half Maximum, Chi Sq: Chi Square, a goodness of fit. Red line: theoretical fitted curve. Dotted black line: experimentally measured curve. Other lines: peaks theoretically introduced to replicate the experimentally determined curve. (b) The silica wafer carton explains a proposed bonding motive based on the XPS results.

In conclusion, this section showed that Pt^{4+} precursor was successfully incorporated on the surface of silanated SiO_2/Si-wafer to liberate a platinised surface. The resultant surface Pt^{2+} complex had a Pt:Cl atomic ratio of 1:2 for grafting and spin coating experiments performed.

3.2.3 Elucidation of the Binding Mode of Immobilised Pseudo-Bidentate Ligand to Pt Centre

The XPS data of platinised Si-wafers suggested that $H_2PtCl_6 \cdot 6H_2O$ reacts with the immobilised allylsilane ligand to form a Pt^{2+} complex most likely resembling surface **4**. The precise nature of allyl coordination to the metal centre could not be determined using the collected XPS data. To elucidate the binding mode of allyl groups to the metal centre, solutions of bidentate and monodentate ligands with olefin functional group were reacted separately with $H_2PtCl_6 \cdot 6H_2O$ solutions in ethanol in two

set of conditions (i) 60 °C for 30 min and (ii) room temperature (*ca*. 25 °C) for 24 h. Among the ligands evaluated, 1,3-divinyltetramethyldisiloxane and allyltrimethoxysilane were most ideal because they closely resemble the backbone of the immobilised pseudo-bidentate ligand in surface **2** (see Figure 3.7). However, these ligands decomposed under the experimental conditions and no products could be conclusively identified.

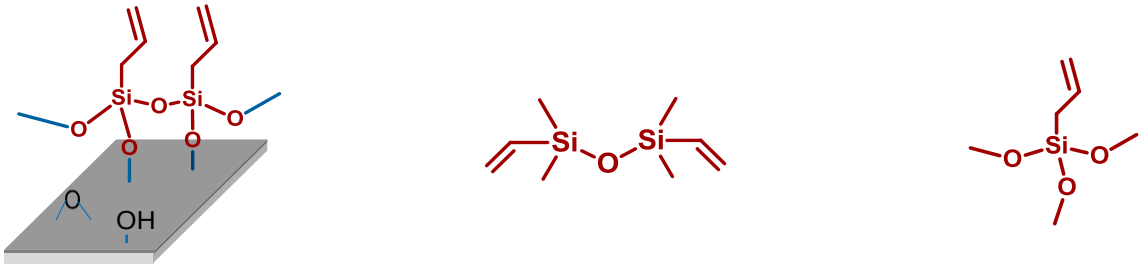

Surface **2** 1,3-divinyltetramethylsiloxane **5** Allytrimethoxysilane **6**

Figure 3.7. A comparison of the immobilised pseudo-bidentate ligand in surface **2** relative to the homogeneous bidentate and monodentate ligands **5** and **6**.

1,5-Cyclooctadiene **7** was identified as a suitable alternative to elucidate the binding mode of the immobilised pseudo-bidentate ligand. At 60 °C, 1,5-cyclooctadiene reacts with $H_2PtCl_6 \cdot 6H_2O$ to form a known complex, dichloro(1,5-cyclootadiene)platinum (II) **8** (Scheme 3.3). The coordination of the 1,5-cyclooctadiene to Pt centre was confirmed by the ^{1}H NMR data of the Pt complex **8** which showed multiplets for axial and equatorial methylene protons at chemical shifts 2.25 and 2.69 ppm due to the locked boat conformation of 1,5-cyclooctadiene. The oxidation state of Pt in **8** was determined by ^{195}Pt NMR analysis where a singlet was detected at -3337.0 pm which is consistent to Pt^{2+} chemical shift properties. ^{195}Pt NMR analysis distinguishes the chemical shift regions for Pt^{0} upfield of -4000 ppm, for Pt^{2+} between -2500 ppm and -4000 ppm, and downfield of -2500 ppm Pt^{4+}.[19,20] The most important feature of **8** is that it retains two Cl atoms and Pt^{2+} oxidation state which is the same as the immobilised π-olefin Pt^{2+} complex on surface **4** (see Scheme 3.2). Since the

Pt and Cl XPS peak positions are very similar to those of the proposed surface **4**, see Figure 3.4 and text above Figure 3.5, one can conclude that the coordination of immobilised pseudo-bidentate ligands to the Pt centre is very similar to the binding of **7** to form Pt^{2+} complex **8**. The crystal structure of **8** is also known.[21]

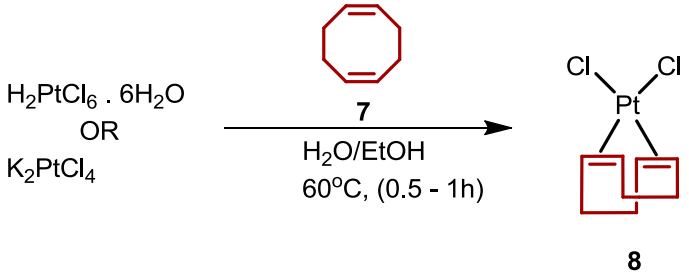

Scheme 3.3. The reaction of 1,5-cyclooctadiene with hexachloroplatinic acid to form dichloro(1,5-cyclootadiene)platinum (II) **8**.

Secondly, the reaction of excess 1-hexene with $H_2PtCl_6 \cdot 6H_2O$ or K_2PtCl_4 at 60 °C formed the π-olefin complex di-μ-chlorodichlorobis[(1,2-η-)-1-hexene]diplatinum(II), **9** which has a π-binding mode similar to the postulated complex on surface **4** (see Figure 3.8). When $H_2PtCl_6 \cdot 6H_2O$ is used as a Pt precursor, only trace amounts of **9** are observed on the ^{1}H NMR spectrum. The reaction of excess 1-hexene with K_2PtCl_4 forms Pt complex **9** in yield of 59 %.

The structure of complex **9** was derived from the ^{1}H NMR data, elemental analysis and the XPS data of the reaction product. The ^{1}H NMR analysis revealed three broad signals at chemical shift range 5.6 to 4.6 ppm corresponding to the protons of coordinated olefin group. When compared to the ^{1}H NMR spectrum of free ligand 1-hexene which has alkene protons centred at 5.8 ppm and 5.0 ppm, the alkene protons of coordinated 1-hexene shift upfield. The observed shift in alkene protons implied the loss of olefinic character after coordination to the metal centre. Elemental analysis of C and H in pure reaction product gave 20.7 and 3.1 % respectively. This C and H content

is very close to the theoretical content of 20.6 and 3.5 % expected for the chemical structure of **9**, $C_{12}H_{24}Cl_4Pt_2$.

(a)

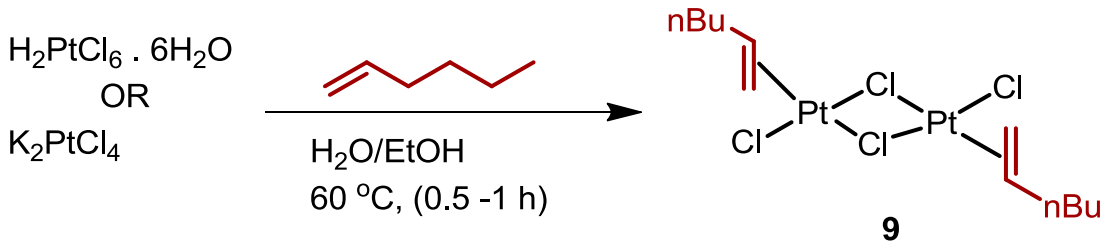

9

(b)

Elemental Analysis (%)		
	Calculated for $C_{12}H_{24}Cl_4Pt_2$	*Found*
C	20.57	20.74
H	3.45	3.14

(c) Alkene protons of neat 1-hexene

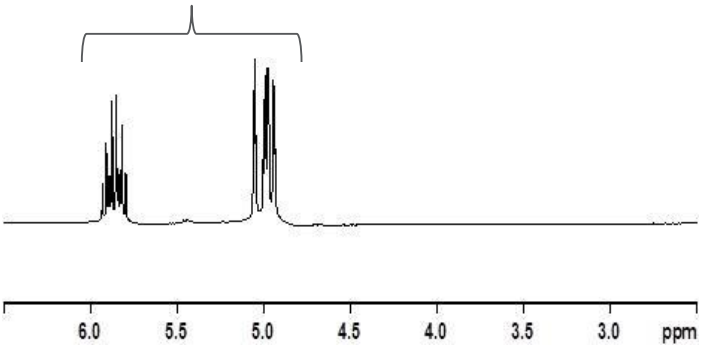

Alkene protons of Pt coordinated 1-hexene

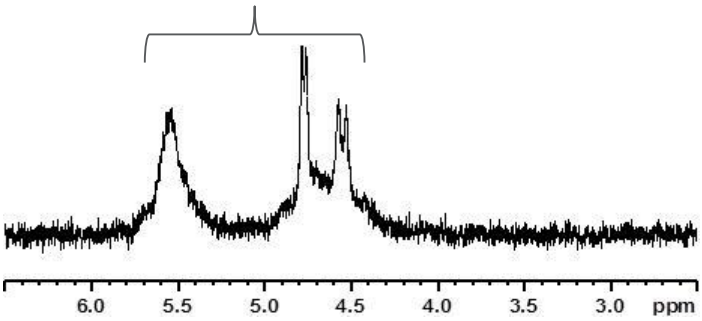

Figure 3.8. (a) The reaction of monodentade ligand, 1-hexene with $H_2PtCl_6 \cdot 6H_2O$ or K_2PtCl_4 to form complex **9** and (b) the results from elemental analysis of **9** and (c) ^{1}H NMR (600 MHz, $CDCl_3$) analysis showing alkene protons of free ligand 1-hexene and alkene protons of coordinated 1-hexene in complex **9**.

The XPS analysis of complex **9** confirmed the Pt^{2+} oxidation state with binding energy of 73.5 eV due to Pt $4f_{7/2}$ contribution. In addition to the Pt^{2+} peak, two additional Pt $4f_{7/2}$ peaks with binding energies of 72.1 and 74.9 eV were observed after the deconvolution of the Pt 4f spin doublet by

curve fitting. The additional peaks correspond to the residual Pt^{4+} for unreacted starting material and Pt^0 due to auto-reduction respectively. The presence of Cl in **9** was confirmed by Cl $2p_{3/2}$ peaks at 199.0 eV and 200.5 eV due to the terminal covalently bonded Cl atoms and the μ-Cl bridged atoms.

In reality, surface **4** is expected to have a mixture of all possibilities shown all through the structures presented in Scheme 3.2, Figure 3.5 and Figure 3.6. Because of the XPS results, the π-olefin complex of Pt^{2+} is expected to be the dominant Pt species formed on surface **4**. The results obtained after the reaction of 1,5-cyclooctadiene with $H_2PtCl_6 \cdot 6H_2O$ and 1-hexene with $H_2PtCl_6 \cdot 6H_2O$ or K_2PtCl_4 at 60 °C supported that the allylsilane groups immobilised on surface **2** react with Pt^{4+} precursor to form a π-olefin complex of Pt^{2+} as postulated for surface **4**. The resultant homogeneous complexes (**8** and **9**) showed the same Pt^{2+} and Cl^- XPS characteristics as the immobilised π-olefin Pt^{2+} complex on surface **4**. Although the analysis done on surface **4** resulted indirectly to the conclusion that the immobilised allyl ligand bind to the Pt centre, the ^1H NMR and elemental analysis of the homogeneous π-olefin complexes showed that the olefin binding to the Pt centre is highly plausible.

3.2.4 Reduction of Platinized Si-wafer and Characterization

The reduction of the immobilised π-olefin Pt^{2+} complex and other possible Pt species coating surface **4** to metallic Pt particles supported on the surface of the Si-wafer is the last step in the preparation of the flat model Pt catalyst (Pt/SiO_2/Si-wafer, **10**). Samples of surface **4** were slowly heated (1 °C/min) in a quartz oven to 300 °C in air (this generates PtO_2), followed by reduction of PtO_2 at 350 °C under a flowing hydrogen atmosphere (Figure 3.9). Under these reductive and combusting conditions, the ligands in the immobilised π-olefin Pt^{2+} complex coating surface **4** and all organics on the surface should decompose to form gases (CO_2, H_2O) which evaporate and leave behind on the surface of silicon wafer after H_2 reduction, supported platinum particles [22] as a final model Pt/SiO_2/Si-wafer catalyst **10**.

To characterise the flat model catalyst **10** after the reduction procedure, again, attention was given to the redox state of Pt and the possible atomic ratio of Pt to Cl. Both these factors were used exhaustively in the previous sections to identify the π-olefin Pt^{2+} complex on surface **4**. XPS analysis of grafted and spin coated samples revealed that the Cl 2p peak in the spectrum, which was previously identified at a binding energy of *ca*. 199 eV, was completely undetectable after reduction at 350 °C under H_2 atmosphere. A definite decrease in binding energy (*ca*. 1 eV) of Pt $4f_{7/2}$ signal in all samples confirmed a successful reduction to the Pt^0 oxidation state (Figure 3.10). In both samples that were prepared by either the grafting or spin coating approach, an additional Pt $4f_{7/2}$ peak was observed at *ca*. 73 eV due to Pt^{2+} contribution. Based on the surface areas of Pt^0 peaks and Pt^{2+} peaks relative to the total surface area of all the peaks in the Pt 4f region, the additional Pt^{2+} species contributes 35.7% of the total Pt in the grafted sample and only 7.4% of the total Pt in the spin coated sample (see Figure 3.10).

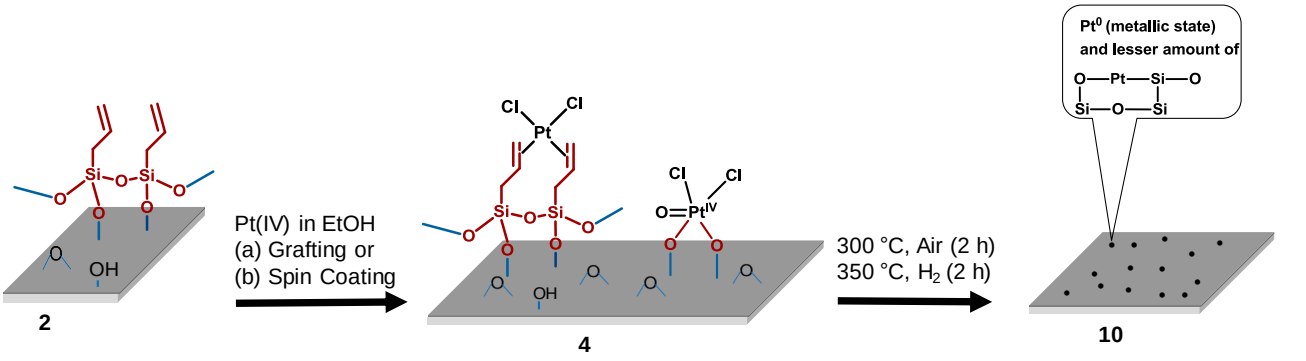

XPS Analysis (Atomic Ratio	
Pt	Cl
1	2

XPS Analysis (Atomic Ratio)	
Pt	Cl
1	0

Figure 3.9. The outline of the procedures used to prepare the final flat model catalyst (surface **10**) from hexachloroplatinic acid. Results from XPS analysis are included in the tables insert. The black dots in surface **10** is the pictorial model that represent the Pt particles on the SiO_2/Si-wafer surface.

Since all the Cl species were removed during reduction at 350 °C, the Pt $4f_{7/2}$ XPS spectral peak at 73 eV is attributable to Pt^{2+} specie formed by the sigma bonding with the SiO_2 support. The

most likely interaction of Pt with SiO_2 is through the oxygen atoms to form the Si-O-Pt-O-Si interphase. During grafting procedure over 24 h, the interaction of the Pt precursor with the surface silanol groups is prolonged. Thus there is more Pt^{2+} species (35.7% of the total surface Pt) in surface **10** from the grafting method (Figure 3.10). The Pt^{2+} $4f_{7/2}$ binding energy (*ca.* 73 eV) of the proposed O-Pt-O component is in good accordance with the Katrib *et al.*[23] results where it was shown that reductive calcination of $PtBr_4/SiO_2$ results in strong metal-support interaction to form -Pt-O-Si-O- specie with binding energy at 72.6 eV.

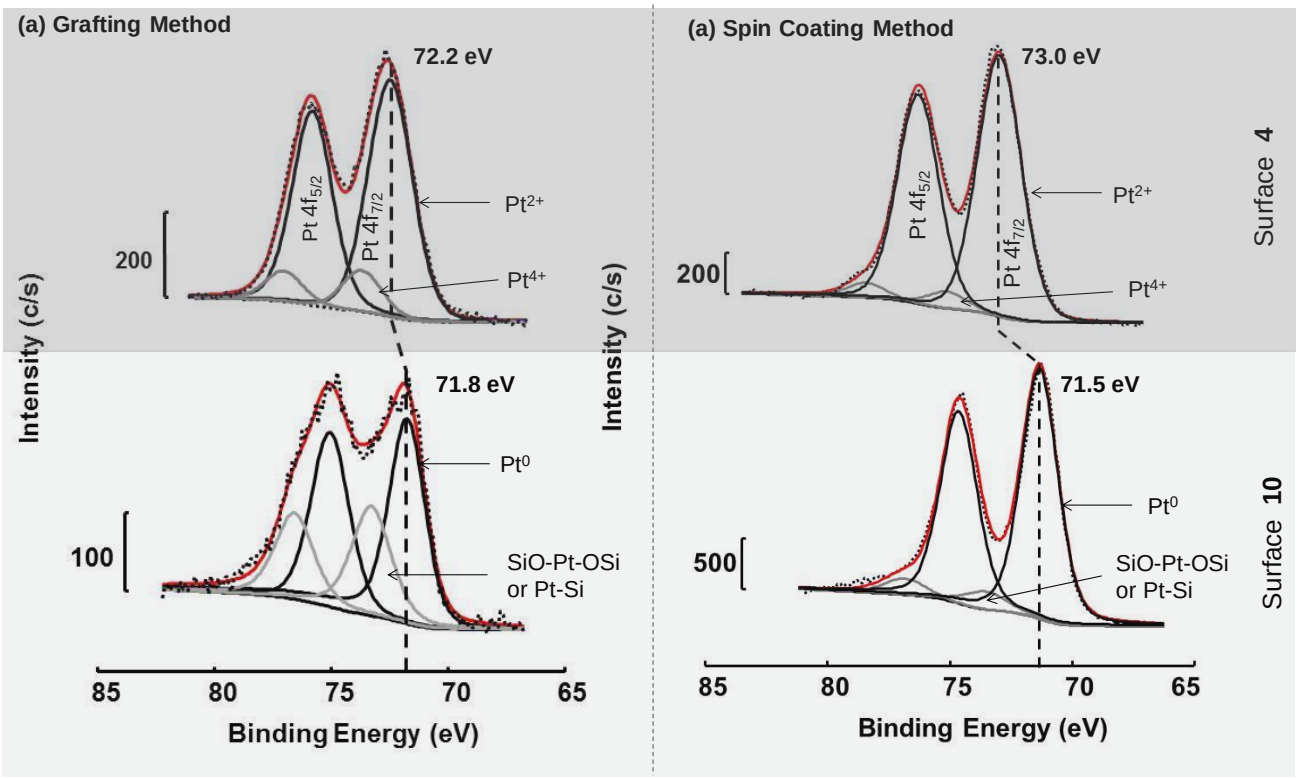

Figure 3.10. XPS spectra of Pt 4f from the analysis of platinised Si-wafers, surface **4** prepared by (a) grafting and (b) spin coating. Underneath the results from analysis of surface **4**, the shift in the Pt 4f peaks due to the reduction of Pt^{2+} complex to form Pt particles, surface **10**, is also shown. Red line: theoretical fitted curve. Dotted black line: experimentally measured curve. Other lines: peaks theoretically introduced to replicate the experimentally determined curve.

The other possibility for the presence of Pt^{2+} species is that the Pt particles interact with surface SiO_2 layer to form platinum silicides (PtSi or Pt_2Si). Supported Pt particles are well known to

interact with amorphous SiO_2 supports at elevated temperatures (>350 °C) to form Pt silicides.[24] Both Pt-O specie and Pt silicides have similar binding energy (Pt $4f_{7/2}$ at *ca*. 73 eV);[25] therefore they probably both are present in the platinised surface **10**, see Figure 3.9. The proposed O-Pt-O and Pt-Si species highlight the probability of the presence of interphase layer fragments between the metal and the support or the strong metal-support interaction. Supported Pt catalysts on SiO_2 support are known to exhibit strong metal-support interaction.[26,27] The interaction of Pt with the surface silica layer observed in this study is similar to the Cr^{6+} ester previously reported on Cr anchored on the surface of functionalised Si-wafer by Niemantsverdriet and co-workers.[28]

The prepared model catalysts Pt/SiO_2/Si-wafer **10** were further characterised by transmission electron microscopy (TEM). Even with the low resolution TEM analysis, Pt particles could be identified in the model catalysts. Figure 3.11 shows the TEM micrographs and particle distribution data of silanated Si-wafer and platinised Si-wafer surface. Very fine Pt particles were obtained by grafting procedure in surface **10** but the resolution in the TEM image (Figure 3.11b) was not good enough to accurately identify the diameters of individual particles. However, utilising a covalent Pt radius of 0.137 nm, it is clear that on average each particle had to have less than 10 Pt atoms per particle.

The Pt particles obtained by spin coating of a 10 mM solution of $H_2PtCl_6 \cdot 6H_2O$ on silanated SiO_2/Si-wafer were clearly visible as circular and few irregular black spots on surface **11** (Figure 3.11c). The average diameter of the adsorbed particles was determined to be 3.0 nm, this on average about 12 Pt atoms per particle. About 94 % of the adsorbed Pt particles were distributed within a small diameter range of 1.5-4 nm (Figure 3.11d). Few of the particles on surface **11** aggregated to form bigger particles that lied outside this range.

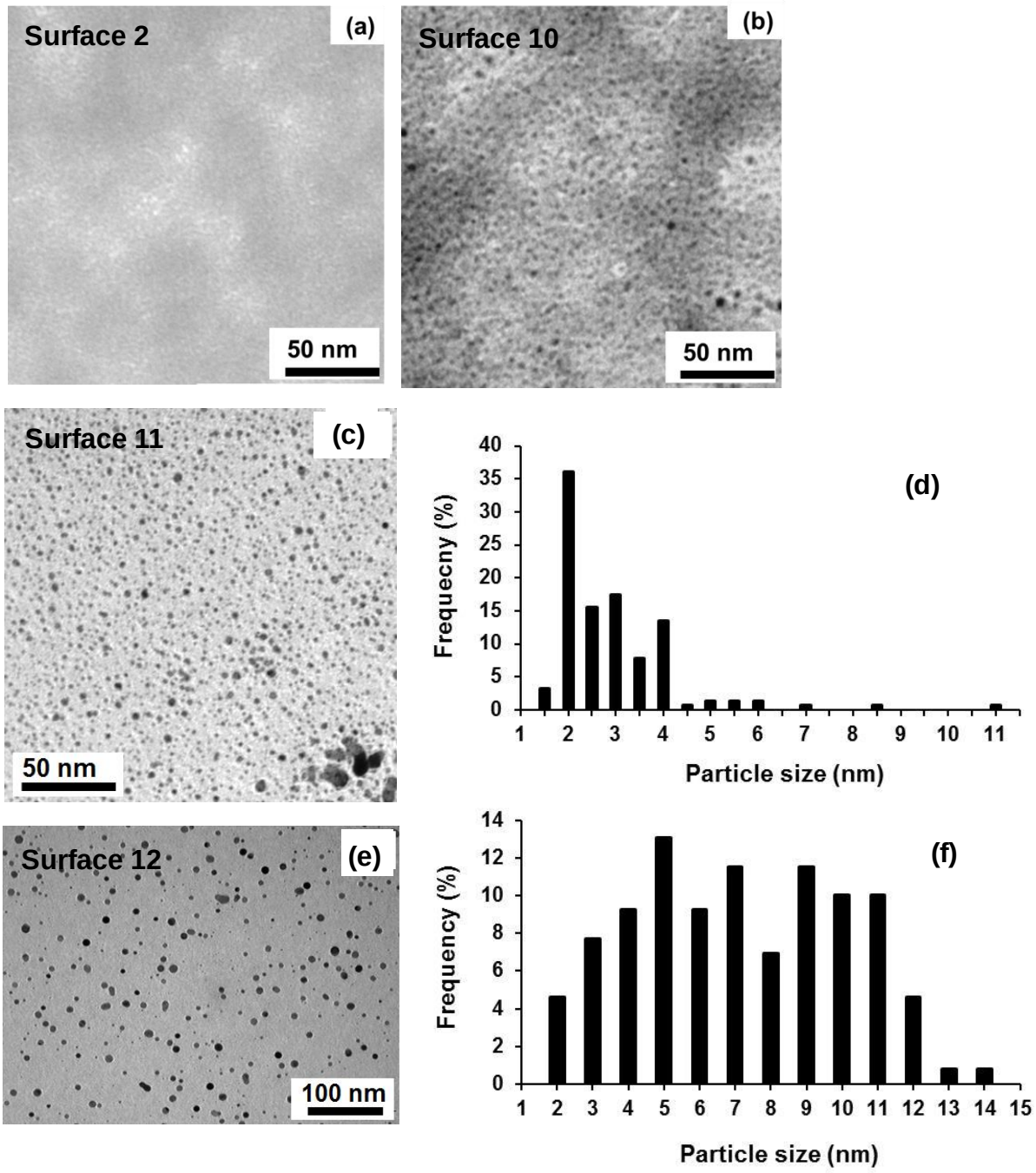

Figure 3.11. Representative TEM micrographs of Si-wafer (a) after silanation with allylmethoxysilane for 12 h under reflux, (b) a flat model Pt catalysts (surface **10**) obtained by grafting a solution of $H_2PtCl_6 \cdot 6H_2O$ on silanated Si-wafer followed by calcination and reduction, (c) flat model Pt catalysts (surface **11**) obtained by spin coating 10.3 mM solution of $H_2PtCl_6 \cdot 6H_2O$ on silanated Si-wafer followed by calcination and reduction and (d) corresponding statistical distribution of adsorbed Pt particles. (e) Representative TEM micrograph of surface **12** obtained by spin coating 20 mM solution of $H_2PtCl_6 \cdot 6H_2O$ on Si-wafer and (f) corresponding statistical distribution of adsorbed Pt particles.

When the concentration of $H_2PtCl_6 \cdot 6H_2O$ solution was increased to 20 mM, the resulting Pt particles on surface **12** were more defined as circular particles (Figure 3.11e). The average diameter of the adsorbed particles increased to 7.1 nm (about 26 Pt atoms per particle) and the particle size distribution increased over a wide diameter range between 2 nm to 12 nm (Figure 3.11f). This small particle size is attributable to the use of the allyl and silanol coordination sites on the surface of the wafer. In its absence, the initially coated or grafted H_2PtCl_2 would agglomerate and sinter together during calcination into particles tens of times larger than what was obtained initially.

Rutherford Backscattering Spectroscopy (RBS) analysis of model catalysts **10** clearly showed the spectral peaks corresponding to the Si of surface SiO_2 and the bulk Si substrate at ion beam energy of 1.2 MeV and 1.0 MeV respectively (Figure 3.12a). At higher ion beam energy, only a small peak corresponding to Pt was observed after magnification of the baseline. It is important to note the tailing nature of the Pt peak due to the isolated large Pt particles as corroborated by the TEM micrograph in Figure 3.11b (For more information about RBS spectrum please refer to Section 2.4.1 in literature review). To get a relative Rutherford Universal Manipulation Program (RUMP)[iii] fit on experimental data, the deposited particles were divided into 13 sub-layers with varying ratios of Pt:Si:O. The reason for these subdivisions is that the RBS analysis detected the entire amount of Pt in the sample, even the quantities embedded beneath the surface *via* strong metal-support interaction as multiple layers with different ion beam energies.[29] Based on the RUMP fit in Figure 3.12b, the amount of Pt deposited on the surface in model catalyst **10** was 0.9 Pt atoms/nm^2. This was less than the amount of Pt loading on surfaces **11** and **12** which was determined using the spin coat equation 3.1 which indicated the Pt loading to be 1.6 Pt atoms/nm^2 and 3.2 Pt atoms/nm^2 respectively. Surface **11** and **12** were prepared by spin coating while surface **10** was prepared by grafting method. Surface **10** and **11** were prepared using the same solution of $H_2PtCl_6 \cdot 6H_2O$ (10 mM). Even so, to

[iii] Rutherford Universal Manipulation Program is the analysis package used to simulate the RBS spectra to get accurate composition of flat surfaces as given by RBS peaks.

find a RBS loading result of 0.9 Pt atoms/nm^2 in surface **10** compared to the spin coat formula result of 1.6 nm Pt atoms/nm^2 in surface **11** is very close to each other and is considered as mutually consistent. The increasing trend in Pt loading on surfaces **10**, **11** and **12** correspond to the observed trend in average particles sizes where the average diameter of particle sizes adsorbed increases with increasing Pt loading (Figure 3.11).

$$\mathrm{m} = 1.35 \times C_o \sqrt{\frac{\eta}{\rho\omega^2 t_{evp}}} \qquad \textbf{3.1}$$

Here, m is the number of moles of catalyst deposited onto the functionalised SiO_2-wafer,
C_0 is the bulk concentration of the catalyst precursor in solution,
η is the viscosity of the solvent,
ρ is the density of the solvent,
ω is the rotation speed and
t_{evp} is the evaporation time.

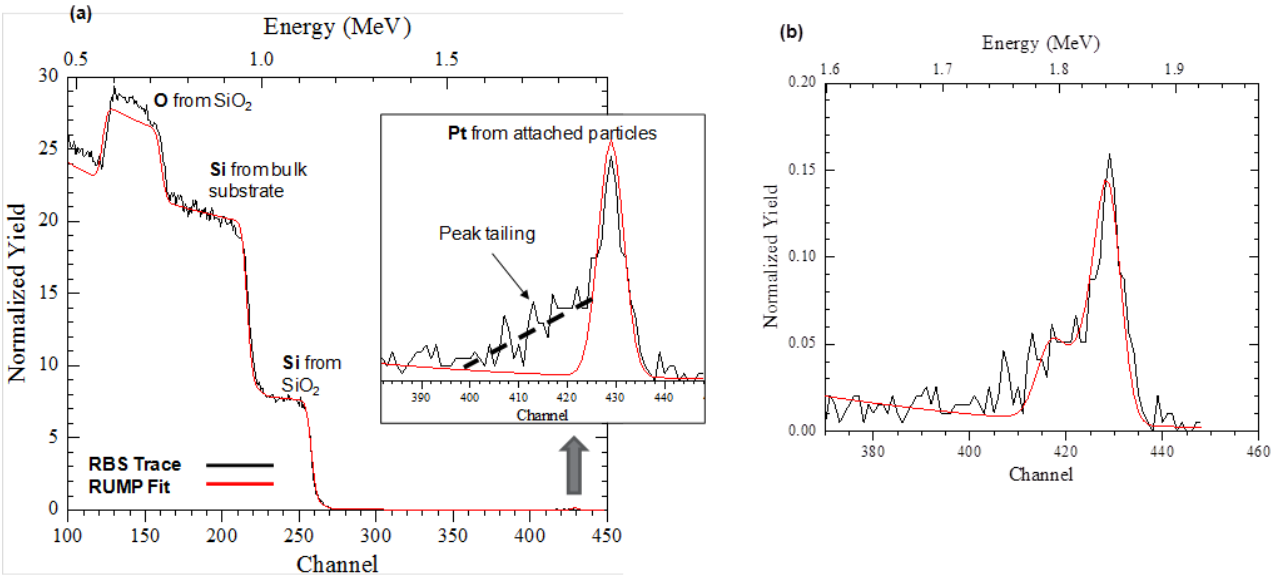

Figure 3.12. (a) RBS spectrum (black line) of surface **10** at normal incident of 2 MeV $^4He^+$ generated by the RUMP software package. The smooth red curve is the theoretical model of the spectrum. The insert is the blow-up of the Pt region with the Rutherford Universal Manipulation Program (RUMP) simulation of uniform Pt film on the surface SiO_2 as preferred by RBS analysis and (b) presents the RUMP fit to non-uniform Pt particles on surface **10**.

The results from XPS, TEM and RBS analysis confirmed that the Pt^{2+} complex which was derived by grafting or spin coating of a Pt^{4+} precursor on the surface of an allyl modified SiO_2/Si-wafer can successfully be reduced to Pt particles adsorbed on the surface of the substrate in relatively small sizes. The particle sizes on the surface of SiO_2/Si-wafer increased with increasing Pt loading with the spin coating procedure which resulted in larger particles (3-5 nm average particle diameter).

3.2.5 Platinisation of Si-wafer: Pt(II) Coordination to Immobilised Pseudo-Bidentate Ligands

The previous section focussed on using a Pt(IV) source, $H_2PtCl_6 \cdot 6H_2O$ to obtain a platinised surface. Since the procedure resulted in auto-reduction of the Pt(IV) source to Pt(II) species, the question arises "can a Pt(II) source be used from the onset?". To test this a solution of 1.25 mM potassium tetrachloroplatinate(II) (K_2PtCl_4) in aqueous ethanol (50% v/v) was identified as an alternative source of Pt to react with the supported allyl groups on surface **2**. Again both procedures, chemical grafting and spin coating as shown in Scheme 3.2, were employed to react the Pt(II) precursor with allyl groups on surface **2**.

3.2.5.1 Chemical Grafting of the Pt(II) Solution on Allyl Functionalised Si-wafer

A solution of 1:1 v/v aqueous ethanol proved to be suitable to dissolve K_2PtCl_4 salt as well as adequately wet the allylsilane functionalised surface of the SiO_2/Si-wafer (surface **2**). The resulting K_2PtCl_4 solution was heated to 50 °C in the presence of surface **2** and kept until a colour change from red to black was observed (about 30 min). Under these grafting conditions, the colour change of solution of K_2PtCl_4 indicated the formation of dispersed colloidal Pt particles as shown in Figure 3.13. At the end of the grafting reaction, the platinised surface **13** and the inside of the vial used in grafting had a faint dark shade possibly due to the deposit of fine Pt particles. When grafting

is carried out at room temperature (*ca.* 25 °C), the colour change is observed after *ca.* 24 h. In aqueous ethanol, the reduction of $PtCl_4^{2-}$ precursor is preceded by hydrolyses to form aquated complexes $PtCl_{4-n}(H_2O)_n$ (here n = 1,2,3 and 4).[30,31] The resulting aquated complexes are easier to reduce to form dispersed colloidal Pt particles than the parent $PtCl_4^{2-}$ precursor.[32] To avoid agglomeration of the unprotected colloidal Pt particles, 30 mM sodium acetate was added as the stabiliser. The ions of acetate chelate the unprotected Pt nanoparticles *via* carboxyl groups and prevent agglomeration of individual particles by electrostatic repulsion.[33,34]

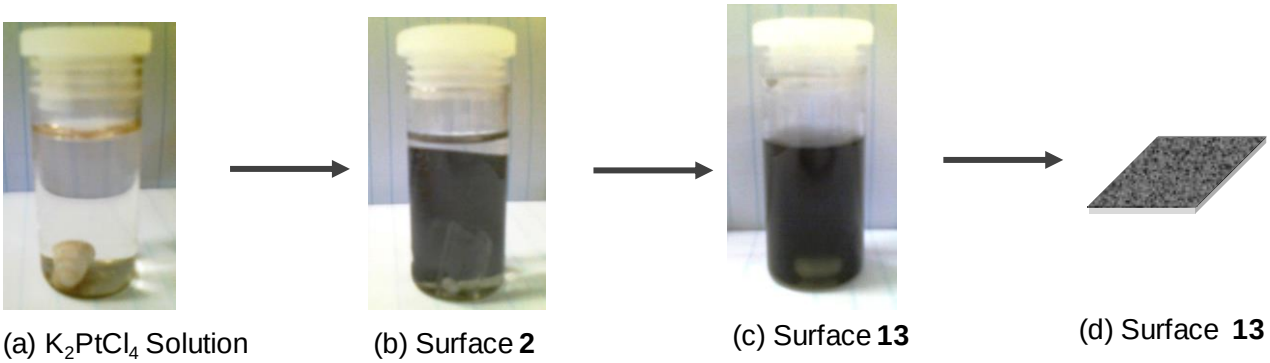

Figure 3.13. (a) 1.25 mM solution of K_2PtCl_4 in aqueous ethanol (b) allylsilane functionalised SiO_2/Si-wafer (surface **2**) submerged in freshly prepared K_2PtCl_4 solution (c) platinised surface **13** submerged in colloidal Pt mixture after heating at 50 °C for 30 min (d) pictorial model of platinised surface **13** with faint dark shade of adsorbed Pt particles.

The nature and composition of immobilised species on surface **13,** in particular, a possible complexation of the Pt^{2+} precursor to the adsorbed allylsilane were determined by XPS analysis. Before XPS analysis, efforts were made to remove weakly adsorbed Pt particles on surface **13** by ultrasonication in aqueous ethanol for 10 sec. Based on XPS data, the surface coverage of surface **13** consisted of Pt with 17.4 atomic % (at %) and negligible amount of Cl (0.2 at %). The rest of the elements on surface **13** were Si (38 at %), O (22 at %) and C (23 at %). The small amount of Cl relative to Pt on surface **13** suggests that the Cl atoms dissociated from the Pt centre during the grafting of K_2PtCl_4. A closer look at the XPS spectra of the Pt 4f bands after peak deconvolution

revealed that about 81% of the attached Pt on surface **13** was in metallic form with Pt 4f spin-orbit-split doublets at 71.3 eV and 74.6 eV (Figure 3.14). The residual Pt detected was in Pt^{2+} and Pt^{4+} oxidation state.

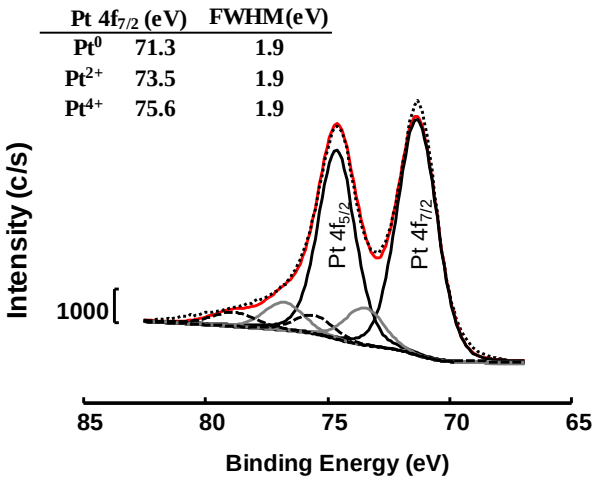

Figure 3.14. XPS data of Pt 4f signals from the analysis of platinised surface **13** prepared by grafting of 1.25 mM solution of K_2PtCl_4 at 60 °C.

The XPS data clearly showed that K_2PtCl_4 was reduced to colloidal Pt particles and remained attached on surface **13** even after ultrasonic rinsing in aqueous ethanol. The direct loading of the preformed colloidal metal particles on the surface of flat model support is known[35] and results in metal particles with defined particle sizes.[36,37] When surfactant-capped particles are immobilised on the flat model support, the surfactant on the surface of the metal particle interacts with the support through ionic interactions and form an interphase layer between the particles and the support.[38] In the present study, it was not clear whether the Pt particles attached on surface allylsilane through direct π-backbonding[39] or by weak interactions such as van der Waals forces.[40] The XPS spectra for C 1s core electrons did not show any conclusive evidence for the interaction between surface allylsilane and the deposited Pt particles.

3.2.5.2 Chemical Grafting of the Pt(II) Solution on Amino Functionalised Si-wafer

To optimise the immobilisation of Pt on the surface of functionalised Si-wafer, Pt(II) precursor was also grafted on 3-aminopropyltrimethoxysilane functionalised SiO_2/Si-wafer. Before the grafting was performed, the XPS analysis of the amino-functionalised surface **3** exhibited a strong peak at 399.2 eV and weaker peaks at 400.4 eV and 401.5 eV due to N 1s core electron binding energies. The peak at 399.2 eV is due to the contribution of free amine groups while the peaks at 400.4 eV and 401.5 eV are caused by the hydrogen-bonded and protonated amines as illustrated in (Scheme 3.4).[9,41]

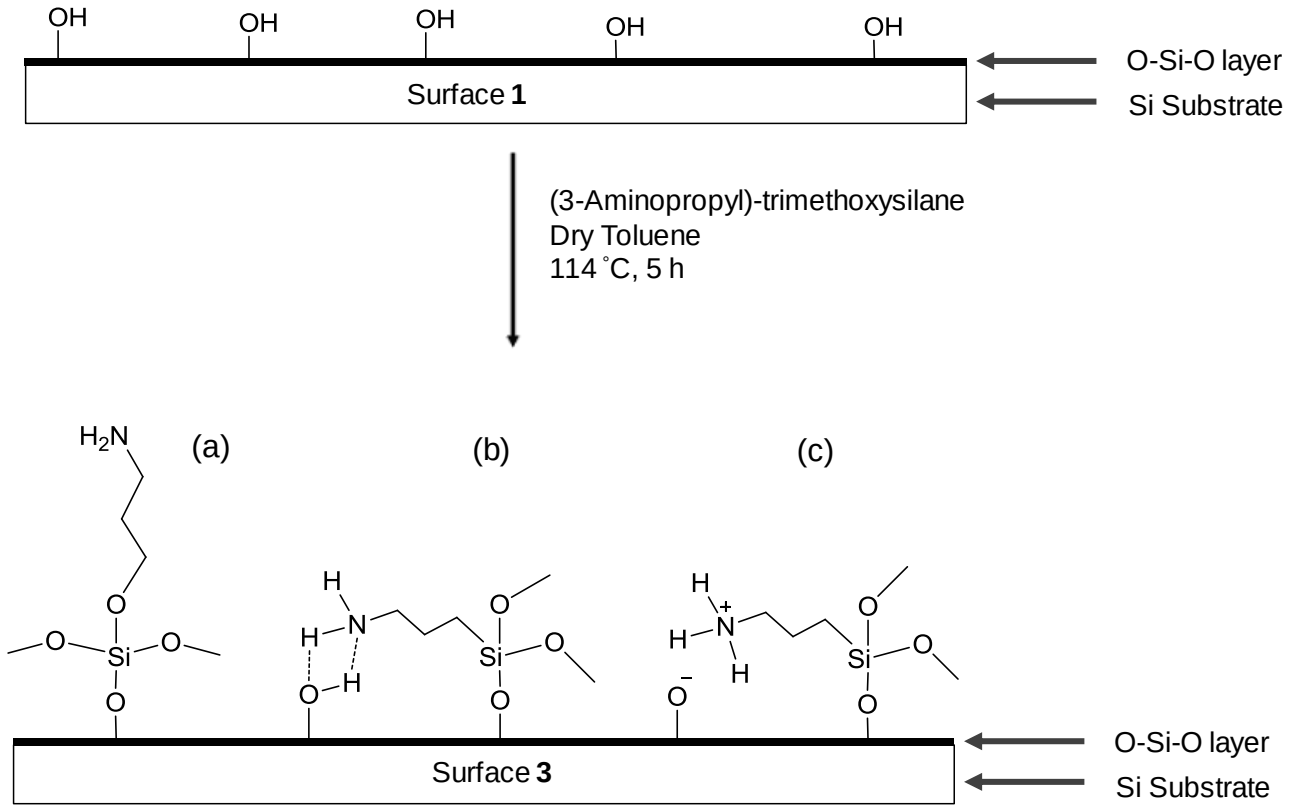

Scheme 3.4 A schematic model illustrating the interaction between the amino group of 3-aminopropyltrimethoxysilane and surface silanol groups on SiO_2/Si-wafer (surface **3**). Surface **3** illustrates immobilised (a) free amine group, (b) amine group with hydrogen bonds with the adjacent silanol group and (c) a protonated amine.

A 1.25 mM solution of K_2PtCl_4 in aqueous ethanol was grafted on 3-aminopropyltrimethoxysilane surface **3** at 60 °C until the colloidal mixture of platinum particles formed, see Scheme 3.5. Subsequent characterisation of the resultant surface **14** by XPS analysis showed the presence of Pt^{2+} and Pt^0 species with Pt $4f_{7/2}$ peaks at 71.8 eV and 72.9 eV respectively. The presence of Pt^0 implied that K_2PtCl_4 was reduced to Pt particles followed by the immobilisation of these Pt particles on surface **14**. The Pt $4f_{7/2}$ peak at 72.9 eV was attributed to the Pt^{2+} species formed by the reaction of surface amino groups with the Pt precursor. To confirm the reaction of the Pt with the amino group, the N 1s peak at 397.7 eV was identified and attributed to the presence of Pt-N bond. The observed N 1s peak for Pt-N bond was consistent with the literature value of 397.9 eV for the Pt-N bond formed on amine modified Pt surface.[9,42] In addition to the N 1s peak identified at 397.9 eV, the N 1s peaks which correspond to free amine (399.3 eV), hydrogen-bonded amine (400.4 eV) and protonated amine (401.6 eV) were also detected in surface **14**. Furthermore, the spin doublets for covalently bonded Cl 2p were observed at 198.3 eV and 199.9 eV as well as the spin doublets for ionic Cl at 197.2 eV and 198.8 eV. Based on the XPS data, the Pt^{2+} formed on surface **14** was postulated as shown in Scheme 3.5.

The final model catalyst (surface **15**) was achieved by calcination of surface **14** at 300 °C for 2 h followed by reduction at 350 in H_2 atmosphere for 2 h (Scheme 3.6). The resultant surface coverage of the model catalyst consisted of 2 % of surface Pt. The majority (85 %) of the detected Pt content was in metallic form with Pt $4f_{7/2}$ binding energy at 71.6 eV. A very small amount of the detected surface Pt (15 %) was in the form of Pt^{2+} and Pt^{4+} species as revealed by the Pt $4f_{7/2}$ binding energies at 72.9 eV and 74.2 eV respectively.

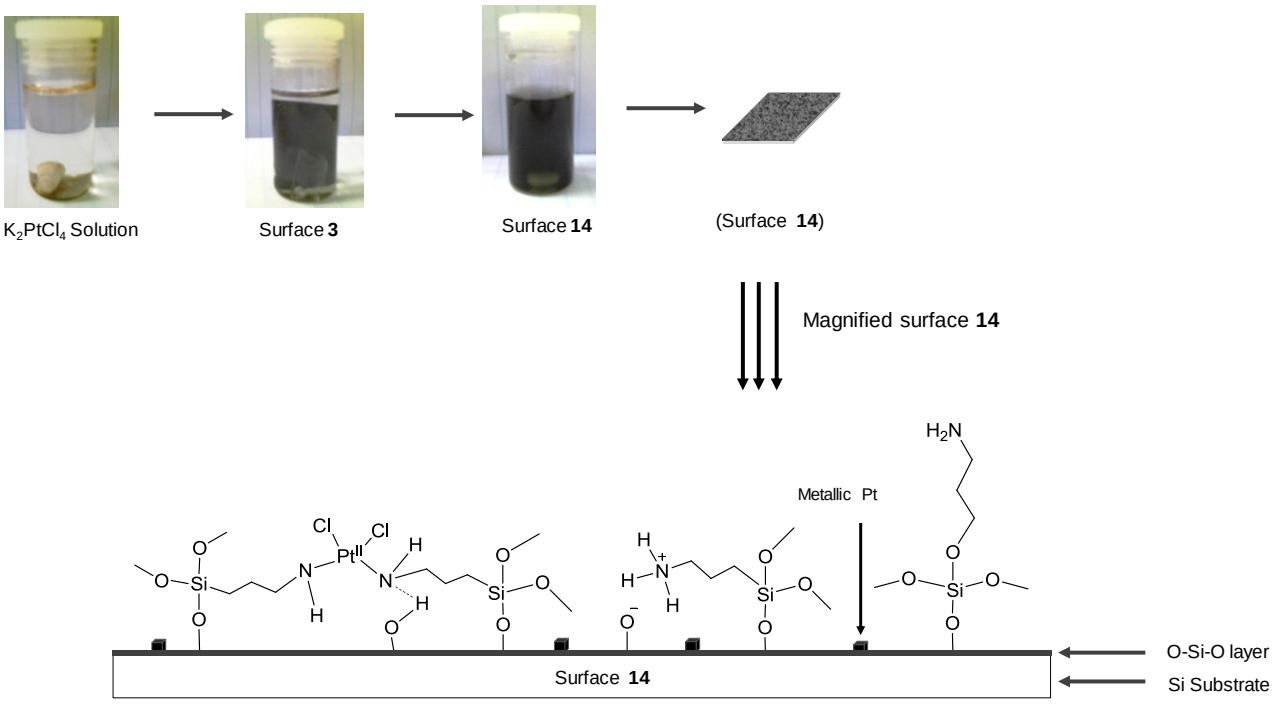

Scheme 3.5. (a) 1.25 mM solution of K_2PtCl_4 in aqueous ethanol, amino functionalised SiO_2/Si-wafer (surface **3**) submerged in freshly prepared K_2PtCl_4 solution and platinised surface **14** submerged in colloidal Pt mixture after heating at 50 °C for 30 min and a pictorial model of platinised surface **14** with faint dark shade of adsorbed Pt particles. (b) A detailed representation of chemical structures on surface **14** based on XPS data of Pt $4f_{7/2}$, N 1s and Cl 2p.

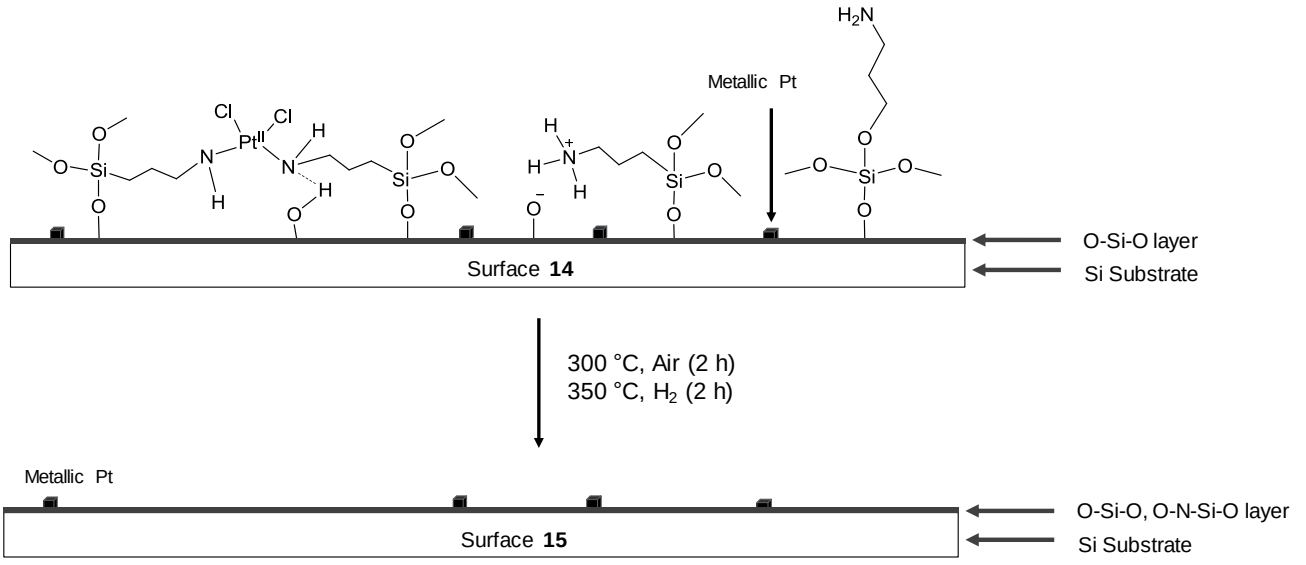

Scheme 3.6. Outline of the calcination and hydrogen reduction of surface **14** to form surface **15** as a final model Pt/SiO_2/Si-wafer catalyst.

The presence of the residual N 1s peak at 397.8 eV due to Pt-N bond (see Figure 3.15c) suggest that a small amount of surface Pt^{2+} species was the residual Pt nitride, most likely, in the interphase between the Pt particle and the surface of the support. In addition to the Pt-N peak in surface **15** sample, the N 1s peak at 400.3 eV was also detected (see Figure 3.15c). In surface **3**, the N 1s peak at 400.4 eV (see Figure 3.15a) was ascribed to hydrogen-bonded amine. Under calcination at 300 °C and reduction at 350 °C, the hydrogenated surface amine will most probably decompose into gases. Therefore the N 1s peak at 400.3 eV is due to the incorporation of the N species into the SiO_2 layer to form a silicon oxynitride, $(Si\text{-}O)_2\text{-}N\text{-}Si$. The observed N 1s binding energy at 400.3 eV is consistent with the literature value at *ca*. 400 eV for $(Si\text{-}O)_2\text{-}N\text{-}Si$.[43,44]

The XPS peaks in Figure 3.15 summarise the changes adopted by (a) surface amino groups on the SiO_2/Si-wafer after (b) platinisation with K_2PtCl_4 solution until the formation of colloidal Pt particles and (c) after calcination at 300 °C followed by reduction at 300 °C to a final model catalyst, surface **15**. No free amine groups at 399.2 eV were detected on surface **15** after reduction to a model catalyst. The N 1s detected by XPS was due to Pt nitride and silicon oxynitride, $(Si\text{-}O)_2\text{-}N\text{-}Si$ (Figure 3.15). The shifts undergone by the N 1s binding energies after platinisation of aminated SiO_2/Si-wafer show that the Pt precursor was successfully adsorbed on the surface and interacted with surface amino groups.

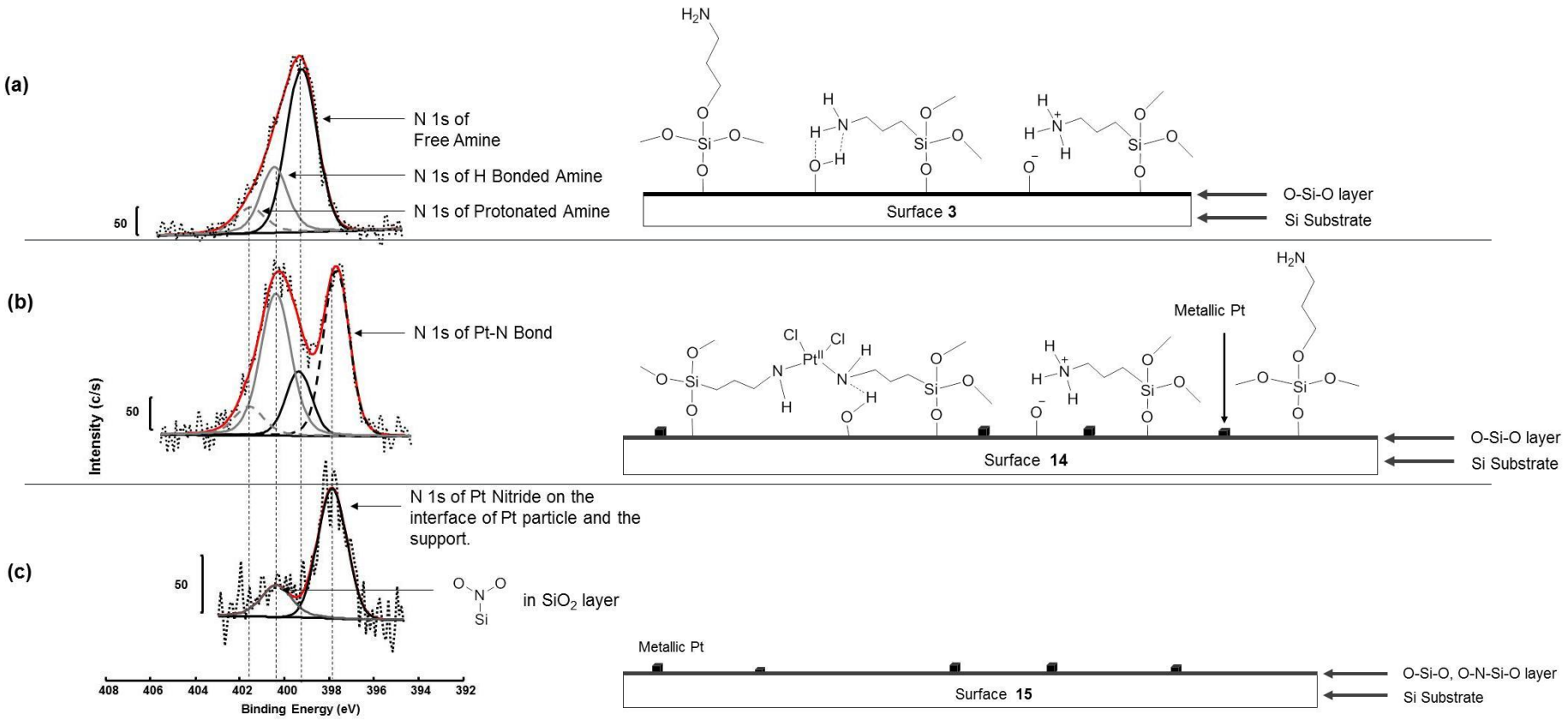

Figure 3.15. XPS spectra of N 1s from the analysis of (a) aminated surface **3**, (b) platinised surface **14** and (c) reduced flat model catalyst (surface **15**). The spectra illustrate changes of surface amine at different phases of model catalyst preparation. The dotted lines represent experimental curve and; the broken lines and solid lines represent fitted curve using Multipak software.

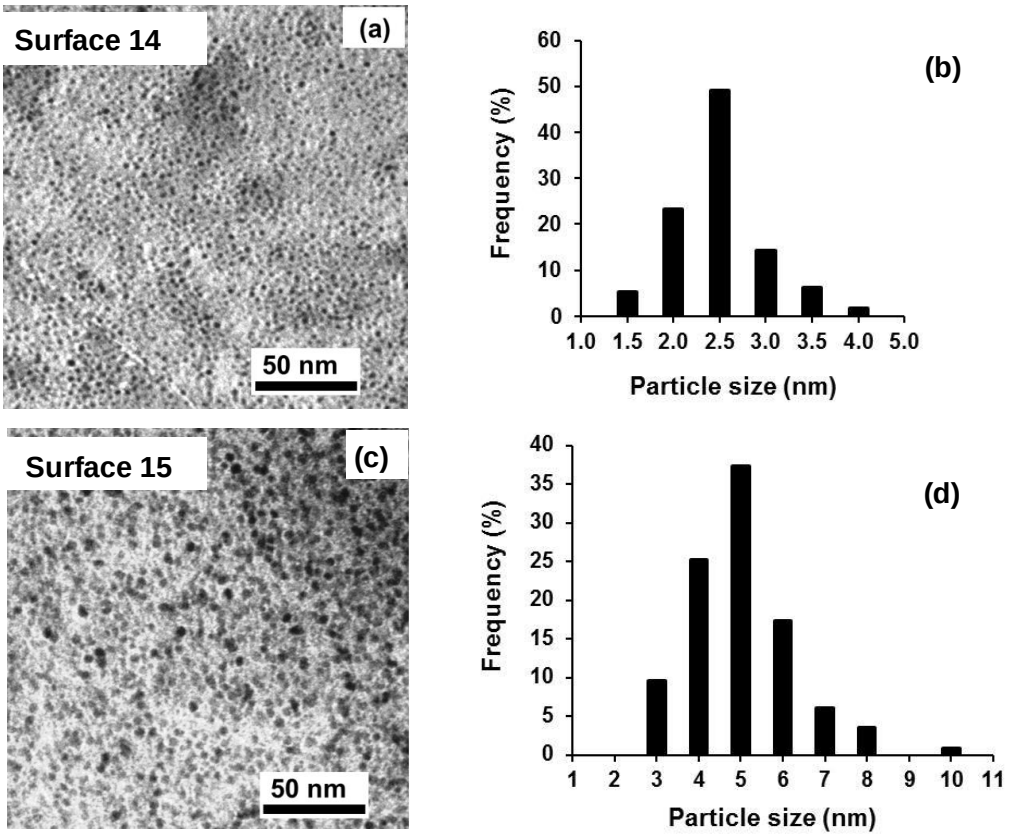

Figure 3.16. (a) Representative sample of TEM micrograph of surface **14** with Pt nanoparticles immobilised by grafting of K_2PtCl_4 solution at 60 °C and (b) corresponding statistical distribution of adsorbed nanoparticles. (c) Representative TEM micrograph of surface **15** achieved by calcination followed by reduction of immobilised Pt nanoparticles and (d) corresponding statistical distribution of adsorbed nanoparticles.

The actual content of Pt on surface **14** was quantified by RBS analysis to the value of 11 Pt atoms/nm^2. Further analysis to determine the morphological characteristics and Pt particle distribution on model catalyst were carried out using TEM which showed monodispersed Pt particles with circular shapes (see Figure 3.16a above). The average diameter of freshly immobilised Pt particles on surface **14** was 2.5 nm and all the particles were within a small diameter range between 1.5 nm and 4 nm. Noteworthy, the Pt particles immobilised on surface **14** double in particle diameter after calcination at 300 °C and reduction at 350 °C in surface **14** (see Figure 3.16b). This indicates possible sintering and agglomeration of small particles during calcination to form enlarged Pt particles.

In a different set of experiments, the K_2PtCl_4 solution was heated to 60 °C and kept at temperature for 30 min in the presence of aminated SiO_2/Si-wafer **3** and kept until black precipitate started forming, followed by cooling the reaction mixture to room temperature (*ca*. 25 °C). The resultant Pt nanoparticles attached on the platinised surface **16** agglomerated after cooling to form large particles (*ca*. 50 nm) even before calcination and reduction, see Figure 3.17. This highlights the importance of removing the platinised Si-wafer from the grafting mixture immediately when the black colour of colloidal Pt particles starts to appear and when the mixture is still at reaction temperature to avoid the formation of larger Pt particles.

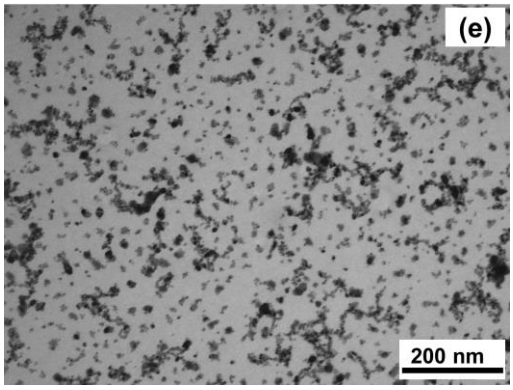

Figure 3.17. (a) TEM micrograph of surface **16** with Pt nanoparticles immobilised by grafting of a K_2PtCl_4 aqueous ethanol solution at 60 °C followed by calcination at 300 °C for 2 h and reduction under H_2 atmosphere at 350 °C for 2h.

In summary, grafting K_2PtCl_4 utilising aqueous ethanol (1:1 v/v) as a solvent results in reduction of Pt^{2+} to form colloidal Pt particles that attach on the surface of allyl or amino functionalised SiO_2/Si-wafer. The colloidal Pt particles attach on 3-aminopropyltrimethoxysilane functionalised SiO_2/Si-wafer (surface **13**) *via* Pt-N bonds. Calcination of platinised SiO_2/Si-wafer (surface **14**) at 350 °C increased the Pt particle from an average diameter of 2.5 nm in surface **14** to 5 nm in surface **15**.

3.2.5.3 Spin Coating of the Pt(II) Solution on Amino Functionalised Si-wafer

In addition to the grafting methodology, a solution of 1.25 mM potassium tetrachloroplatinate(II) (K_2PtCl_4) in aqueous ethanol was spin coated on allyl and amino functionalised SiO_2/Si-wafers **2** and **3** to liberate platinised surface **17**. Unlike grafting, the Pt particles obtained after spin coating tend to aggregate and form localised clusters after calcination and reduction. This resulted in non-uniform distribution of Pt particles throughout surface **17** as observed by TEM analysis. The catalysts prepared by spin coating of K_2PtCl_2 solution were not further characterised or used in subsequent applications.

3.3 Application of Model Flat Pt/SiO_2/Si-wafer in Oxidation Reactions

The model Pt catalysts prepared by grafting of K_2PtCl_4 from a solution (surface **15**), grafting of $H_2PtCl_6 \cdot 6H_2O$ from a solution (surface **10**) and spin coating of a $H_2PtCl_6 \cdot 6H_2O$ solution (surface **11**) on functionalised SiO_2/Si-wafer were validated by using them as realistic model catalysts in a chemical reaction. A solvent free aerobic oxidation of 1-octadecanol **(18**) to its corresponding oxidation products was used as a probe reaction as outline in Scheme 3.7.

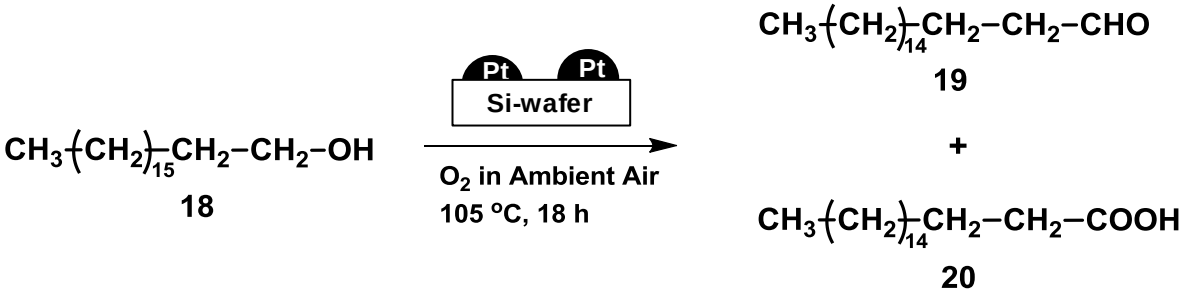

Scheme 3.7. The oxidation of 1-octadecanol **18** to form oxidation products octadecanal **19** and octadecanoic acid **20** in an open glass vial, under controlled reaction temperature and ambient atmospheric air. Another set of oxidation reactions was done in a closed Parr Reactor, under controlled temperature at a constant flow of molecular oxygen at ambient pressure.

3.3.1 Application of Surface 15 Flat Model Pt/SiO_2/Si-wafer in Oxidation Reactions

A detailed analysis and discussion of the oxidation products obtained using surface **15** [iv] as the model catalyst in oxidation of 1-octadecanol are given in this section. The reaction was monitored using Attenuated Total Reflectance Fourier Transform Infrared (ATR FTIR) analysis which could detect the formation of the oxidation products bearing a carbonyl (C=O) group (compounds **19** and **20**) by the appearance of the characteristic FTIR stretching frequency at *ca*. 1730 cm^{-1}. This approach could also be used to monitor the consumption of the starting material **18** by the disappearance of the FTIR stretching frequency at *ca.* 3200 cm^{-1} which indicated the conversion of the hydroxyl group (O-H) to the oxidised products.

Figure 3.18 presents the progression of substrate **18** oxidation over surface **15**. It should be noted that the strong FTIR C=O stretching frequency centred at 1725 cm^{-1} is not product specific and it could correspond to the formation of any of the oxidation products, octadecanal (**19**) and octadecanoic acid (**20**) or other secondary oxidation products.

A closer look at the major FTIR C=O stretching frequency revealed that it was made up of two overlapping peaks at 1716 cm^{-1} and 1732 cm^{-1} (see Figure 3.18b). The FTIR C=O stretching frequency at 1716 cm^{-1} was the favourable product until the reaction progressed beyond 180 min at 105 °C. At about 240 min, the oxidation product with FTIR C=O stretching frequency at 1732 cm^{-1} started to increase to become the major oxidation product.

[iv] Surface **15** was prepared by calcination followed by reduction of surface **14** at 350 °C. Surface **14** was prepared by grafting 1.25 mM K_2PtCl_4 solution on 3-aminopropyltrimethoxysilane functionalised SiO_2/Si-wafer. XPS and TEM analysis showed that surface **15** consists of Pt particles with Pt-N-Si-O interface.

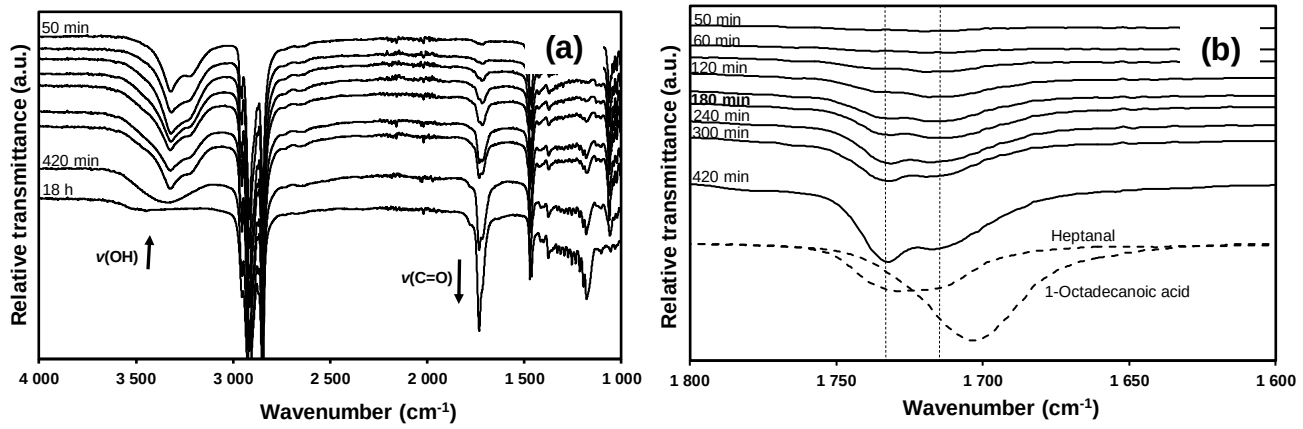

Figure 3.18. (a) FTIR spectra of the product mixture from the oxidation of 1-octadecanol catalysed by surface **15**, a model $Pt/SiO_2/Si$-wafer catalyst at 105 °C in ambient air. (b) Enlarged section of the FTIR C=O stretching frequency.

To determine the actual oxidation products with the FTIR C=O stretching frequency observed at 1732 cm^{-1} and 1716 cm^{-1}, commercially sourced heptanal and octadecanoic acid were used as reference standards in FTIR analysis. It was assumed that heptanal will give the same FTIR C=O stretching frequency as octadecanal. The FTIR C=O stretching frequency for heptanal and octadecanoic acid appeared at 1727 cm^{-1} and 1703 cm^{-1} respectively. The results from commercial samples gave an impression that the FTIR C=O stretching frequency observed at 1732 cm^{-1} belong to octadecanal and the stretching frequency at 1716 cm^{-1} belong to octadecanoic acid. However, it was unlikely that the FTIR C=O stretching frequency at 1732 cm^{-1} which appears later in the reaction belongs to octadecanal only, the primary product of the oxidation of 1-octadecanol.[45]

Another product possibility includes the formation of octadecanyl octadecanoate the secondary product formed by condensation of 1-octadecanol and octadecanoic acid. Additional analysis using Proton Nuclear Magnetic Resonance spectroscopy (^{1}H NMR) confirmed the product with FTIR C=O stretching frequency at 1732 cm^{-1} as octadecanyl octadecanoate ($CH_3(CH_2)_{15}CH_2COOCH_2(CH_2)_{16}CH_3$). The characteristic methylene protons of the starting material **18** (-C$\underline{H_2}$OH), the product aldehyde **19** (-C$\underline{H_2}$CHO) and the product carboxylic acid **20** (-C$\underline{H_2}$COOH)

in the crude product mixture were identified by ^{1}H NMR as triplets (J_{HH} = 7-7.5 Hz) centred at 3.64 ppm, 2.42 ppm and 2.35 ppm respectively, see Figure 3.19a.

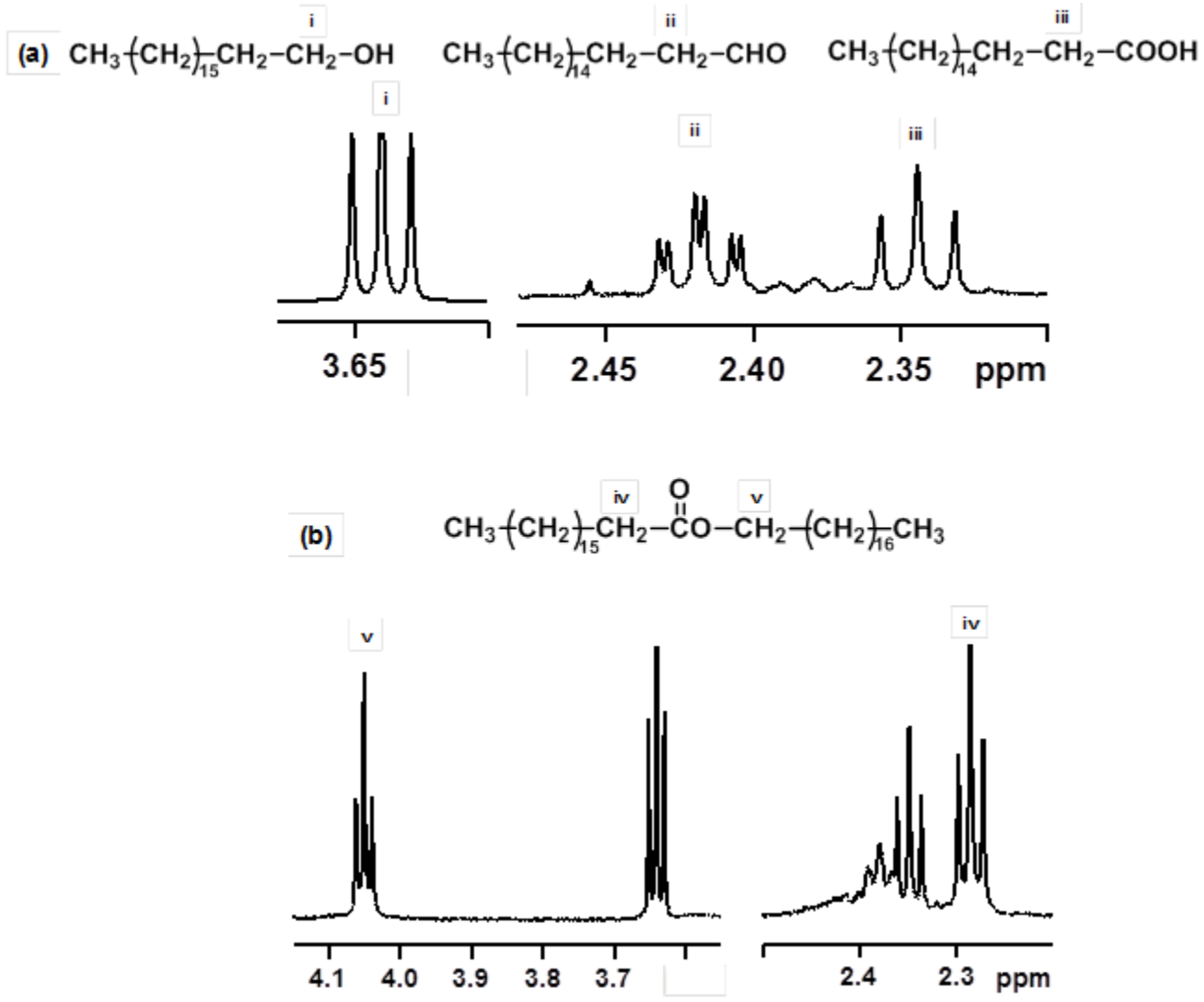

Figure 3.19. (a) ^{1}H NMR signals of labelled methylene protons of 1-octadecanol and oxidation products octadecanal and octadecanoic acid and (b) labelled methylene protons of octadecanyl octadecanoate.

The spin-spin splitting observed in the identified methylene protons was due to the coupling with the adjacent methylene protons of the octadecanyl chain. Additional spin-spin splitting due to coupling with the aldehyde proton was also observed in methylene protons of octadecanal. Hence the

signal of methylene protons at 2.42 ppm resonates as a doublet of triplets (J_{HH} = 7.3 Hz and J_{HH} = 1.9 Hz). The methylene protons of octadecanyl octadecanoate resonated at 4.05 ppm for the methylene group attached directly to oxygen ($CH_3(CH_2)_{15}\underline{CH_2}COO\underline{CH_2}(CH_2)_{16}CH_3$) and at 2.28 ppm for the methylene group which is adjacent to the carbonyl group (labelled with IV) as presented in Figure 3.19b above. The methylene protons of octadecanyl octadecanoate (labelled IV and V in Figure 3.19b) resonated as triplets due to the neighbouring methylene groups of the parent alkyl chain.

By collecting ^{1}H NMR data over time, it was possible to monitor the progress of 1-octadecanol oxidation and identify different products that are formed at various stages of the reaction. The advantage of using ^{1}H NMR analysis to monitor the oxidation of 1-octadecanol is the ability to identify the characteristic proton signals of any of the oxidation products. ATR FTIR analysis which was used to collect the data in Figure 3.18 is easy to use in terms of sample preparation and data collection. However the different products formed from oxidation of 1-octadecanol cannot be identified and characterised uniquely using ATR FTIR analysis.

The ATR FTIR data was useful to monitor the depletion of the starting material by following the disappearance of the FTIR hydroxyl stretching frequency at *ca.* 3200 cm^{-1}. Relative intensities of the hydroxyl stretching frequencies before the start of the reaction and at given time intervals during the reaction, were used to determine the 1-octadecanol depletion shown in Figure 3.20.

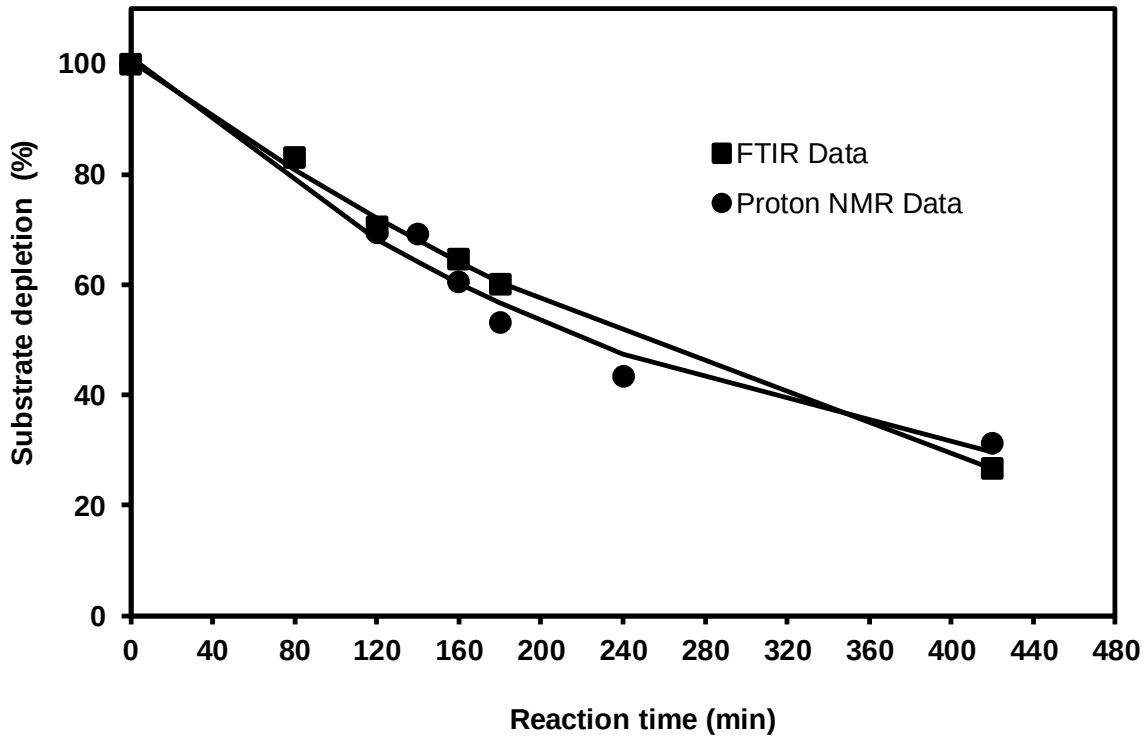

Figure 3.20. The 1-octadecanol depletion as a function of reaction time over 440 min. The data shown was from the analysis of oxidation product mixture using ATR FTIR and ^{1}H NMR.

The data from ATR FTIR and ^{1}H NMR analysis were fitted to the first-order kinetic equation $[A]_t = [A]_0\ e^{(-kobst)}$ with $[A]_t$ and $[A]_0$ representing the stretching frequency peak amplitude or the resonance peak integration of the reactant 1-octadecanol at time t and at $t = 0$. It was found that the first order rate constant for the data obtained by NMR and FTIR was $k_{obs} = 6(1)x10^{-5}\ s^{-1}$ and $3.8(4)x10^{-5}\ s^{-1}$ respectively. The large experimental error associated with the NMR data relates to the method of data collection. The FTIR analysis is performed on the formed oxidation product without further treatment such as dissolving in a solvent. For the NMR data, reaction samples had to be collected and dissolved to a predetermined concentration before peak integration gave kinetic data. Regardless of the experimental error, the k_{obs} values indicate that the different techniques, NMR and FTIR were mutually consistent in monitoring the oxidation of 1-octadecanol.

The changes in the sample composition of the oxidation product mixture over 240 min were monitored *ex situ* by ^{1}H NMR spectroscopy and the results are presented in Figure 3.21. Significant

change in the product composition was observed at 100 min when about 15 % of 1-octadecanol was converted into octadecanoic acid and octadecanal (see Figure 3.21a).

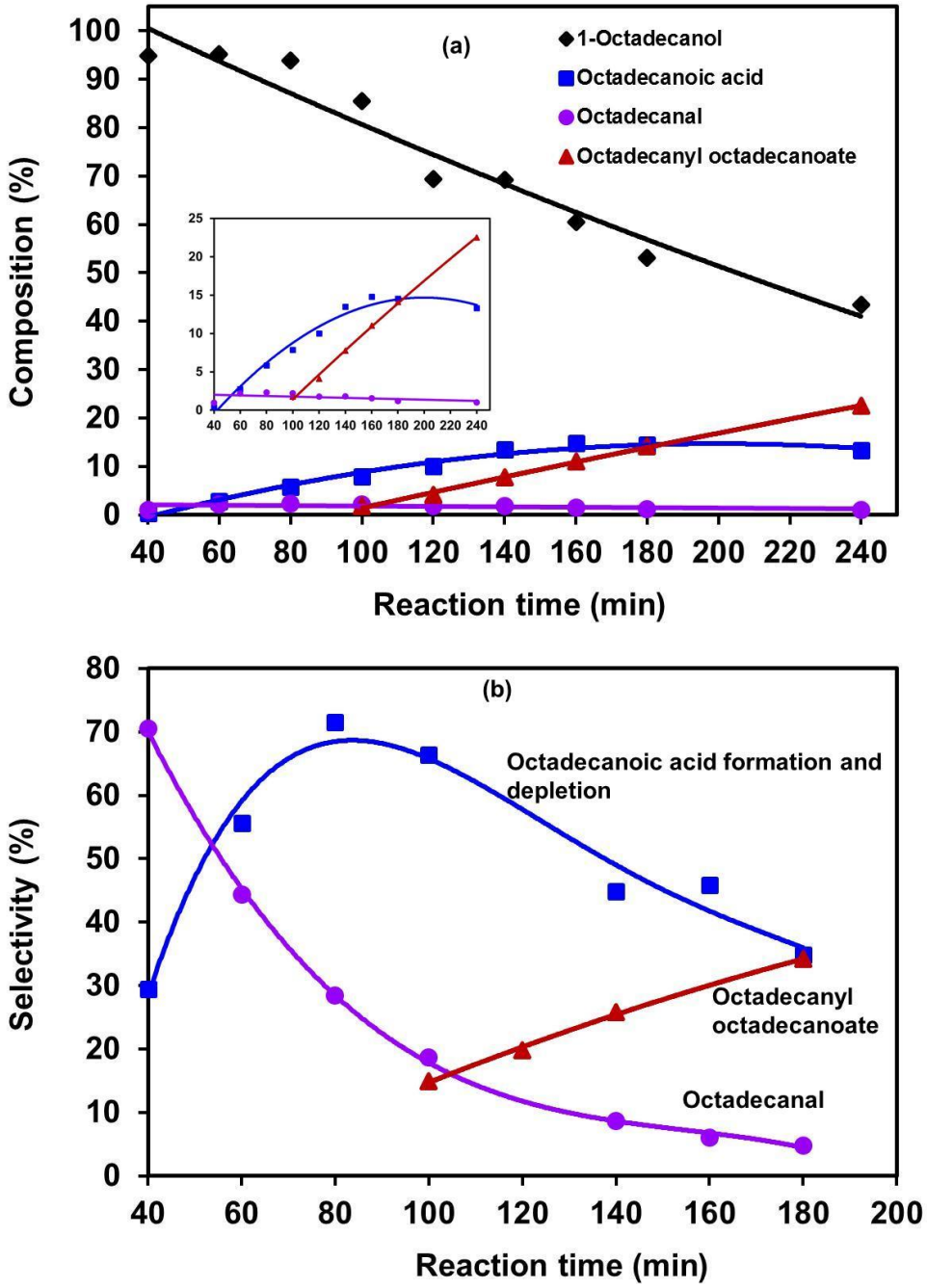

Figure 3.21. Reaction data from the oxidation of 1-octadecanol over flat model $Pt/SiO_2/Si$-wafer catalyst (surface **15**). (a) The changes in oxidation product composition as a function of reaction time during 240 min. The data was derived from a ^1H NMR analysis of the reaction medium. The insert chart is the y-axis enlarged section of the figure showing composition changes of products at less than 25 % content. (b) Selectivity of oxidation products as a function of time over 180 min.

The selectivity to octadecanoic acid and octadecanal was 66 % and 18 % respectively (Figure 3.21b). Octadecanoic acid was the major product in the product mixture reaching up to 71 % selectivity until the reaction progressed beyond 180 min. After 180 min, significant amounts of octadecanyl octadecanoate (40 % selectivity) were formed. This trend in respect to the production of octadecanoic acid and octadecanyl octadecanoate agrees very well with the IR data recorded in Figure 3.18b. The IR data showed that, the FTIR C=O stretching frequency at 1716 cm^{-1} was the favourable product until the reaction progressed beyond 180 min. At *ca.* 240 min, the FTIR C=O stretching frequency at 1732 cm^{-1} started to increase to become the major oxidation product. A very small amount of octadecanal was formed (*ca.* 2 % level was maintained during the course of the reaction) in this oxidation and could be identified by ^{1}H NMR analysis. The minute amount of octadecanal formed during the reaction is immediately oxidised further to octadecanoic acid as could be deduced from the increasing formation of the carboxylic acid.

According to the product trends outlined in Figure 3.21a, the oxidation of 1-octadecanol followed a mechanism where octadecanal is formed first by oxidative dehydrogenation.[45] The resultant octadecanal is subsequently oxidised further to form octadecanoic acid. In the reaction mixture, the amount of octadecanal remains constant at a steady state content of 2 % regardless of the increasing amount of octadecanoic acid and the consumption of the 1-octadecanol. This implies that the octadecanal is consumed constantly to form octadecanoic acid.

There was a noticeable connection between the formation of octadecanyl octadecanoate and the consumption of the 1-octadecanol. At about 120 min, the conversion of 1-octadecanol increased to about 30 % when the octadecanyl octadecanoate started forming in the reaction mixture. At the same time, the amount of octadecanoic acid in the reaction mixture started to stabilise at 15 % and ultimately decreased to 13 % (Figure 3.21). It is deduced that octadecanyl octadecanoate is formed by self-catalysed condensation of octadecanoic acid and 1-octadecanol (see Scheme 3.8). In this esterification reaction, octadecanoic acid acts as both a catalyst and a reactant.[46,47] A number of

self-catalysed esterifications of alcohols have been reported in the literature.[48,49] Solvent free self-esterification of 1-octadecanol provides a unique way to long chain esters. No literature on solvent free self-esterification on flat model catalyst was found.

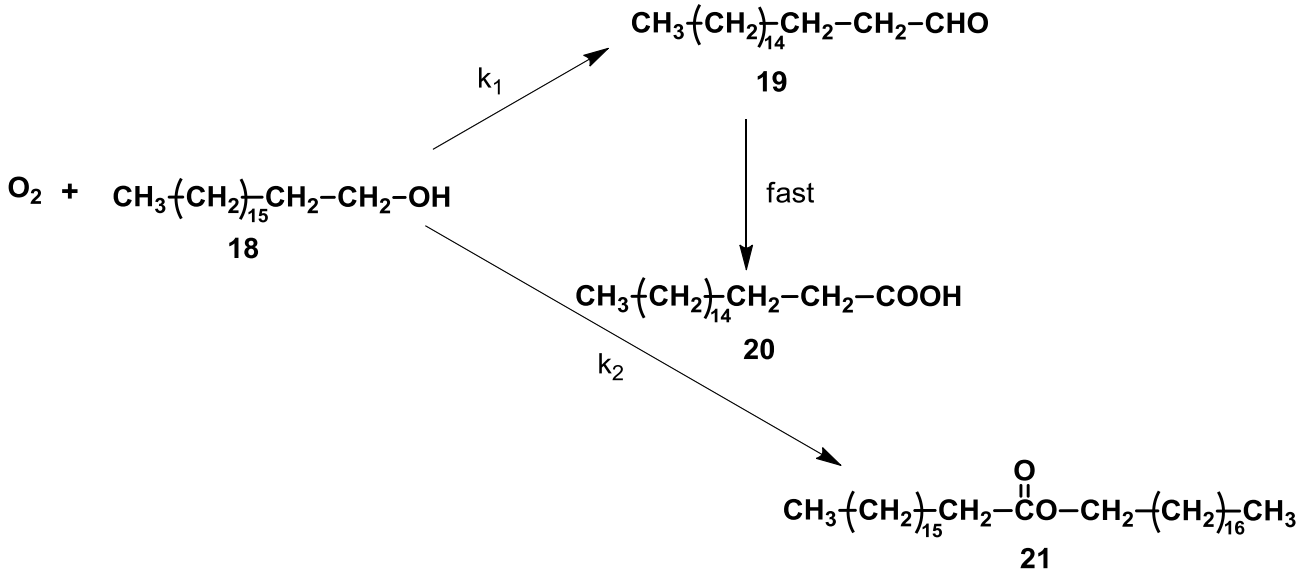

Scheme 3.8. Outline of the reaction pathway to esterification of 1-octadecanol to form octadecanyl octadecanoate.

Based on the RBS analysis, the amount of Pt loaded on the flat model $Pt/SiO_2/Si$-wafer catalysts prepared by grafting of K_2PtCl_4 solution (surface **14** and surface **15**)[v] was 11 atoms/nm^2. On a 81 mm^2 flat model $Pt/SiO_2/Si$-wafer catalyst used in the oxidation of 1-octadecanol, there was therefore 8.91×10^{14} Pt atoms loaded. In terms of oxidation turnover frequency (TOF) calculations, the challenge was to determine the number of available and active Pt atoms by titration techniques since the surface area covered by the Pt nano particles is very small relative to the entire model catalyst. Another challenge was the esterification of 1-octadecanol which takes place parallel to oxidation. In every mole of ester formed, a mole of oxidation product, octadecanoic acid and a mole of 1-octadecanol are consumed (Scheme 3.8). The oxidation TOF of the catalyst was determined

[v] Only surface **14** was analysed by Rutherford Backscattering Spectroscopy (RBS) to determine loaded Pt.

utilising equation 3.2 which is based on the loaded Pt atoms and final oxidation product mixture collected after the experiment. Of the 100 mg of 1-octadecanol used, about 15-20% sublimed and collected on the walls of the glass reactor. After 21 h, 80 mg of 1-octadecanol (0.30 mmol) was completely converted to the oxidation products and an ester. The oxidation TOF obtained after 21 h was 2.2 s^{-1}. The observed oxidation TOF indicated a fast reaction and comparable to the TOF = 3 s^{-1} for the solvent free oxidation of 1-phenylethanol over supported palladium nanoclusters.[50]

$$TOF = \frac{\left[\dfrac{(\text{Moles converted}) - \left(\dfrac{\text{Moles of an ester}}{2}\right)}{\text{Moles of Pt loaded}}\right]}{\text{Time(s)}} \qquad \textbf{3.2}$$

Here, TOF is the turnover frequency.

The model $Pt/SiO_2/Si$-wafer catalyst derived by grafting of K_2PtCl_4 solution followed by calcination and reduction at 350 °C (surface **15**) was also applied in solvent-free 1-octadecanol oxidation under a gentle stream of pure molecular oxygen at 105 °C (the discussion above used ambient air). The FTIR data of the oxidation product sample collected after 180 min is shown in Figure 3.22. A significant amount of 1-octadecanol was consumed after 180 min and the FTIR C=O stretching frequency corresponding to oxidation products was evident at 1714 cm^{-1}. The ^1H NMR showed 10 % residual 1-octadecanol after 180 min of reaction time. Surface **14** which was obtained by grafting of K_2PtCl_4 solution in aqueous ethanol without calcination and reduction steps at 350 °C gave similar results in oxidation of 1-octadecanol. In both model catalysts, the reaction was complete within 4 h. There was a slow but an observable consumption of 1-octadecanol when the flat model support without the Pt catalyst was used as a control reaction under the same experimental conditions. The significant difference between the results obtained from the control reaction and the

catalytic reaction was that the 1-octadecanol conversion in the control reaction resulted in unintended products with FTIR stretching frequency between 1978 cm^{-1} to 2165 cm^{-1}. Only small amount of oxidation products (less than 1 %) in the control reaction was detected which further proved that the observed oxidation that took place over surfaces **14** and **15** as shown by the FTIR C=O stretching frequency at 1714 cm^{-1} were assisted by the catalyst and is not due to auto-oxidation, or silicon-induced.

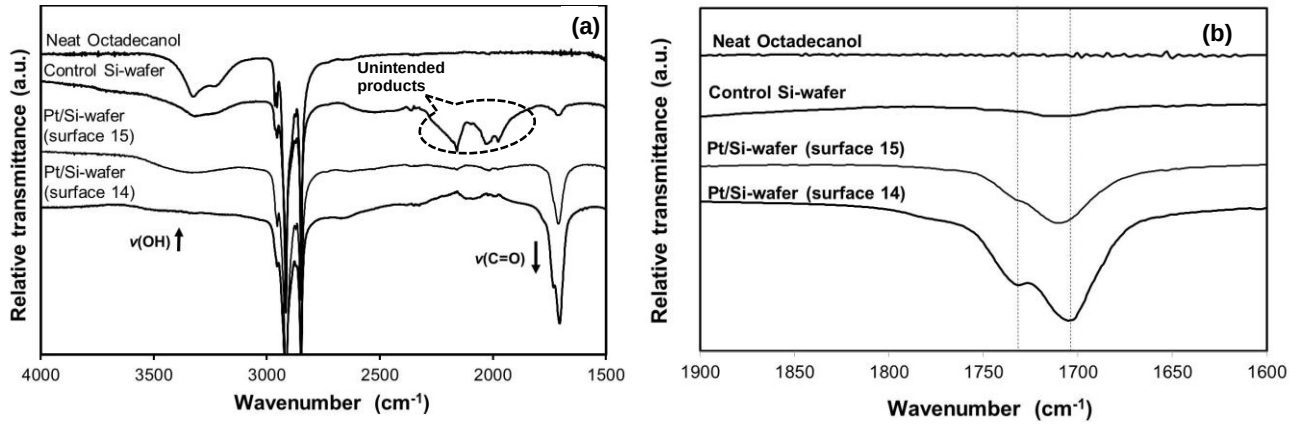

Figure 3.22. (a) Fourier Transform Infrared (FTIR) spectra of the product mixture from the oxidation of 1-octadecanol catalysed by surfaces **14** and **15**, the model Pt/SiO2/Si-wafer catalysts at 105 °C under a gentle stream of molecular oxygen. (b) Enlarged section of the FTIR C=O stretching frequency region.

Oxidation of 1-octadecanol over surface **15** with a gentle flow of molecular oxygen achieved higher conversions and selectivity to octadecanoic acid than oxidation done in ambient air. Noteworthy is that the presence of molecular oxygen did not only increase the 1-octadecanol conversion, but suppressed the formation of secondary product octadecanyl octadecanoate (Figure 3.23). At more than 90 % conversion of 1-octadecanol, the ratio of an ester to the octadecanoic acid was 1:2. The reverse is observed when ambient air is used as an oxidant. In ambient air, the oxidation is sluggish and 1-octadecanol react with the oxidation products when oxygen is depleted. In the presence of pure molecular oxygen (*i.e.* larger quantities), 1-octadecanol undergoes oxidative dehydrogenation to form

water and an aldehyde which ultimately form carboxylic acid. The 1-octadecanol oxidation TOF increased in the presence of pure molecular oxygen to 6.1 s^{-1}. Both TOFs obtained in oxidation of 1-octadecanol over surface **14** in the presence of ambient air or molecular oxygen are higher than the reported TOF ($1.3x10^{-3}$ s^{-1}) for the oxidation of hydroquinone over flat model Co/porphyrin/Si-wafer catalyst in the presence of molecular oxygen.[51] The activity of monometallic $Pt/SiO_2/SiO_2$/Si-wafer (surface **14**) is, however, lower than the activity of bimetallic flat model $Pd^{IV}Co^{III}/SiO_2$/Si-wafer catalyst which gave TOF of 12-14 s^{-1} in solvent free oxidation of 1-octadecanol in ambient air. [8]

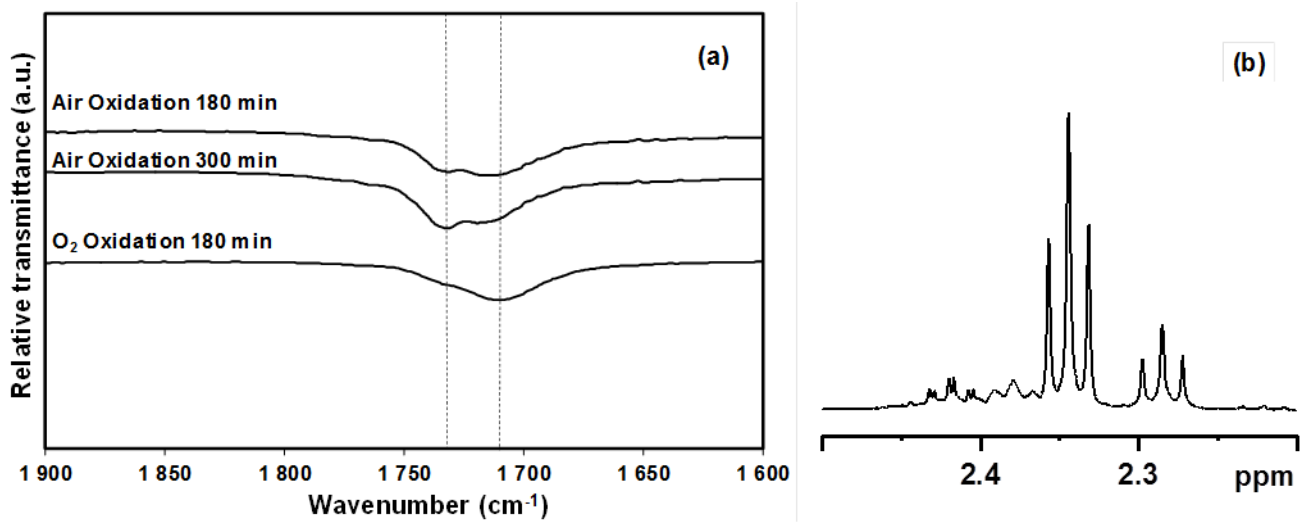

Figure 3.23. (a) The FTIR C=O stretching frequency region of the product mixture from the oxidation of 1-octadecanol catalysed by surface **15** using air (first 2 FTIR traces) and pure molecular oxygen (last FTIR trace) as oxidants. (b) The ^{1}H NMR spectrum of the oxidation product mixture which was obtained when pure molecular oxygen was used as an oxidant. The ^{1}H NMR spectrum shows signals of methylene protons of octadecanoic acid (2.35 ppm) and octadecanyl octadecanoate (2.28 ppm) adjacent to the carbonyl group.

3.3.2 Application of Surface 11 Flat Model Pt/SiO_2/Si-wafer in Oxidation Reactions

$H_2PtCl_6 \cdot 6H_2O$ was used as a precursor to prepare the model Pt/SiO_2/Si-wafer catalysts; surface **10** by grafting and surface **11** by spin coating. Surface **10** had fine particles with size diameter below the detection limit of the low resolution TEM used in this study. No reaction was obtained when surface **10** containing Pt, PtO and Pt-O-Si was utilised in the oxidation of 1-octadecanol in the presence of ambient air as oxidant. This is probably the result of too small platinum particles to allow surface adsorption by both oxidant (O_2 in air) and substrate (1-octadecanol) on the same particle.

Surface **11**[vi] had well defined Pt particles with average diameter of *ca*. 3 nm and also contained interface Pt-O, Pt-Si as determined by XPS analysis. When utilised for the oxidation of 1-octadecanol with ambient air as oxidant, FTIR analysis could detect C=O stretching frequency of oxidation products only after 10 h (Figure 3.24). The conversion of 1-octadecanol as determined by the decrease of FTIR stretching frequency intensity of the hydroxyl group showed that there was an induction period of about 10 h before the substrate was consumed steadily according to the same trends as observed in oxidation over surface **15** in ambient air. It was clear from the FTIR data that surface **11** was less active in oxidation of 1-octadecanol at the initial stages of the reaction relative to surface **15**. It has been shown previously that flat model catalysts prepared by grafting are superior to catalysts prepared by spin coating in oxidation of 1-octadecanol.[8] The particle size difference between the two catalysts may also play a role in the observed inequality of the oxidation activity. Surface **15** which was prepared by grafting of K_2PtCl_4 from solution has Pt particles with average diameter of *ca.* 5 nm while the Pt particles on surface **11** are *ca.* 3 nm in average diameter. On surface **15**, there was also Pt-N detected due to most probably the interphase layer between the Pt

[vi] Surface **11** was prepared by spin coating of 10 mM $H_2PtCl_6 \cdot 6H_2O$ solution on activated Si-wafer with surface allyl groups followed by calcination at 300 °C for 2 h and H_2 reduction at 350 °C for 2 h. XPS and TEM analysis showed Pt particles with interphase Pt-O-Si and Pt-Si.

particles and the support. The influence of surface N atoms in the oxidation of 1-octadecanol was not determined since it was not within the boundaries of this study, the allocated time for the study allowed the proof of concept that the prepared model Pt/SiO_2/Si-wafer catalysts have catalytic activity in oxidation of the substrate.

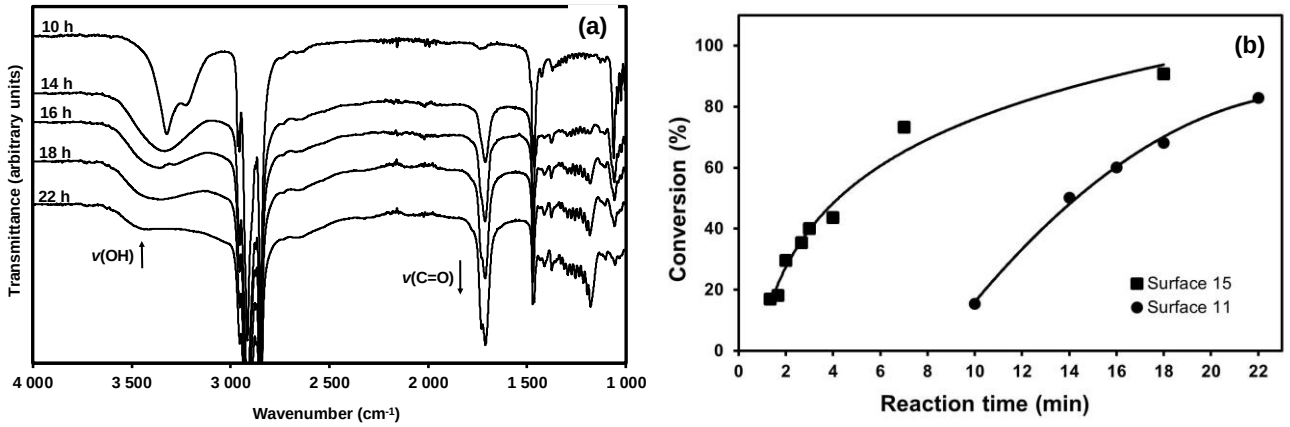

Figure 3.24. The FTIR spectra of the reaction mixture of the oxidation of 1-octadecanol catalysed by surface **11**, a model Pt/SiO_2/Si-wafer catalyst at 105 °C in ambient air. (b) 1-Octadecanol conversion as a function of reaction time from the analysis of oxidation product mixture catalysed by model Pt/SiO_2/Si-wafer catalysts (surface **15** and surface **11**).

According to the spin coating formula (equation 3.1), the Pt load on Pt/SiO_2/Si-wafer model catalyst was 1.6 Pt atoms/nm^2. Based on 83 % conversion, the oxidation TOF of surface **11** after 22 h was 8.6 s^{-1} which was higher than the TOF obtained over surface **15**. The catalyst loading on surface **11** was smaller than the Pt loading on surface **15**, which is why high TOF is observed even though there was a lag time for about 10 h before any product could be observed over surface **11**.

In summary, the flat model catalysts on SiO_2/Si-wafer (surfaces **11**, **14** and **15**) were successfully validated in solvent free oxidation of 1-octadecanol in ambient air and in molecular oxygen. The oxidation rates over these catalysts were determined by using the FTIR data and ^{1}H NMR data. Higher oxidation rates were obtained in the presence of pure molecular oxygen. The

oxidation rate over surface **15** increased in the presence of molecular oxygen from TOF = 2.2 s^{-1} in ambient air to 6.1 s^{-1} in molecular oxygen.

3.4 Application of Flat Model Pt/SiO_2/Si-wafer in Hydrogenation Reactions

Beside oxidation reactions discussed in the previous sections, the model Pt catalysts prepared by platinisation of functionalised flat model support SiO_2/Si-wafer were further validated as realistic model catalysts in hydrogenation of simple substrates with one alkene functional group (cyclohexene) and more complex substrates (benzaldehyde and cinnamyldehyde) with multiple functional groups such as aromatic, alkene and carbonyl functionalities. Since grafting of K_2PtCl_4 solution in aqueous ethanol also involves direct reduction of the Pt precursor to form colloidal Pt particles which adsorb on the surface of functionalised SiO_2/Si-wafer, the resultant platinised surface **14** was used in hydrogenation reactions.

Surfaces **11** and **15** which were obtained by oxidation and reduction of platinised surfaces did not show activity in hydrogenation reactions. The calcination and reduction at high temperature caused sintering of Pt particles to form larger particles[vii] and lose the shape (morphology) necessary for structure-sensitive hydrogenation reactions.[52] The following discussion is based on the results from hydrogenation over surface **14** which has the same Pt load as surface **15**. The difference between the two catalysts is the calcination and hydrogenation steps at 350 °C which were done to prepare surface **15**.

[vii] The average diameter of Pt particles in surface **14** increased from 2.5 nm to 5.0 nm in surface **15** after calcination at 300 °C for 2 h followed by reduction at 350 °C for 2 h.

3.4.1 Hydrogenation Over Surface 14 Flat Model Pt/SiO$_2$/Si-wafer Catalysts

Hydrogenation of a cyclohexene solution (1.7 M in hexane) was used as a benchmark to evaluate the activity of surface **14** containing Pt and Pt-N, in hydrogenation reactions. The conversion of cyclohexene to cyclohexane was determined by making use of ^{1}H NMR spectroscopy where the disappearance of the olefin proton signal at 5.70 ppm (see Figure 3.25) was used to monitor the activity of the catalyst.

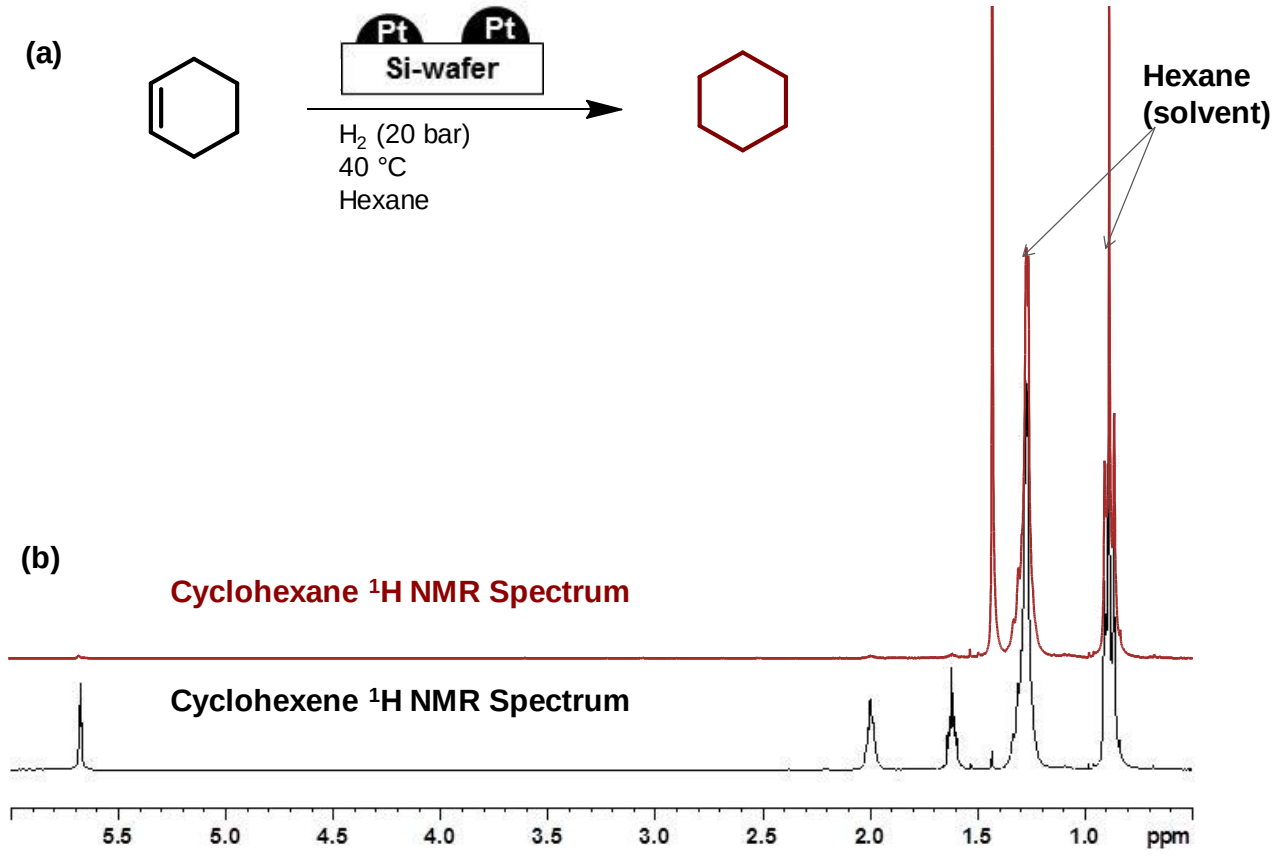

Figure 3.25. (a) The hydrogenation of cyclohexene over surface **14**, a model Pt/SiO$_2$/Si-wafer catalyst with 11 Pt atoms/nm^2, to form cyclohexane. (b) An overlay of the ^{1}H NMR spectrum of the solution of cyclohexene and *n*-hexane as a solvent before hydrogenation and the spectrum of hydrogenation product, cyclohexane, in the presence of the reaction solvent *n*-hexane. The ^{1}H NMR solvent was $CDCl_3$.

Based on the ^{1}H NMR data of crude product, the catalyst achieved 40 % conversion after 12 h at 40 °C and 20 bar H_2. When the reaction time is increased to 72 h, the conversion is quantitative. In both cases, cyclohexane is the only product detected as revealed by the intense singlet of cyclohexane protons at 1.49 ppm (see Figure 3.25). Hydrogenation of cyclohexene is uncomplicated and is often used as a probe reaction to determine the catalytic properties of supported catalysts in liquid phase hydrogenation of olefins.[53]

Hydrogenation of benzaldehyde is more challenging than cyclohexene because it has a less reactive carbonyl group which can be hydrogenated to form an alcohol group (Scheme 3.9). The aromatic phenyl ring may be hydrogenated by Pt catalysis to cyclohexyl analogues but this reaction requires substantial amount of energy.[54] A solution of benzaldehyde (1.6 M) in *n*-hexane was hydrogenated over surface **14** at 55 °C and 20 bar H_2 pressure. The target product for hydrogenation reaction was benzyl alcohol which would form by hydrogenation of the carbonyl group. After a 12 h reaction, the ^{1}H NMR analysis of the crude product sample showed a new signal at 4.7 ppm which corresponds to the methylene protons of benzyl alcohol. The conversion of benzaldehyde to benzyl alcohol was determined from the ^{1}H NMR data to be 70 % with *ca.* 61 % yield in this time period. The reported yield was based on the collected crude sample after the evaporation of the solvent. Some product material could be lost during product work up. No other products, especially cyclohexyl analogues, were detected by ^{1}H NMR. The reaction TOF at 70 % aldehyde conversion was determined using equation 3.3 to be 7.5 per moles per Pt moles per second.

$$\mathrm{TOF} = \frac{\left[\dfrac{(\text{moles of substrate converted})}{\text{moles of Pt loaded}}\right]}{\text{time(s)}} \qquad \textbf{3.3}$$

The solvation effect of *n*-hexane, which was used as a solvent, may have minor contribution to high selectivity towards benzyl alcohol.[54,55] Aprotic solvents such as *n*-hexane have high affinity to solvation of an aromatic ring and orientate the carbonyl group towards the metal surface leading to hydrogenation.[56] Hydrogenation of an aromatic ring is more likely when the reaction is done with a polar solvent[54] where the aromatic ring is orientated towards the metal surface.[56] The experiment was repeated under the same conditions over oxidised Si-wafer with no Pt particles loaded. After 12 h, only traces of benzyl alcohol were detected and almost all of the starting material was present with no apparent transformation. This confirmed that the hydrogenation of benzyl alcohol observed over surface **14** was accelerated by Pt particles.

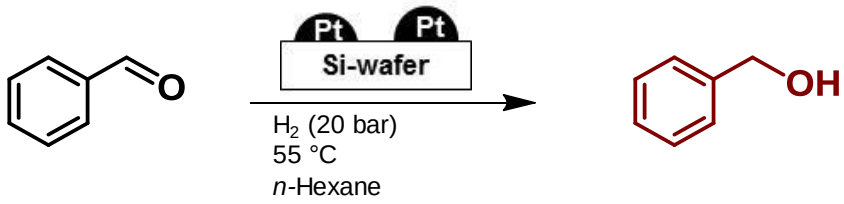

Scheme 3.9. The hydrogenation of benzaldehyde over surface **14**, a model Pt/SiO_2/Si-wafer catalyst 11 Pt atoms/nm^2, to form benzyl alcohol.

An aromatic analogue of benzaldehyde, cinnamaldehyde, was used as a more complex substrate to determine the activity of the model Pt/SiO_2/Si-wafer catalysts. Cinnamaldehyde has two main functional groups, an alkene and an aldehyde group, which are susceptible to catalytic hydrogenation. Hydrocinnamaldehyde is formed when hydrogenation took place on the alkene group while cinnamyl alcohol is formed when the aldehyde carbonyl group is hydrogenated. Total hydrogenation of the alkene and the carbonyl group results in the formation of 3-phenyl-1-propanol as depicted in Scheme 3.10.

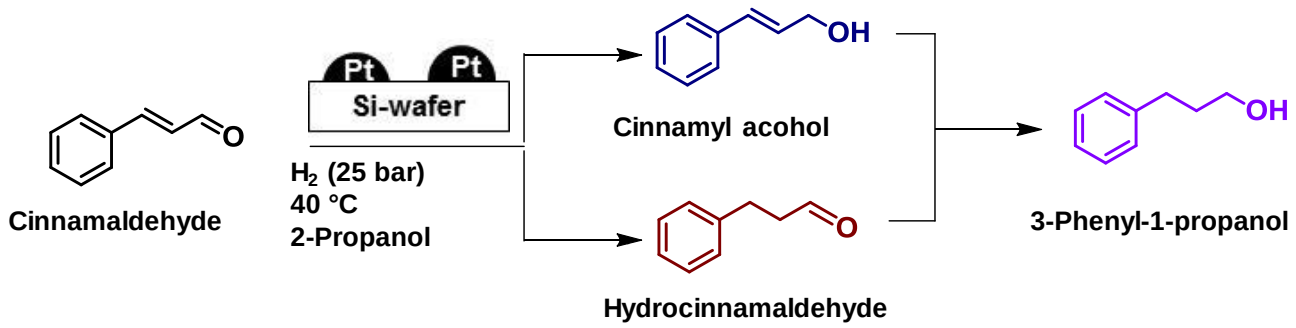

Scheme 3.10. An outline of the hydrogenation of cinnamaldehyde solution in 2-propanol to form cinnamyl alcohol, hydrocinnamaldehyde and 3-phenyl-1-propanol over surface **14**, a model $Pt/SiO_2/Si$-wafer catalyst with 11 Pt atoms/nm^2.

A solution of cinnamaldehyde (3.2 M) in 2-propanol was hydrogenated over surface **14** at 40 °C and 25 bar H_2 pressure. The ^{1}H NMR spectrum of the crude product showed multiple signals at 6.5 ppm and also in the region 1.5 ppm to 4.5 ppm which belong to the methine and methylene protons of the hydrogenation products (see Figure 3.26). In addition to these signals, a characteristic aldehyde proton signal of hydrocinnamaldehyde resonated as a triplet at 9.82 ppm. The peak integrals of methylene protons at 2.96 ppm, 3.70 ppm, 4.35 and the internal standard, 1,1,2,2,-tetrachloroethane were used to quantify the hydrogenation products in the product mixture. After 24 h in reaction, the conversion of cinnamaldehyde to hydrogenation products was 60 % and the product distribution indicated that saturation of α-olefin to hydrocinnamaldehyde was more favoured with 36.6 % selectivity. The rest of hydrogenation products formed were cinnamyl alcohol (15 % selectivity) and 3-phenyl-1-propanol in 36 % selectivity. It should be noted that the solvent, 2-propanol was not detected by ^{1}NMR in the crude product. Analysis of the gas samples using mass spectroscopy showed a molecular ion which correspond to propane. Thus, under the experimental conditions, 2-propanol hydrolysed to form volatile propane *via* a well-known catalytic hydrogenolysis mechanism.[57]

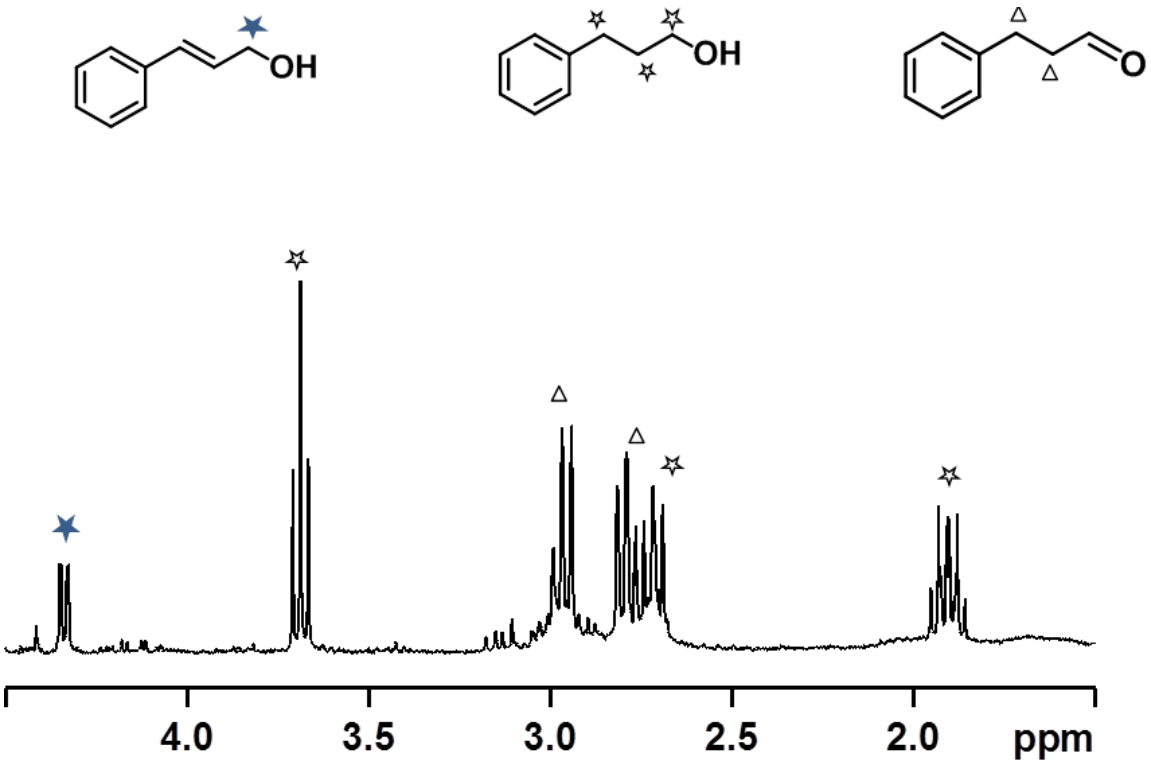

Figure 3.26. ^{1}H NMR spectrum of the reaction mixture of cinnamaldehyde hydrogenation catalysed by surface **14**, a model Pt/SiO_2/Si-wafer catalyst with 11 Pt atoms/nm^2. Only the region showing the methylene proton signals is provided.

In addition to methylene protons of the hydrogenation products, the ^{1}H NMR analysis showed two sets of doublets centred at 6.3 ppm and 7.6 ppm which belong to the olefinic methine protons of cinnamic acid (12.5 % selectivity) as highlighted in Figure 3.27a in page 119.[58] The presence of cinnamic acid in the hydrogenation product mixture implied that during hydrogenation, cinnamyldehyde is competitively oxidised likely by the classical hydration to geminal diol followed by dehydrogenation to cinnamic acid as illustrated in Scheme 3.11.[59,60] The presence of the intermediate products to cinnamic acid was not detected in this study and the water involved in the postulated hydration pathway to cinnamic acid might have been present in the reagents.

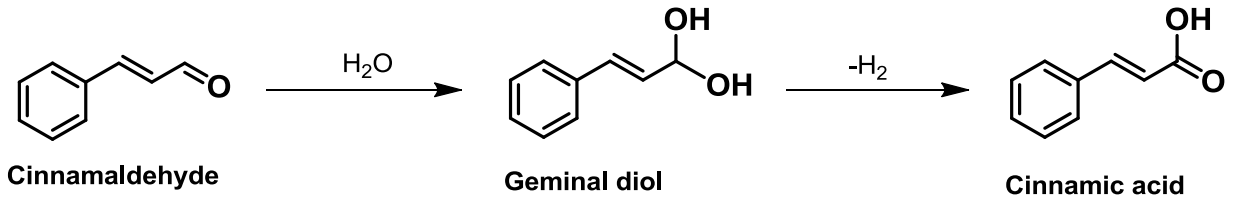

Scheme 3.11. Outline of cinnamaldehyde dehydration to cinnamic acid.

The addition of $NaHCO_3$ solution (4 mM in water) to the reaction solution suppressed the formation of side products especially cinnamic acid as illustrated by the overlay of ^{1}H NMR spectra of hydrogenation product mixture in Figure 3.27. At the same time, there was no improvement in the conversion of cinnamaldehyde to the desired products after the addition of the $NaHCO_3$ solution. When NaOH solution (4 mM in water) was added to the hydrogenation solution, the formation of side products was suppressed completely. Furthermore, cinnamaldehyde was converted completely after 24 h at 40 °C and 25 bar H_2 pressure. The main products detected by ^{1}H NMR analysis were 3-phenyl-1-propanol and hydrocinnamaldehyde with 75 % and 25 % selectivity respectively.

It has been previously shown that the co-impregnation of alkali ions increases the electronic density of metal particles supported on porous powder such as zeolites and CeO_2.[61,62,63] The alkali ions further improve the adsorption of cinnamaldehyde on electron rich Pt particles by polarising the C=O bond and enhance hydrogenation to cinnamyl alcohol.[64] The activation of C=O bond to form cinnamyl alcohol suppresses the hydration reaction and formation of side products such as acetals and ethers.[64,63] Both hydrocinnamaldehyde and cinnamyl alcohol are further hydrogenated to 3-phenyl-1-alcohol. NaOH solution has better promoting effect than $NaHCO_3$ as could be seen by the cinnamaldehyde conversion (100 % *vs* 59 % respectively) obtained when these bases have been added to the reaction solution.

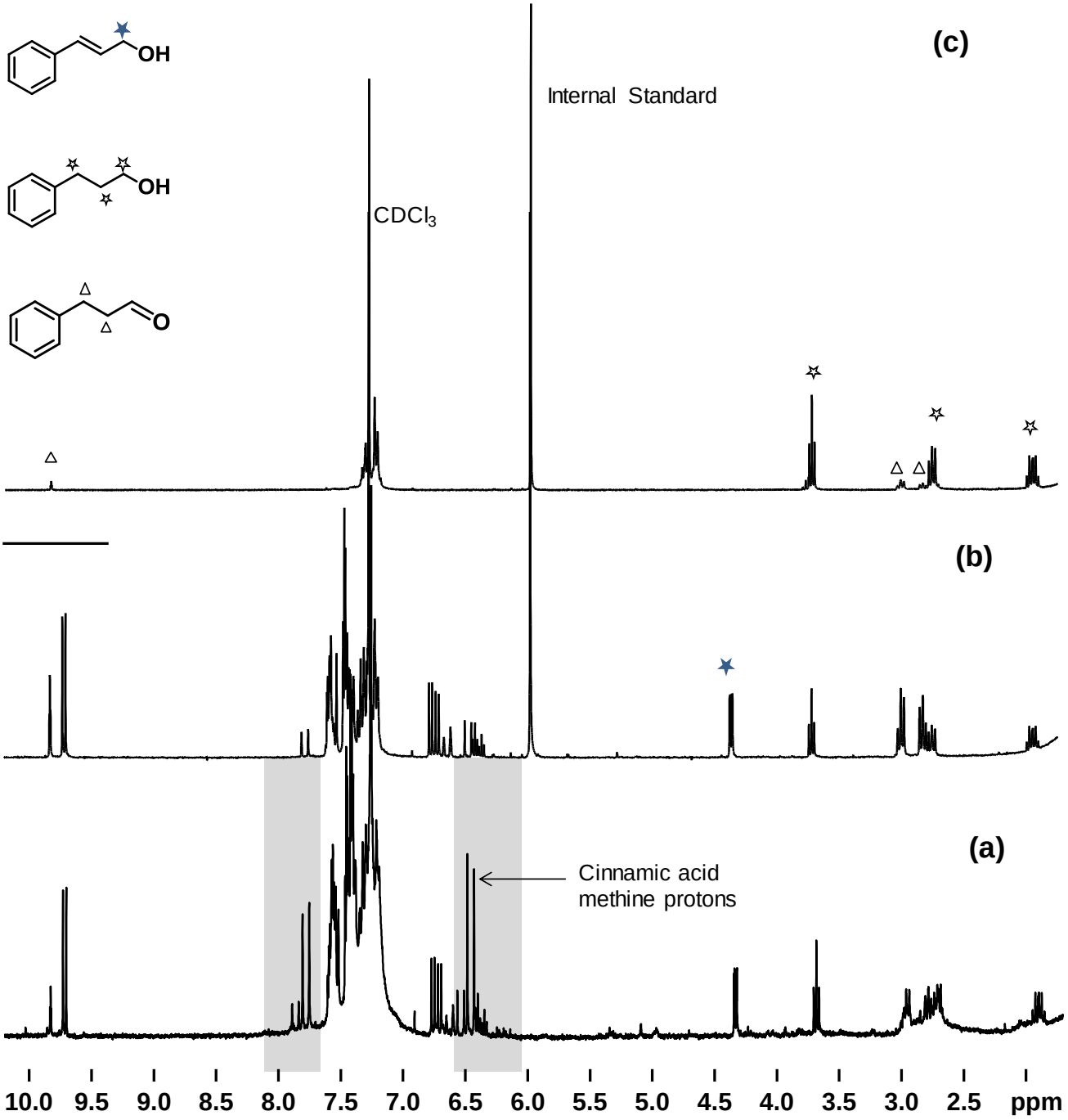

Figure 3.27. An overlay of ^{1}H NMR spectra of the reaction mixture of cinnamaldehyde hydrogenation catalysed by surface **14** with (a) no base added, (b) with 24 mM $NaHCO_3$ solution added and (c) 4 mM NaOH solution added to the hydrogenation solution. The shaded area in (a) shows the signals due to the side products such as cinnamic acid.

To get more understanding of the product slate achieved by hydrogenation of cinnamaldehyde in the presence of NaOH solution, the reaction was monitored by ^{1}H NMR over time. The

cinnamaldehyde conversion and product selectivities as function of reaction time are presented in Figure 3.28. After 6 h of reaction time, hydrocinnaldehyde was the major product with 62 % selectivity. Hydrocinnamaldehyde was depleted over 24 h reaction time in favour of 3-phenyl-1-propanol. A small amount of cinnamyl alcohol was quantified with only 21 % selectivity observed after 9 h of reaction time.

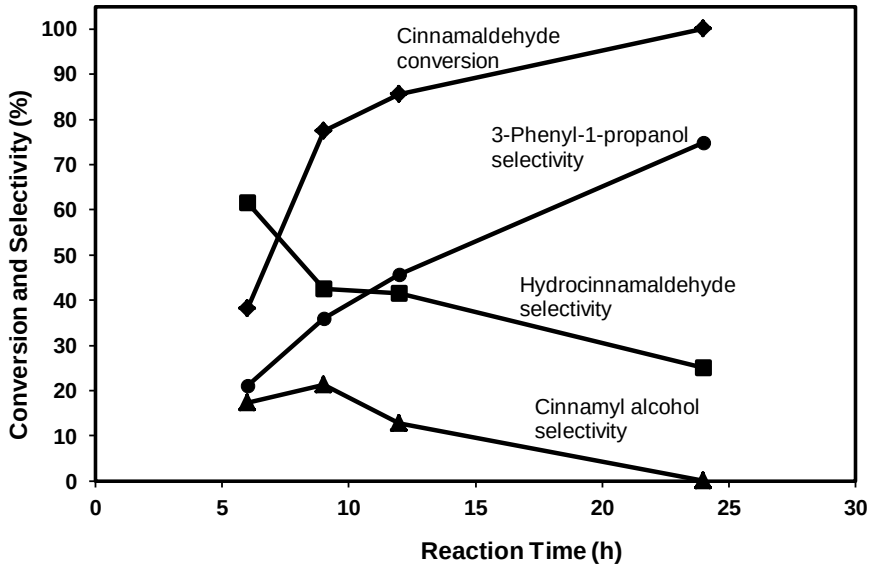

Figure 3.28. The curves of cinnamaldehyde conversion to its hydrogenation products and relative selectivities of hydrocinnamaldehyde, cinnamyl alcohol and 3-phenyl-1-propanol plotted against reaction time. The curves were derived from the ^{1}H NMR signals of the methylene protons and the olefin protons of the starting material and the hydrogenation products.

The overall TOF of the reaction after complete hydrogenation of cinnamaldehyde at 24 h was 3.3 s^{-1}. The observed hydrogenation TOF was within the same range as the TOFs (2-5 s^{-1}) of the bimetallic $PtAu/SiO_2$ catalyst and higher than the TOFs (0.03 to 0.24 s^{-1}) of monometallic Pt/SiO_2 which were used in cinnamaldehyde hydrogenation at 150 °C and 10 bar hydrogen partial pressure.[65] It should be noted that the observed TOF of flat model Pt/SiO_2/Si-wafer catalyst (surface **14**) is based on the total Pt load that is 11 atoms/nm^2. Therefore, this activity given by TOF could be under estimated since some of the Pt atoms are not exposed to the substrate. A highly active Pt catalyst on

powder support, can achieve between 10 to 20 s^{-1} cinnamaldehyde hydrogenation TOF under similar conditions used in this study.[64]

The results implied that the hydrogenation of cinnamaldehyde at alkene carbonyl group (3,4-addition) was more preferred than the hydrogenation of the carbonyl group (1,2-addition) especially in the first 12 h of the reaction time. The selectivity to hydrocinnamaldehyde is influence by the Pt particle size among other factors. The average particle size of Pt on surface **14** used as a model catalyst was 2.5 nm according to the low resolution TEM analysis. Larger Pt particle sizes (5-12 nm) favour hydrogenation of carbonyl bond to form cinnamyl alcohol.[64,66] Therefore the majority of Pt particles on surface **14** would favour the formation of hydrocinnamaldehyde in agreement with the results in Figure 3.28. Surface **15** with larger particles (5 nm average diameter) did not have activity in the hydrogenation reaction because the morphology of the particles was altered during calcination and reduction at 350 °C.

The validation of the flat model catalysts Pt/SiO_2/Si-wafer (surface **14**) in liquid phase hydrogenation of various substrates was achieved. Based on TOF values obtained from the hydrogenation of benzaldehyde and cinnamaldehyde, activity of surface **14** is within the same ranges as the published literature. The hydrogenation of cinnamaldehyde which has multifunctional groups follows a thermodynamically favoured route where the alkene functional group is hydrogenated to form hydrocinnamaldehyde followed by the hydrogenation of the carbonyl group to cinnamyl alcohol.

3.5 Supported Pt Catalysts on Porous (3-D) Zeolites for Organic Transformations

After the above described Pt catalyst systems supported on 2-D Si-wafers, the attention was focussed on Pt catalysts supported on 3-D supports, specifically zeolites. Supported Pt catalysts were successfully prepared by impregnation of porous zeolite supports, the so called KL-zeolite and

HY-zeolite. Zeolites are porous materials composed of a defined framework of silicates and aluminates in specific ratio. KL-zeolites are basic in nature due to the presence of K^+ cation in the structure, and the Si: Al ratio is frequently 3 but can be 1 to 20. HY zeolites are acidic in nature due to the presence of the proton H^+ in the structure. Various techniques were used to determine the extent of catalyst loading on the support, the oxidation states of the catalyst and available active sites. The catalysts were then applied in transformation of organic substrates to valuable building blocks. Some of the catalytic reactions done over the prepared catalysts were only used as probe reactions to understand the catalytic activity of the catalysts.

3.5.1 Characterisation of Fresh Pt/Zeolite Catalysts

The extent of platinum loading on Pt/zeolite catalysts was confirmed by inductively coupled plasma – optical emission spectroscopy (ICP-OES) after calcination at 350 °C. The Pt content in catalysts with theoretical loading of 1 wt% was found to range between 0.9 wt% and 1.0 wt% at 95% confidence interval for catalysts prepared by incipient wetness impregnation and vapour phase impregnation respectively. These results confirmed that the metallic phase, platinum, was successfully incorporated into the zeolitic porous support.

Successful loading of Pt on KL-zeolite support was also confirmed by the changes in specific surface area and porosity of the support. The adsorption isotherms of nitrogen gas (N_2) for KL-zeolite sample before impregnation and after impregnation with platinum precursors are shown in Figure 3.29, surface and porosity properties are summarised in Table 3.3. It could be noted that the isotherm curves for the adsorbed nitrogen are similar in shape (see Figure 3.29) which means that there was no major structural changes such as the collapse of zeolite channels that took place during impregnation or calcination. The shape of the isotherm curves resembles type 1 isotherm which is the characteristic of materials with small pores.[67]

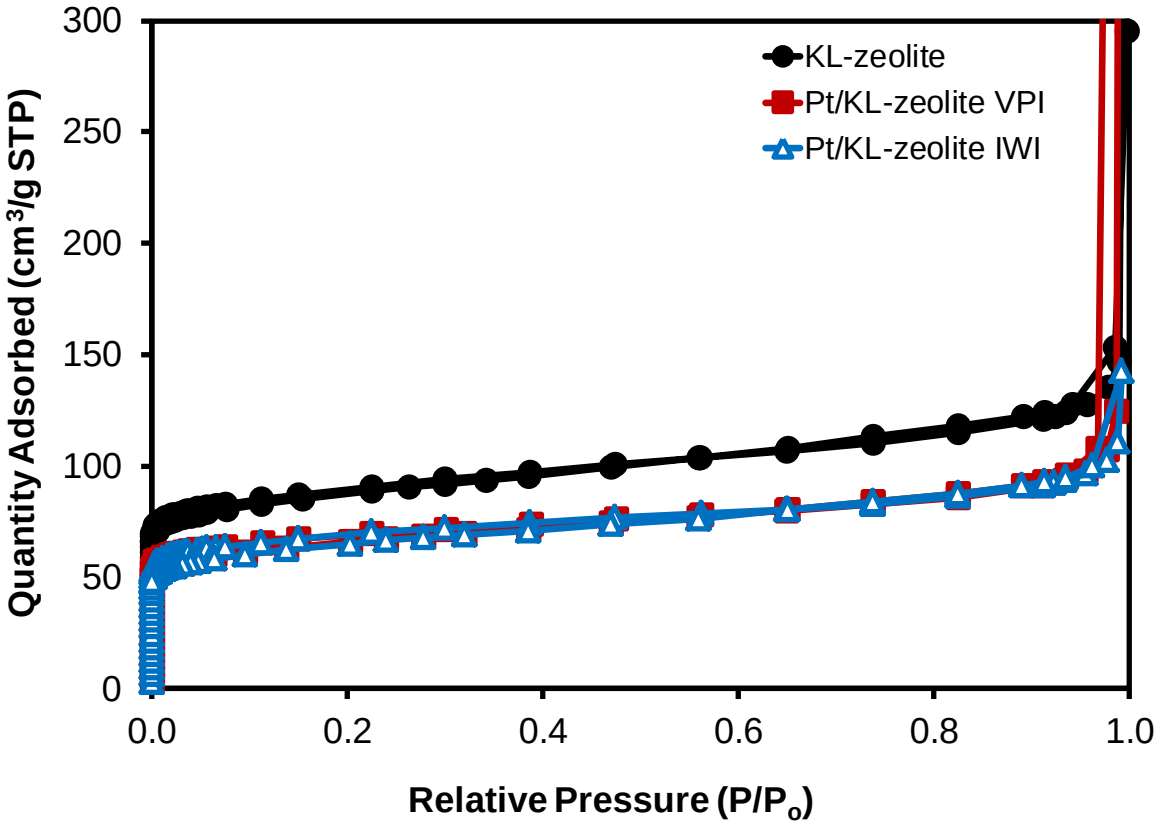

Figure 3.29. Adsorption isotherms of nitrogen for KL-zeolite before impregnation with the Pt precursor and after impregnation with $Pt(acac)_2$ using vapour phase method (Pt/KL-zeolite VPI) and incipient wetness impregnation of $Pt(NH_3)_4(NO_3)_2$ solution (Pt/KL-zeolite IWI). The physisorption was done on Pt/KL-zeolite samples after calcination at 300 °C.

Table 3.3. The surface and porosity properties of KL-zeolite before impregnation with the Pt precursor and after impregnation with $Pt(acac)_2$ using vapour phase method (Pt/KL-zeolite VPI) and incipient wetness impregnation of $Pt(NH_3)_4(NO_3)_2$ solution (Pt/KL-zeolite IWI).

Sample	Surface Area (BET, m^2/g)[a]	Micropore Volume (cm^3/g)
KL-zeolite	301 (290)[b]	0.10
Pt/KL-zeolite-VPI	238	0.08
Pt/KL-zeolite-IWI	191	0.06

a: based on Brunauer, Emmett and Teller (BET) theory[68], b: surface area given by the value in brackets refers to the value given by the KL-zeolite supplier, Tosoh Corporation, Japan.

In addition to the shape of the isotherm curves, it could be notable that the nitrogen quantity adsorbed decreases after the Pt impregnation. The decrease in nitrogen quantity adsorbed after Pt impregnation indicated that the channels of the support were partially filled with Pt after impregnation. This influenced the surface area which decreased from 300 m^2/g to 191 m^2/g in Pt catalyst prepared by incipient wetness impregnation with $Pt(NH_3)_4(NO_3)_2$ (Pt/KL-zeolite IWI). The surface area in catalyst prepared by vapour phase impregnation with platinum acetylacetonate (Pt/KL-zeolite VPI) decreased to 259 m^2/g in Pt/KL-zeolite VPI (see Table 3.3). The effect of impregnation was minimal on micropore volume which remained at *ca.* 0.1 cm^3/g in both catalysts. This implied that the pores remained open after impregnation and could be used for catalysis purposes.

The colour of freshly impregnated Pt/KL-zeolite catalyst was either white after incipient wetness impregnation with $Pt(NO_3)_2(NH_3)_4$ or light yellow after vapour phase impregnation with $Pt(acac)_2$. After calcination and reduction of these catalysts, the colour changed to light grey indicating the presence of the platinum metallic state.[69]

The results from the XPS analysis of the Pt oxidation states of the prepared Pt/KL-zeolite catalysts are recorded in Figure 3.30. The Pt 4f signals from Pt/KL-zeolite catalysts after charge correction with C 1s peak (at 284 eV), were comparable to the XPS data from Pt/SiO_2/Si-wafer model catalysts. A good similarity was observed in the binding energies of Pt $4f_{7/2}$ from catalysts prepared by incipient wetness impregnation and spin coating impregnation (see Figure 3.30b and Figure 3.30d). Only Pt^0 oxidation state could be identified when the Pt/KL-zeolite catalyst was prepared by incipient wetness impregnation. In Pt/KL-zeolite catalysts prepared by vapour phase impregnation, the Pt $4f_{7/2}$ peaks at 70.7 eV and 72.0 eV are attributable to Pt^0 and Pt^{2+} contribution respectively (see Figure 3.30c). Similarly, the Pt/HY-zeolite catalyst prepared by incipient wetness impregnation had the same Pt $4f_{7/2}$ peaks at 71.5 eV and 72.9 eV which correspond to the Pt^0 and Pt^{2+} species respectively (see Figure 3.30d).

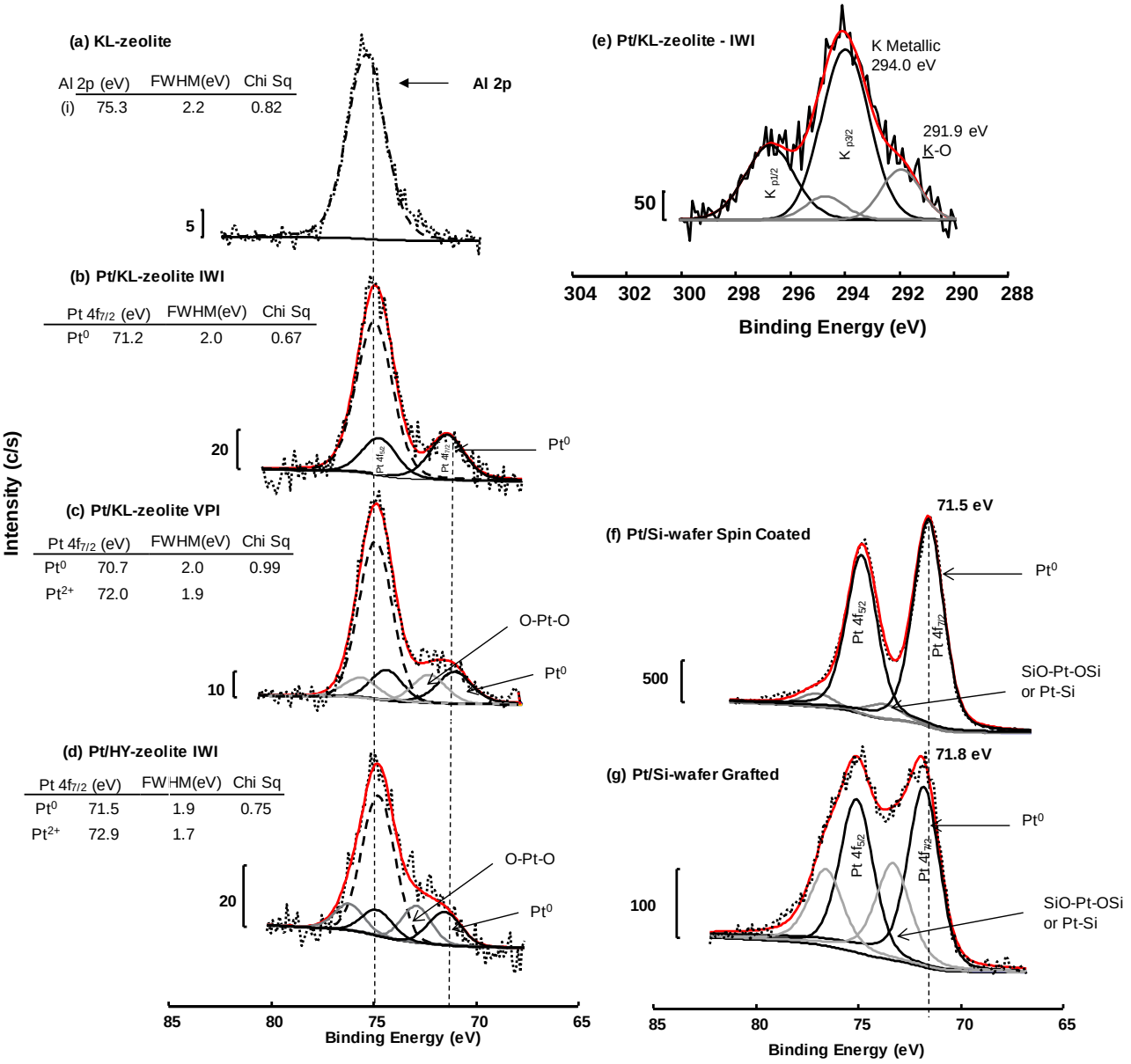

Figure 3.30. XPS data of Al 2p and Pt 4f from the analysis of (a) KL-zeolite, (b) Pt/KL-zeolite catalyst prepared by incipient wetness impregnation (IWI) and (c) Pt/KL-zeolite catalyst prepared by vapour phase impregnation (VPI), (d) Pt/HY-zeolite catalysts prepared by incipient wetness impregnation and (e) K 2p from the analysis of Pt/KL-zeolite-IWI. Also shown is the XPS data of Pt 4f from the analysis of the flat model catalysts (f) prepared by spin coating the Pt precursor and (g) Pt/SiO2/Si-wafer prepared by grafting of Pt precursor. The table inserts present the binding energies of Al 2p and Pt $4f_{7/2}$, the full width at half maximum (FWHM) and the goodness of fit (Chi Square). Red line: theoretical fitted curve. Dotted black line: experimentally measured curve. Other lines: peaks theoretically introduced to replicate the experimentally determined curve.

The Pt^{2+} specie in the prepared Pt/zeolite catalysts is due to the interaction of the metal with the support[70] and is consistent with the XPS data collected from Pt/SiO_2/Si-wafer model catalyst where a Pt^{2+} species due to Pt-O bond were detected at *ca.* 72.5 eV to 73 eV (see Figure 3.30c and Figure 3.30f). The presence of Pt^{2+} specie indicates that the Pt clusters in Pt/KL-zeolite prepared by vapour phase impregnation method form a sigma bonding with the support. Attempts to determine the binding energy of the core level electrons of O 1s which correspond to Pt-O specie were unsuccessful since the Al-O species which makes up the zeolite matrix also exhibits the same binding energy *ca*. 530.7 eV.[71,72] Previous reports showed that the Pt/KL-zeolite catalysts which are prepared by the vapour phase impregnation have small Pt clusters with strong interaction with the walls of the support resulting in Pt-O bond formation.[73,74] However, the metal-support interaction is relatively poor when the Pt/KL-zeolite catalyst is prepared by incipient wetness impregnation.[73]

In addition to the XPS data of Pt 4f, the Al 2p signal of the zeolite support was detected at *ca*. 25 eV in the calcined KL-zeolite and reduced Pt/zeolite catalysts. The resolution of the XPS spectra was good enough to identify the Pt 4f spin doublet after curve fit even though it overlaps with the Al 2p spectral peak (see Figure 3.30). Also detected by XPS analysis were the K 2s and K 2p spectral peaks centred at 379.2 eV and 294.0 eV respectively in KL-zeolite and Pt/KL-zeolite catalyst samples. It is important to retain K^+ ions in the KL-zeolite matrix after Pt impregnation to maintain the basic nature of the support.

The volumetric titration of carbon monoxide (CO) and hydrogen (H_2) was used to determine the chemisorption properties of Pt/KL-zeolite catalysts recorded in Table 3.4 and to determine the dispersion and the crystallite sizes of impregnated Pt. The H_2 uptake by Pt/KL-zeolite catalysts prepared by incipient wetness impregnation is higher than the CO uptake and thus the H_2/Pt ratio is higher than the CO/Pt ratio. The observed chemisorption behaviour is in accordance to the previously reported results where Pt/KL-zeolite catalyst chemisorbs more H_2 than CO.[75] This trend implies that the Pt particles are not easily accessible to larger CO gas molecules. At the same time,

the CO chemisorption data give a true reflection of the amount of Pt active sites inside the pores that are available for catalytic reactions since the reactants are larger than the H_2 gas molecules.

Based on CO chemisorption data, the Pt/KL-zeolite catalyst prepared by vapour phase impregnation have high particle dispersion of up to 91.5 % relative to 75.8 % obtained for incipient wetness impregnated catalyst as summarised in Table 3.4. The average diameter of Pt crystallite in Pt/KL-zeolite prepared by vapour phase impregnation is 1.2 nm while for incipient wetness impregnated catalyst is 1.5 nm. In both catalysts, the Pt crystallites that are smaller than the average diameter are likely to be found inside the zeolite channels (*ca*. 1.3 nm in diameter).

Table 3.4. CO and H_2 chemisorption data collected at 35 °C on freshly reduced Pt/KL-zeolite and Pt/HY-zeolite catalysts. IWI: Incipient Wetness Impregnation and VPI: Vapour Phase Impregnation.

Catalyst	Adsorbed Gas [(a)] (μmol/g of catalyst)		Gas : Metal Ratio [(b)]		CO Chemisorption	
	CO	*H_2*	*CO/Pt*	*H_2/Pt*	*Dispersion (%)*	*mean diameter (nm)*
Pt/KL-zeolite IWI	32.3	47.6	0.75	1.1	75.8	1.5
Pt/KL-zeolite VPI	42.2		0.92		91.5	1.2
Pt/HY-zeolite IWI	42.0		0.93		92.0	1.2

(a): moles of irreversible gas chemisorption which is equivalent to the available metal for catalysis, (b): Molar ratio of chemisorbed gas to Pt loading.

The Pt/HY-zeolite catalyst prepared by incipient wetness impregnation had similar chemisorption data to Pt/KL-zeolite catalyst prepared by vapour phase impregnation. The HY-zeolite support has large pores (*ca*. 0.75 nm dimeter)[76] and micropore volume (0.242 cm^3/g *vs* 0.10 cm^3/g in KL-zeolite)[77] which make it easy for the solution of the Pt precursor to fill in the zeolite cages with minimum agglomeration or pore-blockages that may cause poor particle dispersion observed in Pt/KL-zeolite IWI catalyst.

3.5.2 Application of Pt/KL-Zeolite Catalysts in Aromatisation of n-Alkanes

The prepared Pt/KL-zeolite catalysts were applied in catalytic aromatisation of neat *n*-hexane, *n*-heptane and *n*-octane to corresponding aromatics (Figure 3.31). *n*-Alkane feeds contaminated with varying concentrations of catalyst poisons acetic acid, propionaldehyde and thiophene were also used in catalytic aromatisation to determine impact of these poisons on aromatisation.

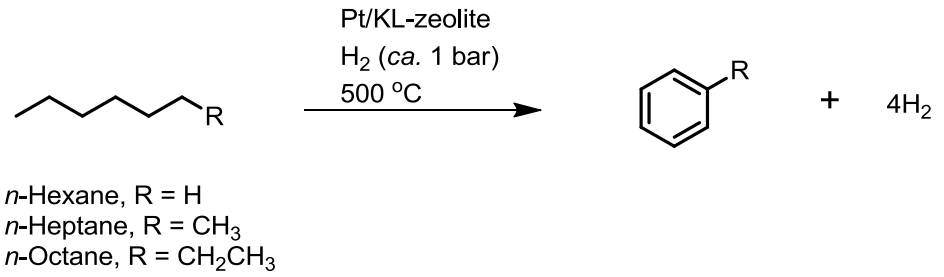

Figure 3.31. Outline of the aromatisation of *n*-alkanes to corresponding aromatics. The weight hourly space velocity which determines the catalyst contact time with the feed was varied between 2.5 h^{-1} to 5 h^{-1}.

3.5.2.1 Aromatisation of n-hexane feeds: Preliminary screening

Initially, the Pt/KL-zeolite catalyst prepared by incipient wetness impregnation was used in aromatisation of neat *n*-hexane and in aromatisation of *n*-hexane feeds contaminated with catalyst poisons propionaldehyde, acetic acid or thiophene at 500 °C with weight hourly space velocity (WHSV)[viii] of 4 h^{-1} and H_2:Hexane molar ratio of 2.5. The activity of the Pt/KL-zeolite catalyst in terms of *n*-hexane conversion and aromatisation selectivity over the duration of 20 h on stream is presented in Figure 3.32. At 10 h on stream, the conversion of neat *n*-hexane was 66 % and declined

[viii] Weight hourly space velocity = (mass of *n*-hexane feed / hour) / (mass of Pt/KL-zeolite catalyst loaded). WHSV indicates the catalyst contact time with the feed. The contact time of the catalyst with the reactants is prolonged at low WHSV. The given WHSV is only based on *n*-hexane feed rate excluding the H_2 feed rate.

to 54 % after 20 h. The observed decline in *n*-hexane conversion indicates the deactivation of Pt/KL-zeolite catalyst over time.

The presence of 0.1 wt% oxygenates propionaldehyde or acetic acid in *n*-hexane feed stream decreased the catalytic conversion of *n*-hexane. In the presence of 0.1 wt% propionaldehyde, the *n*-hexane conversion decreased to 63 % whereas acetic acid (0.1 wt%) in *n*-hexane feed resulted in 53 % conversion at 10 h on stream. The lowest *n*-hexane conversion, 41 %, was observed when $14x10^{-5}$ wt% thiophene was present in the *n*-hexane feed. In all experimental runs recorded Figure 3.32, a similar decreasing slope which indicates catalyst deactivation was observed.

The aromatisation selectivity to benzene was stable between 56 – 52 % when neat *n*-hexane was used as a feed over 20 h on stream (see Figure 3.32). Other identified products formed during aromatisation include C_1-C_5 alkanes (*ca.* 12 %), hexenes (*ca.* 3 %) and hydrogen (6-10 %). Some of the feed was transformed *via.* aromatisation into coke deposits as could be seen by the high amount of deposited carbon on spent catalyst (up to 3 % carbon, see section 3.5.2.4).

The effect of propionaldehyde and acetic acid on benzene selectivity was not substantial. Only a slight decrease to 50 % benzene selectivity was observed when 0.1 wt% propionaldehyde or acetic acid was present on feed stream. The impact of these oxygenates was clearly observed on benzene yield where the suppression was *ca.* 10 mol% when acetic acid was present in the feed stream. Similarly to the trend observed in *n*-hexane conversion, $14x10^{-5}$ wt% thiophene has an evident negative impact on benzene selectivity and yield. After 20 h on stream, the benzene selectivity and the yield was as low as 18 % and 6 % respectively when $14x10^{-5}$ wt% thiophene was present in the feed stream. Based on the *n*-hexane conversion trends and benzene yields from various experiments recorded in Figure 3.32, acetic acid has more effect in deactivation of Pt/KL-zeolite catalyst among the oxygenates tested.

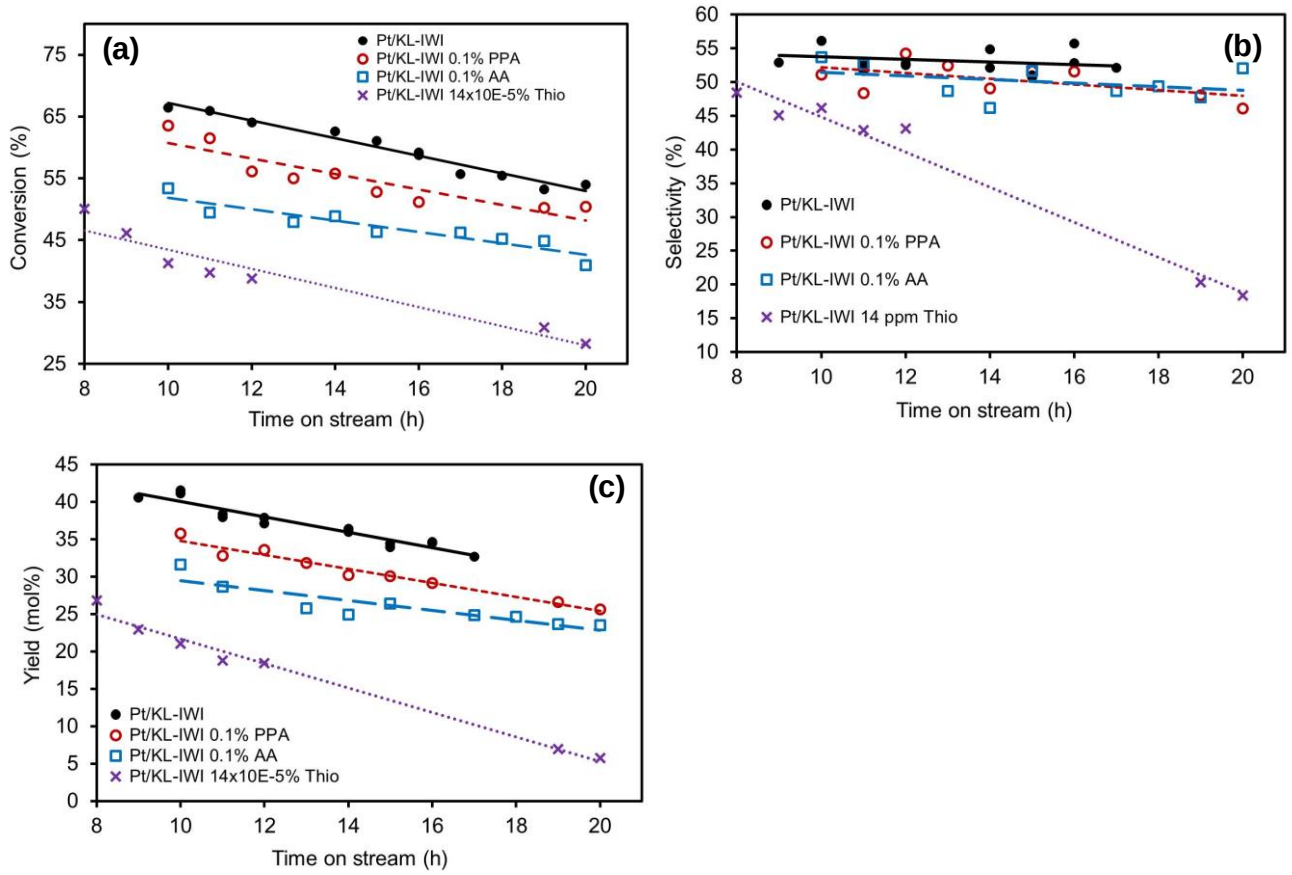

Figure 3.32. (a) The comparative catalytic conversion of neat *n*-hexane and *n*-hexane feeds contaminated with various catalyst poisons (b) benzene selectivity from aromatisation of various *n*-hexane feeds and (c) benzene yield from aromatisation of *n*-hexane feed against time on stream. • Pt/KL-IWI: catalytic aromatisation of neat *n*-hexane with Pt/KL-zeolite catalyst prepared by incipient wetness impregnation, ○ Pt/KL-IWI 0.1 % PPA: catalytic aromatisation of *n*-hexane contaminated with 0.1 % propionaldehyde, □ Pt/KL-IWI 0.1 % AA: catalytic aromatisation of *n*-hexane contaminated with 0.1 % acetic acid and x Pt/KL-IWI $14x10^{-5}$ % Thio: catalytic aromatisation of *n*-hexane contaminated with $14x10^{-5}$ % thiophene. Experimental conditions: weight hourly space velocity = 4 h^{-1}, H_2/*n*-hexane molar ratio = 2.5, temperature = 500 °C and ambient pressure.

To determine the effect of acetic acid concentration in *n*-hexane feed, a special set of aromatisation experiments were carried out with WHSV of 2.5 h^{-1} and H_2: Hexane molar ratio of 2.5. It should be noted that the WHSV was reduced from 4 h^{-1} to 2.5 h^{-1} to increase the catalyst contact time with the feed. There was a clear trend showing that the addition of 0.1 %, 0.5 % and 1 % acetic

acid in the *n*-hexane feed has a detrimental effect on *n*-hexane conversion as illustrated by the conversion curves in Figure 3.33. Without acetic acid in the *n*-hexane feed, the conversion was *ca.* 70 % at 14 h time on stream. The addition of 0.1 % acetic acid in the feed decreased the *n*-hexane conversion to 64 %. A severe decreased to 22 % *n*-hexane conversion was observed when 1 % acetic acid was added in the feed stream.

The severity of catalyst deactivation increases in the presence of the sulphur containing compound, thiophene. The effect of acetic acid and thiophene on aromatisation of n-alkanes was further evaluated at high weight hourly space velocity rates and H_2/alkane molar ratios in the following section.

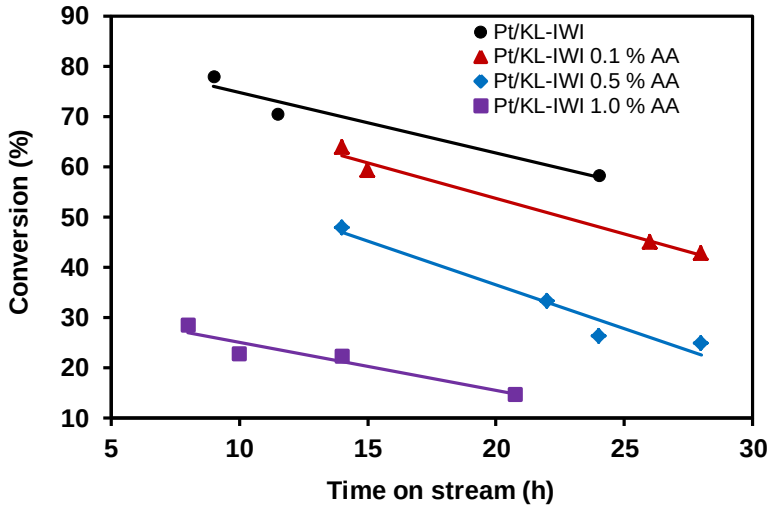

Figure 3.33. The comparative catalytic conversion of neat *n*-hexane and *n*-hexane feeds contaminated with various amounts of acetic acid against time on stream. Pt/KL-IWI: catalytic aromatisation of neat *n*-hexane with Pt/KL-zeolite catalyst prepared by incipient wetness impregnation, Pt/KL-IWI 0.1 % AA: catalytic aromatisation of *n*-hexane contaminated with 0.1 % acetic acid, Pt/KL-IWI 0.5 % AA: the *n*-hexane feed is contaminated with 0.5 % acetic acid and Pt/KL-IWI 1.0 % AA: the *n*-hexane feed is contaminated with 1.0 % acetic acid. Experimental conditions: weight hourly space velocity = 2.5 h^{-1}, H_2/*n*-hexane molar ratio = 2.5, temperature = 500 °C and ambient pressure.

3.5.2.2 Comparative Study of n-Alkanes Aromatisation over Pt/KL-zeolite Catalysts

Pt/KL-zeolite catalysts prepared by incipient wetness impregnation and vapour phase impregnation were used in aromatisation of neat n-hexane, n-heptane and n-octane. In this instance, the weight hourly space velocity was increased to 5 h^{-1} and H_2/alkane molar ratio was increased to 6.

The results obtained from the aromatisation of neat *n*-hexane are reported in Figure 3.34. Under the same experimental conditions, the catalysts prepared by vapour phase impregnation achieved higher *n*-hexane conversion and aromatisation selectivity than the catalysts prepared by incipient wetness impregnation. At 12 h on stream, the n-hexane conversion was constant at 72 % and benzene selectivity was 58 % when vapour phase impregnated catalyst was used. A slight decrease to 69 % conversion and 54 % benzene selectivity was observed when incipient wetness impregnated catalyst was used. Notable is the decline in n-hexane conversion to 64 % over 16 h on stream when the incipient impregnated catalyst was used.

Similarly, the impact of catalyst deactivation over time is clearly visible in the decreasing trend of benzene yield as reported in Figure 3.34b. Based on the n-hexane conversion and benzene yield obtained over 20 h on stream, the catalyst prepared by vapour phase impregnation was more robust towards catalyst deactivation. The superiority of Pt/KL-zeolite catalyst prepared by vapour phase impregnation over the catalyst prepared by incipient wetness impregnation is probably due to better Pt particle dispersion as determined by CO chemisorption (see Table 3.4, 91.5 % vs 75.8 %). Furthermore, the average particles size of vapour phase impregnated Pt was estimated to be 1.2 nm which implies that the majority of particles will be inside the L-zeolite channels (1.3 nm). Pt/KL-zeolite catalyst with most of the Pt particles inside the L-zeolite channels is resistant to 3-D carbonaceous deposits due to the protected environment provided by the channels where bimolecular reactions leading to coke are inhibited.[78]

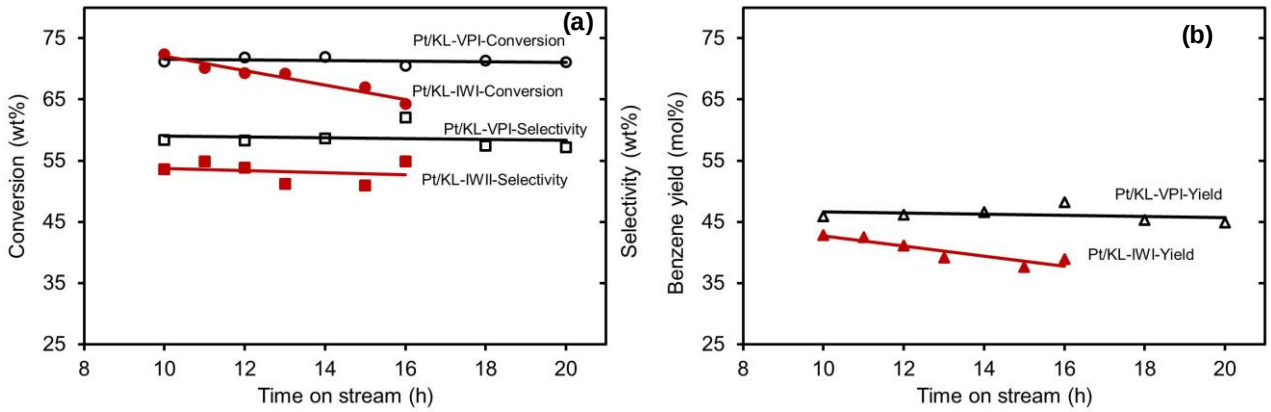

Figure 3.34. (a) The comparative catalytic conversion of *n*-hexane and benzene selectivity against time on stream (b) benzene yield from aromatisation of *n*-hexane over Pt/KL-zeolite against time on stream. Pt/KL-VPI is the Pt/KL-zeolite catalyst prepared by vapour phase impregnation and Pt/KL-IWI is the Pt/KL-zeolite catalyst prepared by incipient wetness impregnation. Open symbols represent catalytic reactions performed over Pt/KL-zeolite-VPI catalyst and solid symbols represent catalytic reactions performed over Pt/KL-zeolite-IWI catalyst. Experimental conditions: weight hourly space velocity = 5 h^{-1}, H_2/*n*-hexane molar ratio = 6, temperature = 500 °C and ambient pressure.

The Pt/KL-zeolite catalyst prepared by vapour phase impregnation was further evaluated in aromatisation of *n*-heptane and *n*-octane which have longer carbon chains than *n*-hexane. When *n*-hexane was used as the feed, the steady state where the reactor temperature is stable was achieved at about 10 h of constant *n*-hexane feed. Thus the analysis of aromatisation products commenced at 10 h. The reactor temperature stabilised within 5 h on stream when *n*-heptane and *n*-octane were used as reactants.

Figure 3.35 shows the results obtained over the first 20 h of catalytic aromatisation of various alkanes using Pt/KL-zeolite catalyst prepared vapour phase impregnation. The Pt/KL-zeolite catalyst activity in respect to *n*-alkane conversion decreased from *n*-hexane to *n*-octane feed. Notable is the slow conversion of *n*-octane over time which is in agreement with the previous reports.[79] The aromatisation of *n*-hexane resulted in higher aromatics yield (*ca*. 45 mol%) than *n*-heptane (30-40 mol%) and *n*-octane (30-20 mol%) as shown in Figure 3.35b. Aromatisation of *n*-hexane resulted in

benzene as the main product while other aromatic compounds such as toluene, ethylbenzene and xylenes were identified when *n*-heptane and *n*-octane were used as feeds to the reactor. The product distribution achieved after 12 h on stream is summarised in Table 3.5. In addition to the different products in Table 3.5, hydrogen (up to 10 % selectivity) was formed due to the dehydrogenation to aromatics. Excessive dehydrogenation of the irreversible adsorbed hydrocarbons also led to the deposition of carbonaceous material on spent catalyst (up to 3 % carbon on spent catalyst was analysed). Some heavy polymeric material of unknown identity was also deposited on the walls of the product vessel.

It is important to note the significant benzene selectivity when *n*-heptane and *n*-octane is used as a feed stream (*i.e.* 24.1 % and 14.2 %) as presented in Table 3.5. The main reason for benzene formation when these *n*-alkanes are used is because the diffusion of alkylbenzenes from confined L-zeolite channels is limited.[79] Therefore benzene is formed due to bond-cracking to form simpler aromatics that can diffuse out of the L-zeolite channels. The selectivity to corresponding cracking products with C_1-C_5 chain length was also high (11-12 %) when *n*-heptane and *n*-octane were used as the feed.

From the reaction curves in Figure 3.35, it is evident that the Pt/KL-zeolite catalyst used was more active and more robust to deactivation in aromatisation of *n*-hexane compared to *n*-heptane and *n*-octane. The deactivation by channel-trapped aromatics is proposed to be the main contributor for poor activity in aromatisation of *n*-heptane and *n*-octane.

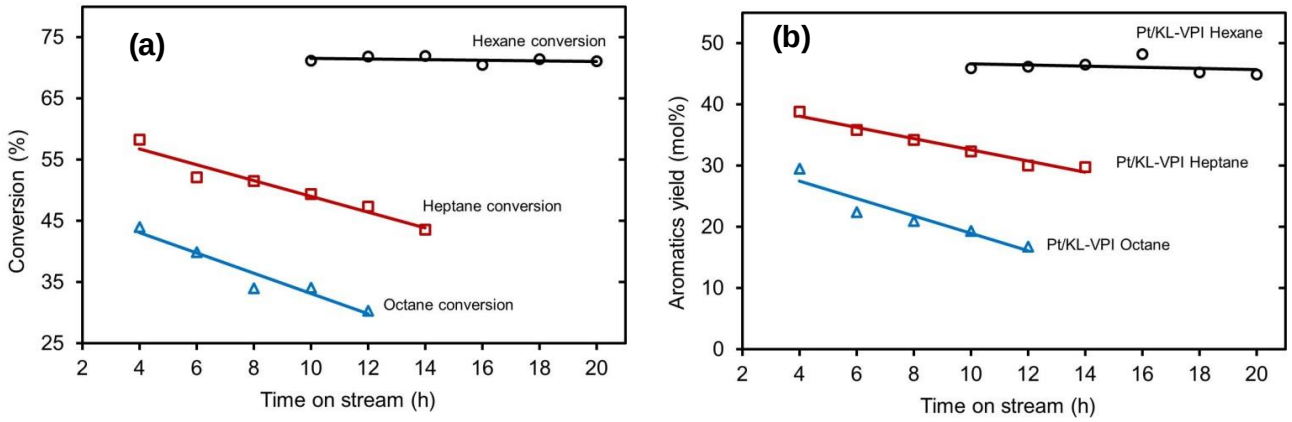

Figure 3.35. (a) The comparative conversion of the *n*-alkane feedstock and (b) aromatics yield from aromatisation of *n*-alkanes against time on stream. Pt/KL-VPI is the Pt/KL-zeolite catalyst prepared by vapour phase impregnation. The *n*-alkanes used are *n*-hexane, *n*-heptane and *n*-octane. Experimental conditions: weight hourly space velocity = 5 h^{-1}, H_2/*n*-hexane molar ratio = 6, temperature = 500 °C and ambient pressure.

Table 3.5. The catalytic conversion of various *n*-alkanes and product distribution achieved after 12 h on stream. Experimental conditions: weight hourly space velocity = 5 h^{-1}, H_2/*n*-hexane molar ratio = 6, temperature = 500 °C and ambient pressure.

Feed	**n-Hexane**	**n-Heptane**	**n-Octane**
Conversion (%)	71.9	47.3	30.3
Selectivity (wt%)[a]			
C_1-C_5 [b]	9.8	11.0	12.2
Hexenes	2.4	0.2	-
Benzene	**58.2**	**24.1**	**14.2**
Toluene	-	**30.0**	**13.9**
Heptenes	-	7.8	-
Octenes	-	-	16.9
Ethylbenzene	-	-	**10.2**
m- and p-Xylene	-	-	**1.7**
o-Xylene	-	-	**4.3**
Other	2.8	3.1	4.6
Total Aromatics	58.2	54.1	44.3

a: The rest of products formed include hydrogen which contribute up to 10 % in product selectivity. Some of the feed was deposited *via* coke formation on the catalyst. b: C_1-C_5 are hydrocarbon products with C_1 to C_5 chain length.

3.5.2.3 Aromatisation of n-Alkane Feeds Contaminated with Catalyst Poisons

The Pt/KL-zeolite catalysts were further evaluated in aromatisation of *n*-alkanes contaminated with catalysts poisons acetic acid and thiophene at 500 °C with weight hourly space velocity of 5 h^{-1} and H_2/alkane molar ratio of 6. The results presented in Figure 3.36 show that the catalysts poisons have similar impact on catalyst deactivation in both incipient wetness impregnated and vapour phase impregnated catalysts as outlined by the *n*-hexane conversions and benzene yields. In the presence of 0.1 wt% acetic acid, the *n*-hexane conversion decreased by *ca.* 5 % in both catalyst types. In the first 10 h on stream, the Pt/KL-zeolite catalyst prepared by vapour phase impregnation was tolerant to 0.1 wt% acetic acid on feed stream. The depression in *n*-hexane conversion became more prominent after 20 h on stream. When the concentration of acetic acid was increased to 0.5 wt%, the *n*-hexane conversion decreased even further by 15 %. The impact of acetic acid on catalyst deactivation is also evident on benzene yield which decreased as the concentration of acetic acid in *n*-hexane feed was increased, following a similar trend as the conversion trend.

The Pt/KL-zeolite catalysts evaluated are relatively more tolerant towards oxygenates than sulphur containing compounds. Previous reports in the literature claim that oxygenates in aromatisation feedstock decompose to form CO which competitively chemisorb onto their Pt active sites and suppress the catalyst activity.[80]

The mode of deactivation by sulphur compounds is twofold: (1) Sulphur adsorbs on the Pt active sites and enhances the growth of Pt clusters by agglomeration and eventually plugging the L-zeolite channels.[74,81] (2) Sulphur in *n*-alkane feedstock interacts strongly with K^+ and suppresses the ability of K^+ to promote aromatisation.[82] XPS analysis of the spent catalyst after aromatisation of *n*-hexane feed contaminated with thiophene showed the presence of sulphur species, which confirms the adsorption of sulphur on Pt/KL-zeolite catalyst. More details on the analysis of spent catalysts are given in the next section (section 3.2.5). No CO gas was detected in the off-gas from the reactor in

this study. Attempts to determine any changes in the characteristics of Pt-O using XPS analysis were unsuccessful.

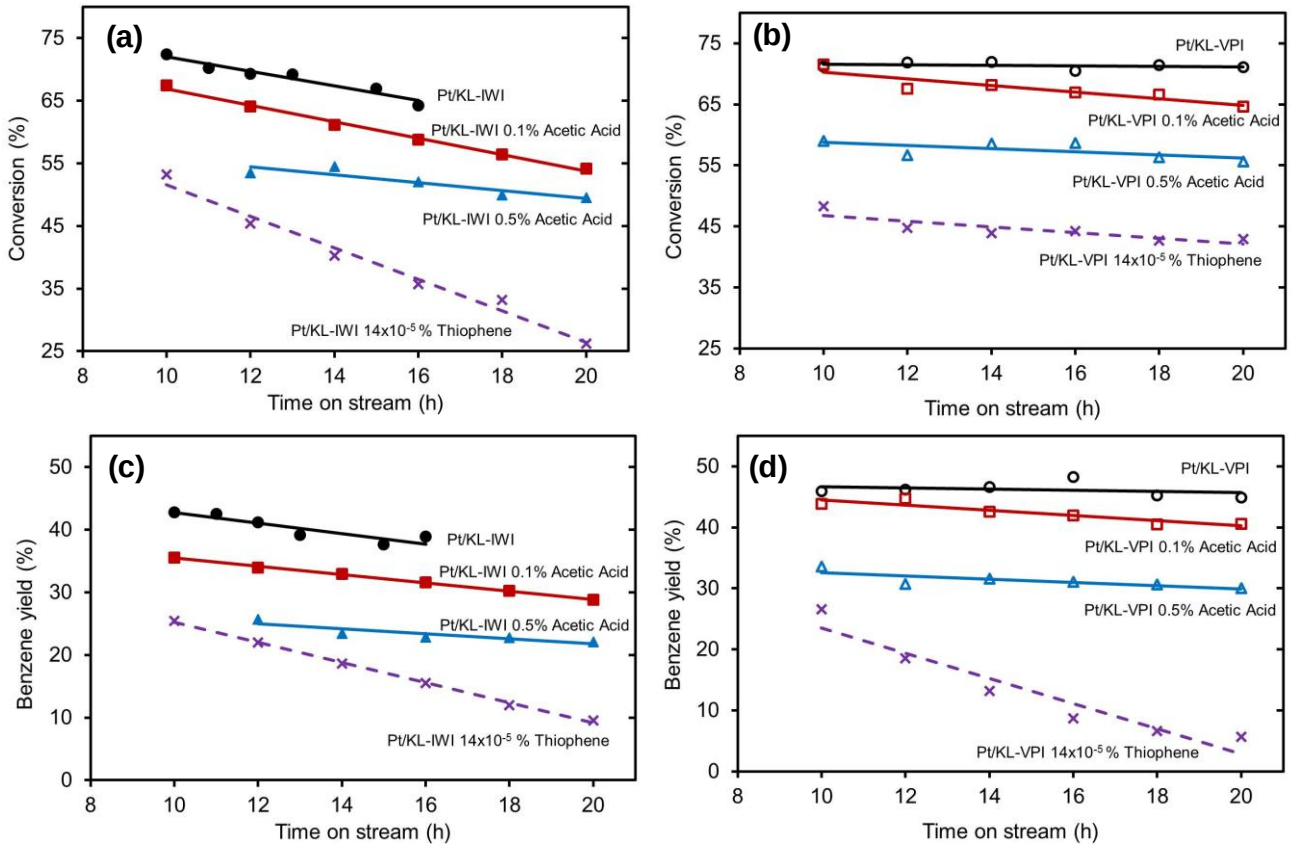

Figure 3.36. The catalytic conversion of neat *n*-hexane and *n*-hexane feed contaminated with various catalyst poisons over (a) Pt/KL-zeolite catalyst prepared by incipient wetness impregnation *versus* time on stream and (b) Pt/KL-zeolite catalyst prepared by vapour phase impregnation *versus* time on stream. The benzene yield from aromatisation of *n*-hexane feeds catalysed by (c) Pt/KL-zeolite catalyst prepared by incipient wetness impregnation *versus* time on stream and (d) Pt/KL-zeolite catalyst prepared by vapour phase impregnation *versus* time on stream. ○Pt/KL-VPI: catalytic aromatisation of neat *n*-hexane with Pt/KL-zeolite catalyst prepared by vapour phase impregnation, □ Pt/KL-VPI 0.1 % acetic acid: catalytic aromatisation of *n*-hexane contaminated with 0.1 % acetic acid, Δ Pt/KL-VPI 0.5 % acetic acid: catalytic aromatisation of *n*-hexane contaminated with 0.5 % acetic acid and x Pt/KL-VPI $14x10^{-5}$ % Thiophene: catalytic aromatisation of *n*-hexane contaminated with $14x10^{-5}$ % thiophene. The closed symbols represent reactions catalysed by Pt/KL-zeolite prepared by incipient wetness impregnation. Experimental conditions: weight hourly space velocity = 5 h^{-1}, H_6/*n*-hexane molar ratio = 6, temperature = 500 °C and ambient pressure.

The Pt/KL-zeolite catalysts prepared by vapour phase impregnation exhibited superior activity in aromatisation of *n*-hexane than catalysts prepared by incipient wetness impregnation and showed a better tolerance to acetic acid. After 20 h on stream, the *n*-hexane conversion stayed well above 65 % even in the presence of 0.1 wt% acetic acid. Therefore, the Pt/KL-zeolite catalysts prepared by vapour phase impregnation were further evaluated in aromatisation of *n*-octane in the presence of acetic acid.

The aromatisation of neat *n*-octane over Pt/KL-zeolite was sluggish and there was a clear catalyst deactivation trend illustrated by the reduction of *n*-octane conversion from 44 % to 30 % between 4 h to 12 h on stream as presented in Figure 3.37a. The addition of 0.5 wt% acetic acid in the *n*-octane feed did not show a significant impact on catalyst deactivation with respect to *n*-octane conversion. A significant decrease in *n*-octane conversion (30 % to 23 % after 12 h on stream) was observed when 1.0 wt% acetic acid was added in the feed stream. As expected, the aromatics yield also decreased as the concentration of acetic acid in the *n*-octane feedstock is increased (Figure 3.37b).

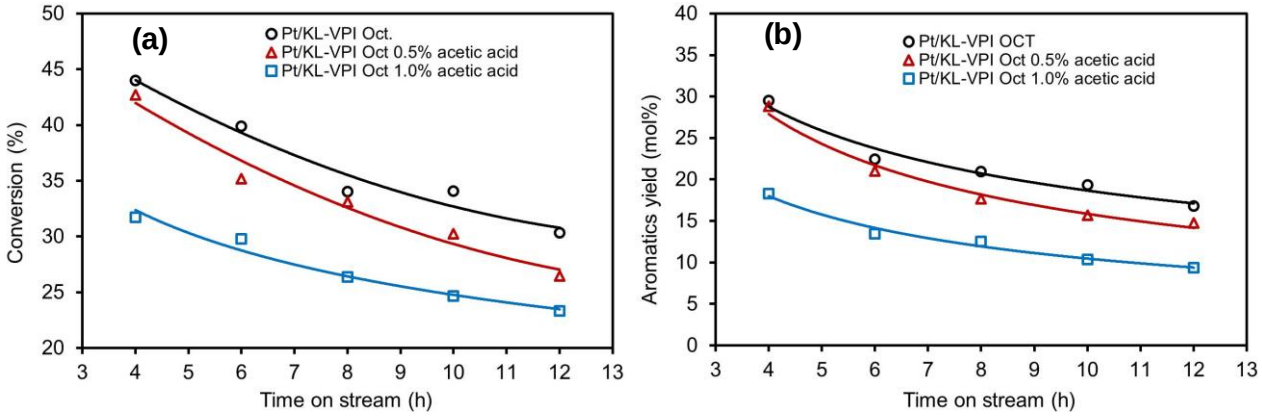

Figure 3.37. (a) The comparative catalytic conversion of neat *n*-octane and *n*-octane feed contaminated with acetic acid *versus* time on stream (b) benzene yield from aromatisation of *n*-octane feeds against time on stream. ○Pt/KL-VPI Oct: catalytic aromatisation of neat *n*-octane with Pt/KL-zeolite catalyst prepared by vapour phase impregnation, Δ Pt/KL-VPI Oct 0.5 % acetic acid: catalytic aromatisation of *n*-octane contaminated with 0.5 % acetic acid, □ Pt/KL-VPI Oct 1.0 % acetic acid: catalytic aromatisation of *n*-octane contaminated with 1.0 % acetic acid. Experimental conditions: weight hourly space velocity = 4 h^{-1}, H_2/*n*-hexane molar ratio = 2.5, temperature = 500 °C and ambient pressure.

The effect of adding 0.5 wt% acetic acid in the feed stream was very minimal on *n*-octane aromatisation compared to *n*-hexane aromatisation as presented in Table 3.6. Only a slight decrease in *n*-octane conversion (4 %) was observed and the product distribution was basically unchanged after 12 h on stream for reactions done with neat and contaminated *n*-octane.

Table 3.6. The catalytic conversion of neat and contaminated *n*-alkanes and product distribution achieved after 12 h on stream. Experimental conditions: weight hourly space velocity = 5 h^{-1}, H_2/*n*-hexane molar ratio = 6, temperature = 500 °C and ambient pressure.

Feed	**n-Hexane**		**n-Octane**	
	Neat	*0.5 wt% Acetic Acid*	*Neat*	*0.5 wt% Acetic Acid*
Conversion (%)	71.9	56.7	30.3	26.5
Selectivity (wt%)[a]				
C1-C5 [b]	9.8	10.7	12.2	13.6
Hexenes	2.4	3.8	-	-
Benzene	58.2	49.1	14.2	14.7
Toluene	-	0.3	13.9	14.6
Octenes	-	-	16.9	15.3
Ethylbenzene	-	-	10.2	9.4
m- and p-Xylene	-	-	1.7	1.7
o-Xylene	1.7	-	4.3	3.9
Other	2.8	3.1	4.6	0.6
Total Aromatics	58.2	49.1	44.3	44.3

a: The rest of products formed include hydrogen which contribute up to 10 % in product selectivity. Some of the feed was deposited *via* coke formation on the catalyst and heavy polymeric material which deposited on the walls of the product vessel. b: C_1-C_5 are hydrocarbon products with C_1 to C_5 chain length.

When *n*-hexane is used as the feed, the conversion decreased by *ca.* 15 % and the benzene selectivity is decreased in favour of hydrocarbons with C_1-C_5 chain and hexenes. Since *n*-hexane aromatisation products diffuse easily from L-zeolite channels, *n*-hexane aromatisation is less susceptible to deactivation by channel-trapped products.[79] At the same time, the Pt active sites are

easily accessible to poisons such as acetic acid and CO which is formed by the decomposition of acetic acid. Therefore, the presence of acetic acid in the feed stream has high negative impact on catalyst activity in aromatisation on *n*-hexane. When *n*-octane is used as the feed stream the catalyst deactivation and coke formation by channel-trapped alkylbenzenes is already high.[78,79] The acetic acid and secondary products do not have easy access to coke-covered Pt active sites and the impact of acetic acid on catalyst deactivation is not as high as in *n*-hexane aromatisation.

3.5.2.4 Analysis of Spent Catalysts from Aromatisation Reactions

A special set of catalytic aromatisation experiments were done with WHSV of 2.5 h^{-1} and an H_2/hexane molar ratio of 2.5 to determine the effect of different concentrations of acetic acid in aromatisation of *n*-hexane. These experiments also provided an opportunity to analyse the amount of deposited carbonaceous material on catalyst since there was a dramatic decrease in *n*-hexane conversions as the amount of acetic acid was increased in each experimental run.

The Thermogravimetric Analysis (TGA) of spent catalysts which was done under argon atmosphere did not show any stepped thermal decomposition except for water loss. The TGA carried out in a medical air atmosphere showed two distinct steps of mass loss at *ca*. 100 °C and *ca.* 440 °C as presented in Figure 3.38 (a). A comparison of the TGA curves of spent catalyst and fresh catalyst (see Figure 3.38) revealed that the mass loss step at 100 °C is common in both samples and is consistence with the loss of moisture. An additional mass loss at *ca.* 440 °C was only observed in spent catalyst samples and was suspected to belong to deposited carbonaceous material. LECO Total Organic Carbon (LECO-TOC) analyser confirmed the presence of carbon based material on spent catalysts.

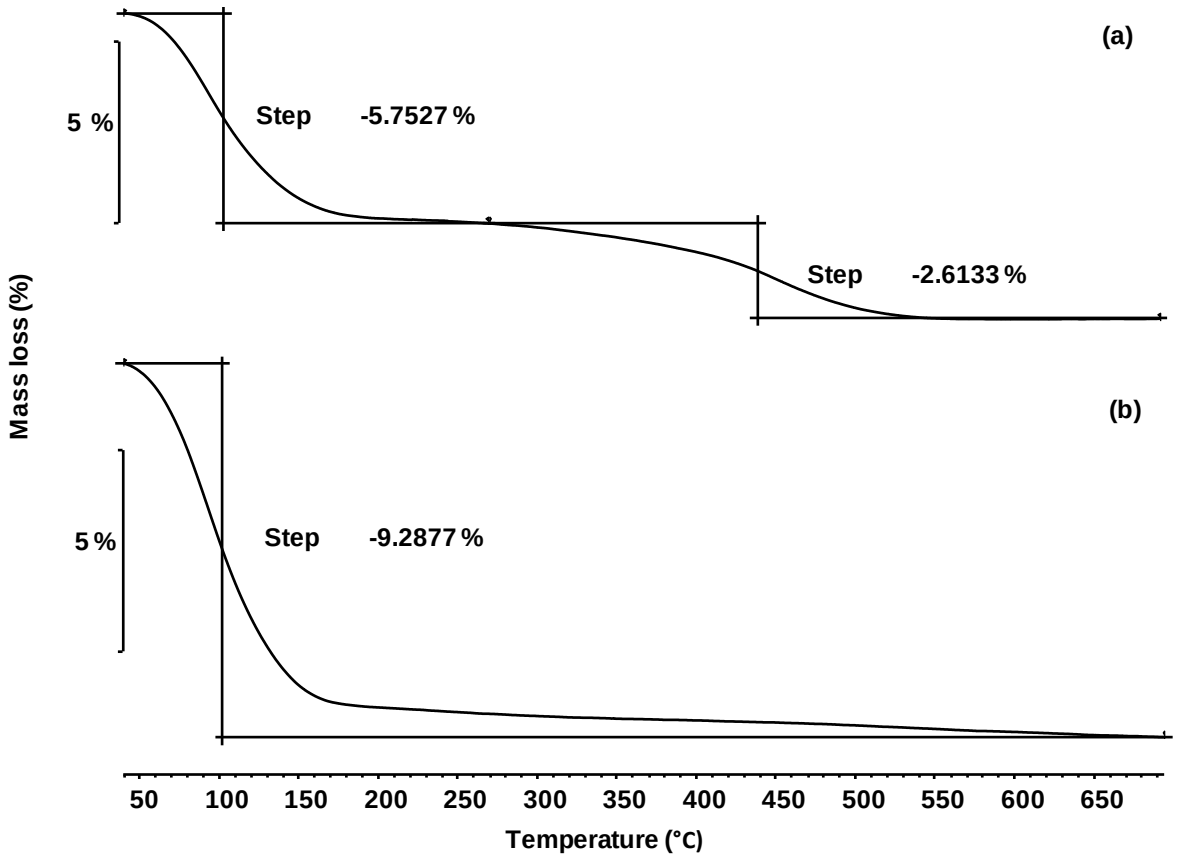

Figure 3.38. TGA curves of (a) spent Pt/KL-zeolite catalyst from the catalytic aromatisation of *n*-hexane and (b) fresh Pt/KL-zeolite catalyst which were analysed under an atmosphere of medical air.

The TGA and LECO-TOC results from the analysis of spent catalyst are presented in Figure 3.39. Higher amount of deposited carbonaceous material was reported by the LECO-TOC analyser than the TGA. The reason for the high amount of carbon content reported by LECO-TOC is because this technique reports the entire carbon content deposited on the catalyst including the high boiling deposits while the reported TGA results only show the carbon content that thermally decompose at temperature range of 250 °C to 550 °C. TGA step curves illustrate that the reaction temperature of 500 °C is still within the temperature range where the carbonaceous deposits can accumulate overtime. Among the gases used in TG analysis, only medical air gave quantifiable TGA step curves and this observation compliments the procedure where air is used at 400 °C to regenerate spent Pt/KL-zeolite catalysts for aromatisation reactions.[79]

Both TGA and LECO-TOC analysis techniques showed that the amount of carbon deposited on spent catalysts increased as the amount of acetic acid increased in the feed stream. The increasing trend of carbon deposited on spent catalyst, especially the results from TG analysis, correlate with the decreasing trend exhibited by the *n*-hexane conversion. In the absence of acetic acid in the *n*-hexane feed, the conversion was 70.6 % (labelled Neat Hex in Figure 3.39) and the carbon content in the spent catalyst was 2.8%. When 2 % acetic acid was added in the feed, the *n*-hexane conversion decreased to 22.4 % while the carbon content increased to 4.4 %.It could be deduced from these trends that the acetic acid in *n*-hexane feed favoured the formation of carbonaceous deposits on the catalyst and results in detrimental effect on the *n*-hexane conversion.

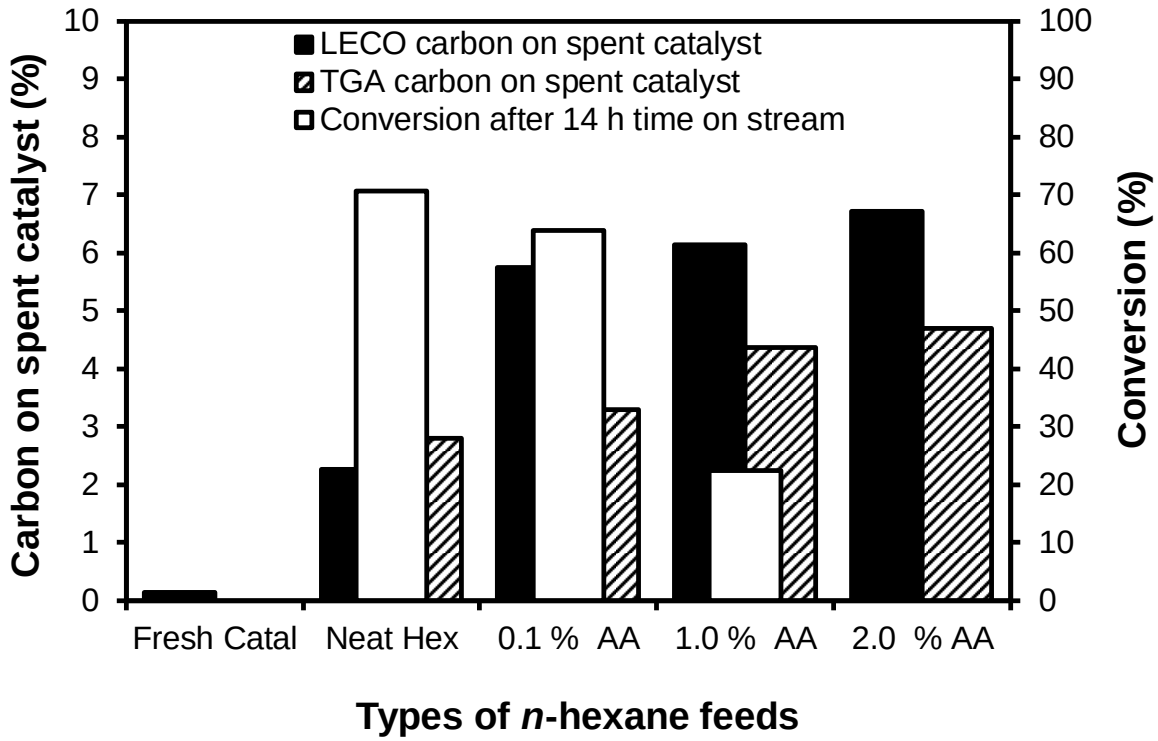

Figure 3.39. A chart of carbon content on fresh Pt/KL-zeolite catalyst and spent catalysts from aromatisation reactions at low WHSV (2.5 h^{-1}) against different *n*-hexane feeds. Also shown is the *n*-hexane conversion obtained after 14 h time on stream for spent catalysts analysed (white columns). Fresh catal: Freshly prepared Pt/KL-zeolite catalyst, Neat Hex = spent catalyst where neat hexane was used a feed, 0.1 % AA: spent catalyst where *n*-hexane feed was contaminated with 0.1 % acetic acid, 1.0 % AA: *n*-hexane feed was contaminated with 1.0 % acetic acid, 2.0 % AA: *n*-hexane feed was contaminated with 2.0% acetic acid.

It is important to note that the rate of carbon deposition on Pt/KL-zeolite catalyst may be exaggerated in aromatisation experiments with low WHSV and low H_2/hexane molar ratio (2.5). Therefore, the spent catalysts from aromatisation experiments with high WHSV (5 h^{-1}) and H_2/hexane molar ratio of 6 were also analysed for carbonaceous deposits recorded in Figure 3.40.

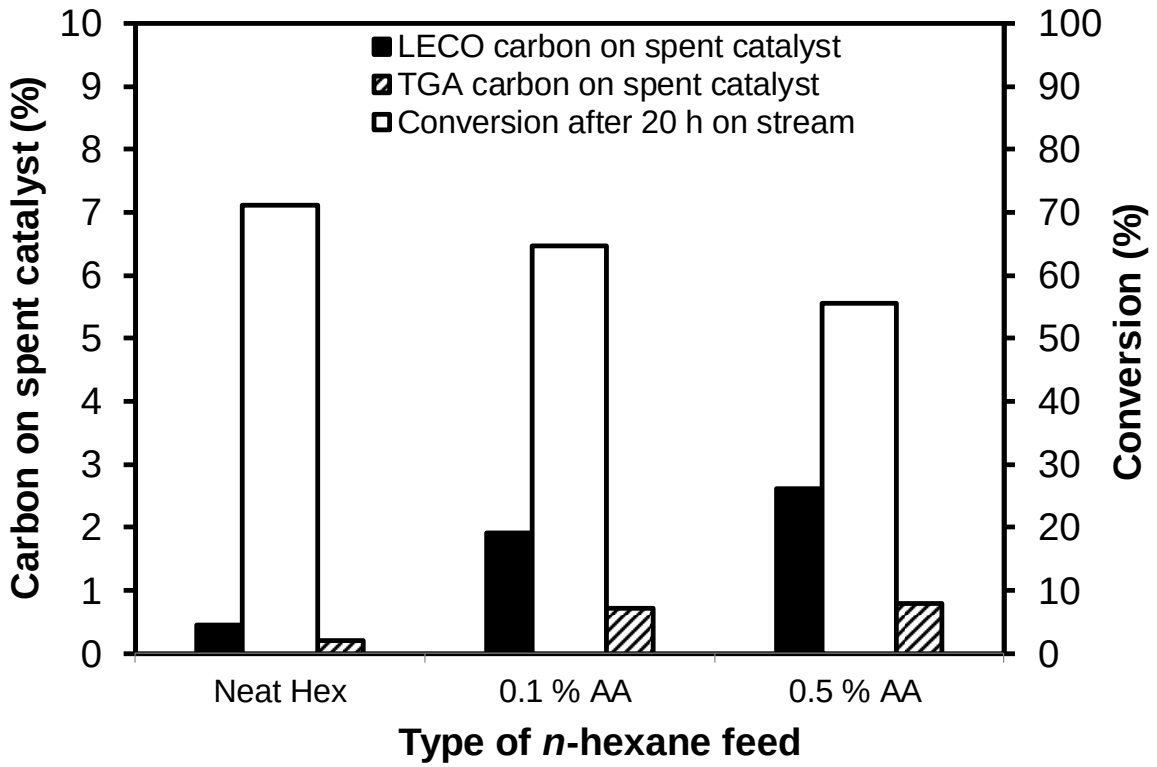

Figure 3.40. A chart of carbon content on spent Pt/KL-zeolite catalysts from aromatisation reactions at high WHSV (5 h^{-1}) against different *n*-hexane feeds. Also shown is the *n*-hexane conversion obtained after 20 h time on stream for spent catalysts analysed (white columns). Neat Hex: spent catalyst where neat *n*-hexane was used a feed, 0.1 % AA: spent catalyst where *n*-hexane feed was contaminated with 0.1 % acetic acid, 0.5 % AA: *n*-hexane feed was contaminated with 0.5 % acetic acid.

The deposited carbonaceous residue from spent catalysts used in the set of experiments carried out with high WHSV (5 h^{-1}) and H_2/hexane molar ratio of 6 was relatively low (see Figure 3.40 above). The amount of carbon content on spent catalysts accumulated in the presence of 0.1 % acetic acid in *n*-hexane feed was 0.7 % relative to 3.3 % obtained when the experiments were carried out at

low WHSV and H_2/hexane molar ratio of 2.5. Again, the LECO-TOC analyser consistently reported high carbon content than the TG analyser and the decrease in *n*-hexane conversion correlated to the increase in carbon content analysed on the catalysts.

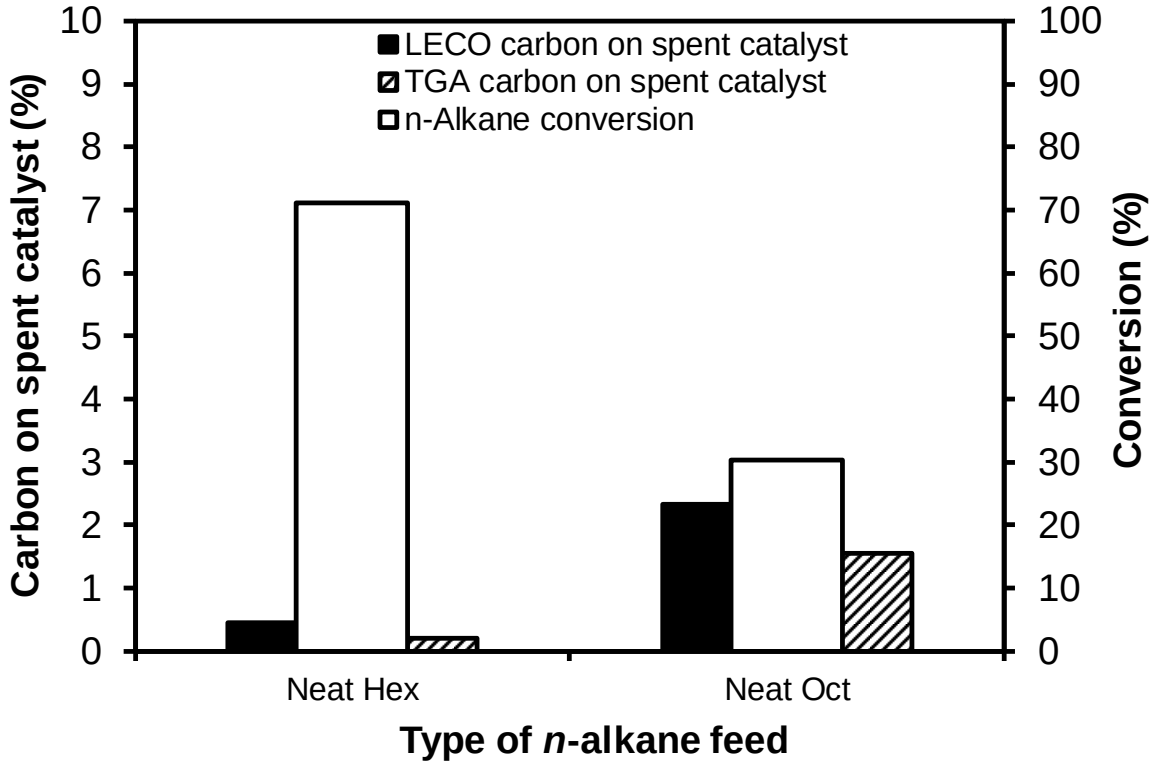

Figure 3.41. A chart of carbon content spent Pt/KL-zeolite catalysts from aromatisation reactions at high WHSV (5 h^{-1}) against different *n*-alkane feeds. Also shown is the *n*-hexane conversion obtained after 20 h time on stream for spent catalysts used in *n*-hexane aromatisation and 12 h on stream for spent catalysts used in *n*-octane conversion (white columns). Neat Hex: spent catalyst where neat *n*-hexane was used a feed, Neat Oct: spent catalyst where neat *n*-octane was used a feed.

The acetic acid on the *n*-alkane feed stream was not the only factor that enhanced the accumulation of carbonaceous deposits on spent catalysts. The longer carbon chain length of the *n*-alkane used in catalytic aromatisation reactions seemed to favour the increase in carbon content on spent catalysts. When *n*-hexane was used as the feed in aromatisation over Pt/KL-zeolite catalyst prepared by vapour phase impregnation, the carbon content analysed by TGA was 0.2 % which was accumulated over 20 h time on stream (see Figure 3.41 above). Under the same reaction conditions,

the longer chain length alkane *n*-octane aromatisation accumulates 1.6 % carbon content over 12 h time on stream. In both cases, the carbonaceous deposit which is known to reduce the activity of Pt/KL-zeolite catalysts[79] affected the *n*-alkane conversion as outlined in the conversion curves in Figure 3.35.

Based on relative amounts of carbon deposits presented in Figure 3.41, the carbonaceous material deposition had a more severe detrimental effect on the *n*-octane conversion than in the *n*-hexane conversion. When *n*-octane is used as the feed, the carbon residues accumulate by decomposition of the trapped C_8-aromatics inside the zeolite pores (see Table 3.6)[83,84]

3.5.2.5 Regeneration of Spent Catalysts from Aromatisation Reactions

The TG analyses showed that the deposited carbonaceous material on spent Pt/KL-zeolite catalysts can be removed in oxidative combustion at *ca*. 450 °C in medical air. As the regeneration step, the spent catalysts were calcined at 500 °C for 2 h under molecular oxygen atmosphere. Analysis of regenerated catalysts using TGA did not show any stepped thermal decomposition at *ca*. 450 °C which confirmed that the deposited coke was removed during regeneration step. However, chemisorption analysis using carbon monoxide as the analysis gas showed that the Pt crystallite sizes had increased from average diameter of *ca*. 1.2 nm in fresh catalyst to average diameter of *ca*. 2.7 nm after aromatisation of neat *n*-hexane followed by the regeneration step. The regenerated catalysts were not re-tested in aromatisation of *n*-hexane to determine the effect of increased particle size on catalyst activity.

In summary, the prepare 1% Pt/KL-zeolite catalysts showed activity in aromatisation of *n*-hexane, *n*-heptane and *n*-octane. The Pt/KL-zeolite catalyst prepared by vapour phase impregnation (Pt/KL-zeolite VPI) showed more activity in aromatisation of *n*-hexane than the Pt/KL-zeolite catalyst prepared by incipient wetness impregnation (Pt/KL-zeolite IWI). The presence of

oxygenates or sulphur compounds decreased the catalytic activity of the catalysts based on *n*-alkane conversion and selectivity to aromatics. Sulphur compounds were more detrimental to the activity of the catalysts than the oxygenates. Pt/KL-zeolite VPI catalyst was more tolerant to oxygenates than Pt/KL-zeolite IWI catalysts. Less than 5 % decrease in conversion was observed when 0.1 wt% acetic acid was present in *n*-hexane during catalytic aromatisation over Pt/KL-zeolite VPI. There was a direct correlation in catalyst deactivation and the amount of carbonaceous material accumulated on the spent catalyst.

3.5.3 Application of Pt/Zeolite Catalysts in Oxidation of Primary Alcohols

The main challenge in oxidation of primary alcohols is selective dehydrogenation to form aldehydes. The enolisable aldehydes formed by oxidation of primary alcohols tend to be over-oxidised to form carboxylic acids and sometimes form secondary products such as esters with the liberation of water as could be seen in oxidation of 1-octadecanol over model Pt/SiO_2/Si-wafer. Oxidation in aqueous medium is ideal with regard to waste disposal especially when carboxylic acids are target oxidation products.[85] When aldehyde oxidation products are desired, organic solvents are sometimes used.[86] This section is dedicated on liquid phase oxidation of benzyl alcohol and 1-octanol over Pt/KL-zeolites and Pt/HY-zeolites.

3.5.3.1 Oxidation of Primary Alcohols in Aqueous Medium

Benzyl alcohol (1.5 M in water) was used as a simple and yet reactive substrate to test the oxidation activity of Pt/KL-zeolite at 100 °C under a gently stream of molecular oxygen. After 24 h of reaction time, 24 % substrate was converted to benzaldehyde when the reaction was performed over Pt/KL-zeolite catalyst. The characteristic ^{1}H NMR signal for aldehyde proton at 10.0 ppm could be easily identified in the reaction mixture.

To rule out the presence of benzoic acid in the reaction mixture, the FTIR spectrum of the oxidation product mixture was compared to the FTIR spectra of commercial benzoic acid and benzaldehyde (see Figure 3.42). The FTIR C=O stretching frequency of the oxidation product and commercial benzaldehyde appeared at the same wavenumber 1699 cm^{-1} while the FTIR C=O stretching frequency of the commercial benzoic acid appeared at 1677 cm^{-1}. The observed FTIR C=O stretching frequency difference was a good proof that the benzaldehyde in the product mixture did not oxidise further to benzoic acid. The high selectivity to benzaldehyde was due to the non-enolisable aldehyde which is stabilised by the phenyl ring and limit subsequent oxidation to benzoic acid (Scheme 3.12).[87,88] One of the factors contributing to low alcohol conversion would be the bulky nature of benzyl alcohol with the phenyl ring which could prevent the substrate from entering the pores of the support.

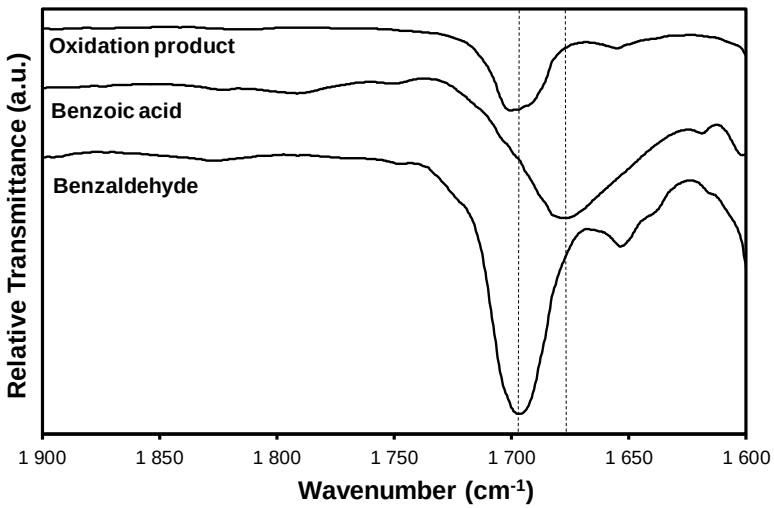

Figure 3.42. The enlarged section of the Fourier Transform Infrared (FTIR) C=O stretching frequency region of the product mixture from the oxidation of benzyl alcohol catalysed by 1% Pt/KL-zeolite at 100 °C under a gentle stream of molecular oxygen and corresponding FTIR spectra of commercial benzoic acid and benzaldehyde .

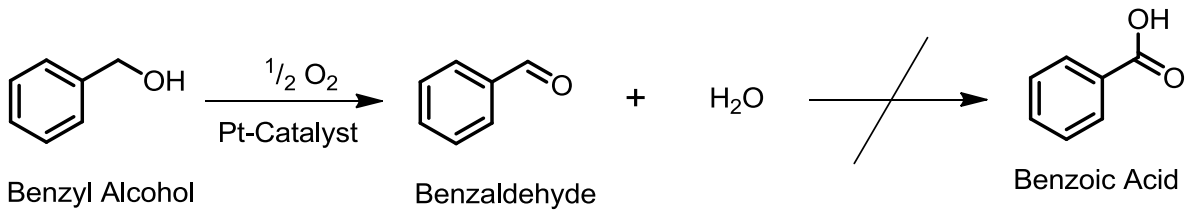

Scheme 3.12. Reaction scheme for the Pt catalysed oxidative dehydrogenation of benzyl alcohol to benzaldehyde and water.

The Pt/zeolite catalysts were also tested in oxidation of 1.3 M 1-octanol in water at 100 °C in the presence of molecular oxygen at ambient pressure. 1-Octanol was chosen because it is linear and could, potentially, enter the pores of the Pt/zeolite catalysts during oxidation. Another advantage of using 1-octanol in liquid oxidation is that the oxidation products have sufficiently high boiling point and could be collected in liquid phase at reaction temperature. After 32 h of reaction time, a 40 % alcohol conversion was achieved when a solution of 1-octanol in water was oxidised over Pt/KL-zeolite catalyst. The major oxidation product was octanoic acid with 70 % selectivity and only 11 % selectivity to octanal was achieved (see Scheme 3.13 and Table 3.7). In addition to the oxidation products, a substantial amount of esterification product, octyl octanoate was formed with 19 % selectivity (see Scheme 3.14 for the reaction to form the identified ester). Octyl octanoate was formed by esterification of 1-octanol with octanoic acid. The formation of an ester in oxidation of 1-octanol is consistent with the results obtained in oxidation of 1-octadecanol over model $Pt/SiO_2/Si$-wafer (surface **15**) where it was shown that the production of an ester is consistent with substrate consumption (as discussed in section 3.3).

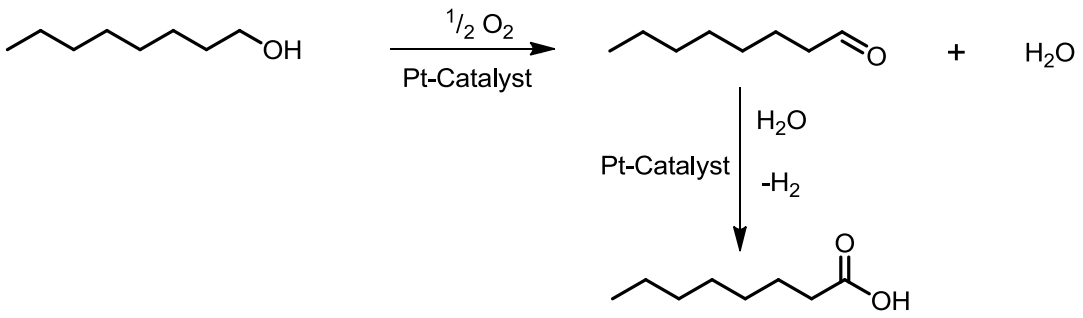

Scheme 3.13. Reaction scheme for the Pt catalysed oxidative dehydrogenation of 1-octanol to octanal and water, and subsequent hydration of octanal to octanoic acid.

Table 3.7. 1-Octanol conversion and selectivities of resultant oxidation products and condensation products over Pt/zeolite catalysts. Reaction conditions: 1-octanol = 1g (0.77 mmol), 1% Pt/zeolite catalyst = 500 mg, water = 5 mL, oxidant = molecular oxygen, temperature = 100 ^{o}C, pressure = ambient.

Catalyst	Time (h)	Additive	Conv. (%)	Selectivity (%)			
				Aldehyde	Organic Acid	Ester	Ether
Pt/KL-zeolite	32	--	40	11	70	19	--
Pt/HY-zeolite	32	--	10	27.5	24	--	48.5
Pt/KL-zeolite	24	K_2CO_3*	10	25	75	--	--
Pt/HY-zeolite	24	K_2CO_3*	--	--	--	--	--

* 7.8 mmol of K_2CO_3 was dissolved in the reaction mixture (1:1 mole ratio with 1-octanol)

When a solution of 1-octanol in water is oxidised over Pt/HY-zeolite catalyst the alcohol conversion is reduced to 10 % compared to when 1-octanol is oxidised over the Pt/KL-zeolite catalyst. Noteworthy is the formation of etherification product, dioctyl ether in 48.5 % selectivity. Octanal was the major product with 27.5 % selectivity amongst the oxidation products and the octanoic acid was the additional oxidation product with 24 % selectivity. Dioctyl ether (which is the most favoured product in oxidation over Pt/HY-zeolite) is the by-product formed by competitive etherification of 1-octanol on the acid sites of the support (HY-zeolite), see Scheme 3.15 for the reaction. Etherification of primary alcohols over acidic zeolites has been reported as the cleaner process to produce ethers which are useful as fuel additives.[89,90,91]

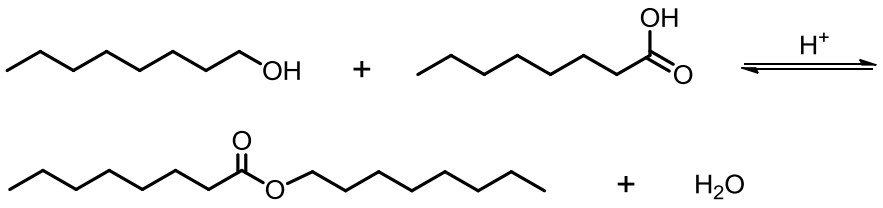

Scheme 3.14. Reaction scheme for the acid catalysed esterification of 1-octanol and octanoic acid to octyl octanoate and water.

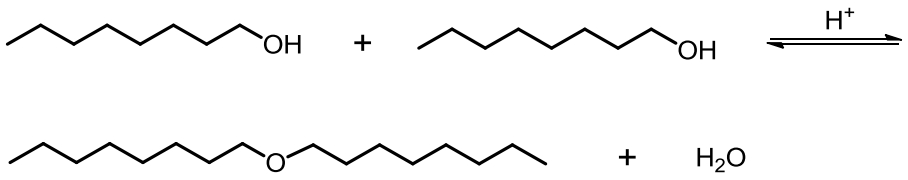

Scheme 3.15. Reaction scheme for the acid catalysed etherification of 1-octanol to dioctyl ether and water.

In an attempt to suppress the acid catalysed reactions *i.e.* esterification to octyl octanoate and etherification to octyl ether (see Scheme 3.14 and Scheme 3.15), 7.8 mmol K_2CO_3 was dissolved in the reaction mixture to make 1:1 mole ratio with 1-octanol. The base completely suppressed the esterification reaction previously observed in oxidation of 1-octanol over Pt/KL-zeolite. At the same time, the alcohol conversion was reduced to 10 %. In Pt/HY-zeolite catalyst the effect of a base on alcohol conversion was detrimental and led to total deactivation of the catalyst.

3.5.3.2 Oxidation of Primary Alcohols in Organic Solvents

The approach used in oxidation of alcohols in aqueous medium was slightly changed and water was replaced by various high boiling solvents, see Table 3.8. The aim was to limit the alcohol over-oxidation to corresponding carboxylic acids observed in the previous section. Benzyl alcohol (1.5 M in xylene) was oxidised over Pt/KL-zeolite and Pt/HY-zeolite catalysts at 130 °C under a gentle

stream of molecular oxygen. After 24 h of reaction time, both catalysts exhibited poor alcohol conversion with only 7 % substrate converted to the aldehyde when the reaction was done over Pt/KL-zeolite catalyst (see Table 3.8). Pt/HY-zeolite catalyst only achieved 3 % alcohol conversion as determined by ^{1}H NMR analysis. The acidity of Pt/HY-zeolite could be the additional contributing factor.

The oxidation of 1-octanol (1.3 M in toluene) over Pt/KL-zeolite resulted in improved selectivity to octanal (75 %) and the selectivity to octanoic acid was 24 %. There was no improvement observed with respect to 1-octanol conversion. The alcohol conversion (10 %) was comparable to the one obtained in aqueous medium. When Pt/HY-zeolite was used as the catalyst, the alcohol conversion was 12 %. What was more interesting in oxidation over Pt/HY-zeolite was that dioctyl ether was formed exclusively. The presence of an ether as the only product suggested that the catalytic oxidation activity of Pt was non-existent under the given reaction conditions and the acid sites on the HY-support were active to catalyse the etherification of 1-octanol instead. Oxidation using dry heptane reduced 1-octanol conversion in both catalysts. Over-oxidation to octanoic acid was suppressed but etherification to octyl ether was favoured.

Table 3.8. 1-Octanol conversion and selectivities of resultant oxidation products and condensation products over Pt/zeolite catalysts. Reaction conditions: 1-octanol = 1g, Pt/zeolite catalyst = 500 mg, oxidant = molecular oxygen, temperature = 100 ^{o}C, pressure = ambient.

Catalyst	Time (h)	Solvent	Conv. (%)	Selectivity (%)			
				Aldehyde	Organic Acid	Ester	Ether
Pt/KL-zeolite	24	Toluene	10.2	75	24	--	--
Pt/HY-zeolite	24	Toluene	12	--	--	--	100
Pt/KL-zeolite	20	Dry Heptane	4.7	40	--	--	59.8
Pt/HY-zeolite	20	Dry Heptane	11	--	--	--	100

3.6 A Summary of the Results and Discussions

The results discussed in this chapter have shown that the flat model support, Si-wafer was successfully functionalised to allow platinisation with K_2PtCl_4 and $H_2PtCl_6 \cdot 6H_2O$. Platinisation with the $H_2PtCl_6 \cdot 6H_2O$ precursor resulted mainly in Pt^{2+} complex coating the surface of SiO_2/Si-wafer which was reduced to form the final flat model Pt/SiO_2/Si-wafer catalyst. Platinisation with K_2PtCl_4 resulted in direct adsorption of catalytically active Pt particles on the surface of amino functionalised SiO_2/Si-wafer. The activities of selected flat model Pt/SiO_2/Si-wafer were investigated in solvent-free oxidation of 1-octadecanol and hydrogenation of cyclooctene, benzaldehyde and cinnamaldehyde. The catalysts showed catalytic activity which is comparable to the data published in the literature.

In addition to the 2-D model catalysts, the 3-D Pt/KL-zeolite catalysts were prepared and applied in aromatisation of *n*-alkanes and liquid phase oxidation. The prepared 1% Pt/KL-zeolite catalysts showed activity in gas phase aromatisation of *n*-hexane, *n*-heptane and *n*-octane. The Pt/KL-zeolite catalyst prepared by vapour phase impregnation (Pt/KL-zeolite VPI) showed more activity in aromatisation than the Pt/KL-zeolite catalyst prepared by incipient wetness impregnation (Pt/KL-zeolite IWI). The presence of oxygenates or sulphur compounds decreased the catalytic activity of the catalysts based on *n*-alkane conversion and selectivity to aromatics. Pt/KL-zeolite VPI catalyst was more tolerant to oxygenates than Pt/KL-zeolite IWI catalysts. There was a direct correlation in catalyst deactivation and the amount of carbonaceous material accumulated on the spent catalyst. Poor catalytic activity was observed when the Pt/KL-zeolite catalysts were used in liquid phase oxidation of alcohols. The porosity of the support might not be suitable for the liquid phase reactions.

3.7 References

[1] P. C. Thune, J. Loos, A. M. de Jong, P. J. Lemstra, J. W. Niemantsverdriet, *Top. Catal*. **2000**, *13*, 67-74.

[2] Z. H. Lu, J. P. McCaffrey, B. Brar, G. D. Wilk, R. M. Wallace, L. C. Feldman, S. P. Tay, *Appl. Phys. Lett.* **1997**, *71*, 2764-2766.

[3] T. Eickhoff, V. Medicherla, W. Drube, *J. Elec. Spec. Rel. Phenom.* **2004**, *137-140*, 85-88.

[4] F. J. Himpsel, F. R. Mc Feely, A. Taleb-Ibrahimi, J. A. Yarmoff, *Phys. Rev. B.* **1988**, *38*, 6084-6095.

[5] Gunter, P.L.J., Niemantsverdriet, J.W., Ribeiro, F.H., Somorjai, G.A., *Catal. Rev. Sci. Eng.* **1997**, *39*, 77-168.

[6] C. M. Castaneda, L. Ashbaugh, P. Wakabayashi, *J. Aerosol Sci.* **2010**, *41*, 99-107.

[7] T. Kyotani, T. Nagai, S. Inoue, A. Tomita, *Chem. Mater*. **1997**, *9*, 609-615.

[8] E. Erasmus, J. W. Niemantsverdriet, J. C. Swarts, *Langmuir*. **2012**, *28*, 16477-16484.

[9] A. Adenier, M. M. Chehimi, I. Gallardo, J. Pinson, N. Vila, *Langmuir*. **2004**, *20*, 8243-8253.

[10] J. Singh, J. E. Whitten, *J. Phys. Chem. C*. **2008**, *112*, 19088–19096.

[11] Q. J. Miao, Z-P. Fang, G. P. Cai, *Catal. Comm.* **2003**, *4*, 637–639.

[12] J. X. McDermott, J. F. White, G. M. Whitesides, *J. Am. Chem. Soc.***1976**, *98*, 6521-6528.

[13] J. F. Moulder, W. F. Stickle, P. E. Sobol, K. D. Bomben, in *Handbook of X-Ray Photoelectroscopy*, (J. Chastain, ed.). Perkin-Elmer Corp., USA, **1992**, p. 181.

[14] T. W. Hanks, R. A. Ekeland, K. Emerson, R. D. Larsen, P. W. Jennings, *Organometallics.* **1987**, *6*, 28-32.

[15] C. Kan, X. Kong, C. Du, D. Liu, *Polymer Journal*. **2002**, *34*, 97-102.

[16] J. L. G. Fierro, J. M. Palacios, F. Tomas, *Surf. Interface Anal.* **1988**, *13*, 25-32.

[17] Z. Paal, R. Schlogl, G. Ertl, *Catal. Lett.* **1992**, *12*, 331-344.

[18] T. L. Barr, *J. Phys. Chem.* **1978**, *82*, 1801-1810.

[19] M. F. Lappert, F. P. A. Scott, *J. Organomet. Chem.* **1995**, *492*, Cll-C13.

[20] A. Kowalewska, W. A. Stańczyk, *Arkivoc*. **2006**, 110-115.

[21] A. Syed, E. D. Stevens, S. G. Cruz, *Inorg. Chem.* **1984**, *23*, 3673-3674.

[22] A. Bakalova, D. Ivanov, *J. Thermal Anal. Calorimetry*. **2007**, *89*, 257-260.

[23] A. Katrib, A. Stanislaus, R. M. Yousef, *J. Mol. Str.* **1985**, *129*, 151-163.

[24] D. Wang, S. Penner, D. S. Su, G. Rupprechter, K. Hayek, R. Schlogl, *J. Catal.* **2003**, *219*, 434-441.

[25] L. K. Ono, B. Yuan, H. Heinrich, B. R. Cuenya, *J. Phys. Chem. C.* **2010**, *114*, 22119-22133.

[26] G. A. Martin, R. Dutartre, J. A. Dalmon, *React. Kinet. Catal. Lett.* **1981**, *16*, 329-332.

[27] C. Hippe, R. Lamber, G. Schulz-Ekloff, U. Schubert, *Catal. Lett.* **1997**, *43*, 195-199.

[28] P. C. Thune, R. Linke, W. J. H. van Gennip, A. M. de Jong, J. W. Niemantsverdriet, *J. Phys. Chem. B.* **2001**, *105*, 3073-3078.

[29] D. R. Pesiri, R. C. Snow, N. Elliott, C. Maggiore, R. C. Dye, *J. Membrane Sci.* **2000**, *176*, 209-221.

[30] C. I. Sanders, D. S. Martin, *J. Am. Chem. Soc.* **1961**, *83*, 807-810.

[31] L. W. Brigitte, E. Schwederski, D. W. Margerum, *Inorg. Chem.* **1990**, *29*, 3578-3584.

[32] A. Henglein, B. G. Ershov, M. Malow, *J. Phys. Chem.* **1995**, *99*, 14129-14136.

[33] G. Yu, W. Chen, J. Zhao, Q. Nie, *J. Appl. Elec.* **2006**, *36*, 1021-1025.

[34] J. Yang, T. C. Deivaraj, H.-P. Too, J. Y. Lee, *Langmuir.* **2004**, *20*, 4241-4245.

[35] P. C. Thune, C. J. Weststrate, P. Moodley, A. M. Saib, J. van de Loosdrecht, J. T. Miller, J. W. Niemanstsverdriet, *Catal. Sci. Technol.* **2011**, *1*, 689-697.

[36] P. Moodley, J. Loos, J. W. Niemantsverdriet, P. C. Thune, *Carbon*. **2009**, *47*, 2002-2013.

[37] P. Moodley, F. J. E. Scheijen, J. W. Niemantsverdriet, *Catal. Today*, **2010**, *154*, 142-148.

[38] C. Dablemont, P. Lang, C. Mangeney, J-Y. Piquemal, V. Petkov, F. Herbst, G. Viau, *Langmuir*. **2008**, *24*, 5832-5841.

[39] L. N. Lewis, J. Stein, Y. Gao, R. E. Colborn, G. Hutchins, *Platinum Metals Rev.* **1997**, *41*, 66-75.

[40] S. V. Aradhya, M. Frei, M. S. Hybertsen, L. Venkataraman, *Nature Mater.* **2012**, 1-5. *DOI:10.1038/NMAT3403*.

[41] E. T. Vandenberg, L. Bertilsson, B. Liedberg, K. Uvdal, R. Erlandsson, H. Elwing, I. Lundstrom, *J. Colloid Interf. Sci.* **1991**, *147*, 103-118.

[42] M. Barczak, R. Dobrowolski, J. Dobrzynska, E. Zieba, A. Dabrowski, *Adsorption*. **2013**, *19*, 733-744.
[43] S. Alexandrova, E. Halova, S. Bakalova, A. Szekeres, A. Marin, P. Osiceanu, M. Gartner, N. Koujuharova, *J. Phys. Conf. Series*. **2014**, *514*, 120351-120355.
[44] Y. Xu, X. Zhu, H. D. Lee, C. Xu, S. M. Shubeita, A. C. Ahyi, Y. Sharma, J. R. Williams, W. Lu, S. Ceesay, B. R. Tuttle, A. Wan, S. T. Pantelides, *J. Appl. Phys.* **2014**, *115*, 335021-335028.
[45] H. G. J. de Wilt, H. S. van der Baan, *Ind. Eng. Chem. Prod. Res. Dev.* **1972**, 11, 374-378.
[46] I. Roberts, H. C. Urey, *J. Am. Chem. Soc.* **1939**, *61*, 2584-2587.
[47] I. W. Ashworth, E. Bush, L. C. Chan, J. C. Cherryman, B. G. Cox, J. Muir, S. R. Korupoju, J. Keshwan, *Org. Proc. Res. Dev.* **2012**, *16*, 1646-1651.
[48] M. T. Sanz, R. Murga, S. Beltran, J. L. Cabezas, J. Coca, *Ind. Eng. Chem. Res.* **2002**, *41*, 512-517.
[49] R. V. Jagadeesh, H. Junge, M.-M. Pohl, J. Radnik, A. Bruckner, M. Beller, *J. Am. Chem. Soc.* **2013**, *135*, 10776-10782.
[50] K. Mori, T. Hara, T. Mizugaki, K. Ebatani, K. Kaneda, *J. Am. Chem. Soc.* **2004**, *126*, 10657-10666.
[51] K. L. E Eriksson, W. W. Y. Chow, C. Puglia, J. E. Backvall, E. Gothelid, S. Oscarsson, *Langmuir*. **2010**, *26*, 16349-16354.
[52] D. Loffreda, F. Delbecq, F. Vigne, P. Sautet, *J. Am. Chem. Soc.* **2006**, *128*, 1316-1323.
[53] E. Bayram, J. Lu, C. Aydin, A. Uzun, N. D. Browning, B. C. Gates, R. G. Finke, *ACS Catal.* **2012**, *2*, 1947-1957.
[54] J. A. Anderson, A. Athawale, F. E. Imrie, F.-M. M^{c}Kenna, A. M^{c}Cue, D. Molyneux, K. Power, M. Shand, R. P. K. Wells, *J. Catal.* **2010**, *270*, 9-15.
[55] R. V. Malyala, C. V. Rode, M. Arai, S. G. Hegde, R. V. Chaudhari, *Appl. Catal. A.* **2000**, *193*, 71-
[56] T. R. Mattson, S. J. Paddison, *Surf. Sci.* **2003**, *544*, L697-
[57] S. N. Delgado, D. Yap, L. Vivier, C. Especel, *J. Mol. Catal. A.* **2013**, *367*, 89-98.
[58] S. M. Kim, Y. S. Kim, D. W. Kim, J. W. Yang, *Green Chem.* **2012**, 2996-2998.
[59] T. Mallat, Z. Bodnar, P. Hug, A. Baiker, *J. Catal.* **1995**, *153*, 131-143.
[60] T. Mallat, A. Baiker, *Chem. Rev.* **2004**, *104*, 3037-3058.
[61] C. Besoukhanova, J. Guidot, D. Barthomeuf, M. Breysse, J. R. Bernard, *J. Chem. Soc., Faraday Trans. 1*. **1981**, *77*, 1595-1604.
[62] A. P. J. Jansen , R. A. Van Santen, *J. Phys. Chem.* **1990**, *94*, 6764–6772.
[63] S. Bhogeswararao, D. Srinivas, *Catal. Lett.* **2010**, *140*, 55-
[64] S. Bhogeswararao, D. Srinivas, *J. Catal.* **2012**, *285*, 31-40.
[65] K-Q. Sun, Y-C. Hong, G-R. Zhang, B-Q. Xu, *ACS Catal.* **2011**, *1*, 1336-1346.
[66] P. Gallezot, D. Richard, *Catal. Rev. Sci. Eng.* **1998**, *40*, 81-126.
[67] P. A. Webb, C. Orr, in *Analytic Methods in Fine Particle Technology*, (R. W. Camp, J. P. Olivier, Y. S. Yunes, contributors), Micromeritics Instrument Corporation, Norcross, **1997**, p. 54-55.
[68] S. Brunauer, P. H. Emmett, E. Teller, *J. Am. Soc.* **1938**, *60*, 309-319.
[69] J. Yoo, Y. Do, *Dalton Trans.* **2009**, 4978-4986.
[70] A. Katrib, A. Stanislaus, R. M. Yousef, *J. Mol. Str.* **1985**, *129*, 151-163.
[71] Z. Paal, R. Schlogl, G. Ertl, *Catal. Lett.* **1992**, *12*, 331-344.
[72] J. F. Moulder, W. F. Stickle, P. E. Sobol, K. D. Bomben, in *Handbook of X-Ray Photoelectroscopy*, (J. Chastain, ed.). Perkin-Elmer Corp., USA, **1992**, p. 45.
[73] G. Jacobs, F. Ghadiali, A. Pisanu, A. Borgna, W. E. Alvarez, D. Resasco, *Appl. Catal. A.* **1999**, *188*, 79-98.
[74] M. Vaarkamp, J. T. Miller, F. S. Modica, G. S. Lane, D. C. Koningsberger, *J. Catal.* **1992**, *138*, 675-685.
[75] D. J. Ostgard, L. Kustov, K. R. Poeppelmeier, W. M. H. Sachtler, *J. Catal.* **1992**, *133*, 342-357.
[76] S. J. Tauster, J. J. Steger, *J. Catal.* **1990**, *125*, 387-389.
[77] J. S. L. Fonseca, A. C. F. Junior, J. M. Grau, M. C. Rangel, *Appl. Catal. A.* **2010**, *386*, 201-210.
[78] E. Iglesia, J. F. Baumgartner, in *New Frontiers in Catal.* (L. Guczi, F. Solymosi, P. Teteny, eds.), *Proc. 10th Int. Congr. Catal.* Akad Kiado, Budapest, **1993**, *B*, 993-1006.
[79] S. Jongpatiwut, P. Sackamduang, T. Rirksomboon, S. Osuwan, D. E. Resasco, *J. Catal.* **2003**, *218*, 1-11.
[80] M. E. Dry, R. J. Nash, C. T. O'Connor, in *Proc. 12th Inter. Zeolite Conf.* Baltimore, **1998**, 2557-2564.

[81] G. B. McVicker, J. K. Lao, J. J. Ziemiak, W. E. Gates, J. L. Robbins, M. M. J. S. B. Rice, T. H. Vanderspurt, V. R. Cross, A. K. Ghosh, *J. Catal*. **1993**, *139*, 48-61.
[82] T. Fukunaga, V. Ponec, *J. Catal.* **1995**, *157*, 550-558.
[83] S. Trakarnroek, S. Ittisanronnachai, S. Jongpatiwut, T. Rirksomboon, S. Osuwan, D. E. Resasco, *Chem. Eng. Comm.* **2007**, *194*, 946–961.
[84] M. M. J. Treacy, *Micropor. Mesopor. Mater.* **1999**, *28*, 271–292.
[85] L. Zhou, W. Yu, L. Wu, Z. Liu, H. Chen, X. Yang, Y. Su, J. Xu, *Appl. Catal. A.* **2013**, *451*, 137-143.
[86] R. Anderson, K. Griffin, P. Johnston, P. L. Alters, *Adv. Synth. Catal.* **2003**, *345*, 517-523.
[87] D. I. Enache, D. W. Knight, G. J. Hutchings, *Catal. Lett.* **2005**, *103*, 43-52.
[88] A. K. Bera, B. Pal, K. S. S. Gupta, *Int. J. Chem. Kinet.* **2012**, *44*, 494-505.
[89] I. Hoek, T. A. Nijhuis, A. I. Stankiewicz, J. A. Moulijn, *Appl. Catal. A.* **2004**, *266*, 109-116.
[90] G. A. Olah, T. Shamma, G. K. Surya, *Catal. Lett.* **1997**, *46*, 1-4.
[91] C. Park, M. A. Keane, *J. Mol. Catal. A.* **2001**, *166*, 303-322.

4. Experimental Procedures

4.1 Introduction

This chapter describes in detail the methods used to prepare various platinum catalysts and the procedures followed in application of these catalysts in organic transformations. A summary of the materials and the suppliers of the materials used to prepare the catalysts and the characterisation techniques are also included.

4.2 Materials

The solid and liquid materials from Sigma Aldrich were used without further purification unless otherwise stated in the procedure. Solvents were dried by distillation over a suitable drying agent such as sodium according to the published methods. Silicon wafers were obtained from Topsil, these are n-type, single crystalline of (100) orientation, with resistivity of 370-410 Ω.m. Catalyst supports KL-zeolite (HSZ-500KOA) and HY-zeolite (HSZ-350HUA) were purchased from Tosoh Corp (Japan) and were used without further modification except calcination.

4.3 Spectroscopic Measurements

Nuclear magnetic resonance (^{1}H and ^{195}Pt) spectra were recorded on a Bruker Avance DPX 300 MHz spectrometer (only ^{1}H) and Bruker Avance DPX 600 MHz (both ^{1}H and ^{195}Pt). The ^{1}H chemical shifts reported were relative to $SiMe_4$ at 0.00 ppm and the ^{195}Pt was measured relative to K_2PtCl_4 at -4104 ppm. The Fourier transform infrared (FTIR) wave numbers of the products and the reactants was recorded on a Bruker Tensor 27 infrared spectrophotometer fitted with Pike MIRacle single bounce diamond Attenuated Total Reflectance (ATR). Rutherford Backscattering Spectroscopy (RBS) was perfomed at iThemba Labs (Somerset West) and the amount of deposited metal was determined by curve fit using the Rutherford Universal Manipulation Program.

The elemental analysis of the catalysts was carried out by the Canadian Microanalytical Service Ltd., the Analytical Chemistry division of the Department of Chemistry, University of the Free State and Sasol Shared Services on a LECO Truspec Micro elemental analyser. The metal particle size analysis was performed by the Centre for Microscopy, University of the Free State.

XPS data were recorded on a PHI 5000 Versaprobe system with monochromatic AlK alpha X-ray source. Spectra were obtained using the aluminium anode (Al Kα = 1486.6 eV) operating at 50 μm, 12.5 W and 15 kV energy. The survey scans were recorded at constant pass energy of 187.85 eV and region scans at constant pass energy of 29.35 eV with the analyser resolution ≤ 0.5 eV. The background pressure was 2 x 10^{-8} mbar. The XPS data were analysed utilising Multipak version 8.2c computer software[1] using Gaussian–Lorentz fits (the Gaussian/Lorentz ratios were always >95%).

4.4 Thermal Analysis

The Mettler/Toledo TGA/SDTA857 equipment was used to perform the thermal analysis of the Pt/zeolite catalysts. About 20 mg of the catalyst was heated to 700 °C at heating rate of 10 °C/min. The TGA data were analysed utilising the Mettler STA^e Evaluation Software to determine mass loss at different temperatures.

4.5 Physisorption and Chemisorption Analyses

All porosity and surface area properties were determined on a Micromeritics ASAP 2020 Surface Area and Porosity Analyzer and the data analysed with ASAP 2020 V2.0 for physisorption. The Pt/zeolite catalyst was activated at 150 °C for 12 hours for porosity analysis and a typical amount of ~20 mg was used for each analysis with the warm and cold free space determined separately. The BET surface area results and micropore volume results were obtained by curve fitting using MicroActive V1.01 Software.

Similarly, the chemisorption properties were determined on a standard Micromeritics ASAP 2020 Surface Area and Porosity Analyzer enabled for standard ASAP Chemi Series chemisorption procedure. The chemisorption analysis was done at 35 °C using CO (Carbon Monoxide) as the titration gas. A Micromeritics reference sample, 0.5 % Pt/Alumina was used to calibrate the method. Freshly calcined Pt/zeolite catalyst (250 mg) was reduced on line with H_2 at 350 °C followed evacuation and cooling to 35 °C; and ultimately titration with CO. The data was analysed with ASAP 2020 V2.0 for chemisorption.

4.6 Preparation Model Pt Catalysts on Flat two-Dimensional Supports

4.6.1 Pre-treatment of Silicon Wafer (Si-wafer) as a Catalyst Support

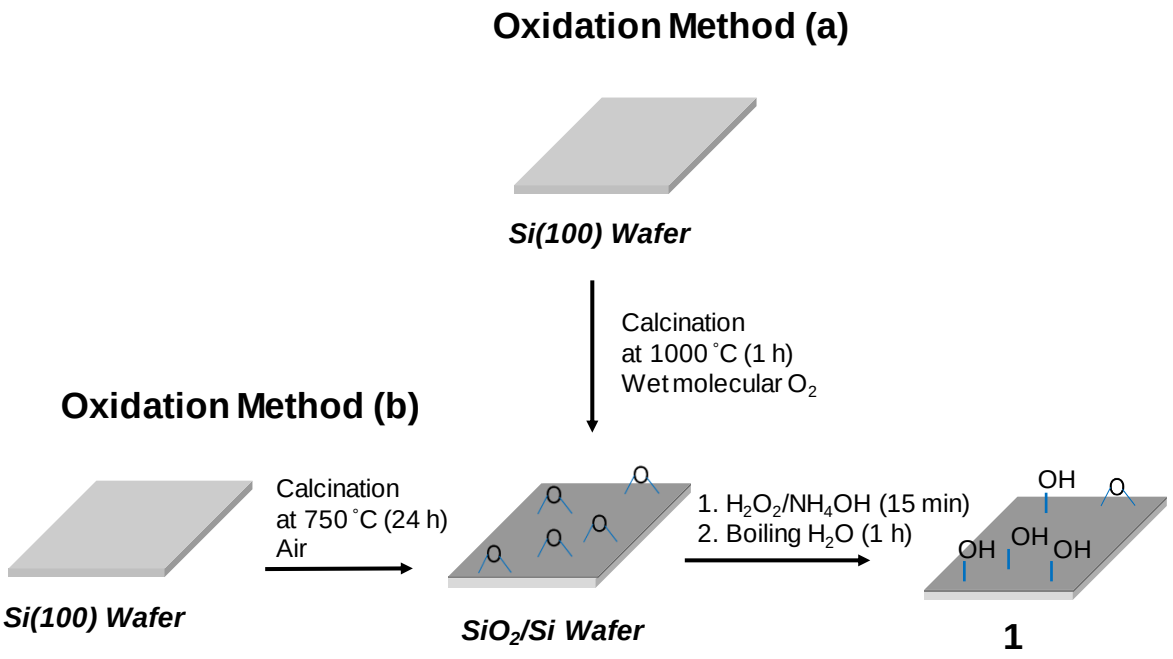

Scheme 4.1. An outline of the methods used to oxidised Si (100) wafer followed by hydroxylation to form surface silanol groups (Si-OH) in surface **1**.

Oxidation Method A: The Si-wafer sample with (100) surface orientation was place in a quartz tube in a calcination oven at 1000 °C (see Scheme 4.1). Molecular oxygen from the gas cylinder was gently bubbled through a distilled water reservoir (gas bubbler). The wet oxygen from the water reservoir was passed through the hot quartz tube in the calcination oven. The oven was cooled down after 1 h and the bluish Si-wafer sample was removed from the oven.

Oxidation Method B: The Si-wafer sample in a quartz chamber was placed in a calcination oven under ambient air. The temperature of the oven was increased to 750 °C (average heating rate = 16 °C/min). After 24 h at 750 °C, the oven temperature was then turned off and the Si-wafer sample was kept inside the oven until the temperature of the oven cooled down to about 25 °C after *ca.* 12 h (see Scheme 4.1). The Si-wafer sample was removed and analysed with XPS.

*Hydroxylation to form silanol groups on surface **1***: The oxidised Si-wafer prepared by oxidation Method B was cleaned by allowing the wafer to stand in a mixture of 1:1 (v/v) H_2O_2 (25% solution) and NH_4OH (35% solution) at *ca.* 40 °C for 15 minutes. Afterwards the Si-wafer samples were hydroxylated to form surface silanol groups (Si-OH) by boiling it in double distilled water for 1 h and dried at room temperature under nitrogen (see Scheme 4.1). The Si-wafer samples were used with no further analysis.

4.6.2 Grafting of Allyltrimethoxysilane or 3-Aminopropyltrimethoxysilane onto Si-OH Groups on the Si-wafers

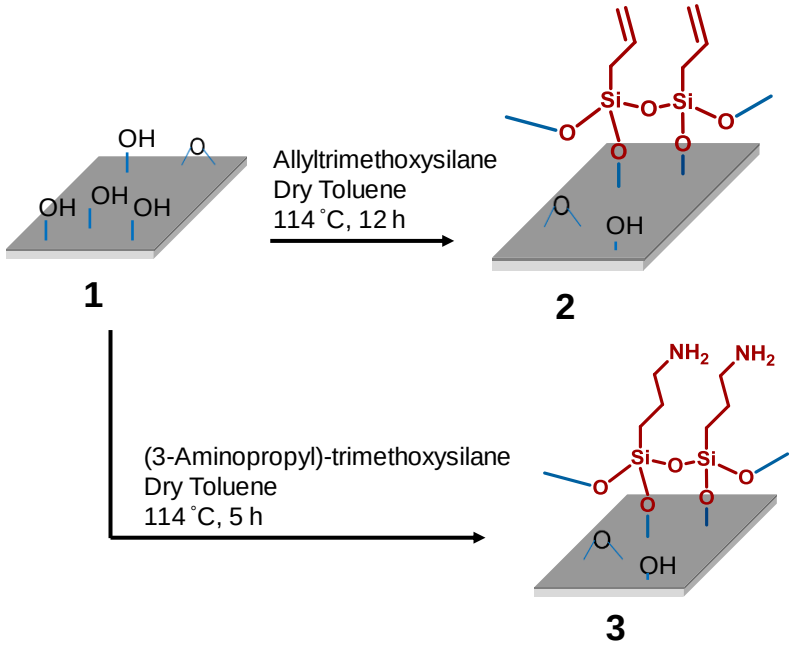

Scheme 4.2. Outline of silanation of Si-OH groups on the SiO_2/Si-wafers.

A solution of allyltrimethoxysilane (2 ml, 4.5 mmol) in dry toluene (70 ml) was prepared in a 250 ml round bottom flask. A sample of hydroxylated Si-wafer was placed in the solution with activated side of the wafer facing up. The solution in the flask was heated to achieve gentle reflux while stirring under nitrogen atmosphere. Extra care is taken to prevent the magnetic stirrer from touching the Si-wafer, by using a small magnetic stirrer. After 12 h under reflux the allyltrimethoxysilane functionalised Si-wafer samples were washed with toluene (20 ml) to remove the unreacted silane followed by washing with absolute ethanol and drying under a stream of argon (see Scheme 4.2).

XPS of surface 2: Binding energy, eV: 284.8 (Allyl C1s), 286.7 (methoxy C1s).

The same procedure described above was used to silanate the hydroxylated Si-wafer with 3-aminopropyltrimethoxysilane. A solution of 3-aminopropyltrimethoxysilane (2 ml, 4.5 mmol) in

dry toluene (70 ml) was used as a silanation solution at 114 °C. The 3-aminopropyltrimethoxysilane solution with a sample of hydroxylated Si-wafer was refluxed for 5 h followed by rinsing in toluene and ethanol and finally drying (see Scheme 4.2).

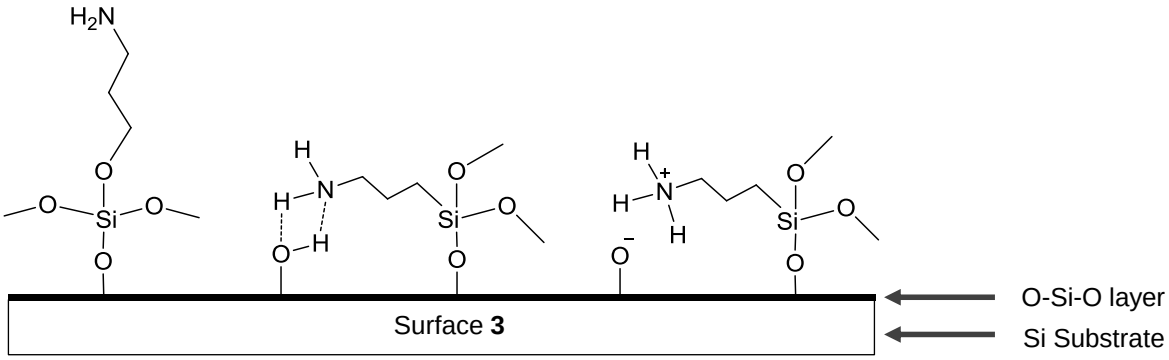

XPS of surface 3: Binding energy, eV: 399.2 (N 1s for free amine), 400.4 (N 1s for hydrogen bonded amine) and 401.5 (N 1s for protonated amine).

4.6.3 Platinisation of Activated Si-water with a Pt(IV) Precursor

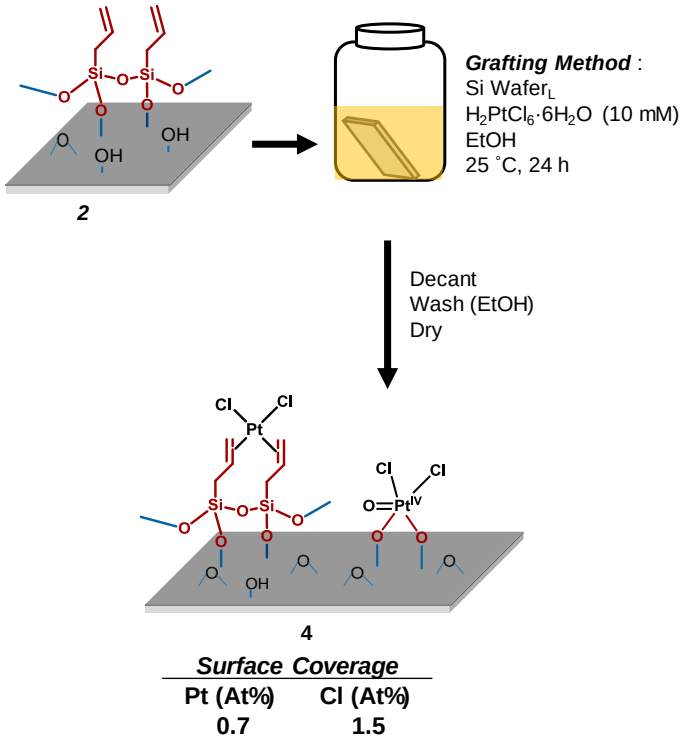

Scheme 4.3. Outline of platinisation of surface **2** by grafting of H_2PtCl_6.

Grafting method: A solution of $H_2PtCl_6 \cdot 6H_2O$ (16 mg, 0.080 mmol) in ethanol (3 mL) was prepared in 5 mL vial. A Si-wafer which was pre-silanated with allyltrimethoxysilane, was placed in $H_2PtCl_6 \cdot 6H_2O$ solution and stirred for 24 h at 25 °C. To prevent scratching of the surface of Si-wafer, the magnetic stirrer bar was separated from Si-wafer by a glass barrier. The reaction solution was decanted and Si-wafer washed with 50 v/v% aqueous ethanol followed by rinsing with distilled water and drying under a flow of nitrogen (see Scheme 4.3).

***XPS of surface 4*:** Binding energy, eV: 72.4 (Pt $4f_{7/2,}$ Pt^{2+}), 73.6 (Pt $4f_{7/2,}$ Pt^{4+}) 198.5 (Cl $2p_{3/2}$, Pt-Cl), 530.7 (O 1s, Pt=O), 531.1 (O 1s, Pt-O), 532.6 (O 1s, Si-O).

Spin coating method: A solution $H_2PtCl_6 \cdot 6H_2O$ (16 mg, 0.080 mmol) in absolute ethanol (3 mL) was prepared. The prepared $H_2PtCl_6 \cdot 6H_2O$ solution (100 μL) was then placed dropwise onto the centre of the allyltrimethoxysilane functionalised Si-wafer mounted on the spin-coater device and it was rotated at 2880 rpm. After the appearance of the Newtonian circles on the surface of Si-wafer, the platinised surface was spun for additional to completely evaporate the solvent. The rotation of the spin-coater was then terminated, the platinized Si-wafer was dismounted and it was analysed with XPS (see Scheme 4.3).

***XPS of surface 4*:** Binding energy, eV: 73.0 (Pt $4f_{7/2,}$ Pt^{2+}), 75.2 (Pt $4f_{7/2,}$ Pt^{4+}) 198.7 (Cl $2p_{3/2}$, Pt-Cl), 199.9 (Cl $2p_{3/2}$, μCl) 532.6 (O 1s, Si-O).

4.6.4 Chemical Grafting of the Pt(II) Solution on Allyl Functionalised Si-wafer

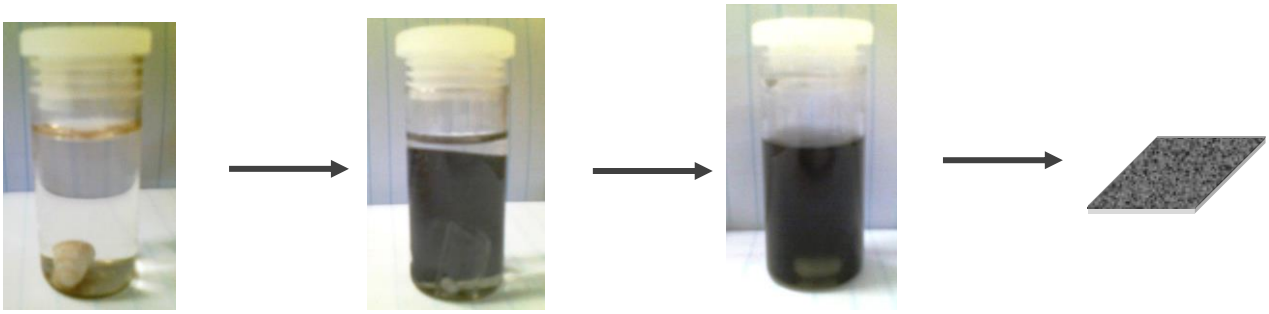

(a) K_2PtCl_4 Solution (b) Surface **3** (c) Surface **13** (d) Surface **13**

Scheme 4.4. (a) 1.25 mM solution of K_2PtCl_4 in aqueous ethanol (b) SiO_2/Si-wafer with surface allyl groups submerged in freshly prepared K_2PtCl_4 solution (c) platinised surface **13** submerged in colloidal Pt mixture after heating at 60 °C (d) pictorial model of platinised surface **13** with faint dark shade of adsorbed Pt particles.

The platinisation of allyltrimethoxysilane functionalised Si-wafer (surface **2**) with K_2PtCl_4 was carried out using grafting method.

Grafting method: A solution of K_2PtCl_4 (6 mg, 0.0145 mmol) in 3 mL distilled water was prepared in 12 mL glass vial followed by filtration through a glass wool. Ethanol (3 mL) was added to the resulting solution. A SiO_2/Si-wafer silanated with allyltrimethoxysilane was place in the Pt solution followed by gently heating to 50 ^oC in water bath for 30 minutes or until the colour changed from red to black. The Si-wafer was then removed from the Pt solution, washed with distilled water and finally rinsed with ethanol before drying at room temperature using a light stream of nitrogen (see Scheme 4.4). The platinized Si wafer was analysed by XPS.

***XPS of surface 13*:** Binding energy, eV: 71.3 (Pt $4f_{7/2,}$ Pt^0), 73.5 (Pt $4f_{7/2,}$ Pt^{2+}), 75.6 (Pt $4f_{7/2,}$ Pt^{4+}).

4.6.5 Chemical Grafting of the Pt(II) Solution on Amino Functionalised Si-wafer

The platinisation of 3-aminopropyltrimethoxysilane functionalised Si-wafer (surface **3**) with K_2PtCl_4 was carried out using two methods, grafting to liberate platinised surface **14** and spin coating to liberate platinised surface **17** as described above in section 4.5.3 and section 4.4.4. The same preparation methods were utilised. The platinised surface **14** was subsequently analysed by XPS. Platinised surface **17** which was prepared by spin coating was not analysed by XPS because TEM analysis showed an ununiform distribution of Pt particles.

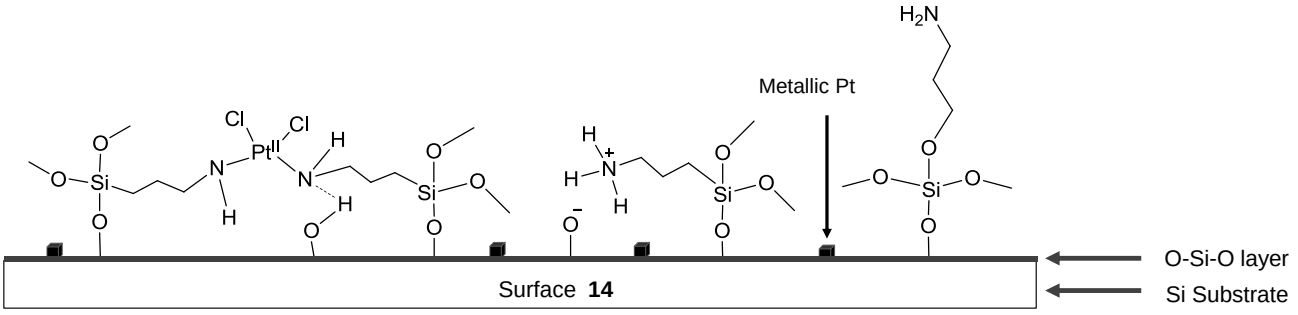

***XPS of surface 14*:** Binding energy, eV: 71.8 (Pt $4f_{7/2,}$ Pt^0), 72.9 (Pt $4f_{7/2,}$ Pt^{2+}), 397.7 (N 1s, Pt-N), 399.2 (N 1s for free amine), 400.4 (N 1s for hydrogen bonded amine) and 401.5 (N 1s for protonated amine).

4.6.6 Elucidation of the Binding Mode of Immobilised Pseudo-Bintate Ligand to Pt Centre

The reaction of the Pt precursors with various olefins was carried out to determine the binding mode of Pt centre to the adsorbed allysilane on the 2-D flat solid support. The method used to react $H_2PtCl_6{\cdot}6H_2O$ or K_2PtCl_4 with 1,5-cyclooctadiene or 1-hexene is described below.

4.6.6.1 Synthesis of Platinum (II) 1,5-Cyclooctadiene Chloride, Complex (8)

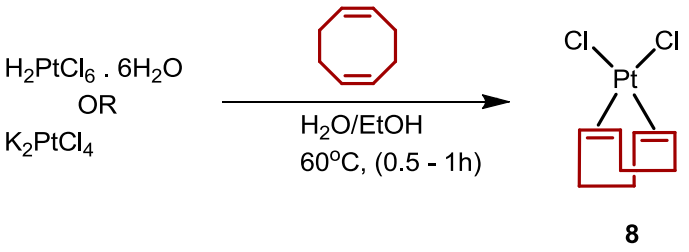

Scheme 4.5. The reaction of 1,5-COD with $H_2PtCl_6 \cdot 6H_2O$ or K_2PtCl_4 to form dichloro(1,5-cyclootadiene)platinum (II) **8**

Method A using $H_2PtCl_6 \cdot 6H_2O$: A solution of $H_2PtCl_6 \cdot 6H_2O$ (50 mg, 0.097 mmol) was dissolved in 3 mL of absolute ethanol in a 25 mL round bottomed flask fitted with the condenser. Water (0.1 mL) and excess 1,5-cyclooctadiene (0.1 mL, 0.8 mmol) was immediately added to the resultant Pt solution followed by vigorous stirring. The reaction solution was transferred into the water bath which was heated to 60 °C and kept at this temperature for 1 h (see Scheme 4.5). The reaction solution was concentrated *in vacuo* followed by dissolving the unreacted $H_2PtCl_6 \cdot 6H_2O$ by the addition of water (5 mL). The crude product was extracted by chloroform to afford crude 1,5-cyclooctadiene chloride complex (**8**) as a light yellow solid (1 mg, 4 % yield). Pure product was recrystallized in aqueous ethanol (1:1 by volume) to achieve white solid needles, mp. 285 °C.

Method B using K_2PtCl_4: A red solution of K_2PtCl_4 (100 mg, 0.24 mmol) in distilled water (1.5 mL) was prepared followed by filtration through a glass wool. Ethanol (2.5 mL) and excess 1,5-cyclooctadiene (1,5-COD) (0.1 mL, 0.8 mmol) were added sequentially to the Pt solution while stirring vigorously. The resulting mixture was heated to reflux in water bath at 60 ^oC. After 30 min at reflux, the stirring was stopped to allow any precipitate to settle and the hot solution was separated and cooled down separately (Scheme 4.5). The white needle shaped crystals which formed immediately (in the filtrate) when the reaction solution cools down were separated, washed with

pentane (5 mL) and dried in reduced pressure using vacuum pump. The final product collected was white needles of complex **8** (24 mg, 26.6% yield).

^{1}H NMR of complex 8 δ_H (600 MHz, $CDCl_3$, Appendix 1b), ppm: 2.25 (4H, m, 2xCH_2), 2.69 (4H, m, 2xCH_2), 5.6 (4H, t, $J_{Pt\text{-}H}$ = 32.8 Hz, 4xCH).

^{195}Pt NMR of complex 8: δ_{Pt} (107 MHz, $CDCl_3$, Appendix 2), ppm: -3337.0 (1Pt, s, Pt^{2+}).

4.6.6.2 Synthesis of di-μ-Chlorobis[(1,2-η-)-1-hexene]diplatinum(II), (9)

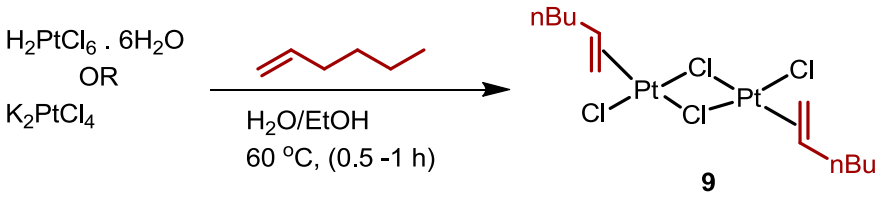

Scheme 4.6. The reaction of monodentade ligand, 1-hexene with $H_2PtCl_6{\cdot}6H_2O$ or K_2PtCl_4 to form complex **9**

Method A using $H_2PtCl_6{\cdot}6H_2O$: A solution of $H_2PtCl_6{\cdot}6H_2O$ (50 mg, 0.068 mmol) in 4 mL ethanol was prepared followed by the addition of water (0.1 mL) and excess 1-hexene (0.2 mL, 1.36 mmol) while stirring vigorously. The resulting solution was heated to reflux in water bath at 60 ^{o}C (Scheme 4.6). After 1 h at reflux, the stirring was stopped and the reaction solution was concentrated *in vacuo* to *ca.* 2 mL followed by the addition of water (5 mL) to dissolve the unreacted $H_2PtCl_6{\cdot}6H_2O$. The product and residual 1-hexene were extracted with chloroform. An oily residue (2 mg) was collected after concentration. ^{1}H NMR analysis showed unquantifiable trace of complex **7**.

Method B using K_2PtCl_4: A red solution of K_2PtCl_4 (50 mg, 0.12 mmol) in distilled water (1.5 mL) was prepared followed by filtration through a glass wool. Ethanol (2.5 mL) and 1-hexene (0.2 mL, 1.36 mmol) were added sequentially to the Pt solution while stirring vigorously. The resulting

solution was heated to reflux in water bath at 60 ^{o}C. The reaction solution was kept at 60 °C for *ca.* 30 min until the colour changed from red to yellow (Scheme 4.6). The stirring was stopped and the reaction solution was concentrated *in vacuo* to *ca.* 2 mL followed by the addition of water (5 mL) to dissolve the unreacted K_2PtCl_4. The product and residual 1-hexene were extracted with chloroform. An oily residue of complex **9** (31 mg, 59 %) was collected after concentration.

^{1}H NMR of complex 9: δ_H (600 MHz, $CDCl_3$, Appendix 3b), ppm: 0.97 (6H. t, J_{HH} = 12 Hz, 2xCH_3), 1.25-22.18 (12H, m, 6CH_2), 4.55 (2H, m, 2xCH), 4.78 (2H, m, 2xCH), 5.55 (2H, m, 2xCH).

Analysis calaculated. for $C_{12}H_{24}Cl_4Pt_2$: C, 20.6, H , 3.5.% Found: C, 20.7, H, 3.1.

XPS of complex 9: Binding energy (Appendix 10), eV: 73.5 (Pt $4f_{7/2}$, Pt^{2+}), 199.0, 200.5 (Cl $2p_{3/2}$).

4.6.7 Calcination and Reduction of H_2PtCl_6 Platinised Si-wafers

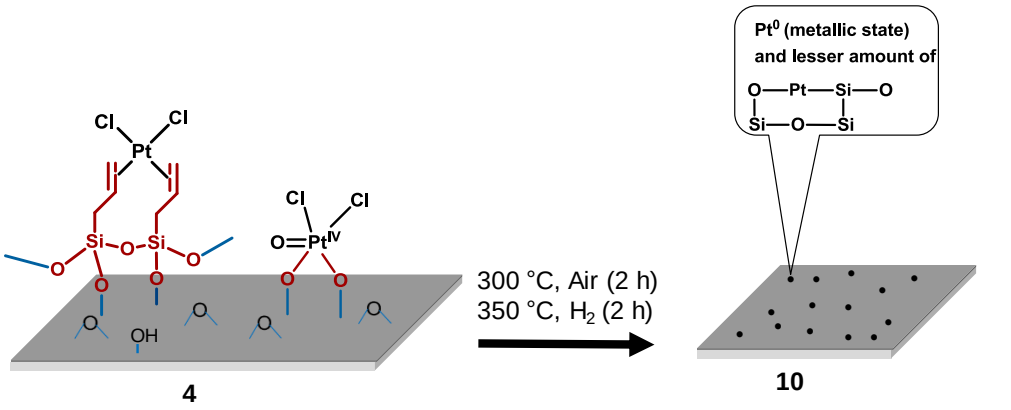

XPS Analysis (Atomic Ratio

Pt	Cl
1	2

XPS Analysis (Atomic Ratio)

Pt	Cl
1	0

Scheme 4.7. The outline of the procedures used to prepare the final flat model catalyst (surface **10**) from H_2PtCl_6. The black dots in surface **10** is the pictorial model that represent the Pt particles on the SiO_2/Si-wafer surface.

Platinized Si-wafers derived from reaction of surface allyl groups and H_2PtCl_6 (about 1 x 1 cm dimension) were placed in a ceramic boat then calcined in the oven quartz tube which was opened at

both ends to allow ambient air to pass through. The temperature of the oven was slowly increased by 1°C/min until it reached 300 °C. After 2 hours at 300 °C, the temperature was cooled down to 100 °C. The inlet of the quartz tube in the oven was connected to the hydrogen (H_2) supply and the outlet was connected to the vent *via* a silicon oil bubbler. A gentle hydrogen flow (about one bubble per second as qualitatively determined by the hydrogen passing through the silicon bubbler) was passed through the quartz tube with the calcinated Pt/Si-wafer samples. The temperature of the oven was increased slowly by 1 °C/min until it reached 350 °C. After 2 h at 350 °C, the temperature of the oven was reduced by 5 °C/min to 50 °C (see Scheme 4.7 for the reaction scheme). The hydrogen flow was stopped and quartz tube was flushed with nitrogen for 30 min. The quartz tube was sealed and removed from the oven to cool down at room temperature. The final model Pt/Si-wafer catalysts were stored in the glove box filled with nitrogen.

XPS of surface 10: Binding energy, (eV) 71.5 (Pt $4f_{7/2}$, Pt^0), 73.0, (Pt $4f_{7/2}$, Pt^{2+}).

4.6.8 Calcination and Reduction of K_2PtCl_4 Platinised Si-wafers

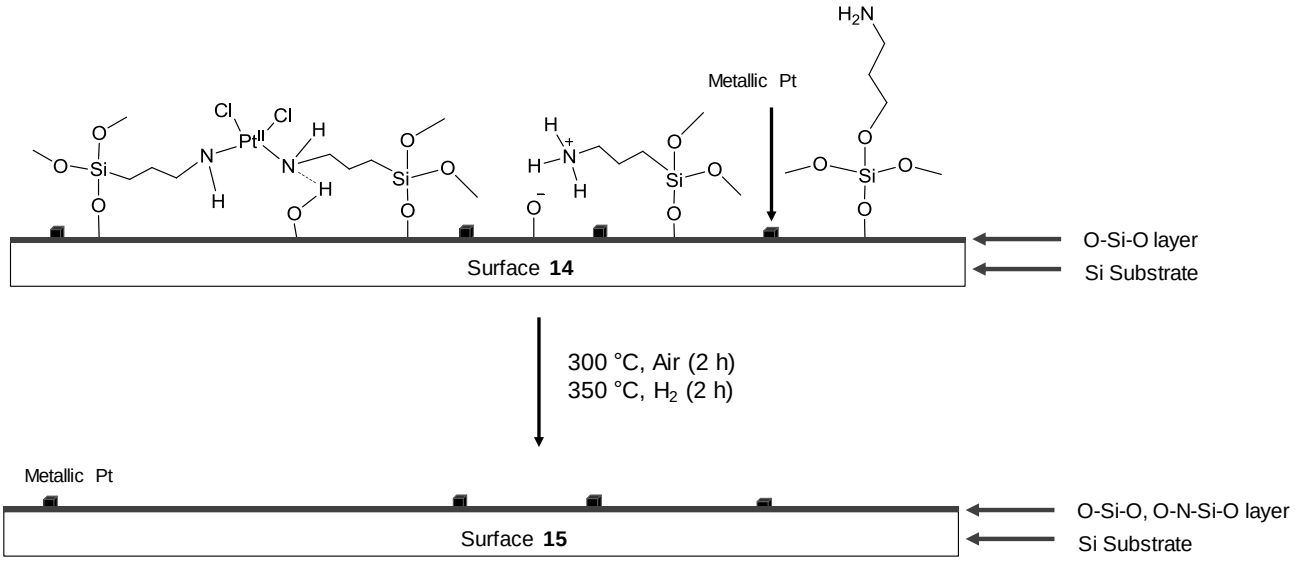

Scheme 4.8. The outline of the procedures used to prepare the final flat model catalyst (surface **15**) by calcination and reduction of surface **14**.

Platinized Si-wafers derived from reaction of surface amino groups and K_2PtCl_4 were calcined and reduced using the procedure described in section 4.5.7 to form surface **15**, see Scheme 4.8 for the reaction scheme.

XPS of surface 15: Binding energy, (eV) 71.6 (Pt $4f_{7/2}$, Pt^0), 72.9, (Pt $4f_{7/2}$, Pt^{2+}), 74.2, (Pt $4f_{7/2}$, Pt^{4+}), 397.8, (N 1s, Pt-N).

4.7 Oxidation of Alcohols Over Flat Model Pt/SiO_2/Si-wafer Catalysts

4.7.1 Oxidation in Ambient Air

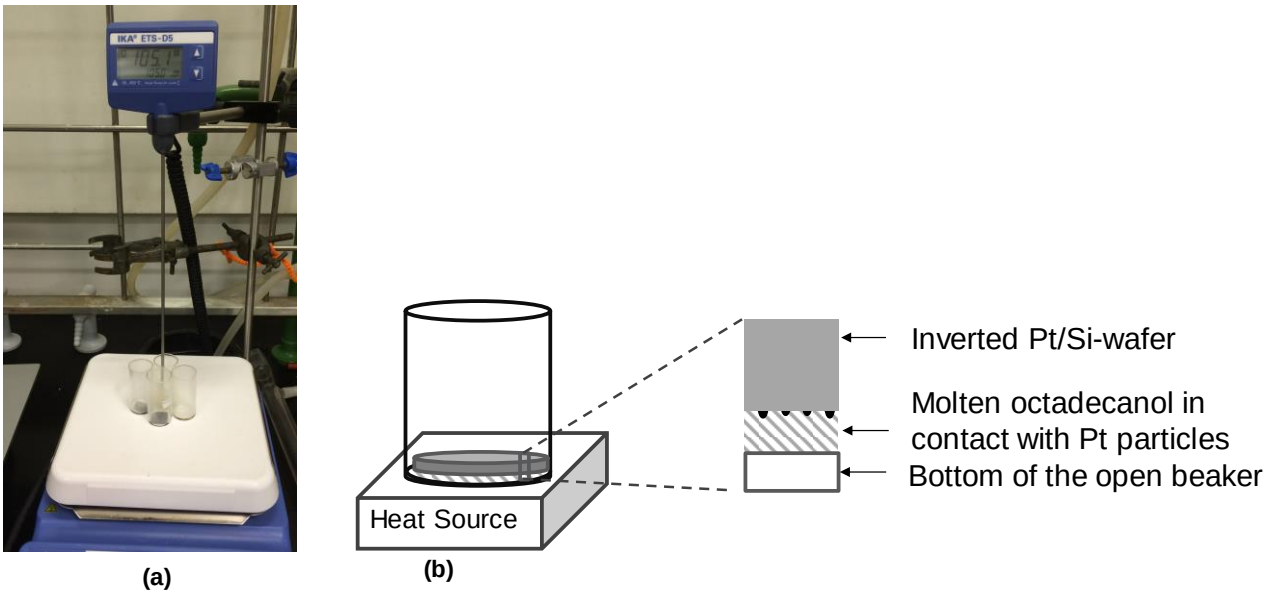

Figure 4.1 (a) Pictorial representation of the reactor set-up used in solvent free-oxidation over flat model Pt/SiO_2/Si-wafer catalyst (b) animation of the reactor set-up.

Oxidation of alcohols in ambient air was carried out in an open 20 mL glass vial or a beaker. The set-up includes a control vial with only alcohol to be oxidised, a control vial with alcohol and un-platinised Si-wafer and vial with platinised Si-wafer (Pt/Si-wafer) facing down in contact with the

oxidation substrate (see Figure 4.1). The catalytic experiment and the control experiment are done on a hot plate with automatic heat control.

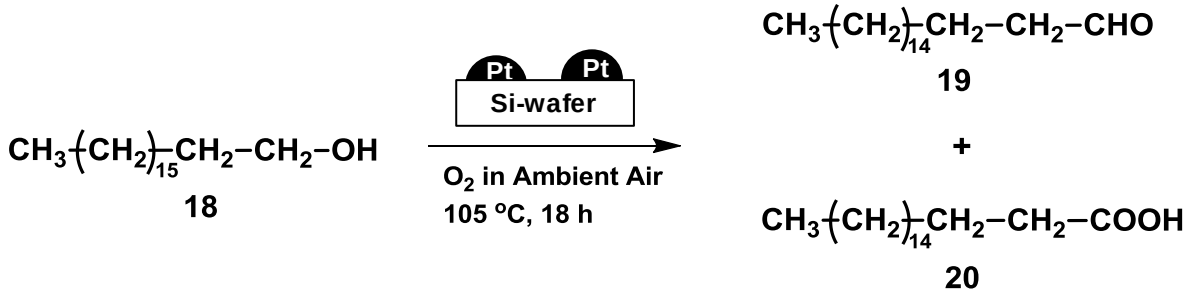

Scheme 4.9. The oxidation of 1-octadecanol **18** to form oxidation products octadecanal **19** and octadecanoic acid **20** in open glass vial, under controlled reaction temperature and ambient atmospheric air.

Oxidation of 1-octadecanol: 1-Octadecanol powder (100 mg, 0.34 mmol) was placed in a 20 ml glass vial and covered with a small piece of platinised SiO_2/Si-wafer (9x9 mm^2) with the polished side in direct contact with 1-octadecanol (see Figure 4.1for the reaction set-up and Scheme 4.9 for the reaction scheme). The glass vial was kept open while the reaction contents were heated slowly to 105 °C. Samples were collected periodically by dipping a spatula in molten oxidation solution under the Pt/Si-wafer and analysed using ATR FTIR to monitor the progress towards the formation of oxidation products. Samples were collected between 1 h and 18 h with 15 min intervals during the first hour, 30 min intervals until the 3rd hour thereafter, the samples were collected hourly until the 7th hour. After the 10th hour, the samples were collected after every 2 h interval. The oxidation samples for proton Nuclear Magnetic Resonance (^{1}H NMR) analysis were collected by dipping the spatula in molten oxidation solution under the Pt/Si-wafer followed by the quick dissolution of the collected sample in chloroform ($CHCl_3$). The solvent was evaporated from the oxidation sample and the remaining residue was weighed accurately, dissolved in 0.5 mL deuterated chloroform ($CDCl_3$) with internal standard 1,1,2,2-tetrachloroethane (2 mg/ml) and analysed by NMR spectroscopy. The

remaining oxidation product (80 mg) under the $Pt/SiO_2/Si$-wafer was also analysed by ATR FTIR and ^1H NMR.

***FTIR* of the product mixture**: ν_{max} (Figure 3.8), cm^{-1}: 3200 (OH), 2918, 2850 (CH), 1736, 1717 (C=O),

^1H NMR of the octadecanal, 19: δ_H (600 MHz, $CDCl_3$, Appendix 4b), ppm: 0.88 (3H, t, J_{HH} = 6.7 Hz, CH_3), 1.25 (28H, s, 14xCH_2), 1.59 (2H, m, CH_2), 2.42 (2H, dt, J_{HH} = 1.9 Hz, J_{HH} = 7.3 Hz, CH_2), 9.76 (1H, t, J_{HH} = 1.9 Hz, CHO).

^1H NMR of the octadecanoic acid, 20: δ_H (600 MHz, $CDCl_3$, Appendix 4a), ppm: 0.88 (3H, t, J_{HH} = 6.7 Hz, CH_3), 1.25 (28H, s, 14xCH_2), 1.59 (2H, m, CH_2), 2.35 (2H, t, J_{HH} = 7.5 Hz, CH_2)

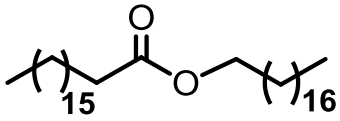

Octadecanyl Octanoate **21**

^1H NMR of an ester 21 in the product mixture: δ_H (600 MHz, $CDCl_3$, Appendix 4a), ppm: 0.88 (3H, t, J_{HH} = 6.70 Hz, CH_3), 1.25 (28H, s, 14xCH_2), 1.59 (2H, m, CH_2), 2.29 (2H, t, J_{HH} = 7.5 Hz, CH_2), 4.05 (2H, 1, J_{HH} = 6.7Z Hz, CH_2).

4.7.2 Oxidation in Molecular Oxygen

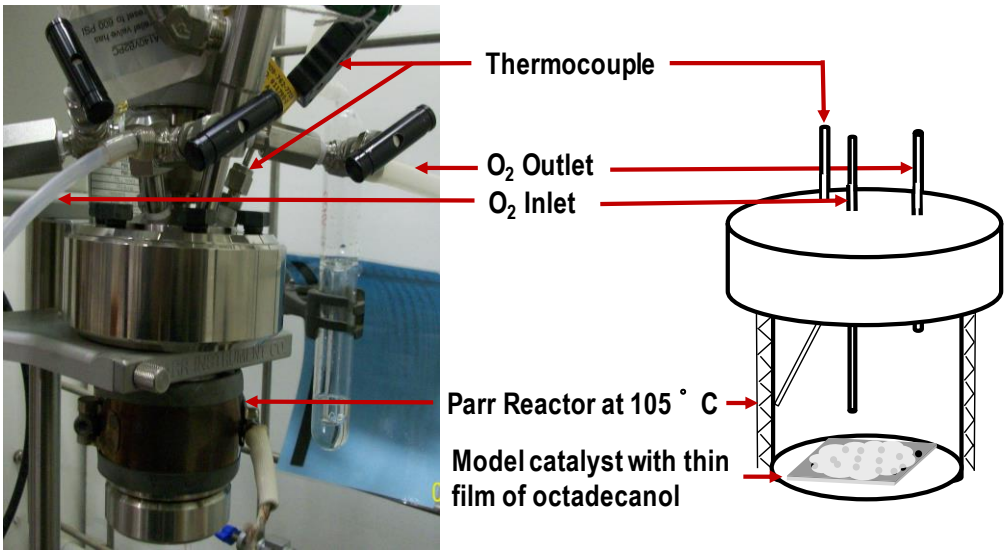

Figure 4.2 (a) Pictorial representation of the reactor set-up used in solvent free-oxidation over flat model $Pt/SiO_2/Si$-wafer catalyst in the presence of molecular oxygen (b) animation of the reactor set-up.

Oxidation of alcohols in molecular oxygen was carried out in a 25 mL Parr Reactor under a gently flow of molecular oxygen. During oxidation experiments, the thermocouple of the reactor was bent to touch the walls of the reactor to prevent over heating (see Figure 4.2).

Oxidation of 1-octadecanol: A flat model Pt/Si-wafer catalyst (18x18 mm^2) was placed flat on the surface of the Parr Reactor facing up. On the Pt/Si-wafer catalyst, 1-octadecanol powder (100 mg, 0.34 mmol) was placed to form a thin film covering the surface. The reactor was sealed followed by heating to 105 °C. When the reactor was at reaction temperature, molecular oxygen was introduced gently in the reactor keeping the gas outlet open. After 3 h oxidation, the reaction was terminated by sequentially switching off the heat supply, switching off the oxygen gas line and replacing it with nitrogen gas flow for about 15 min. When the reactor finally cools down to about 30 °C, the reactor was opened and the Pt/Si-wafer covered with a thin solid film of oxidation mixture

was removed from the reactor. The crude oxidation product was analysed using ^{1}H NMR spectroscopy. Same oxidation products were identified as described above in section 4.6.1.

4.8 Hydrogenation Over Flat Model Pt/Si-wafer Catalysts

4.8.1 Hydrogenation of 1-Cyclohexene

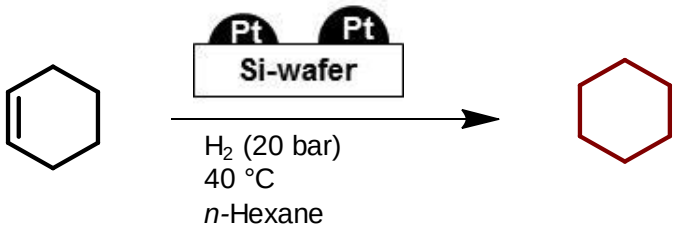

Scheme 4.10. (a) The hydrogenation of cyclohexene over surface **14**, a model Pt/SiO_2/Si-wafer catalyst with 11 Pt atoms/nm^2, to form cyclohexane.

A platinised Si wafer (21 x 23 mm^2) was placed in a 25 mL Parr Reactor. The reactor was flushed with nitrogen and finally sealed under hydrogen pressure (10 bar) and heated to 150 °C. After 12 h, the reactor temperature was decreased to room temperature and evacuated while flushing with nitrogen. The Pt/Si-wafer was covered by a solution of 1-cyclohexene (0.5 mL) in n-hexane (2.5 mL). The reactor was sealed under hydrogen pressure (19.8 bar) followed by temperature increase to 40 °C and allowed to stand for 12 h while stirring the H_2 gas at 300 rpm.[i] The same experiment was repeated and prolonged for 3 days. The reaction conditions were subsequently decreased to ambient temperature and pressure (see Scheme 4.10 for the reaction scheme). The crude reaction products were analysed by NMR. Based on ^{1}H NMR data, conversion = 40 %.

^{1}H NMR of cyclohexane: δ_H (300 MHz, $CDCl_3$), ppm: 1.43 (12H, s, CH_2).

[i] The stirring only affected the H_2 gas and the cyclohexane solution in the reactor was not stirred.

4.8.2 Hydrogenation of Benzaldehyde

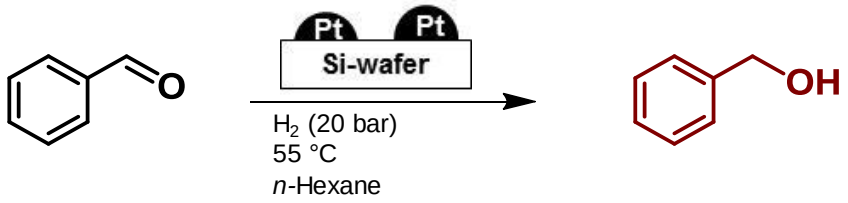

Scheme 4.11. The hydrogenation of benzaldehyde over surface **14**, a model Pt/SiO_2/Si-wafer catalyst 11 Pt atoms/nm^2, to form benzyl alcohol.

A platinised Si wafer (21 x 23 mm^2) was placed in a 25 mL Parr Reactor. The reactor was flushed with nitrogen and finally sealed under hydrogen pressure (10 bar) and heated to 150 °C. After 12 h, the reactor temperature was decreased to room temperature and evacuated while flushing with nitrogen. The Pt/Si wafer was covered by a solution of benzyldehyde (0.1 mL, 1.1 mg) in n-hexane (0.5 mL). The reactor was sealed under hydrogen pressure (20 bar) followed by temperature increase to 55 °C and allowed to stand for 10 h while stirring the H_2 gas at 300 rpm. The reaction conditions were subsequently decreased to ambient temperature and pressure. To obtain a crude product, the solvent was evaporated at room temperature (90 mg of the crude product was collected). The reaction products were analysed by NMR spectroscopy. Based on ^{1}H NMR data, benzaldehyde conversion was 70 %.

^{1}H NMR of benzyl alcohol: δ_H (300 MHz, $CDCl_3$, Appendix 5), ppm: 4.71 (2H, s, CH_2), 7.37 (5H, m, ArH).

4.8.3 Hydrogenation of Cinnamaldehyde

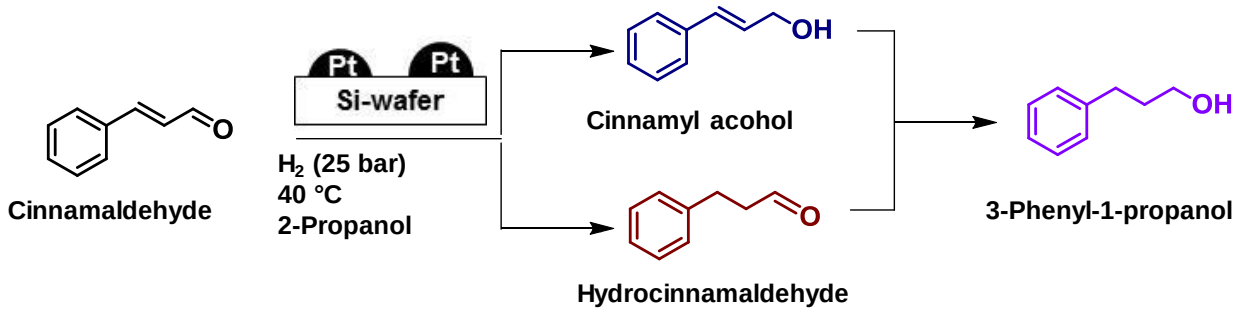

Scheme 4.12. An outline of the hydrogenation of cinnamaldehyde solution in 2-propanol to form cinnamyl alcohol, hydrocinnamaldehyde and 3-phenyl-1-propanol over surface **14**, a model Pt/SiO_2/Si-wafer catalyst with 11 Pt atoms/nm^2.

Method A: A 50 v/v% cinnamaldehyde solution in 2-propanol was prepared. The prepared cinnamaldehyde solution (0.45 mL) was mixed with 80 µL of 2-propanol to achieve 3.2 M cinnamaldehyde solution. A Pt/SiO_2/Si-wafer model catalyst (20 mm x 20 mm) was placed in a 25 mL Parr Reactor and covered with a 40 µL of cinnamaldehyde solution. The reactor was flushed with nitrogen for 2 min. The reactor was then filled with hydrogen (10 bar) followed by releasing the pressure to *ca*. 1 bar. The sequence of filling and releasing H_2 in the reactor was done 3 times. The reactor was finally sealed under hydrogen pressure (25 bar) and heated to 40 °C while stirring the H_2 gas at 300 rpm. After 24 h, the reactor temperature was decreased to room temperature and then evacuated (see Scheme 4.12 for the reaction). The crude hydrogenation products were analysed by NMR spectroscopy and the overhead gas products were analysed by mass spectroscopy (MS). Based on ^{1}H NMR data, the cinnamaldehyde conversion was 60 %.

Method B: A 50 v/v% cinnamaldehyde solution in 2-propanol was prepared. The prepared cinnamaldehyde solution (0.45 mL) was mixed with 80 µL solution of NaOH or $NaHCO_3$ (24 mM in distilled water) to achieve a final concentration of 3.2 M cinnamaldehyde solution. The final concentration of the base in the reaction solution was 4 mM. The subsequent steps described in

Method A were then followed until the end of the reaction. Based on ^{1}H NMR data, the cinnamaldehyde conversion was 59 % in the presence of $NaHCO_3$ and 100 % in the presence of NaOH.

In order to follow the product formation over time in the presence of 4 mM NaOH solution, the Pt/SiO_2/Si-wafer catalysts that were cut from the same big piece of Pt/SiO_2/Si-wafer were used. The same sized Pt/SiO_2/Si-wafer catalysts stored under nitrogen were used independently in hydrogenation as described in *Method B.* The reactions were performed over different reaction times of 6 h, 8 h, 12 h and 24 h. The substrate conversions and product selectivity base on ^{1}H NMR data of the crude hydrogenation product mixture were plotted as a function of reaction time.

^{1}H NMR of cinnamyl alcohol: δ_H (300 MHz, $CDCl_3$, Figure 3.28), ppm: 4.34 (2H, dd, J_{HH} = 1.46 Hz, J_{HH} = 5.66 Hz, CH_2), 6.38 (1H, dt, J_{HH} = 5.66 Hz, J_{HH} = 15.87 Hz, CH), 6.6 (1H, m, J_{HH} = 16.01 Hz, CH), 7.3 (5H, m, ArH).

^{1}H NMR of hydrocinnamaldehyde: δ_H (300 MHz, $CDCl_3$, Figure 3.28), ppm: 2.79 (2H, t, J_{HH} = Hz, CH_2), 2.97 (2H, t, J_{HH} = Hz, CH_2), 7.3 (5H, m, ArH) 9.83 (1H, t, J_{HH} = 1.35 Hz, CHO).

^{1}H NMR of 3-Phenyl-1-propanol: δ_H (300 MHz, $CDCl_3$, Figure 3.28), ppm: 1.93 (2H, m, CH_2), 2.72 (2H, t, J_{HH} = 6.43 Hz, CH_2), 3.69 (2H, t, J_{HH} = 7.50 Hz, CH_2), 7.3 (5H, m, ArH).

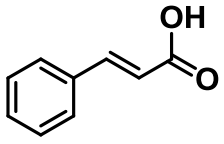

Cinnamic acid

^{1}H NMR of Cinnamic acid: ^{1}H NMR: δ_H (300 MHz, $CDCl_3$, Figure 3.28), ppm: 6.48 (1H, d, J_{HH} = 16.00 Hz, -CH=CH-), 7.50 (5H, m, ArH), 7.81 (1H, d, J_{HH} = 16.00 Hz, -CH=CH-).

MS of the gas sample: *m/z* (Appendix 10): 2 (H_2), 18 (H_2O), 44 (Propane).

4.9 Preparation of Platinum Catalysts Supported on Zeolites

Pt catalysts on zeolite supports were prepared by incipient wetness impregnation and vapour phase impregnation. Before use in catalyst preparation, the zeolite supports were heated slowly (2 °C/min) in calcination oven to 400 °C under a gently stream of nitrogen. After 5 h, the temperature was reduced to room temperature and the zeolite supports were transferred and stored in the glove box under inert atmosphere of nitrogen.

4.10 Incipient Wetness Impregnation of Zeolite Supports

The Pt/KL-zeolite and Pt/HY-zeolite were prepared by incipient wetness impregnation on either the alkaline KL-zeolite or acidic HY-zeolite.

4.11 Preparation of Pt/KL-zeolite by Incipient Wetness Impregnation

The freshly calcined KL-zeolite support was impregnated drop-wise with an aqueous solution of tetraammineplatinum(II)nitrate $Pt(NH_3)_4(NO_3)_2$. The adequate Pt loading into the zeolite support (KL-zeolite of HY-zeolite) was determined from the content of Pt in $Pt(NH_3)_4(NO_3)_2$ salt. For example, to load 0.88 wt% Pt on 19.8 g of KL-zeolite support, a solution of 400 mg $Pt(NH_3)_4(NO_3)_2$ in 12 mL distilled water was added to the support with constant stirring. A liquid/solid ratio of about 0.6 mL/g gave suitable incipient wetness for KL zeolite. The amount of liquid to be used in solution was predetermine by adding drop-wise distilled water to the zeolite of known mass until the mixture form a wet solid paste with no flowing water. The freshly impregnated crude catalyst samples were left to stand at room temperature for 12 h to slowly evaporate the solvent followed by the complete solvent evaporation at 110 $^{\circ}$C for 12 h. The catalyst samples were then calcined in the oven by heating slowly at 0.8 °C/min to 300 °C in ambient air. After 5 h at 300 °C, the oven was cooled down to room temperature. The calcined Pt/zeolite catalysts were analysed by ICP for Pt content.

ICP-OES of Pt/KL-zeolite: 1.0 % Pt content.

4.12 Preparation of Pt/HY-zeolite by Incipient Wetness Impregnation

The Pt salt solution was prepared by dissolving 20 mg of tetraammineplatinum(II)nitrate $Pt(NH_3)_4(NO_3)_2$ in 2.1 mL distilled water. The resultant solution was added drop-wise to 990 mg HY-zeolite while stirring to form a wet solid paste. The final mixture was left standing for 12 h at room temperature. When the solvent had evaporated, the impregnated material was dried at 110 °C for 12 h. The subsequent steps were carried out as described in the preparation of Pt/KL-zeolite.

ICP-OES of Pt/HY-zeolite: 0.9 % Pt content.

4.13 Vapour Phase Impregnation (VPI) on Zeolite Supports

The VPI procedure was done as outlined by Jacobs *et al.*[2] A freshly calcined zeolite support was mixed with neat platinum acetylacetonate $Pt(acac)_2$[ii] in a two neck round-bottomed flask with a tap on one neck, under inert atmosphere. The flask was sealed and the solid mixture was mixed by stirring with the magnetic stirrer. The neck with the tap was connected to the vacuum line and the volatiles in the zeolite pores were evacuated using a vacuum pump to 0.07 mbar for 24 h. The solid mixture in the sealed flask was then placed in the pre-heated oil at 80 °C and kept at this temperature for 1 h while stirring to remove volatile impurities. The flask was removed and immediately placed under vacuum for 15 min. The flask was subsequently sealed and placed in pre-heated heating oil at 100 °C for 1 h. The temperature of the heating oil was finally increased to 130 °C and the reaction flask was kept at this temperature for 30 min. After cooling to *ca.*25 °C, the impregnated zeolite was calcined as described previously.

[ii] $Pt(acac)_2$ decompose after melting at 240 °C, therefore this experiment was done at reduced pressure (0.07 bar) at 130 °C to sublime the $Pt(acac)_2$ into zeolite pores.

ICP-OES of Pt/KL-zeolite: 0.94 % Pt content.

4.14 Aromatisation Experiments

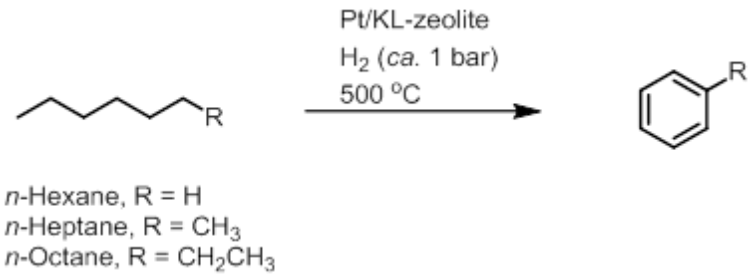

Scheme 4.13. Outline of the aromatisation of *n*-alkanes to corresponding aromatics.

The catalysts used in aromatisation reactions were 0.9% Pt/KL-zeolite prepared by vapour phase impregnation or 1.0% Pt/KL-zeolite prepared by incipient wetness impregnation. The experimental conditions varied on feed rate and hydrogen feed depending on the weight hourly space velocity (WHSV) and the molar ratio of hydrogen: *n*-alkane used. To simplify the procedure, details on experimental conditions WHSV = 5 h^{-1} and hydrogen: *n*-hexane molar ratio = 6 are given.

4.15 Reactor Set-up and Catalytic Procedure

The aromatisation of *n*-alkanes to corresponding aromatics was done in a down-flow continuous reactor packed with a fixed-bed of Pt/KL-zeolite catalyst. The reactor was a stainless steel tube with internal diameter of 12 mm and 40 mL total volume. The reactor was designed in such a way that there is a thermocouple well running through the middle of the reactor. Before packing the reactor, the feed line to the reactor and the product lines to the sample vessel were rinse with the *n*-alkane (*ca.*50 mL) to be used in the next experiment followed by flushing with nitrogen for 20 min. The catalyst (1.5 g) was packed on the pre-determine hottest spot in the reactor between two beds of inert carborundum (SiC). The catalyst bed was separated from the inert material by a thin layer of quartz wool. The packed catalyst was activated by heating the catalyst to 500 ℃ at

1 °C/min while flowing hydrogen at 4 L/h. The catalyst was kept under these conditions for 4 h thereafter; the hydrogen flow was increased to experimental conditions (12 L/h) using a mass flow controller. During this period the hydrogen pressure after the mass flow controller was monitored by the pressure indicator which was at ambient pressure (*ca.* 1 atm). The experiment was initiated by feeding *n*-hexane from HPLC pump at 0.25 mL/min and the reactor was kept at 500 °C and ambient pressure. The aromatisation product from the reactor was collected periodically in the liquid sample vessel at -5 °C and the gas samples were collected after the chilled liquid sample vessel. The rest of the gas coming out of the reactor was measured in the wet gas flow before the vent line. The outline of the reactor set-up used in this experiment is presented in Figure 4.3.

For experiments where *n*-hexane feed was spiked with catalysts poisons, acetic acid, propanaldehyde or thiophene, the feed was prepared separately to achieve the desired concentration of the catalyst poison followed by the procedure as described above. Similarly, other *n*-alkane feeds were used using the described procedure. For experiments with WHSV = 2.5 h^{-1} and hydrogen: *n*-hexane molar ratio = 6, the feed rate was reduced to 1.3 mL/min and the hydrogen flow was reduced to 6 L/h.

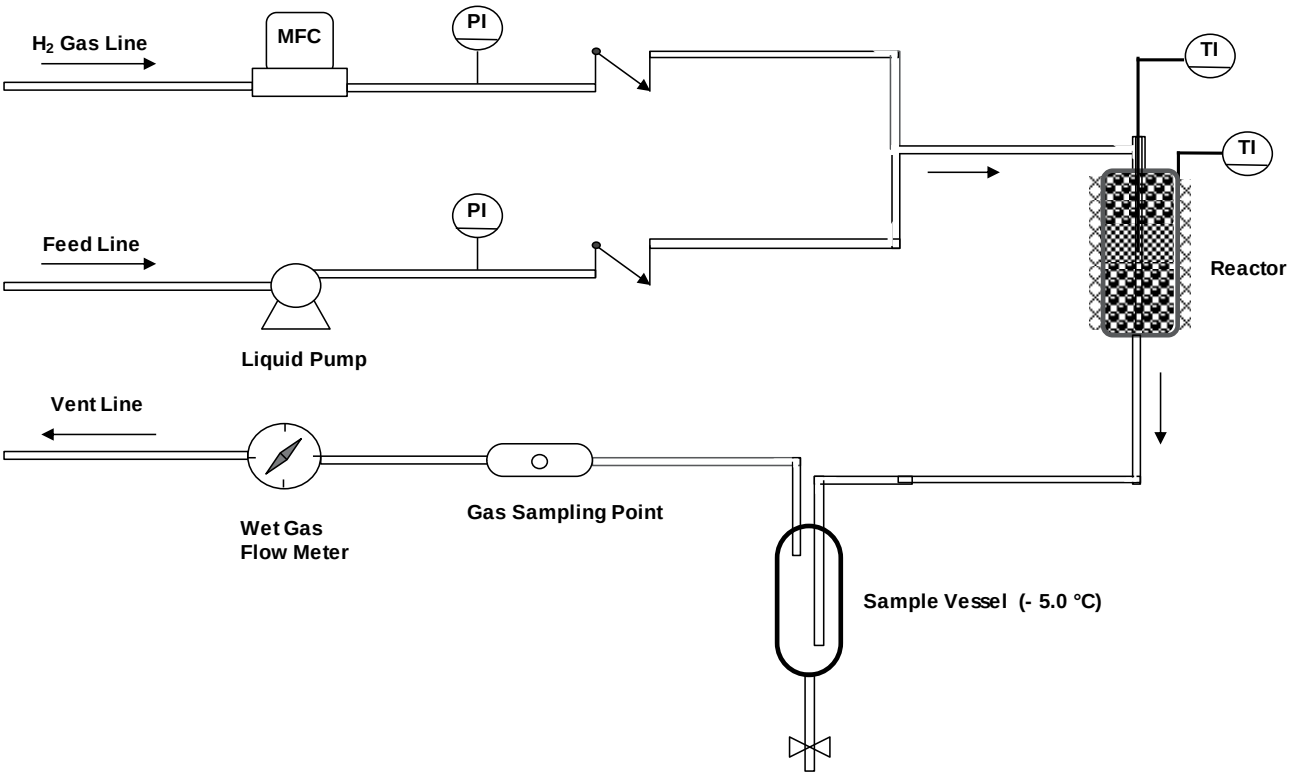

Figure 4.3. The outline of the reactor set-up used in aromatisation of *n*-alkanes over Pt/KL-zeolite catalysts. MFC = Mass Flow Controller, PI = Pressure indicator, TI = temperature indicator.

4.16 Analytical Methods

The liquid products from the chilled product vessel were analysed in a 6850 Agilent series gas chromatography (GC) equipped with flame ionisation detector (FID) and capillary column (HP-PONA Methyl Siloxane, 50 m x 200 μm x 0.5 μm, Agilent). The automated oven temperature program for the GC analysis was as follows: 30 °C (5 min hold), 30 to 280 °C (ramp rate = 5 °C/min) and 280 °C (5 min hold). The concentration of the liquid reactants and the products was determined using freshly distilled pure *n*-heptane or *n*-nonane as an internal standard (see Appendix 12).[3] The gas products were analysed in a separate gas chromatography, Agilent 6850 series gas chromatography equipped with FID and capillary column (PLOT Alumina KCL 40 m x 530 μm x 10.0 μm). The automated oven temperature program for the GC analysis was as follows: 70 °C (5

min hold), 70 to 180 °C (ramp rate = 8 °C/min) and 180 °C (10 min hold). The concentrations of the gaseous products in the off gas and liquid products collected in the chilled product vessel were used to determine the substrate conversion (wt%), product selectivity (wt%) and product yields (mol%) using the following equations as outlined in reference [4]:

$$\text{Substrate conversion} = \left[\frac{(\text{Weight of alkane in the feed}) - (\text{Weight of alkane out})}{\text{Weight of alkane in the feed}}\right] x100 \quad \textbf{4.1}$$

$$\text{Product Selectivity} = \left[\frac{\text{Weight of the desired product}}{(\text{Weight of alkane in the feed}) - (\text{Weight of alkane in the products})}\right] x100 \quad \textbf{4.2}$$

$$\text{Product Yield} = \left[\frac{\text{Moles of product}}{\text{Moles of alkane in}}\right] x100 \quad \textbf{4.3}$$

Here, alkane in = *n*-alkane in the feed, alkane out = unreacted *n*-alkane collected in the product vessel.

4.17 Oxidation of Alcohols in Aqueous Medium Over Pt/zeolite catalysts

4.17.1 Oxidation of Benzyl Alcohol

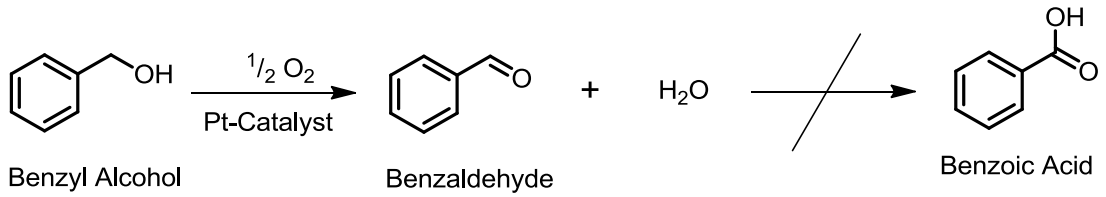

Scheme 4.14. Reaction scheme for the Pt catalysed oxidative dehydrogenation of benzyl alcohol to benzaldehyde and water.

Method A, oxidation in aqueous medium: A solution of benzyl alcohol (1.0 g, 0.92 mmol) in distilled water (10 mL) was prepared in 250 mL 3-neck round bottomed flask coupled with the condenser. 1% Pt/KL-zeolite catalyst (500 mg) was mixed with the benzyl alcohol solution. The reaction contents were heated to reflux at *ca*. 100 °C while stirring with the magnetic stirrer and bubbling molecular oxygen in the reaction mixture. After 24 h, the temperature was cooled down to *ca*. 25 °C and the molecular oxygen tap turn off (see Scheme 4.14 for the reaction scheme). The crude product was extracted with pentane followed by ATR FTIR and ^{1}H NMR analysis and compared with authentic samples. Based on the ^{1}H NMR analysis, benzyl alcohol conversion was 24 %.

Method B, oxidation in organic medium: A solution of benzyl alcohol (1.0 g, 0.92 mmol) in toluene or dry heptane (10 mL) was prepared in 250 mL 3-neck round bottomed flask coupled with the condenser. The subsequent steps are the same as described in Method A. Based on the ^{1}H NMR analysis, benzyl alcohol conversion was 7 %.

^{1}H NMR of benzyldehyde: δ_H (300 MHz, $CDCl_3$, Appendix 6), ppm: 7.55-7.91 (5H, m, ArH), 10.03 (1H, s, CHO).

FTIR of benzaldehyde: ν_{max} (Appendix 9), cm-^{1}: 1699 (C=O).

4.17.2 Oxidation of 1-octanol

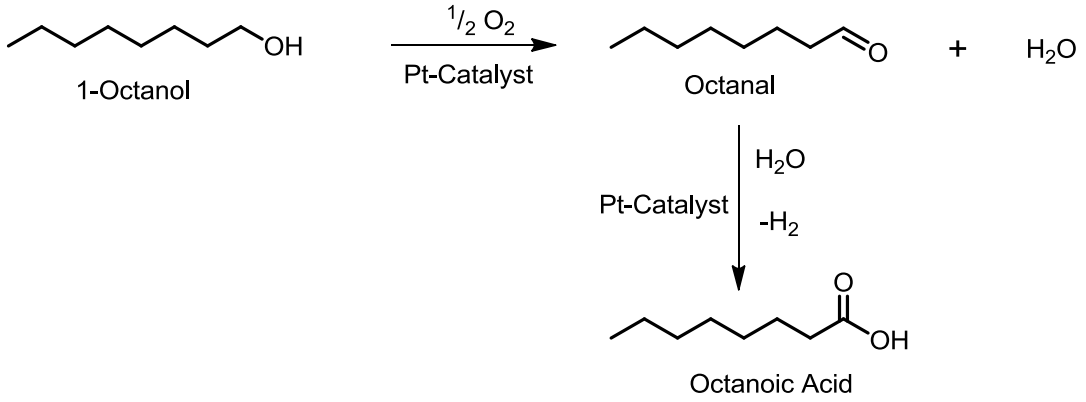

Scheme 4. 15. Reaction scheme for the Pt catalysed oxidation of 1-octanol.

Method A, Method Oxidation in aqueous medium: In a typical 1-octanol oxidation, a solution of 1-octanol (1.0 g, 7.7 mmol) in distilled water (10 mL) was prepared in 250 mL 3-neck round bottomed flask coupled with the condenser. 1% Pt/KL-zeolite catalyst (500 mg) was mixed with the 1-octanol solution. The reaction contents were heated to reflux at *ca*. 100 °C while stirring with the magnetic stirrer and bubbling molecular oxygen in the reaction mixture. After 32 h, the temperature was cooled down to *ca*. 25 °C and the molecular oxygen tap turn off (see Scheme 4. 15 for the reaction scheme). The crude product was extracted with pentane followed by ATR FTIR and ^{1}H NMR analysis and compared with authentic samples. The substrate conversion and product selectivity were determined using ^{1}H NMR analysis with internal standard 1,1,2,2-tetrachloroethane. Based on the ^{1}H NMR analysis, 1-octanol conversion was 40 %.

Method B, Oxidation in the presence of a base: A solution of 1-octanol (1.0 g, 7.7 mmol) in distilled water (10 mL) was prepared in 250 mL 3-neck round bottomed flask coupled with the condenser, then K_2CO_3 (1.06 g, 7.8 mmol) was dissolved in the alcohol solution. The subsequent steps are the same as described in Method A. Based on the ^{1}H NMR analysis, 1-octanol conversion was 10 % after 24 h reaction.

Method B, Oxidation in organic medium: a solution of 1-octanol (1.0 g, 7.7 mmol) in dry toluene or heptane (10 mL) was prepared in 250 mL 3-neck round bottomed flask coupled with the condenser. The subsequent steps are the same as describe in Method A. Based on the ^{1}H NMR analysis, 1-octanol conversion was 10.2 % after 24 h reaction.

^{1}H NMR of octanal: δ_H (300 MHz, $CDCl_3$, Appendix 7), ppm: 0.88 (3H, t, J_{HH} = 6.54 Hz, CH_3), 1.20-1.70 (12H, m, 6xCH_2), 2.42 (2H, dt, J_{HH} = 1.87 Hz, J_{HH} = 7.43 Hz, CH_2), 10.03 (1H, t, J_{HH} = 1.88 Hz, CHO).

^{1}H NMR of octanoic acid: δ_H (300 MHz, $CDCl_3$, Appendix 7), ppm: 0.88 (3H, t, J_{HH} = 6.54 Hz, CH_3), 1.20-1.70 (12H, m, 6xCH_2), 2.32 (2H, t, J_{HH} = 7.38 Hz, CH_2).

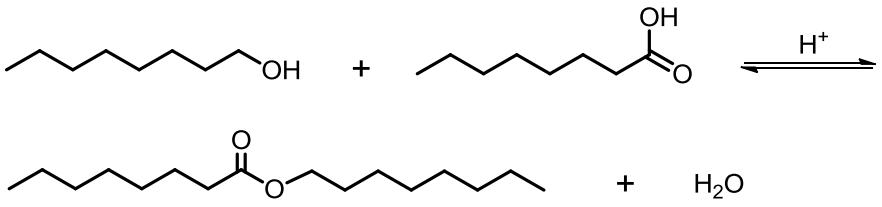

^{1}H NMR of octyl octanoate: δ_H (300 MHz, $CDCl_3$, Appendix7), ppm: 0.88 (6H, t, J_{HH} = 6.54 Hz, 2xCH_3), 1.20-1.70 (22H, m, 11xCH_2), 2.30 (2H, t, J_{HH} = 7.44 Hz, CH_2), 4.07 (2H, t, J_{HH} = 6.70 Hz, CH_2).

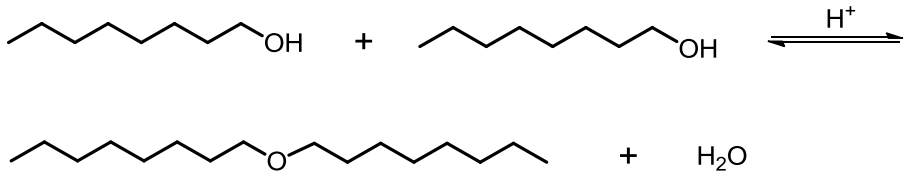

[1]H NMR of dioctyl ether: δ_H (300 MHz, $CDCl_3$, Appendix 8), ppm: 0.88 (6H, t, J_{HH} = 6.54 Hz, 2xCH_3), 1.20-1.70 (24H, m, 12xCH_2), 3.43 (2H, t, J_{HH} = 6.87 Hz, CH_2).

4.18 References

[1] F. Moulder, W.F. Stickle, P.E. Sobol, K.D. Bomben, In *Handbook of X-ray Photo- 367 electron Spectroscopy*, ULVAC-PHI, Inc., 370 Enzo, Chigasaki 253-8522, Japan, 368 **1995**, pp. 45, 57, 143.

[2] G. Jacobs, F. Ghadiali, A. Pisanu, A. Borgna, W. E. Alvarez, D. Resasco, *Appl. Catal. A.* **1999**, *188*, 79-98.

[3] S. Ito, In *Analysis of aromatic hydrocarbons in gasoline and naphtha with Agilent 6820 series gas chromatography and a single polar capillary column*, Agilent Inc. **2003**, p. 1-15.

[4] M. Yin, R. H. Natelson, A. A. Campos, P. Kolar, W. L. Roberts, *Fuels.* **2013**, *103*, 408-413.

5. Conclusions and Future Perspectives

5.1 Conclusions

This chapter describes the outputs achieved to fulfil the objectives set as goals 1-7 at the beginning of the study.

To achieve goal 1 of this study (chapter 1), two-dimensional (2-D), Si-wafer supports were reacted to have a silanol (Si-OH) surface. The silanol groups were then successfully reacted with allyltrimethoxysilane and 3-aminopropyltrimethoxysilane to generate an allyl or an amino surface. These two surfaces both allowed platinisation with Pt^{2+} and Pt^{4+} precursors. The immobilised surface allyl derivatives reacted with H_2PtCl_6 to form a Pt^{2+} complex as the dominant surface species. Metallic Pt/SiO_2/Si-wafer catalysts were then obtained by calcination followed by H_2 reduction to form metallic Pt particles on the wafer surface. Flat model Pt/SiO_2/Si-wafer catalysts prepared by grafting had smaller Pt particles (< 1 nm particle diameter) while model catalysts prepared by spin coating had larger particle sizes (3.0 nm average diameter). It was concluded that the surface allyl and silanol coordination sites influence the formation of small Pt particles in grafting more than the spin coating method. The grafted Pt species are less susceptible to agglomeration and sintering during calcination.

In contrast, platinisation of the allyl or amino surfaces with K_2PtCl_4 (rather than H_2PtCl_6) in aqueous ethanol resulted in a mixture of metallic Pt particles and Pt^{2+} species immobilised on the surface of flat model Si-wafer support without the additional calcination and reduction step. The Pt(II) precursor and the dispersed colloidal Pt particles which are formed during platinisation K_2PtCl_4 interact with immobilised surface amino groups to form a Pt-N bond with XPS binding of N 1s core electrons energy at 397.8 eV. The adsorbed Pt particles are evenly distributed and has particle diameter in the range of 1.5 - 4.0 nm. Calcination to remove the immobilised amino ligands

led to the sintering and agglomeration of the adsorbed Pt particles. This caused a slight increase in average particle diameter to 2.5 - 5.0 nm.

To achieve goal 2 of this study, the freshly prepared flat model Pt/SiO_2/Si-wafer catalysts with particle diameter within the range of 1.5 - 5 nm were investigated for any catalytic activity in solvent free aerobic oxidation of 1-octadecanol to octadecanoic acid at 105 °C in ambient air. Oxidation over the Pt/SiO_2/Si-wafer catalysts (prepared by direct grafting of dispersed colloidal Pt particles on amino surfaces followed by calcination and H_2 reduction) was monitored *ex situ* using FTIR and ^{1}H NMR spectroscopies. The rate of substrate depletion obtained by FTIR and ^{1}H NMR measurements was 3.8(4) x 10^{-5} s^{-1} and 6(1) x 10^{-5} s^{-1} respectively; these values are mutually consistent. The catalyst exhibited a turnover frequency (TOF) of 2.2 s^{-1} in the oxidation of 1-octadecanol in ambient air, based on the ^{1}H NMR data. The observed TOF increased to 6.1 s^{-1} when the oxidation is performed in the presence of molecular oxygen in ambient pressure at 105 °C. Application of model Pt/SiO_2/Si-wafer catalysts prepared by spin coating of H_2PtCl_6 on allyl surfaces in the oxidation of 1-octadecanol in ambient air resulted in an induction period of about 10 h before the formation of oxidation products was observed. The factors contributing to the observed induction period were not investigated in this study.

Only Pt/SiO_2/Si-wafer catalysts prepared by grafting of dispersed colloidal Pt particles on amino surface showed activity in the hydrogenation reactions at 40 °C to 55 °C and 20 bar to 25 bar. The catalyst TOF for the hydrogenation of benzaldehyde to benzyl alcohol was 7.5 s^{-1} while the catalyst TOF in more complex substrate, cinnamaldehyde was 3.3 s^{-1}. The application of the prepared flat model Pt/SiO_2/Si-wafer catalysts in catalytic oxidation and hydrogenation validated these catalysts as realistic model catalysts and fulfilled goal 2 of this study.

In addition to the model Pt catalysts prepared on 2-D Si-wafers, Pt catalysts supported on 3-D supports specifically KL-zeolites and HY-zeolites were successfully prepared *via* incipient wetness

impregnation and vapour phase impregnation. The Pt/KL-zeolite catalysts prepared by vapour phase impregnation had high particle dispersion (91.5 % *vs.* 75.8 %) and smaller particles sizes (average diameter = 1.2 nm *vs.*1.5 nm) compared to the Pt/KL-zeolite catalysts obtained by incipient wetness impregnation. The Pt/KL-zeolite catalysts remained porous with micropore volume of 0.06 cm^3/g to 0.08 cm^3/g which is close to the micropore volume of the support (0.10 cm^3/g) even after calcination at 350 °C. The Pt/HY-zeolite catalysts had a particle dispersion of 92.0 % and a particle mean diameter of 1.2 nm even though they were only prepared by incipient wetness impregnation. The reducibility of the prepared Pt/zeolite catalysts to form supported metallic Pt at 400 °C in H_2 was confirmed by the presence of an XPS Pt $4f_{7/2}$ peak in the XPS spectral region of 70.7 eV to 71.5 eV which can be attributed to the Pt^0 contribution.

The prepare 1% Pt/KL-zeolite catalysts showed activity in gas phase aromatisation of *n*-hexane, *n*-heptane and *n*-octane. The Pt/KL-zeolite catalyst prepared by vapour phase impregnation (Pt/KL-zeolite VPI) showed about 5% more activity in aromatisation of *n*-hexane than the Pt/KL-zeolite catalyst prepared by incipient wetness impregnation (Pt/KL-zeolite IWI). The presence of oxygenates or sulphur compounds decreased the catalytic activity of the catalysts based on *n*-alkane conversion and selectivity to aromatics. In the presence of 0.1 wt% acetic acid in *n*-hexane feed, the conversion over Pt/KL-zeolite VPI catalysts decreased by 6.9 % after 20 h. When Pt/KL-zeolite IWI catalyst was used, the difference between the initial *n*-hexane conversion at 10 h and the conversion at 20 h was 18 %. In the presence of 0.5 wt% acetic acid in the feed, the *n*-hexane conversion over Pt/KL-zeolite VPI catalyst decreased by 16 % and the amount of hydrocarbon products with C_1 to C_5 chain length increased (9.8% to 10.7%). Formation of hexenes also increased (2.4% to 3.8%).

After regeneration of the spent Pt/KL-zeolite VPI catalysts by oxidative combustion of the deposited coke at 500 °C, the original surface area and micropore volume were retained. At the same

time the crystallite sizes of supported Pt increased in mean diameter to *ca.* 2.7 nm and thus particle dispersion decreased to 41%. The effect of crystallite size increase on catalytic aromatisation and the activity of regenerated catalysts were not determined.

Analysis of the spent Pt/KL-zeolite catalysts showed a correlation between the amount of coke accumulated on the spent catalyst and the presence of acetic acid in the *n*-alkane feed stream. In the presence of acetic acid in the feed stream, the amount of coke deposits increased and consequently decreased the catalytic conversion of *n*-alkane. At a low weight hourly space velocity (WHSV) of 2.5 h^{-1} and low H_2:*n*-hexane molar ratio = 2.5, the presence of 1 wt% acetic acid in the feed stream resulted in *ca.* 6 % coke deposits on the spent Pt/KL-zeolite IWI catalyst relative to *ca.* 3 % coke deposits when neat *n*-hexane is used. The *n*-hexane conversion decreased from 70 % in neat *n*-hexane feed to 20 % in the presence of 1 wt% acetic acid. In aromatisation of neat *n*-hexane at high WHSV (5 h^{-1}) and high H_2:*n*-hexane molar ratio = 6 over Pt/KL-zeolite VPI catalysts, the amount of deposited coke was 0.5 % on spent catalyst after 20 h on stream. The amount of coke deposits increased to 3 % in the presence of 0.5 wt% acetic acid in *n*-hexane feed. The increase in coke deposits on spent catalysts had a detrimental effect on *n*-hexane conversion which was reduced from 70 % to 57 %. The observed correlations in coke deposits and *n*-hexane conversion fulfilled goal 5 set in chapter 1.

The 1% Pt/KL-zeolite and 1% Pt/HY-zeolite catalysts prepared by incipient wetness impregnation were applied in liquid phase oxidation of 1-octanol. The highest alcohol conversion of 40 % was achieved when 1.2 M aqueous alcohol was oxidised over Pt/KL-zeolite catalyst at 100 °C in the presence of molecular oxygen. The selectivity to the oxidation products octanoic acid and octanal was 70 % and 11 % respectively. Oxidation over 1% Pt/HY-zeolite catalyst achieved only 10 % 1-octanol conversion to form octanal and octanoic acid in 27.5 % and 24.0 % selectivity. In the presence of 1% Pt/HY-zeolite catalyst, the major product is dioctyl ether (48.5 % selectivity) which is formed by acid catalysed etherification. It was concluded that the porosity of the prepared

Pt/zeolite catalysts might not be suitable for the liquid phase reactions as could be seen by poor activity in catalytic oxidations.

5.2 Future Perspectives

The study of 2-D model Pt/SiO_2/Si-wafer catalysts provided valuable outcomes that can be applied in preparation of Pt catalysts on 3-D powder support. Through model Pt/SiO_2/Si-wafer catalysts, it was shown that the dispersed colloidal Pt particles can be directly immobilised on the surface of the support. This avoids the reduction step which is often carried out at high temperature and lead to sintering and agglomeration of metal particles. In future studies, porous zeolite supports may be used to immobilise the colloidal Pt particles using the same procedure designed in 2-D catalysts systems. These catalysts should be tested for catalytic activity parallel to the model Pt/SiO_2/Si-wafer catalysts.

In the oxidation of 1-octadecanol over Pt/SiO_2/Si-wafer prepared by spin coating of $H_2PtCl_6 \cdot 6H_2O$, an induction period of 10 h was observed. Future studies may explore the factors affecting the observed induction period and comparative studies in oxidation of other alcohols including poly alcohols such as glycerol.

The Pt/SiO_2/Si-wafer catalyst with average particle diameter of 2.5 nm displayed activity in hydrogenation of cinnamaldehyde. Hydrogenation of the alkene to hydrocinnamaldehyde was more favoured than hydrogenation of the carbonyl group to an alcohol. In future studies, the preparation of Pt/SiO_2/Si-wafer catalyst may be refined to form larger Pt particles (5– 12 nm). The catalysts with larger particles will probably be more suitable for selective hydrogenation of the carbonyl group.[1]

The Pt/KL-zeolite prepared by vapour phase impregnation exhibited activity in aromatisation of *n*-alkanes even in the presence of acetic acid. The lowest concentration of acetic acid spiked into the *n*-hexane feed was 0.1 wt% which decreased conversion by 7% only after 20 h. There is still a

need to determine the effect of lower concentrations of acetic acid and other oxygenates in the feed stream. Furthermore, the catalyst regeneration procedure used to remove the deposited coke on spent catalyst can easily be applied to regenerate loaded catalysts on line without adjusting the experimental temperature. However, due to the lack of time and limited access to suitable equipment, the activity of the regenerated Pt/KL-zeolite catalysts was not evaluated in this study. This leaves scope for future studies to devise catalyst regeneration procedures which will maintain the activity of the original catalyst and the evaluation of regenerated catalysts in aromatisation.

5.3 References

[1] P. Gallezot, D. Richard, *Catal. Rev. Sci. Eng.* **1998**, *40*, 81-126.

Appendices

Appendix 1. Reaction of $H_2PtCl_6 \cdot 6H_2O$ with 1,5-cyclooctadine

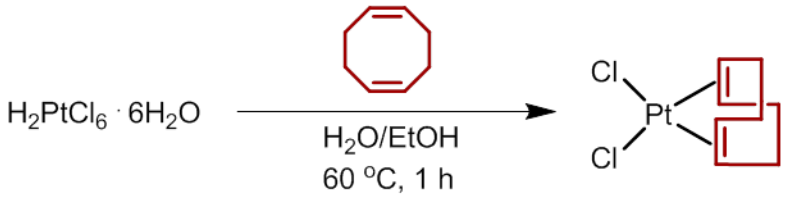

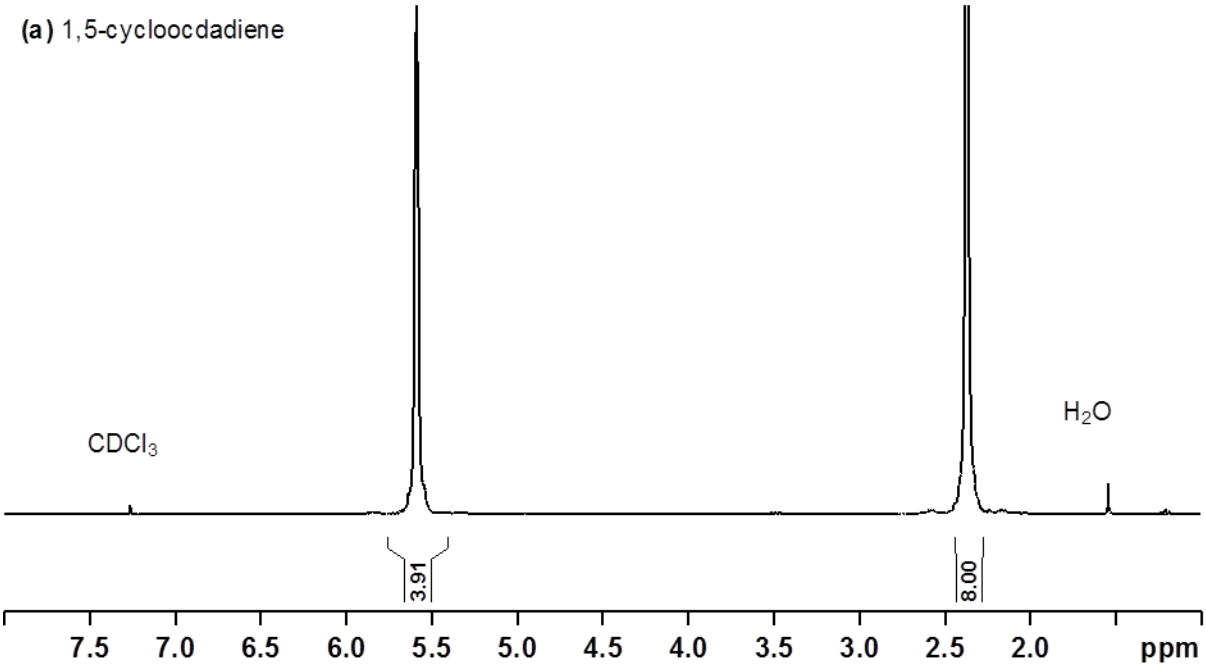

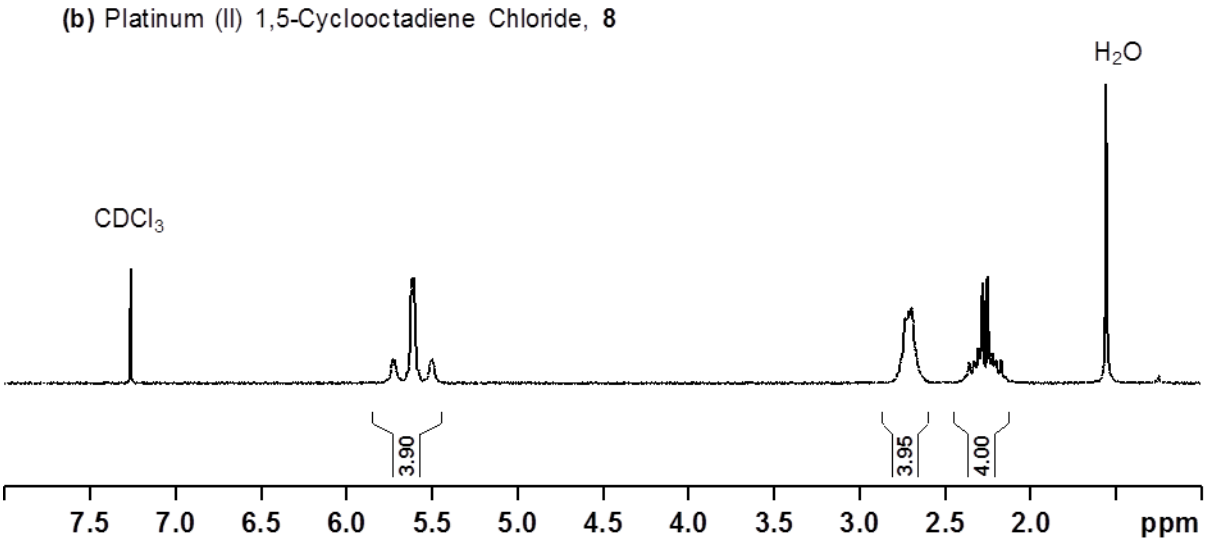

Appendix 2. ^{195}Pt NMR spectrum of Platinum(II) cyclooctadiene chloride

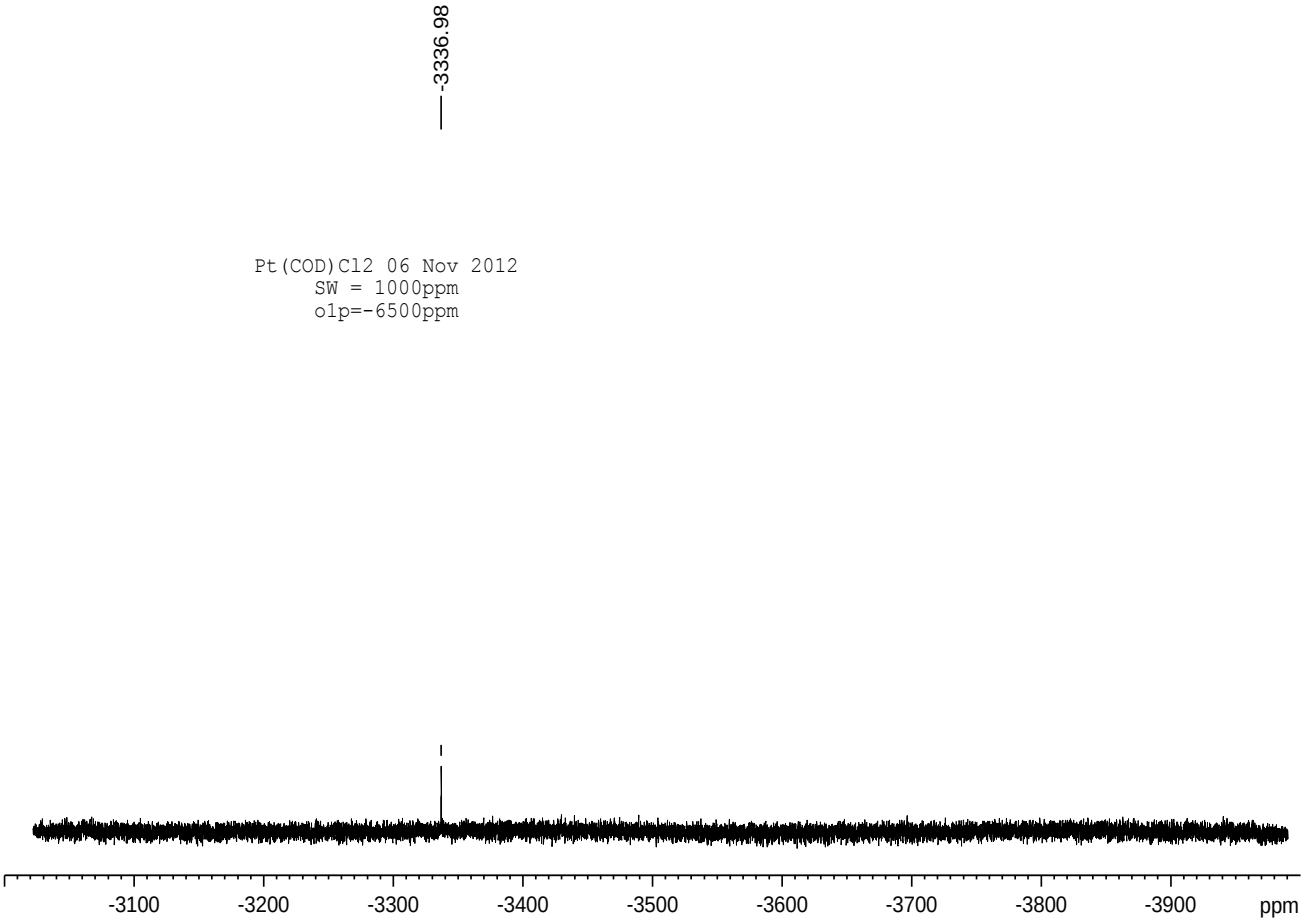

Appendix 3. Reaction of K_2PtCl_4 with 1-hexene

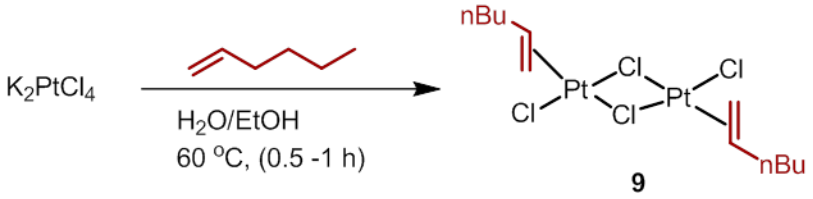

9

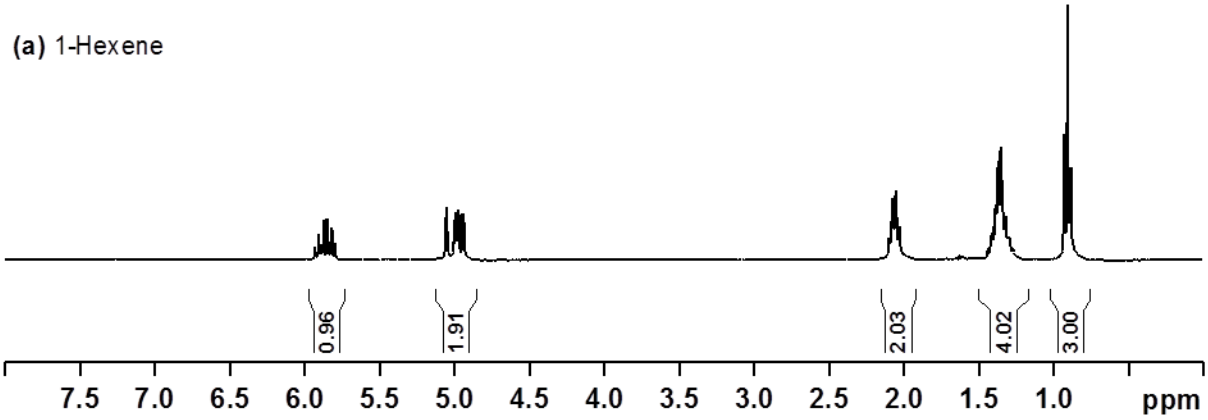

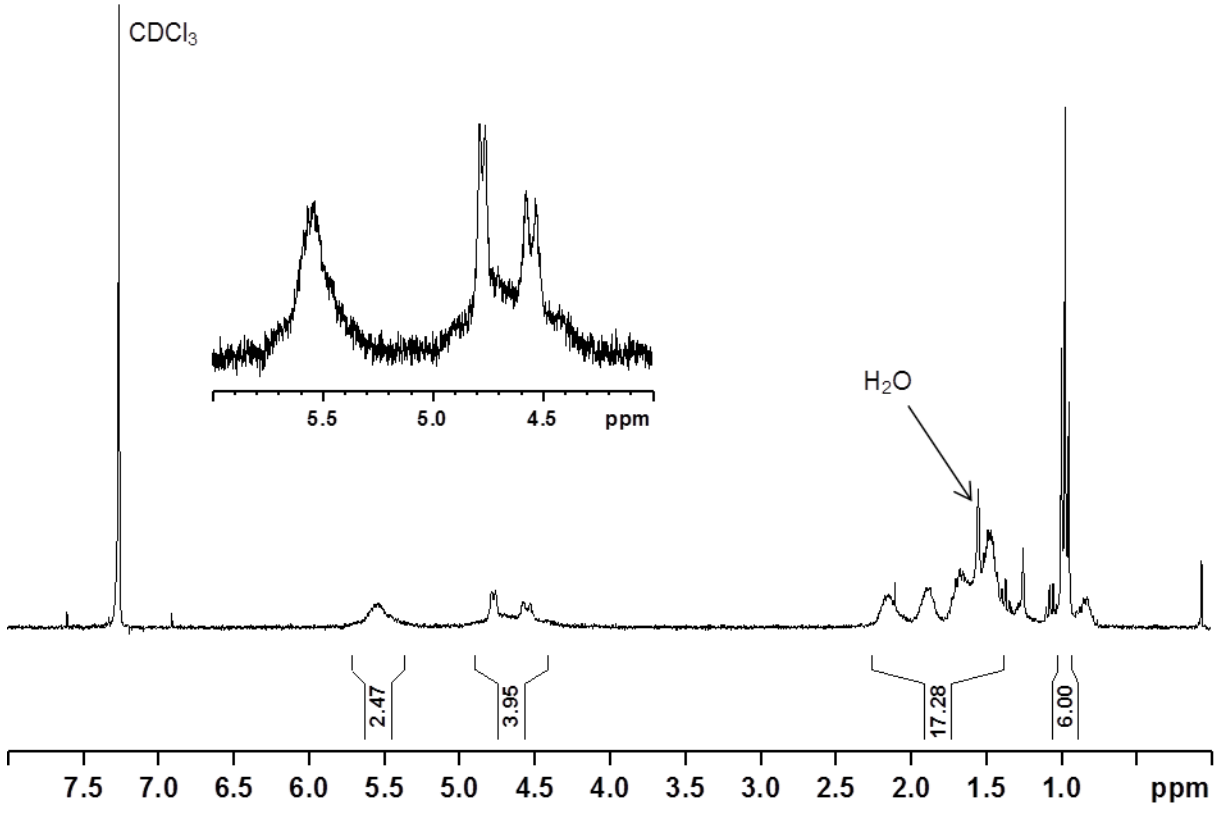

Appendix 4. Oxidation of 1-octadecanol

(a) Oxidation of 1-octanol reaction mixture after 240 min reaction time

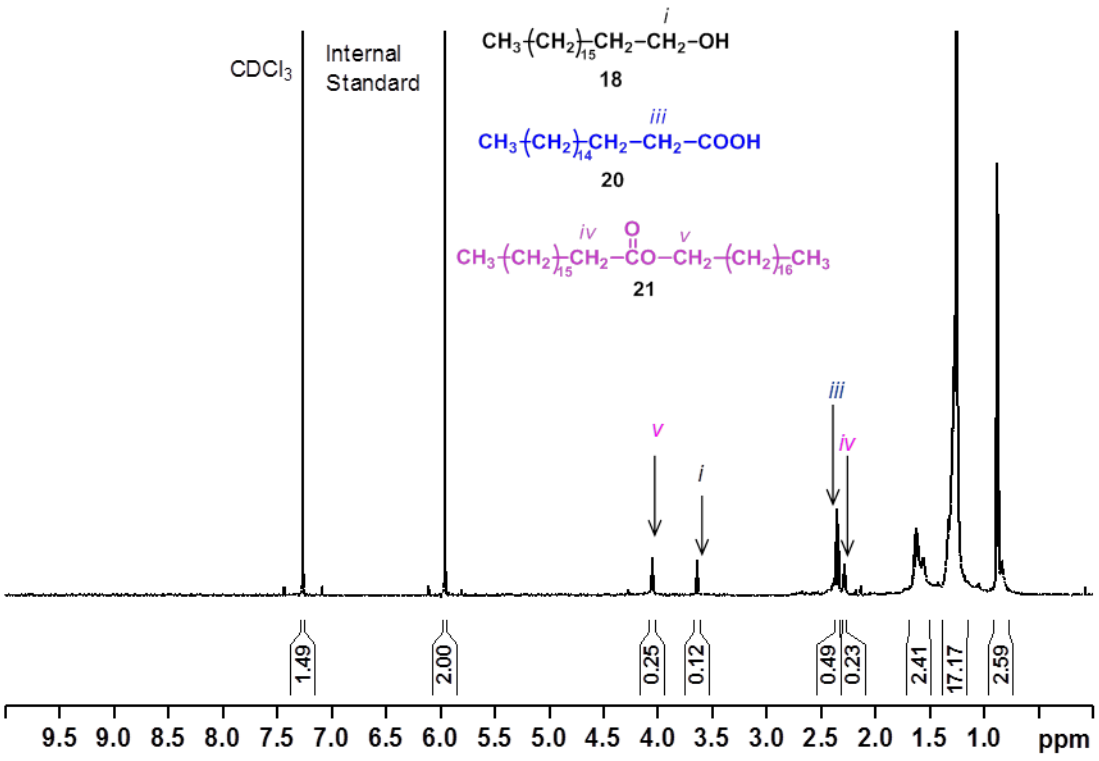

(b) Oxidation of 1-octanol reaction mixture after 60 min reaction time

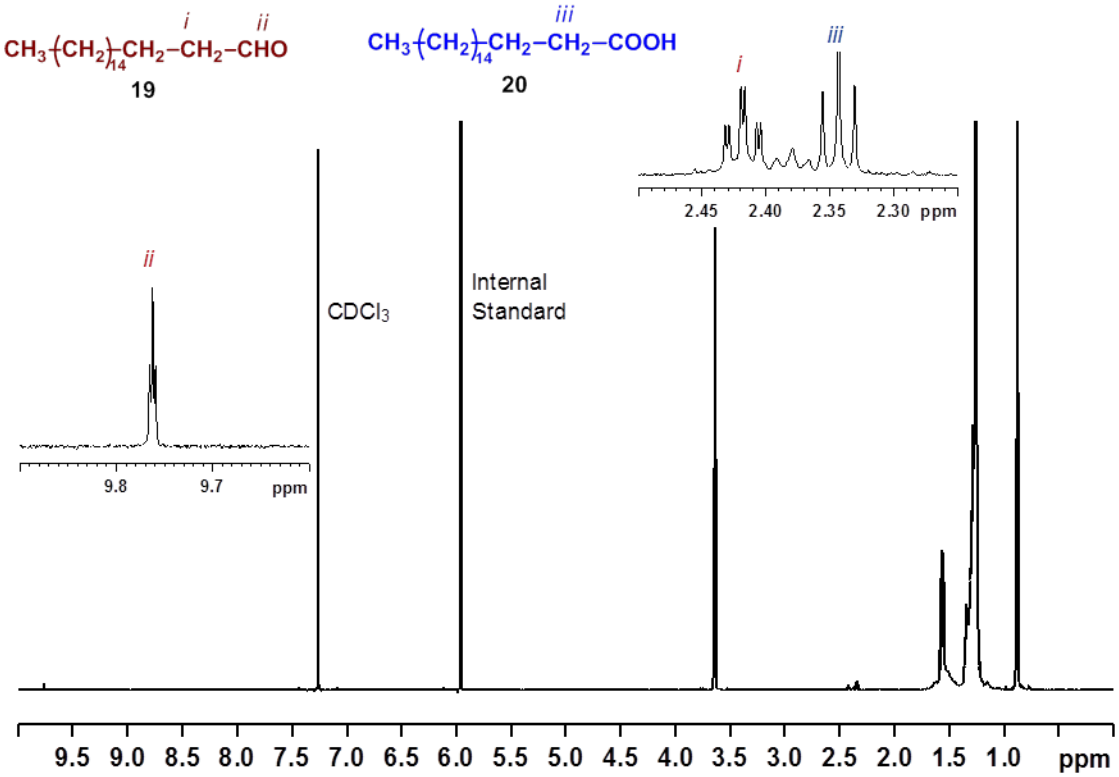

Appendix 5. Hydrogenation of benzaldehyde reaction mixture

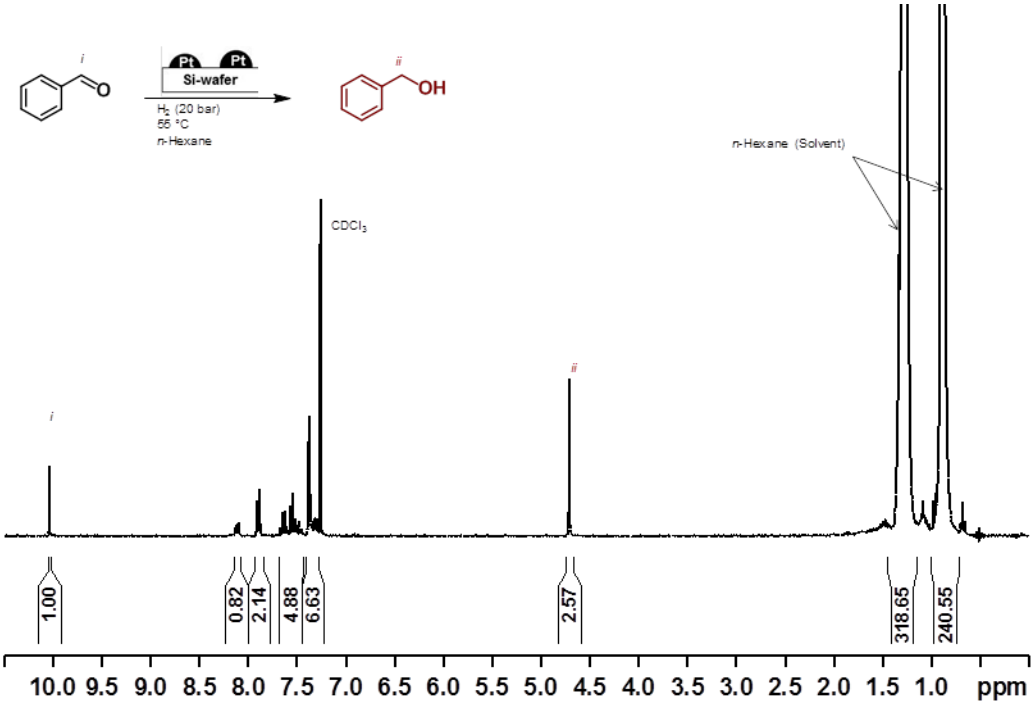

Appemdix 6. Oxidation of benzaldehyde

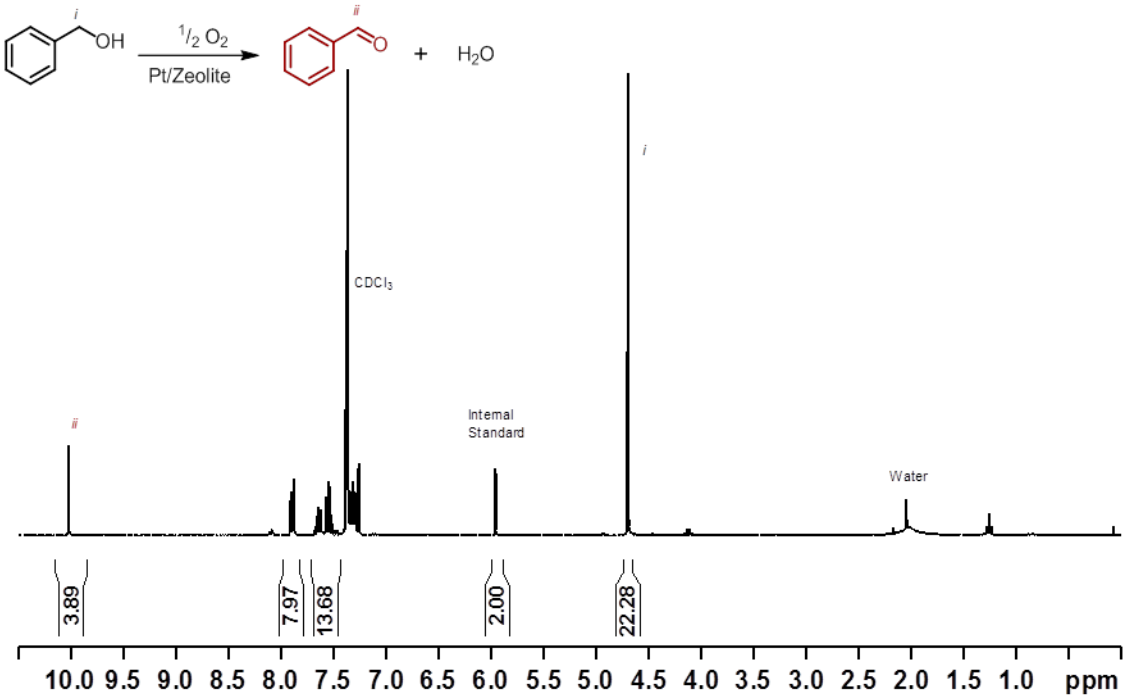

Appendix 7. Oxidation of 1-octanol reaction mixture (starting material and oxidation products)

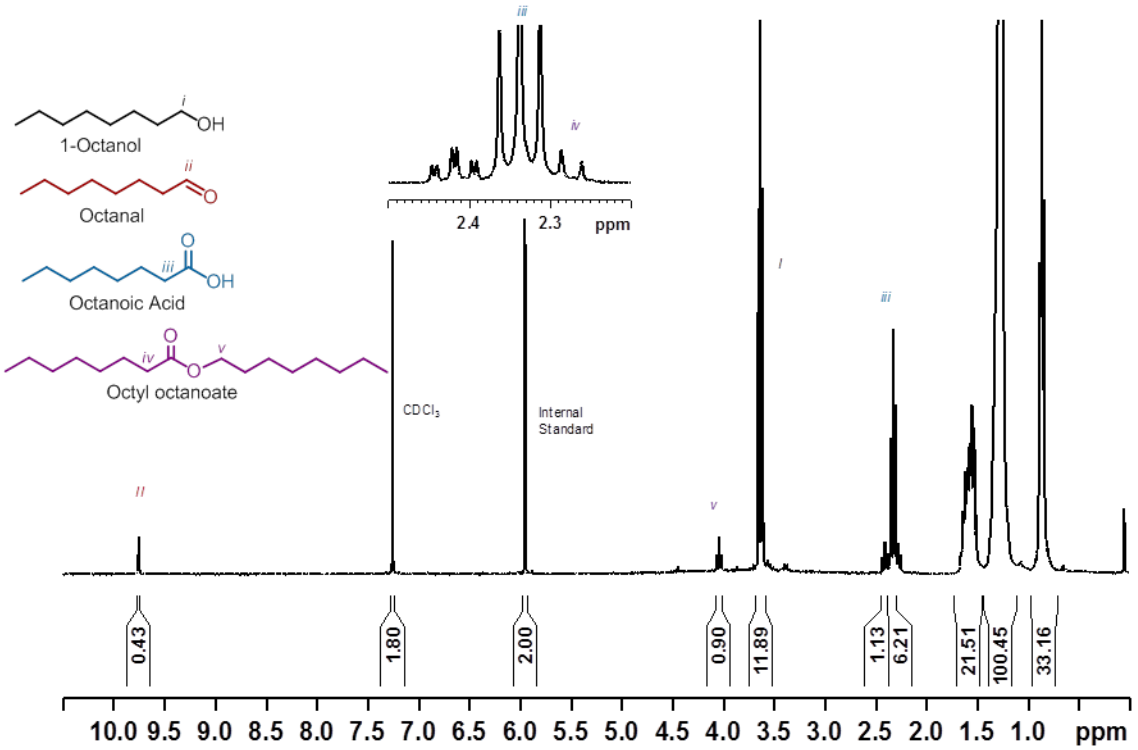

Appendix 8. Oxidation and etherification of 1-octanol reaction mixture

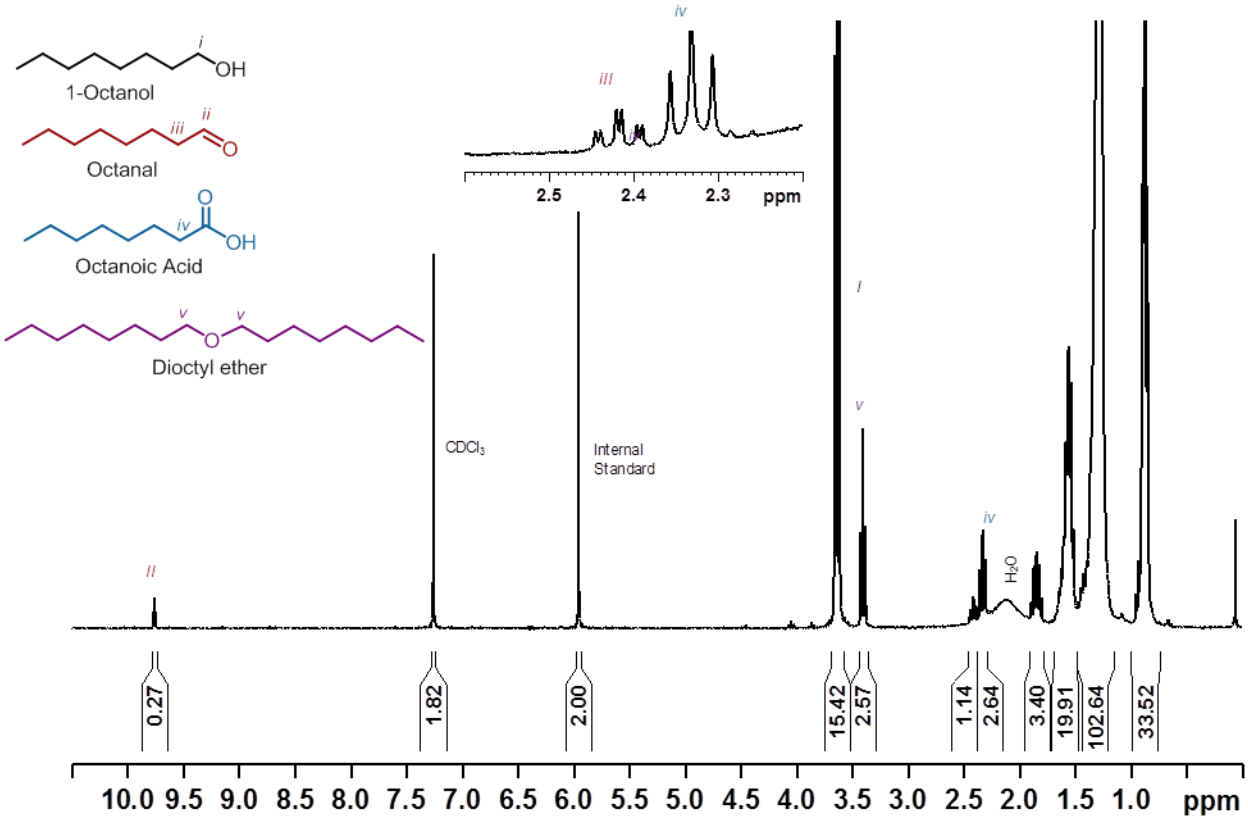

Appendix 9. Oxidation of benzyl alcohol reaction mixture

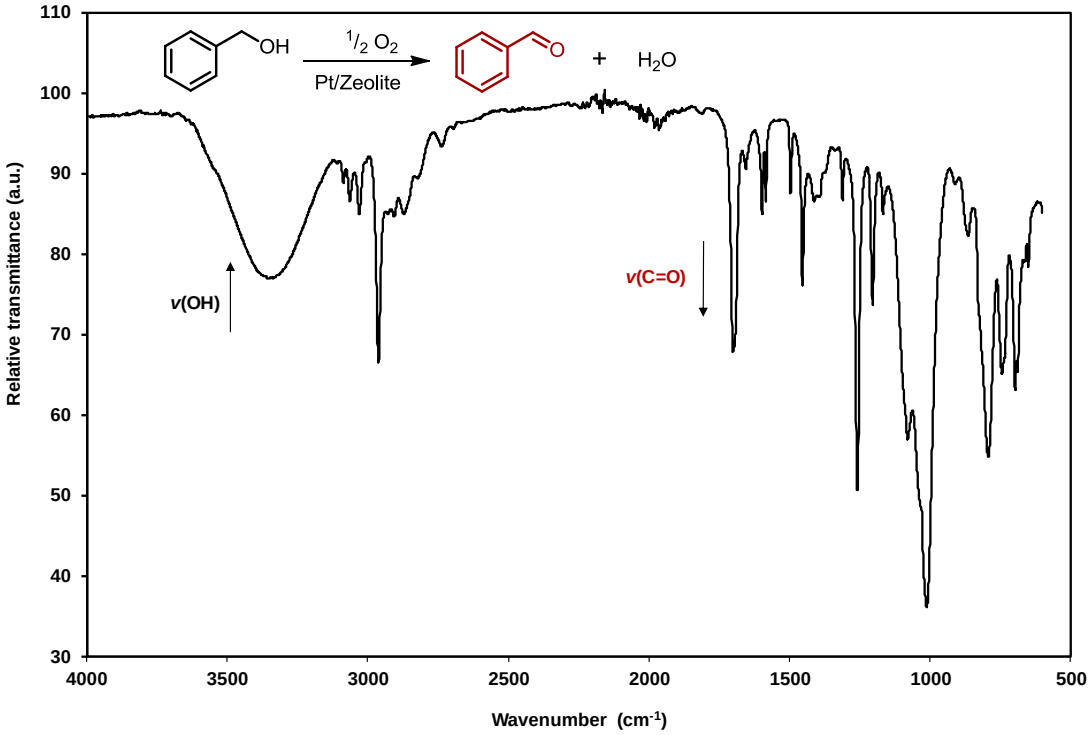

Appendix 10. XPS Data of di-μ-chlorobis[(1,2-η-)-1-hexene]diplatinum(II), 9

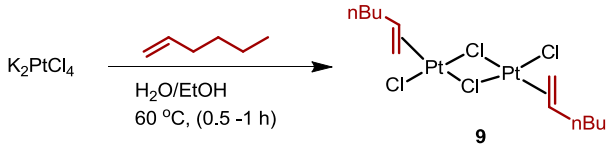

9

Pt 4f7/2 (eV)		FWHM(eV)	Chi Sq
Pt^0	72.1	2.0	1.5
Pt^{2+}	73.5	1.9	
Pt^{4+}	74.9	1.9	

Cl 2p (eV)		FWHM(eV)	Chi Sq
Pt-Cl	199.0	1.6	1.4
Pt-Cl	200.6	1.6	
μ-Cl	200.6	1.6	
μ-Cl	202.2	1.6	

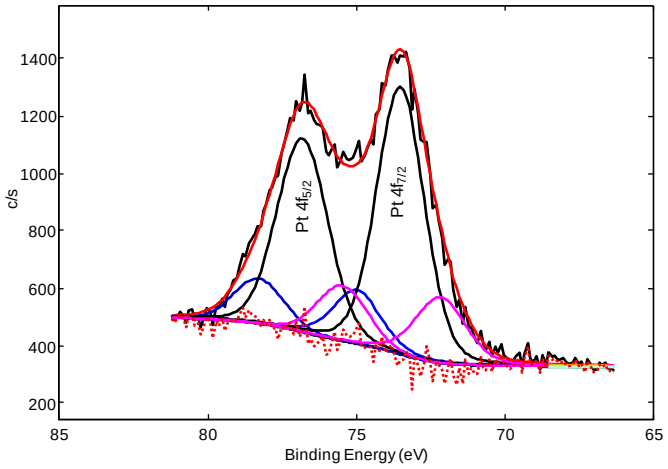

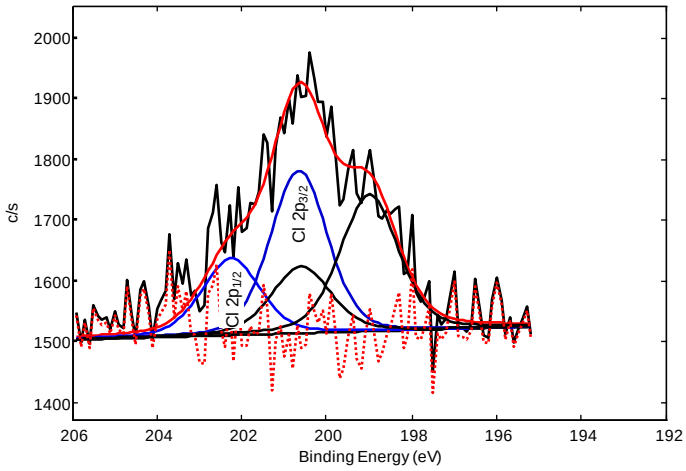

Appendix 11. Mass spectrum of propane formed after hydrolysis 2-propanol during the hydrogenation of cinnamaldehyde (see section 3.4.1).

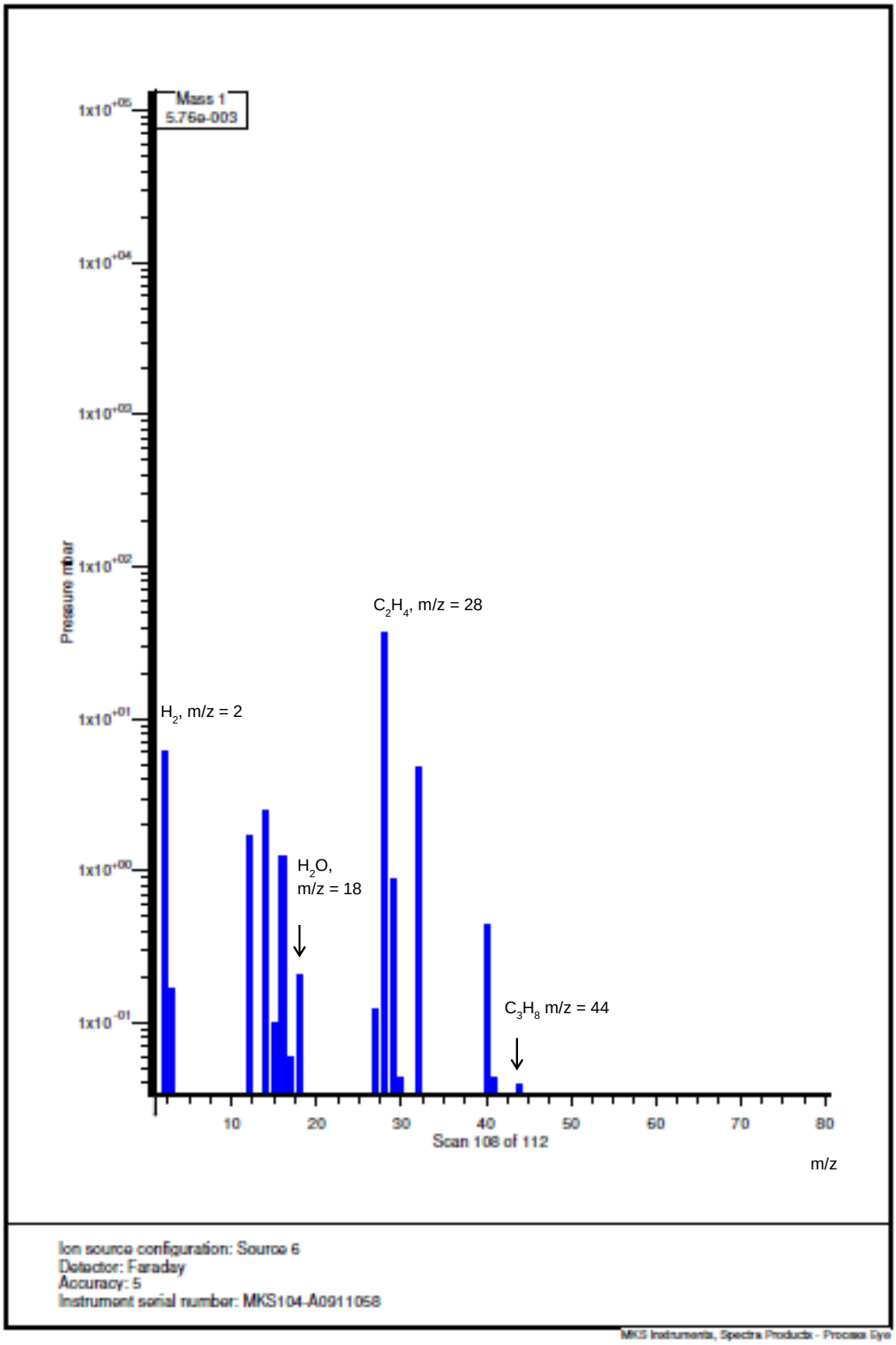

Appendix 12. A chromatogram (GC FID) from the aromatisation of *n*-hexane. The product matrix and retention times: *n*-hexane (*ca.* 3 min), benzene (*ca.* 4 min), heptane internal standard (*ca.* 6 min), naphthalene (*ca.* 21 min).